

**DEVELOPMENT of SIMULATION TOOLS for DISTRIBUTED ENERGY
CONVERSION SYSTEMS towards SMART GRIDS**

HABILITATION THESIS

Associate Professor Dr. Eng. Lucian MIHEȚ-POPA

June 2014

ACKNOWLEDGEMENT

I would like to express my gratitude to all my teachers, professors and mentors who helped me to understand and to love this great profession. Many thanks to my ex-supervisor, Professor Ion Boldea, for his supervision and his patience during my Ph. D stage. I would also like to thank Professor Frede Blaabjerg, Associate Professor Birgitte Bak-Jensen and Associate Professor Ewen Ritchie, from Aalborg University – Denmark, for their help and suggestions. They hosted my experiments in their laboratories. I spent 4 month (October 2000-January 2001) at Aalborg University, when I visited Prof. Frede Blaabjerg and I worked on a project entitled “Power Plant Characteristic of Wind Farms”, and then I spent 15 month (October 2001-December 2002) also at Aalborg University, when I visited Assoc. Prof. Ewen Ritchie and I worked on a project entitled “Condition Monitoring of Wind Generators”. I also want to thanks Professor J. M. Pacas, from Siegen University, Germany, for very interesting discussions and valuable advices, during my PostDoc stage in his Department of Power Electronics and Electrical Drives.

I am very grateful for having the chance to work again in Denmark, between 2011-2014, at RISO – Danish National Laboratory for Sustainable Energy and Technical University of Denmark-DTU. It was an amazing experience to plan work, fight, laugh, eat cakes and cry together with my colleagues and friends from all over the world. Working with the members of the PowerLab.dk and SYSLAB.dk is such an extraordinary experience. Also, teaching to the 3rd Technical University in Europe is a great challenge, as well. Many thanks to Assoc. Professor Arne Nielsen, Senior Scientist Henrik Bindner, Vice-Rector Anders Troi for interesting discussions, financial support and for their exceptional work that contributed to some of me achievements and currently ongoing projects.

Also thanks to my parents who gave me great support. Special thanks to my wife and my soon for giving me the motivation, inspiration and balance that I needed to actually finish this work. I would also like to thank to my colleagues and friends from University Politehnica of Timișoara who helped me with their valuable advices.

Timisoara,

Lucian MIHET-POPA

23 June 2014

Rezumatul Tezei de Abilitare

Teza de Abilitare cu titlul "Dezvoltarea unor modele și biblioteci de simulare dedicate sistemelor distribuite de conversie a energiei într-o rețea inteligentă", reprezintă principalele cercetări pe care le-am realizat în ultimii zece ani în domeniul surselor regenerabile conectate la rețele energetice de distribuție a energiei. Lucrarea se bazează pe contribuții originale, efectuate în cadrul activităților de cercetare, finanțate de Universitatea Politehnica din Timișoara, Universitatea din Aalborg-Danemarca, Universitatea din Siegen-Germania, Laboratorul Danez National de cercetare/dezvoltare-RISO și Universitatea Tehnică din Danemarca (DTU). Realizările și rezultatele obținute în această teză se bazează pe suportul a 11 granturi obținute prin competiție, de echipele de cercetare cu care am lucrat și pe care le-am coordonat, atât la nivel național cât și internațional, după cum urmează: 7 granturi/proiecte internaționale precum și 4 granturi naționale (CNCSIS). În urma rezultatelor obținute am publicat mai mult de 75 de lucrări, atât în reviste naționale cât și internaționale și în volumele unor conferințe de prestigiu.

Prima parte a tezei de abilitare, care face referire la realizările științifice și profesionale, conține 5 capitole. **Primul capitol** oferă o privire de ansamblu asupra structurii tezei, subliniind obiectivele, principalele contribuții, granturi de cercetare și premiile obținute. Scopul celui **de al-doilea capitol** este de a dezvolta modele/biblioteci de simulare pentru diferite componente și sisteme ale surselor de energie regenerabilă, ca parte integrantă în sistemele energetice de distribuție, cu ajutorul a două pachete de programe software dedicate, MATLAB / Simulink și DigSILENT PowerFactory. Aceste modele au fost validate cu ajutorul măsurătorilor/testelor de laborator, utilizând componente reale, și vor fi utilizate în continuare în următoarele capitole pentru dezvoltarea strategiilor de conducere și control a diferitelor scenarii pentru proiectarea și implementarea unei rețele inteligente (*Smart Grid*). Dezvoltarea modelelor de simulare va include panouri și sisteme fotovoltaice, turbine de vânt (generatoare eoliene), sisteme de stocare a energiei și de control al acestora în rețelele de distribuție a energiei, incluzând de asemenea casele inteligente cu diverși consumatori controlați automat. **Al treilea capitol** cuprinde trei părți principale și este dedicat strategiilor de control elaborate pentru sistemele energetice de putere având în componență surse regenerabile dintr-o rețea de distribuție. Prima parte a acestui capitol, oferă o imagine de ansamblu asupra strategiilor de control pentru turbine eoliene de puteri mari, folosind generatoare de inducție. De asemenea, sunt descrise și analizate cele mai performante strategii de comandă și control a turbinelor de vânt, atât cu viteză constantă și control activ al paletelor, cât și cu viteză variabilă și controlul unghiului de înclinare a paletelor. În a doua parte a capitolului 3, se prezintă implementarea pe o platformă/micro-controller digital(ă) în timp real a două strategii diferite de control al mașinilor electrice, utilizate în diferitele topologii ale turbinelor eoliene cu viteză variabilă. În ultima parte a acestui capitol au fost implementate și testate cu succes două tipuri diferite de regulatoare/controlere; Unul pentru reglarea tensiunii într-o rețea de distribuție, folosind consumatorii unei case inteligente (birou), și al doilea controler folosind sistemele de stocare

a energiei (diferite tipuri de baterii/acumulatori). Cele două tipuri de controlere/algoritmi de reglare pentru controlul tensiunii, au fost, de asemenea, implementați în MATLAB / Simulink și DlgSILENT PowerFactory și testați experimental cu ajutorul platformei inteligente de tip Smart Grid, descrisă în capitolul 2. **Capitolul patru** se axează pe testarea componentelor surselor de energie regenerabile care utilizează dispozitive de stocare și consumatori/sarcini controlați (controlate) în mod activ și, de asemenea, la testarea bateriilor vehiculelor electrice și hibride pentru a studia impactul asupra degradării bateriei în timpul efectuării unor teste de încărcare inteligentă și a unei încărcări rapide (la curenți de ordinul sutelor de amperi). Au fost testate două tipuri diferite de baterii Li-ion dedicate autoturismelor electrice și hibride. Scopul **Capitolului 5** este de a proiecta o rețea de distribuție, cu diferite componente ale surselor regenerabile, conectate împreună la aceeași stație de alimentare, și de a identifica situațiile cele mai defavorabile din punct de vedere energetic, punându-se un accent special pe provocările impuse de introducerea unor tehnologii/aparate noi, specifice rețelelor inteligente. Un alt aspect important al acestui capitol este de a identifica cazurile critice de încărcare, maxime și minime (impuse de standardele în vigoare), a rețelelor de distribuție și studiul variațiilor de tensiune generate prin conectarea surselor regenerabile.

Contribuția echipelor/grupurilor noastre în zona de cercetare și dezvoltare, în ultimii zece ani, a avut un impact semnificativ atât în Comunitatea Academică Internațională, precum și în industrie. Publicațiile noastre au primit mai mult de cinci sute de citări în baze de date internaționale. De asemenea, capitol de carte "Modelarea și simularea unui parc eolian de 12 MW", publicat de Editura internațională INTECH în 2011, în cartea intitulată „Studiul Impactului integrării surselor regenerabile în sistemele energetice de putere și alternative pentru a îmbunătăți integrarea acestora” a fost vizualizată și descărcată de peste 5000 de ori. Un alt aspect important pentru recunoașterea activității de cercetare la nivel internațional este premiul al doilea obținut pentru articolul “Wind Turbine Generator Modeling and Simulation where Rotational Speed is the Controlled Variable”, publicat în revista IEEE-IAS Transactions on Industry Applications, în ediția ianuarie/februarie 2004, Vol. 40, No. 1, pp. 3-10, (ISI Journal - ISI Web of Knowledge). Revista are un factor de impact de 2.578, și a primit 50 de citări în baza de date ISI Web of Knowledge, 90 de citări în SCOPUS și peste 150 de citări în Google Scholar.

Cea de a doua parte a tezei, referitoare la planurile de evoluție și dezvoltare a carierei, se bazează pe aptitudinile dovedite de a desfășura și coordona grupuri/echipe de cercetare la nivel înalt și activități de predare la nivel academic și de a iniția colaborări internaționale de succes în domeniul sistemelor de conversie a energiei regenerabile. Ca planuri de viitor vom încerca să accesăm fonduri naționale și Europene (granturi Orizont 2020) pentru a extinde și îmbunătăți laboratoarele departamentului nostru și a centrului de cercetare "Controlul inteligent al conversiei și stocării energiei" de la Universitatea Politehnica din Timișoara, Departamentul de Inginerie electrică, și să extindem cooperarea internațională și rețeaua existentă de cercetare. Un alt aspect important referitor la dezvoltarea carierei academice este de a crea și dezvolta o platformă de tip *Smart Grid*,

similară cu aceia din Danemarca (www.powerlab.dk), unde am petrecut trei ani și de a folosi experiența mea pentru a crea un centru de cercetare cu studenții de la master și doctorat, coordonați ca urmare a obținerii tezei de abilitare.

Abstract

The Habilitation Thesis “DEVELOPMENT of SIMULATION TOOLS for DISTRIBUTED ENERGY CONVERSION SYSTEMS towards SMART GRIDS” points out the main research that I have performed during the last ten years in the area of Energy Conversion Systems with Renewable Energy Resources and Battery Storage Solutions. It is based on original contributions performed during the research activities financed by POLITEHNICA University of Timisoara, Aalborg University-Denmark, Siegen University-Germany, The Danish National Laboratory-RISO and Technical University of Denmark (DTU). The work made in this Thesis has been funded by 7 international grants/projects and by 4 national (CNCSIS) grants, as well. We have also been published more than 70 papers, in national and international journals and conference proceedings, based on the obtained results.

The first part of the Habilitation Thesis, regarding scientific and professional achievements, contains 5 chapters.

The first chapter gives an overview of the research roadmap of the thesis, pointing out the objectives, the main contributions, research grants and awards.

The aim of **the second chapter** is to develop simulation models of DER components in Power System, using two dedicated software packages MATLAB/Simulink and DigSILENT PowerFactory. These models will also be validated against measurements and further used in the next chapters for developing of control strategies and different scenarios for a future smart grid. Development of simulation models will include PV panels and Systems, Wind Turbine Generators, Energy Storage Systems and Demand-Side Control in Distribution Networks with focus on intelligent houses with actively controlled loads.

The third chapter contains 3 main parts and is dedicated to control strategies developed for renewable energy systems in a distribution network. The first part, gives an overview of the state of the art control strategies for large wind turbines using induction generators. An active-stall constant-speed wind turbine controller with its actuator system for variable pitch angle and a control strategy for a pitch-controlled variable-speed wind turbine are described. Afterwards, in the second part, two different control strategies developed for variable-speed wind turbines using induction generators are described and implemented on a real-time digital platform. In the last part of this chapter two different types of voltage controllers in a distribution grid, using active loads/office building appliances and battery energy storage systems, have been implemented and tested successfully. Using the model of an intelligent office building a controller for load shifting has been developed. Two types of controllers for voltage regulation using battery energy systems have also been developed and implemented in MATLAB/Simulink and DigSILENT PowerFactory.

The Chapter four is focuses on testing of DER components with storage devices and actively controlled loads and also on electric vehicle batteries testing to study the impact of

smart charging and fast charging on the power system and on the battery degradation. Two different types of EV battery packs have been tested.

The purpose of **the Chapter 5** is to design a distribution network with different DER Components connected along the feeders and to identify limitations of existing simulation and planning tools, with a particular focus on the challenges imposed by the introduction of Smart Grid technologies. Another important issue of this chapter is to identify critical load cases and voltage variations for the designed scenarios.

Our work in research and development area, during the last ten years, has had a significant impact both in the International Academic Community, as well as in the industry. Our publications have received more than three hundreds of citations in international data bases. Also, our book chapter „**Modeling and simulation of a 12 MW wind farm**“ published by INTECH in 2011 in the book entitled Wind Farm-Impact in power system and alternatives to improve the integration has reached to more than 5000 downloads.

The second part of the Thesis, regarding to future plans for advancement and career development is based on the proven skills to conduct and coordinate high-level research and teaching activities at academic level and to initiate successful international collaborations in the field of renewable conversion systems. As future plans I am trying to attract national and EU funds (Horizon 2020 grants) to extend and improve our research lab “Intelligent control of energy conversion and storage” from POLITEHNICA University of Timisoara, Electrical Engineering Departments, and to extend our international cooperation and network. Another plan is to create and develop a Smart Grid platform, similar with that one from Denmark (www.powerlab.dk) where I spent 3 years and to use my experience to create a research center for Master and Ph.D. students, coordinated as a result of the Habilitation Thesis.

Contents of the Thesis

- ACKNOWLEDGEMENT 2
- Rezumatul Tezei de Abilitare..... 3
- Abstract 6
- Contents of the Thesis..... 8
- Part I: SCIENTIFIC and PROFESIONAL ACHIEVEMENTS..... 12
- Chapter 1: Introduction..... 13
 - 1.1. Overview and Motivation..... 13
 - 1.2. Objectives..... 14
 - 1.3. Summary of the contributions and Impact 14
 - 1.3.1. Major contributions..... 14
 - 1.3.2. Citation 15
 - 1.3.3. Awards..... 15
 - 1.4. Research Environment and Funding 16
 - 1.4.1. Research Grants/Projects..... 16
- Chapter 2:..... 18
- Development, Implementation and Validation of Simulation Models for DER components in a Distribution Network..... 18
- 2. Development, Implementation and Validation of Simulation Models for DER components in a Distribution Network..... 20
 - 2.1. INTRODUCTION 20
 - 2.1.1. Generalities 20
 - 2.1.2. Aim and objectives 20
 - 2.1.3. Abstract 21
 - 2.2. Experimental Facilities of SYSLAB Research Laboratory 22
 - 2.3. SIMULATION MODELS DEVELOPED for PV Panels and SYSTEMS 25
 - 2.3.1. Introduction..... 25
 - 2.3.2. Mathematical Modeling, Implementation and Validation of a Polycrystalline PV panel using MATLAB/Simulink 25
 - 2.3.3. Implementation and validation of the simulation model for PV Array..... 32
 - 2.3.3.3 Graphical user interface 44
 - 2.3.4. Simulation Model of PV System developed in DIgSILENT PowerFactory for distribution networks 46
 - 2.3.4.1. Description of the PV System Model Implementation..... 47
 - 2.3.4.2 Comparison between simulations and measurements..... 51

2.4. Wind Turbine Systems Modeling and Simulation	53
2.4.1. Introduction.....	53
2.4.2 Wind Turbine Modeling.....	53
2.4.3 Simulation Results	59
2.5 Energy Storage Systems in a Distribution Network.....	65
2.5.1 Analytical model of the VRB	66
2.5.2 VRB model implemented in Matlab/Simulink.....	69
2.5.3 Validation of the simulation model	75
2.5.4 Simulation Model of VRB System developed in DigSILENT PowerFactory for distribution networks	76
2.5.4.1 Description of the Battery System Simulation Model Implementation.....	77
2.5.2 Simulation Results and Model Validation	80
2.6 Modeling, simulation and validation of an office building model.....	83
2.6.1 Flex House Modeling & Implementation	83
2.6.1.2 Simulation Results	88
2.7 Conclusion	89
Appendix	91
Chapter 3:.....	94
Control Strategies Developed for	94
Renewable Energy Systems.....	94
3. Control Strategies developed for Renewable Energy Systems	96
3.1. Introduction.....	96
3.2. Dynamics of Control Strategies for Wind Turbine Systems	98
3.2.1. Control Strategies for Wind Turbines.....	98
3.2.2. Active Stall Constant-Speed Wind Turbines using Cage-Rotor Induction Generators.....	101
3.2.3. Control Design for a Variable-Speed Wind Turbine	103
3.2.4 Simulation Results	106
3.3. Control Strategies developed for Variable-Speed Wind Turbine Generators.....	110
3.3.1. Control Strategy of the DFIG based Wind Turbines	110
3.3.2. Control Strategies developed for Variable-Speed Wind Turbines with CRIG and implemented using a real-time digital platform	117
3.4. Control Strategies of DER Components in a Distribution Network.....	122
3.4.1. Voltage control by active power	122
3.4.1.1. Voltage Control by Load Shifting	123
3.4.1.2. Voltage Control using BESS	127
3.5. Discussion and Conclusion	132
Chapter 4. Testing of DER Components with Storage Devices	134
and Actively Controlled Loads in a Smart Grid.....	134
4.1. Introduction.....	136

4.2. Experimental Testing for Stability Analysis of D E R Components with Storage Devices and Loads	138
4.2.1. DER Components with Storage Devices and (Controllable) Loads.....	138
4.2.2. Components Testing under different Modes of Operation	141
4.3. Electric Vehicle Batteries Testing in a Smart Grid using Renewable Energy.....	147
4.3.1. Smart Grid Energy System Infrastructure	147
4.3.1.1. Battery Management System Test Platform	147
4.3.2. Experimental Tests and Results.....	149
4.4. Discussion and Conclusions	161
Appendix.....	163
Chapter 5	164
Modeling and implementation of different scenarios designed to identify critical cases in a future Smart Grid	164
Chapter 5. Modeling and implementation of different scenarios	166
Designed to identify critical cases in a future Smart Grid	166
5.1. Introduction.....	166
5.2. Grid model components and implementation.....	167
5.2.1. Description of the grid models and scenarios.....	167
5.2.2. Grid model implementation in NEPLAN and DIgSILENT PowerFactory	169
5.3. Steady-state simulation results. Power flow calculation analysis.....	174
5.4. Time-series simulation results.....	178
5.4.1. Steady-state simulations	178
5.4.2. Time-series simulations using dynamic models	187
5.4.2.1. PV system modeling	187
5.4.2.2. Active and Dynamic Loads Modeling	191
5.4.2.3. EV battery modeling and implementation	193
5.4.2.4. Simulation Results	196
5.5. Discussion and Conclusion	198
Appendix:	199
Part II: Future Plans for Career Development and Evolution.....	200
A) Main Directions for career development	200
B) Main Directions for research and planning objectives.....	203
B1) Distribution planning objectives	205
B2) Recommendations for Smart Plan Tools: Analytical and Software Packages.....	206
Part III: References	208

References for Chapter 2	208
References for Chapter 3	211
References for Chapter 4	214
References for Chapter 5	217

Part I: SCIENTIFIC and PROFESIONAL ACHIEVEMENTS

Chapter 1: Introduction

This habilitation thesis is a summary of the research work I have been performed over a period of around ten years, in the area of modeling, simulation, control and testing of renewable energy systems with distributed generation. The habilitation covers the research performed after the defense of my Ph.D. Thesis in December 2003.

This chapter gives an overview of the research roadmap of the thesis, pointing out the objectives, the main contributions, research grants and awards.

1.1. Overview and Motivation

Renewable energy systems are growing up due to not only environmental aspect but also due to social, economic and political interest. The European Union is aiming at a specific CO₂ reduction in the electricity sector in the near future (20% reduction by 2020). This will involve a significant growth of Wind Turbines and PV installation all over Europe resulting in a few hundred Giga watts of capacity.

Due to variable nature of power generation from Wind Turbines (WT) and Photo Voltaic (PV) Systems, storage systems and Demand-Side Management (DSM) and response as flexibility options gain particular importance for the secure and cost-efficient operation of power systems and best utilization of available WT and PV resources. These both options provide the shift in time which would help accommodate high penetration levels of PV in the system.

The distributed generation is taking importance pointing out that the future utility line will be formed by distributed energy resources and micro-grids. The flexible micro-grid has to be able to import/export energy from/to the grid, control the active and reactive power flows and manage of the storage energy systems.

An efficient way of controlling the voltage in a distribution network is to control the local power consumption at the bus-bar. The consumption can be influence by shifting load or using energy storage. The ability to control active units can reduce the stress on the low-voltage grid by consuming the PV/Wind production locally.

It is anticipated that new home appliances [e.g., Electric Vehicles (EVs) and Heat Pumps (HPs)], and embedded generations will be introduced to the power system. In addition, control strategies of various energy resources are going to be implemented in the current power system.

To capture the behaviors of such elements, and to handle the correlation of behaviors in time, time series simulation is one of the key function that should be implemented in the future grid design. Moreover, it is of interest that how Smart Grid control strategies can be represented and how concurrent control of units is handled in the simulation tools.

The modeling of DER components in power systems and the relative control architecture are an important part for the introduction of relevant quantity of renewable energy in the future smart grid. Therefore it is a strong necessity to have proper validated

models to help operators to perform better studies and to be more confident with the results.

1.2. Objectives

The objectives of this thesis are to develop simulation models of DER components in Power System, using three dedicated software packages MATLAB/Simulink, NEPLAN and DigSILENT PowerFactory. These models will also be validated against measurements and used for developing of control strategies and different scenarios for a future smart grid. Development of simulation models will include PV panels, Wind Turbine Generators, energy storage systems and demand-side control in distribution networks with focus on intelligent houses with actively controlled loads.

Another objective is to evaluate the performance for an active stall constant speed wind turbine using Cage Rotor Induction Generator (CRIG) versus a pitch controlled variable speed wind turbine using Doubly Fed Induction Generator (DFIG).

To study its steady state and dynamic behavior of a DFIG of 11 kW fed by a vector controlled back-to-back PWM-VSI inverter on the rotor side and a CRIG of 11 kW rating with a vector controlled back-to-back PWM-VSI inverter on the stator side will be implemented and tested using a real-time digital platform, based on a flexible dSPACE digital signal processor system.

Two different types of voltage controllers in a distribution grid using active loads/office building appliances and battery energy storage systems will be implemented and tested using a research lab with real components designed for distributed control and smart grids.

To study the impact of smart charging and fast charging on the power system, on the battery state of health and degradation, and to find out the limitation of the batteries for a future smart grid, a test platform, including three Lithium-ion batteries, will be used. The platform will be designed for EV applications, for testing impacts on different advanced loadings of EV batteries, and will contains a battery management system.

1.3. Summary of the contributions and Impact

My research has been focused on modeling, simulation and testing of different components, control strategies and systems in the area of renewable energy with distributed generation towards smart grids.

1.3.1. Major contributions

The major contributions are summarizes as follows:

- Modeling and simulation of a real wind farm of 12 MW with 6 active stall constant speed wind turbines, using two different software packages, MATLAB/Simulink and DigSILENT PowerFactory [2.53-2.55];
- Development, design, implementation and testing of a condition monitoring system used for variable-speed wind turbines [3.45-3.49]; The system was also implemented on real wind turbines in Denmark.
- Development and testing of different control strategies implemented for variable-speed wind turbine generators, using a real-time simulator platform [3.38, 3.44, 3.49];
- Development of tools for Distributed Energy Resources (DER) Components in a distribution network and validated the simulation models using a research lab with real components designed for distributed control and smart grids with a high share of renewable energy production [2.23-2.26, 3.25-3.27, 3.35]; These tools are used to test new components and to extend the distribution network of the platform.
- Designing a Battery Management System (BMS) devoted to electric and hybrid vehicle batteries testing to study the impact of smart charging and fast charging on the power system and on the battery degradation. Using this system two different types of EV battery packs have been tested: a 16 kWh Lithium-Ferro type, optimized for hybrid EV applications, and a 26 kWh Lithium polymer type, optimized for full EV applications [4.29, 4.45-4.48].
- Designing a distribution network with different DER Components connected along the feeders and identifying limitations of existing simulation and planning tools for distribution networks, with a particular focus on the challenges imposed by the introduction of Smart Grid technologies [5.18-5.20].

1.3.2. Citation

Our publications have got more than five hundreds of citations in international data bases, such as ISI Thomson/ISI Web of Knowledge, SCOPUS, INSPEC, IEEE Explore and Google Scholar.

Our book chapter „**Modeling and simulation of a 12 MW wind farm**” published by INTECH in 2011 in the book entitled Wind Farm-Impact in power system and alternatives to improve the integration has reached to more than 5000 downloads.

1.3.3. Awards

Our paper published in January / February 2004, Vol. 40, No. 1, by the IEEE IAS Transactions on Industry Applications, entitled “Wind Turbine Generator Modeling and Simulation Where Rotational Speed is the Controlled Variable”, received in 2005 the Second Prize Paper Award; This Journal is indexed in ISI Web of Knowledge/ISI Thomson and has an impact factor of 2.58.

Another paper published in 2003 by IEEE IAS received the best paper of the session: “Condition Monitoring of Wind Generators”, Record of IEEE-IAS 38th Annual Meeting, Salt

Lake City-USA, 2003, 12-16 October, Vol. 3, pp. 1839-1846, ISBN: 0-7803-7883-0, Accession Number: WOS: 7798516 (ISI Proceedings, INSPEC, IEEE Explore), The paper received 5 Citations in ISI Web of Knowledge, and more than 70 in Google Scholar.

1.4. Research Environment and Funding

The work presented in this thesis is the result of much collaboration with different research groups from international research institutions and universities and partners from industry. The international research teams, in which I was involved, are from Denmark (I spent 2 year at Aalborg University and 3 year at Technical University of Denmark) and Germany (at Siegen University). At Aalborg University, IET Department we have built a research GREEN LAB with many set-ups able to cover the area of renewable energy conversion systems. These labs are used for teaching and research, as well. At Riso DTU, Electrical Engineering Department we have been developed a research and education platform dedicated to Smart Grids, with real components (wind turbines, PV systems, EV, BESS, heat pumps, diesel genset, intelligent houses etc). The SYSLAB is a laboratory for research and development in distributed control and smart grids with a high share of renewable energy production (www.powerlab.dk). The components are all connected in one distributed control and measurement system that enables very flexible setup with respect to experimental configuration. The data acquisition and control system (hardware and software) is responsible for the supervision and control of the research platform for distributed intelligent energy systems with a high penetration of renewable energy.

1.4.1. Research Grants/Projects

This work has been funded by International and Romanian grants. The funds for all these projects were obtained in competition and provided by European Union (EU), Danish Technical University (DTU), Aalborg University (Denmark), Siegen University (Germany), Danish Energy Agency and CNCSIS.

Below is provided the list of research grants/projects connected to this work:

International Projects in which I was responsible & Work Packages/Milestones Leader

[1] "Smart Modelling of Optimal Integration of High Penetration of PV-Smooth PV", (<http://www.smooth-pv.info/>), PV ERA NET - EU International Project, 2011-2013; In this project were involved 5 Partners from 4 EU countries.

[2] "Distribution System Planning for Smart Grids-Smart Plan", ForskEL ID no. 10680, 2012-2013. This Grant/project was financed by Danish Energy Agency (Energynet.dk) & Danish Technical University-DTU.

[3] "Application of smart grid in photovoltaic power systems-PVNET.dk", ForskEL Project ID 55802, 2012-2014; The project was sponsored by Danish Energy Agency -Energinet.dk and Danish Technical University-DTU, under the Electrical Energy Research.

[4] "Distributed Energy Resources Research Infrastructures-DErri", Seventh Framework Programme-FP7, EU Project No. 228449, 2011-2012; (www.der-ri.net). This project has had 16 Partners from 12 countries.

International research grants/projects in which I participated as a research team member

[1] "Improvement of the structures and efficiency of small horizontal axis wind generators with non regulated blades", POS_CCE-SEE-RO 018. Beneficiary UPT/Institutul de cercetări pentru energii regenerabile, Contract nr.13/01.03.2009.

[2] "Condition Monitoring of Electrical Drive Systems", Postdoc grant of the „Hagen Tschoeltsch-Stiftung”- Universitat Siegen-Germany, Beneficiary: Department of Electrical Drives, Siegen University, Germany, (May 2004-August 2004).

CNCSIS National Grants

[1]. Cod CNCSIS A 628/2005, no. 26 – „New research regarding novel topologies of energy conversion systems using induction generators” (team member).

[2]. Cod CNCSIS 628/2006, no. 29, „New research regarding novel topologies of energy conversion systems using induction generators” (team member).

[3]. Cod CNCSIS 372, Tip A-2007, no. 46GR/11.05.2007: title: “Researches regarding the control of new wind aggregates structures, with non-regulated blades and permanent magnet synchronous generator”, (team member).

[4]. Cod CNCSIS 372, Tip A-2008, no. 98GR / 11.06.2008, title: “Researches regarding the control of new wind aggregates structures, with non-regulated blades and permanent magnet synchronous generator”, (team member).

[5] Acționări electrice și Conversoare Statice – AECS, Cod CNCSIS – D 117/1998, Tema 42. Beneficiar CNCSIS (50 000 USD)

Chapter 2:

Development, Implementation and Validation of Simulation Models for DER components in a Distribution Network

Contents of the chapter

Chapter 2:Development, Implementation and Validation of Simulation Models for DER components in a Distribution Network..... 18

2.1. INTRODUCTION 20

 2.1.1. Generalities 20

 2.1.2. Aim and objectives 20

 2.1.3. Abstract 21

2.2. Experimental Facilities of SYSLAB Research Laboratory 22

2.3. SIMULATION MODELS DEVELOPED for PV Panels and SYSTEMS 25

 2.3.1. Introduction..... 25

 2.3.2. Mathematical Modeling, Implementation and Validation of a Polycrystalline PV panel using MATLAB/Simulink 25

 2.3.3 Implementation and validation of the simulation model for PV Array 32

 2.3.3.3 Graphical user interface 44

 2.3.4 Simulation Model of PV System developed in DIgSILENT PowerFactory for distribution networks 46

 2.3.4.1. Description of the PV System Model Implementation..... 47

 2.3.4.2 Comparison between simulations and measurements..... 51

2.4.Wind Turbine Systems Modeling and Simulation 53

 2.4.1. Introduction..... 53

 2.4.2 Wind Turbine Modeling..... 53

 2.4.3 Simulation Results 59

2.5 Energy Storage Systems in a Distribution Network..... 65

 2.5.1 Analytical model of the VRB 66

 2.5.2 VRB model implemented in Matlab/Simulink..... 69

 2.5.3 Validation of the simulation model 75

 2.5.4 Simulation Model of VRB System developed in DIgSILENT PowerFactory for distribution networks 76

 2.5.4.1 Description of the Battery System Simulation Model Implementation 77

 2.5.2 Simulation Results and Model Validation 80

2.6 Modeling, simulation and validation of an office building model..... 83

 2.6.1 Flex House Modeling & Implementation 83

 2.6.1.2 Simulation Results 88

2.7 Conclusion 89

Appendix 91

2. Development, Implementation and Validation of Simulation Models for DER components in a Distribution Network

2.1. INTRODUCTION

2.1.1. Generalities

Renewable energy systems are growing up due to not only environmental aspect but also due to social, economical and political interest. The European Union is aiming at a specific CO₂ reduction in the electricity sector in the near future (20% reduction by 2020). This will involve a significant growth of PV installation all over Europe resulting in a few hundred Giga watts of capacity [1-2].

The increased PV capacity will influence power system operation and design. Power supplied from a PV array depends mostly on present ambient conditions such as: irradiation and temperature [3-6].

When integrating a high share of PV into the power system, the variability of the power output should be considered, since there is a difference between day and night. This problem might be solved by using storage systems. The battery package is an interesting option for storing excess energy from the hybrid grid (wind intermittency) for later use. It may also act as a peak shaving unit and thereby contribute to a stronger grid [7-10].

The distributed generation is taking importance pointing out that the future utility line will be formed by distributed energy resources and micro-grids. The flexible micro-grid has to be able to import/export energy from/to the grid, control the active and reactive power flows and manage of the storage energy [11-14].

The modeling of DER components in power systems and the relative control architecture are an important part for the introduction of relevant quantity of renewable energy in the future smart grid. Therefore it is a strong necessity to have proper validated models to help operators to perform better studies and to be more confident with the results.

This work has been funded by 3 international EU grant/projects: "Smart Modelling of Optimal Integration of High Penetration of PV-Smooth PV", PV ERA NET and partial by the ForskEL "Smart Plan" project 55807 and by POS_CCE-SEE-RO 018, „Improvement of the structures and efficiency of small horizontal axis wind generators with non-regulated blades" and 2 national grants (CNCSIS): **„New research regarding novel topologies of energy conversion systems using induction generators"** (Cod CNCSIS A 628/2005, no. 26 and Cod CNCSIS 628/2006, no. 29).

Also, this chapter is based on our papers, developed in national and international partnerships and collaborations, and published in International Journals and Conference Proceedings highlighted in Part III of this thesis, to the end of each reference list.

2.1.2. Aim and objectives

The aim of this chapter is to develop simulation models of DER components in Power System, using two dedicated software packages MATLAB/Simulink and DIgSILENT PowerFactory. These models will

also be validated against measurements and further used in the next chapters for developing of control strategies and different scenarios for a future smart grid.

Development of simulation models will include PV panels, Wind Turbine Generators, energy storage systems and demand-side control in distribution networks with focus on smart houses with actively controlled loads.

A relevant model with LV feeders with electricity storage and controllable units will also be modeled. The model development will have a particular focus on implementation of the controls of the active units to enable operation with PV system. Different control strategies will be implemented and tested for a time scale of seconds to minutes/hours.

Validation of simulation models will be carried out using RISO experimental facility SYSLAB (see subchapter 2.2) which include PV Systems, Wind Turbines as well as a Vanadium Redox Flow Battery-VRB and various loads including an office building-FlexHouse in a LV network which can be operated in different configurations. SYSLAB also provides a flexible control system which will be used for testing control strategies for the validation of the relevant models.

A number of tests will be specified and carried out for the validation of the models. The tests will be both at the component level and on the feeder level.

2.1.3. Abstract

In **subchapter 2** an overview about SYSLAB experimental facility is given with some details about its components and architecture.

Subchapter 3 is dedicated to simulation models of PV systems developed and implemented in MATLAB/Simulink and DlgSILENT PowerFactory. The PV panels have been modeled using a single-diode four parameters model based on the data sheet values. To point out the strong dependency on ambient conditions and to validate the simulation models a complex data processing subsystem model has also been developed and implemented.

Subchapter 4 is devoted to modeling and simulation of wind turbine generators, while **subchapter 5** described a Vanadium Redox Battery-VRB system model based on the efficiency of different components, such as: cell stacks, electrolytes, pumps, power converter and the power losses. Details about the models implemented in MATLAB/Simulink and PowerFactory are also presented. The models have been validated against measurements using SYSLAB. Different control strategies of the VRB system for over voltage control were implemented and some simulation results have been presented.

In subchapter 6 is presented the modeling, simulation and validation of an office building model and its local voltage controller operating as an active load in the SYSLAB distribution system. The building is heated by 10 electrical heaters of 1 kW each which can be used as a controllable load in the system. The model contains two parts, a thermal model of the house and a voltage controller which is based on a thermostatic control for the building, so that when the temperature inside is below a certain set-point the heaters turn on and when the temperature is above another set-point the heaters turn off.

Subchapter 7 presents the conclusions regarding the findings in previously subchapters mentioned before.

2.2. Experimental Facilities of SYSLAB Research Laboratory

The SYSLAB is a laboratory for research and development in distributed control and smart grids with a high share of renewable energy production, placed in Roskilde-Denmark. Its experimental facility is a Wind/PV/Diesel Hybrid Mini-Grid with local storage and a novel control infrastructure. The facility is spread across three sites located several hundred meters apart, as can be seen in Fig. 2.1 [15].



Fig. 2.1. SYSLAB Risø's new laboratory for intelligent, active and distributed power systems.

It includes two wind turbines (10kW and 11kW), three PV-plants (one of around 8 kW and two of them of 10kW), a diesel gen-set (48kW/60kVA), an intelligent office building with controllable loads (20kW), a number of passive loads (75kW, 3*36kW), a Vanadium Battery of 15 kW/190 kWh and three containers, each with an EV battery pack and a bidirectional converter.

At each of the three sites there is a switchboard that allows the components installed at the site to be connected to either of two bus bars. The two bus bars at each site are connected to a crossbar switchboard allowing the flexible setup of the system(s) to be studied. The bus bars can be either connected to the national grid or can be part of an isolated system. It allows components and systems to be in grid connected operation, island operation, or operation in parallel with wind turbine or PV-plant, as can be seen in Fig. 2.2.

The components are all connected in one distributed control and measurement system that enables very flexible setup with respect to experimental configuration.

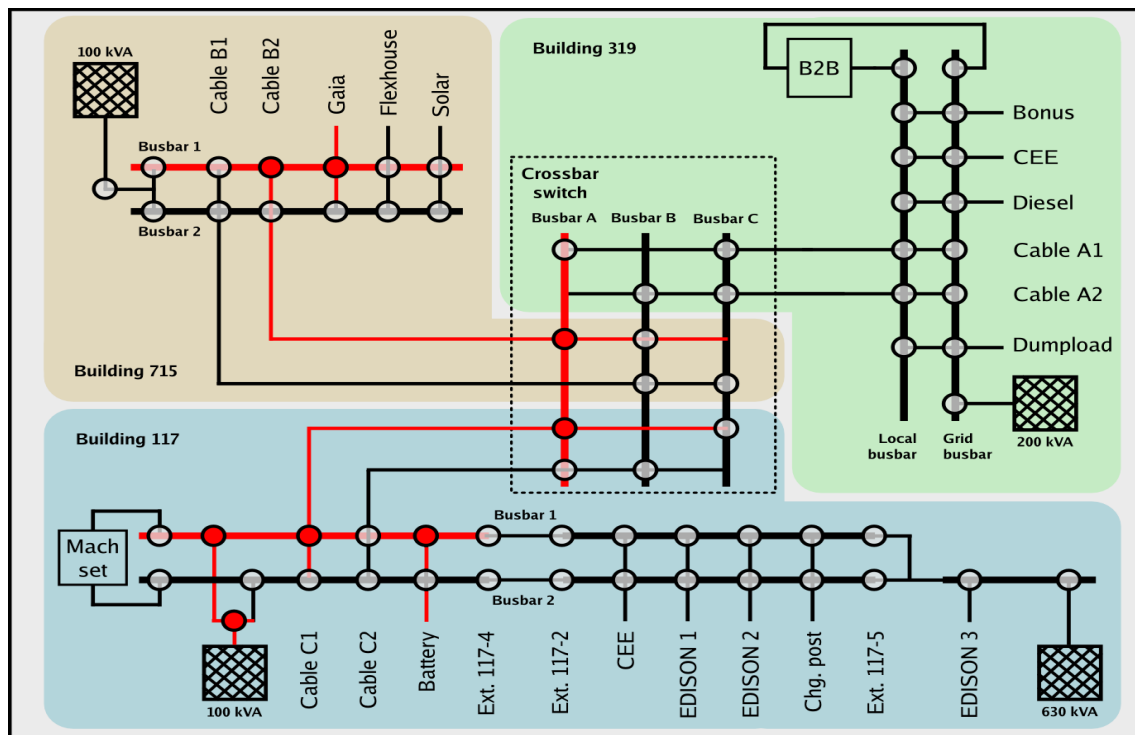


Fig. 2.2. Details about SYSLAB Micro-Grid architecture (plant components) in islanding mode.

All units on the grid – generators, loads, storage systems, switchgear – are automated and remote-controllable. Each unit is supervised locally by a dedicated controller node. The node design combines an industrial PC, data storage, measurement and I/O interfaces, backup power and an Ethernet switch inside a compact, portable container. All nodes are interconnected via Ethernet, in a flexible setup permitting on-line changes of topology and the simulation of communication faults.

The data acquisition and control system (hardware and software) is responsible for the supervision and control of the research platform for distributed intelligent energy systems with a high penetration of renewable energy. The supervisory software code is written in Java and is able to manage the data acquisition, processes the data and executes the control loop and outputs the control variables. The sensors outputs are connected to a signal conditioning board, which in turn is connected to the data acquisition (DAQ) board based on a PC (SCADA System).

Some loads in FlexHouse can be controlled by the central building controller which receives data and events from wireless switches and sensors. In one room, a small touch-screen user interface can be used to influence the controller policy (Fig. 2.3). Through its own grid control node, the building controller can get information on the status of the power grid, and adapt its control strategy accordingly. Active policies, measurement data and user settings can be communicated back to the grid.

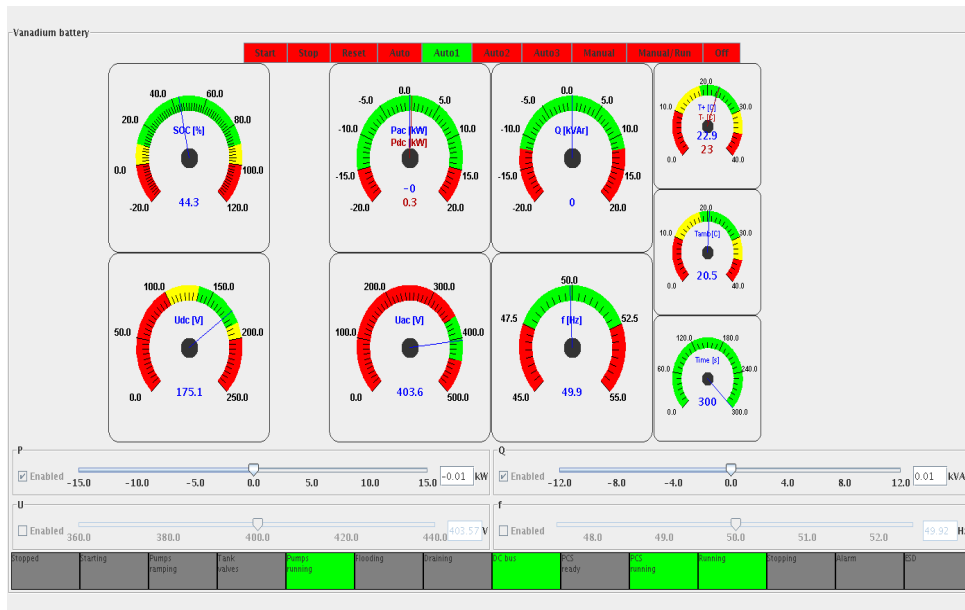


Fig. 2.3. Graphical user interface for control system.

A dedicated controller node is collocated with each of the components. The nodes combined an X86-based computer, local disk storage, analogue measurement hardware, field-bus interfaces, status display backup power and an Ethernet switch inside a portable rack.

2.3. SIMULATION MODELS DEVELOPED for PV Panels and SYSTEMS

2.3.1. Introduction

Power supplied from a PV array depends mostly on present atmospheric conditions such as: irradiation and temperature [3-6]. PV output voltage changes mainly with temperature while PV output current changes mainly with irradiation. Therefore in order to develop a very precise simulation model the local wind speed and the solar radiation incidence angle, in terms of the slope and surface azimuth, should also be considered [4-10].

In order to determine the incident radiation on a surface of any orientation it is necessary to evaluate the ratio of incident radiation on the tilted surface to that on a horizontal surface considering beam, sky diffuse and ground reflected radiation separately [16-19].

2.3.2. Mathematical Modeling, Implementation and Validation of a Polycrystalline PV panel using MATLAB/Simulink

The electrical power available from a PV device can be modeled using an equivalent circuit. This circuit could include a series resistance and a diode in parallel with a shunt resistance. The circuit can be used either for an individual cell, for a module consisting of several cells or for an array consisting of several modules [4, 7, 14, 20-22, 27-28].

A) Equivalent circuit, fundamental parameters and PV characteristics

To be able to develop an accurate PV panel model it is necessary to define the proper equivalent circuit. A solar cell is usually represented by an electrical equivalent one-diode model.

The model used in this report is a single diode model for PV cells described by a simple exponential function (1), as it is shown in Fig. 2.4 [4-7, 23-28]. The model contains a current source, one diode and a series resistance.

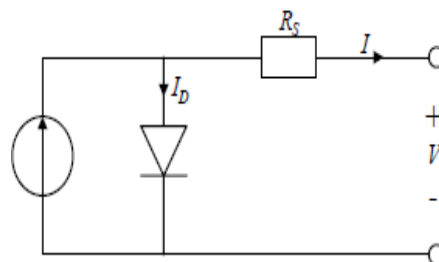


Fig. 2.4. Equivalent circuit of a PV cell with a single diode and a series resistance model.

The double diode model is considered, by many researchers, to be more accurate than the single diode model; the latter one is blamed for being imprecise particularly at low irradiance levels. However, it has been found out that when it was used for modeling the behavior of many interconnected modules, the single diode model is preferred by many of the authors in the literature. [20-22]

The general current-voltage (I-V) characteristic (relationship) of a PV panel based on the single exponential model, at a fixed cell temperature and solar radiation, is described by (2.1):

$$I = I_{sc} - I_0 \cdot \left(e^{(V+I \cdot R_s)/n_s \cdot V_T} - 1 \right) \quad (2.1)$$

In which I_{sc} represents the short-circuit or photo generated current, I_0 – dark saturation current, R_s – panel series resistance, n_s are the number of cells and V_T represents the junction thermal voltage expressed by:

$$V_T = \frac{K_B \cdot T_c \cdot A}{q} \quad (2.2)$$

Where K_B – the Boltzmann’s constant, q – the charge of the electron, A – diode ideality factor and T_c is the absolute cell temperature.

A real solar cell can be characterized by the following **fundamental parameters**, which are also sketched in Fig. 2.5:

(a) Short circuit current: I_{sc} . It is the greatest value of the current generated by a cell. It is produced under short circuit conditions: $V=0$.

(b) Open circuit voltage corresponds to the voltage drop across the diode (p-n junction), when it is traversed by the photocurrent I_{sc} (namely $I_D=I_{sc}$), namely when the generated current is $I=0$. It reflects the voltage of the cell in the night and it can be mathematically expressed as:

$$V_{oc} = \frac{K_B T_c A}{q} \ln \left(\frac{I_{sc}}{I_0} \right) = V_T \ln \left(\frac{I_{sc}}{I_0} \right) \quad (2.3)$$

(c) Maximum power point is the operating point, $A (V_{max}, I_{max})$ in Fig. 2, at which the power dissipated in the resistive load is maximum: $P_{max}=I_{max} U_{max}$.

(d) Maximum efficiency is the ratio between the maximum power and the incident light power:

$$\eta = \frac{P_{max}}{P_{in}} = \frac{I_{max} V_{max}}{A G_a} \quad (2.4)$$

Where G_a is the ambient irradiation and A is the cell area.

(e) Fill factor is the ratio of the maximum power that can be delivered to the load and the product of I_{sc} and V_{oc} :

$$FF = \frac{P_{max}}{V_{oc} I_{sc}} = \frac{V_{max} I_{max}}{V_{oc} I_{sc}} \quad (2.5)$$

The fill factor is a measure of the real I-V characteristic. Its value is higher than 0.7 for good cells (FF=0.737 in our models). The fill factor diminishes as the cell temperature is increased [6-7].

Fig. 2.5 also shows the I-V characteristics of the solar cell for a certain ambient irradiation and a certain/fixed cell temperature. A sign convention is used which takes as positive the current generated by the cell when the sun is shining and a positive voltage is applied on the cell’s terminals.

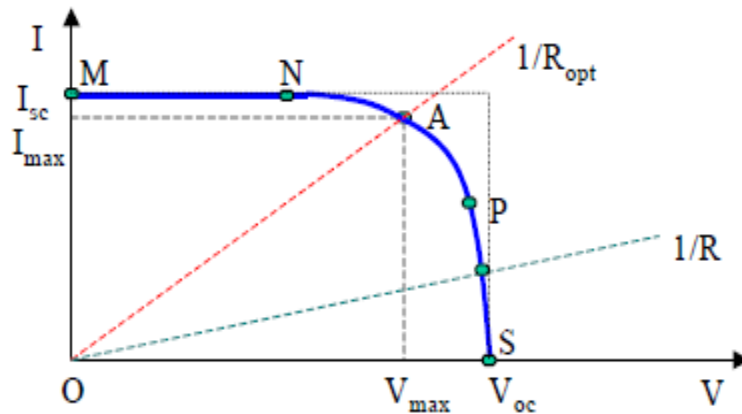


Fig. 2.5. A typical current-voltage curve for a solar cell [7].

B) Determination of the parameters from datasheet values

Manufacturers typically provide only limited operational data for photovoltaic panels. These data are available only at standard rating conditions, for which the irradiance is 1000 W/m^2 and the cell temperature is 25°C , except for the nominal operation conditions (NOCT) which is determined at 800 W/m^2 and an ambient temperature of 20°C .

A list with input parameters contains the values from the panel datasheet is presented in Table 2.1:

Table 2.1: Operational data for PV panels

Parameter name	Measurement unit	Description
for STC – solar irradiance (G_a)= 1000 W/m^2 , cell temperature(T_c)= 25°C , wind speed 1 m/s		
P_{mpp}	W	Rated output power
V_{mpp}	V	Nominal voltage
I_{mpp}	A	Nominal current
$V_{\text{oc}25}$	V	Open circuit voltage
$I_{\text{sc}25}$	A	Short circuit current
$\alpha (P_{\text{mpp}})$	$\%/^\circ\text{C}$	Temperature coefficient for change in (P_{mpp})
$\beta (I_{\text{sc}})$	$\%/^\circ\text{C}$	Temperature coefficient for change in (I_{sc})
$\chi (V_{\text{oc}})$	$\%/^\circ\text{C}$	Temperature coefficient for change in (U_{oc})
$\delta (I_{\text{mpp}})$	$\%/^\circ\text{C}$	Temperature coefficient for change in (I_{mpp})
$\varepsilon (V_{\text{mpp}})$	$\%/^\circ\text{C}$	Temperature coefficient for change in (U_{mpp})

$$\begin{aligned}
I_{sc} &= I_{sc25} \cdot (1 + \beta \cdot \Delta T) \\
V_{oc} &= V_{oc25} \cdot (1 + \chi \cdot \Delta T) \\
\Delta T &= T_c - T_a
\end{aligned}
\tag{2.10}$$

To complete the model it is also necessary to take into account the variation of the parameters with respect to irradiance.

The irradiance dependence is felt only by the short-circuit current:

$$I_{SC} = I_{SC25} \frac{G_a}{1000} \tag{2.11}$$

Model Implementation in MATLAB/Simulink

The model used to obtain the static characteristics of the PV panels has been implemented in MATLAB and Simulink. The equations from the previous section have been implemented, using function blocks from standard library of Simulink, in order to verify the model at different temperature and irradiance conditions [23-26].

The model developed for one panel, as a function of irradiance and absolute temperature, can be seen in Fig. 2.6. The model has as inputs: the solar irradiance (G), the cell temperature ($tempCell$) and the ambient temperature (T_{c25}) and it sweeps the voltage range of the PV panel in order to calculate the output current and power.

Function blocks were used to implement the I_{sc} and V_{oc} values (from eq. 2.11) and also for calculating the output current i (2.1).

For each different input, both the output current considering series resistance and the output current disregarding this parameter are computed. Because the mathematical equation of the output current is implicitly, the “algebraic constraint” block from standard toolbox of Simulink has been used in order for it to be solved.

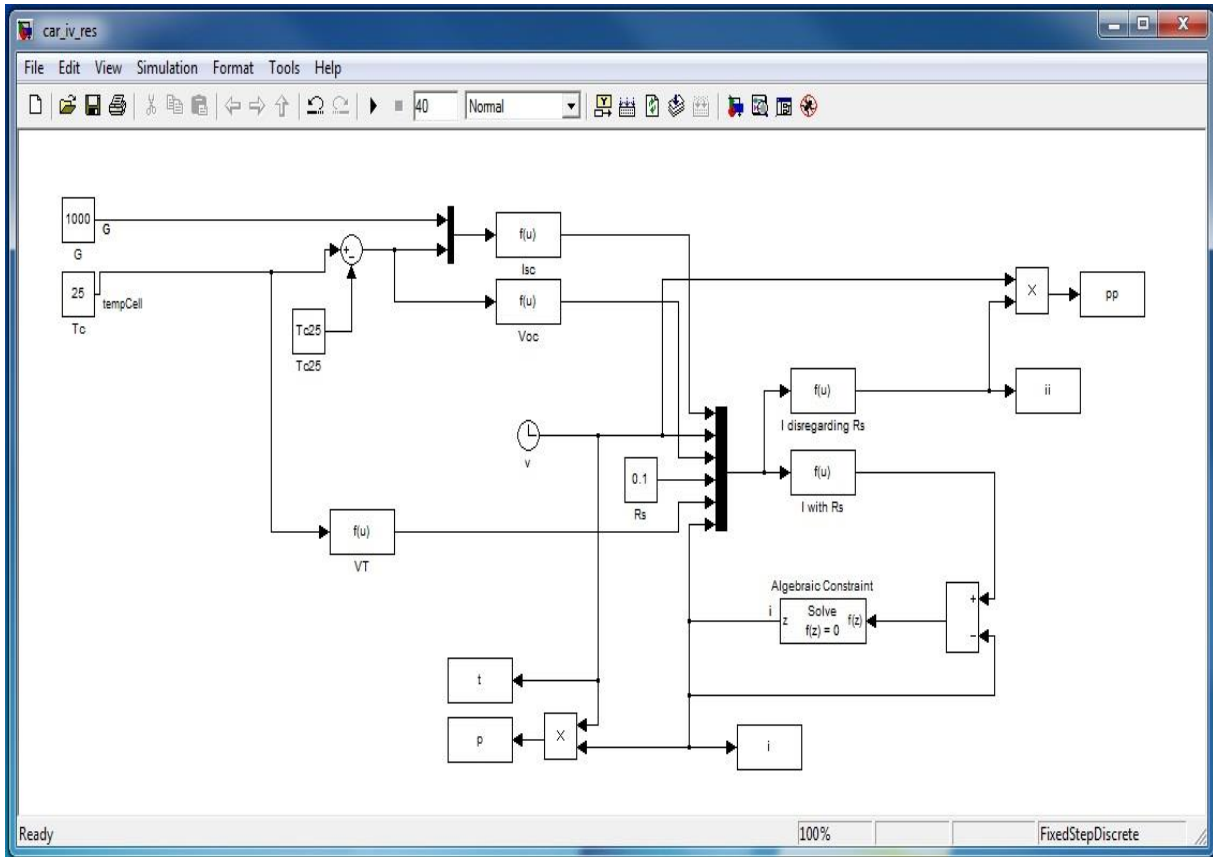
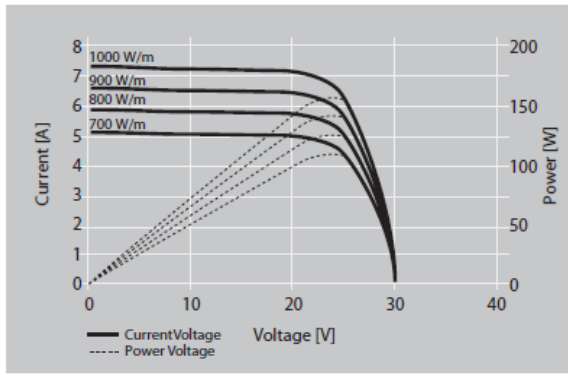


Fig. 2.6. Simulink model implementation for one panel with constant values as inputs.

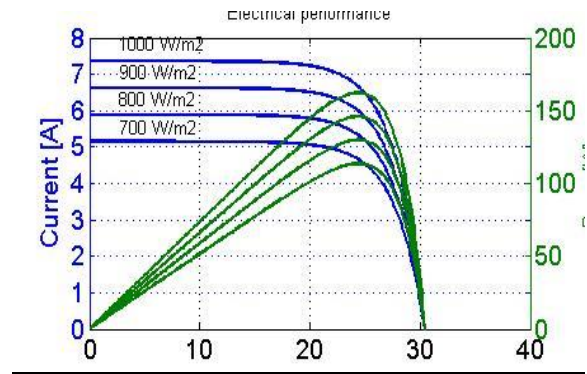
The parameters from the technical data sheet of the panels used in the simulation model are depicted in Appendix.

Validation of the simulation model for one PV panel

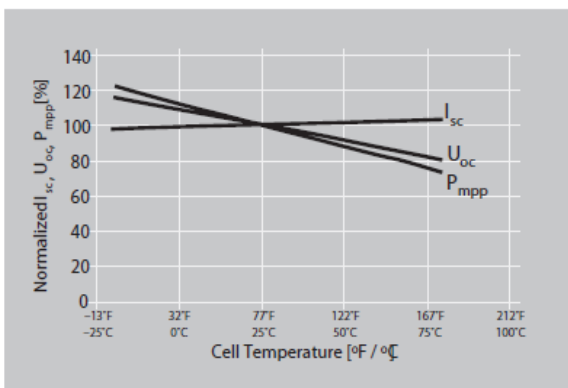
PV cells have nonlinear V-I and V-P characteristics. Its output voltage and power change according to temperature and irradiation. Fig. 2.7 shows the typical characteristics for a PV model and also a comparison between technical characteristics of the Schuco S 165-SP PV module from datasheet (appendix) and simulation results for one panel.



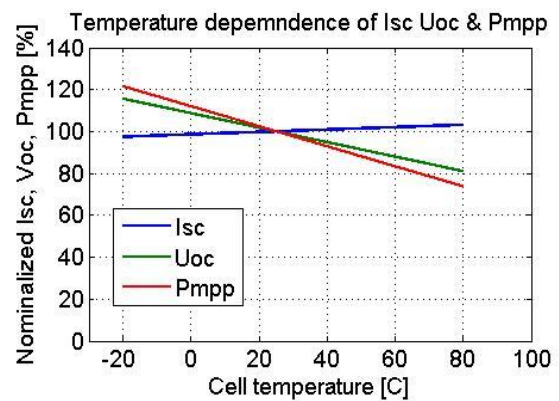
Electrical Performance



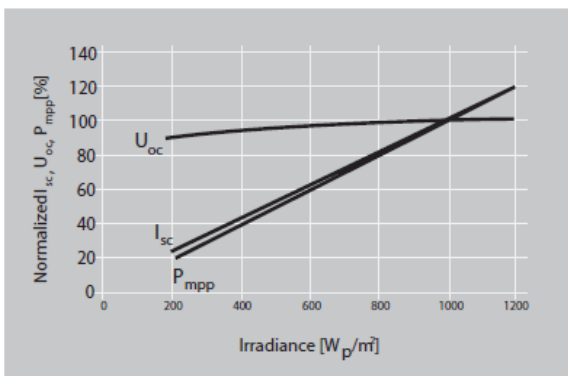
a)



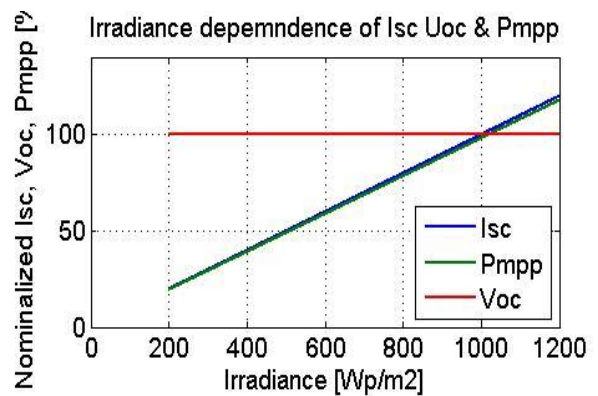
Temperature Dependence of I_{sc} , U_{oc} & P_{mpp}



b)



Irradiance Dependence of I_{sc} , U_{oc} & P_{mpp}



c)

Fig. 2.7. Comparison between PV technical characteristics from datasheet (on the left side) and simulation results for one panel.

These characteristics are computed for specific cell temperature and solar irradiance, under standard conditions (STC).

Fig. 2.7 a) shows a comparison between I-V and P-V characteristics obtained from the simulation model versus technical characteristics from datasheet. In Fig. 2.7 b) and 2.7 c) are shown the temperature dependence and irradiance dependence of the short-circuit current, the open circuit

voltage and the maximum power for the Schuko PV panels. As we can also be seen in Fig. 2.7 the PV output voltage changes mainly with the temperature, while the PV output current changes mainly with irradiation. Also, with constant irradiation specified, the PV output power decreases when the temperature rises and increases when the irradiation increases.

The electrical characteristics are plotted using results from the model simulation; meanwhile the other characteristics are implemented directly from equations described above.

2.3.3 Implementation and validation of the simulation model for PV Array

The stated problem was the development of a PV model for the solar array from RISO SYSLAB. The solar array consists of three solar panel strings: two strings of 18 Schuko 165-SP panels each and one string of 12 SOLEL SE100x panels [23-26, 29], and a Sunny Tripower 10000 TL inverter from SMA Solar Technology; this inverter enables the connection of two different types of solar panels on each of its two inputs. Each input having its own maximum power point tracking (MPPT) [31].

The SYSLAB facility disposes of two types of available measured data: ambient parameters (took from a weather station as can be seen in Fig. 2.8) and electrical parameters (taken from the DAQ board of the PV inverter).

The ambient data are the wind speed, the ambient temperature and the horizontal solar irradiance. The data read from the weather station is measured in different conditions as the PV array: the irradiance is measured on a horizontal plane and the station is positioned further and higher than the PV array. The electric data represent the DC current, voltage and power on each of the three PV input strings, measured directly by the inverter.



Fig. 2.8. Photo with PV panels and weather station at RISØ Campus.

The two main directions in obtaining a reliable model for a PV system have been developed. The first one contains the development, implementation and modeling of a model for the PV panels as a function of solar irradiance and cell temperature that returns current, voltage and power. The second direction was to obtain these values (solar irradiance and cell temperature) with the data read from the weather station. To point out the strong dependency on ambient conditions and to validate the simulation models a complex data processing subsystem model has also been developed, as can be seen in Fig. 2.9.

A) Implementation and Modeling of the PV array

Replacing equations (2.2), (2.6)-(2.8) in (2.1) and the equations (2.11)-(2.12) related to parameters variation with respect to temperature and irradiation and also introducing the number of panels in series and the number of strings in parallel we can obtain the current of the PV array. The I-V characteristics for a solar panel string depending on irradiance G_a and temperature T , for a four parameters model, have the following expressions [20-26]:

$$V = n_{ps}V_{OC} + n_{ps}n_sV_T \ln \left(1 - \frac{I}{n_{sp}I_{SC}25 \frac{G_a}{1000}} \right) \quad (2.12)$$

$$I = n_{sp}I_{SC} \left(1 - e^{\frac{v - n_{ps}V_{OC} + R_s I}{n_{ps}n_sV_T}} \right) \quad (2.13)$$

In which n_s is the no. of cells in series in one panel, n_{ps} – no. of panels in series and n_{sp} – no. of strings in parallel.

The output power of the panel can be calculated as:

$$P = V.I = V.I_{SC} \left(1 - e^{\frac{V - V_{OC}}{n_s V_T}} \right) \quad (2.14)$$

For obtaining the maximum power point of the panel, the condition (15) should be fulfilled:

$$\frac{dP}{dV} = 0 \quad (2.15)$$

That means:

$$\frac{dP}{dV} = n_{sp}I_{SC} \left[1 - e^{\frac{V - n_{ps}V_{OC} + R_s I}{n_{ps}n_sV_T}} - \frac{v}{n_{ps}n_sV_T} e^{\frac{v - n_{ps}V_{OC} + R_s I}{n_{ps}n_sV_T}} \right] = 0 \quad (2.16)$$

The PV array model is based on the equations (2.12-2.14). These equations represent the PV characteristics taking into account the no. of strings in parallel and the no. of panels in series.

Solving the equation (2.15) we can determine the maximum power point, which the inverter should track precisely, because in the PV systems there are no mechanical parts involved, and thus, the time constants are very small, being all electrical in nature (e.g. compared to wind turbine systems).

The simulation model, developed before and implemented in MATLAB/Simulink for one PV panel, has been improved and modified for a PV array with three strings. A block diagram of the complete model can be seen in Fig. 2.9.

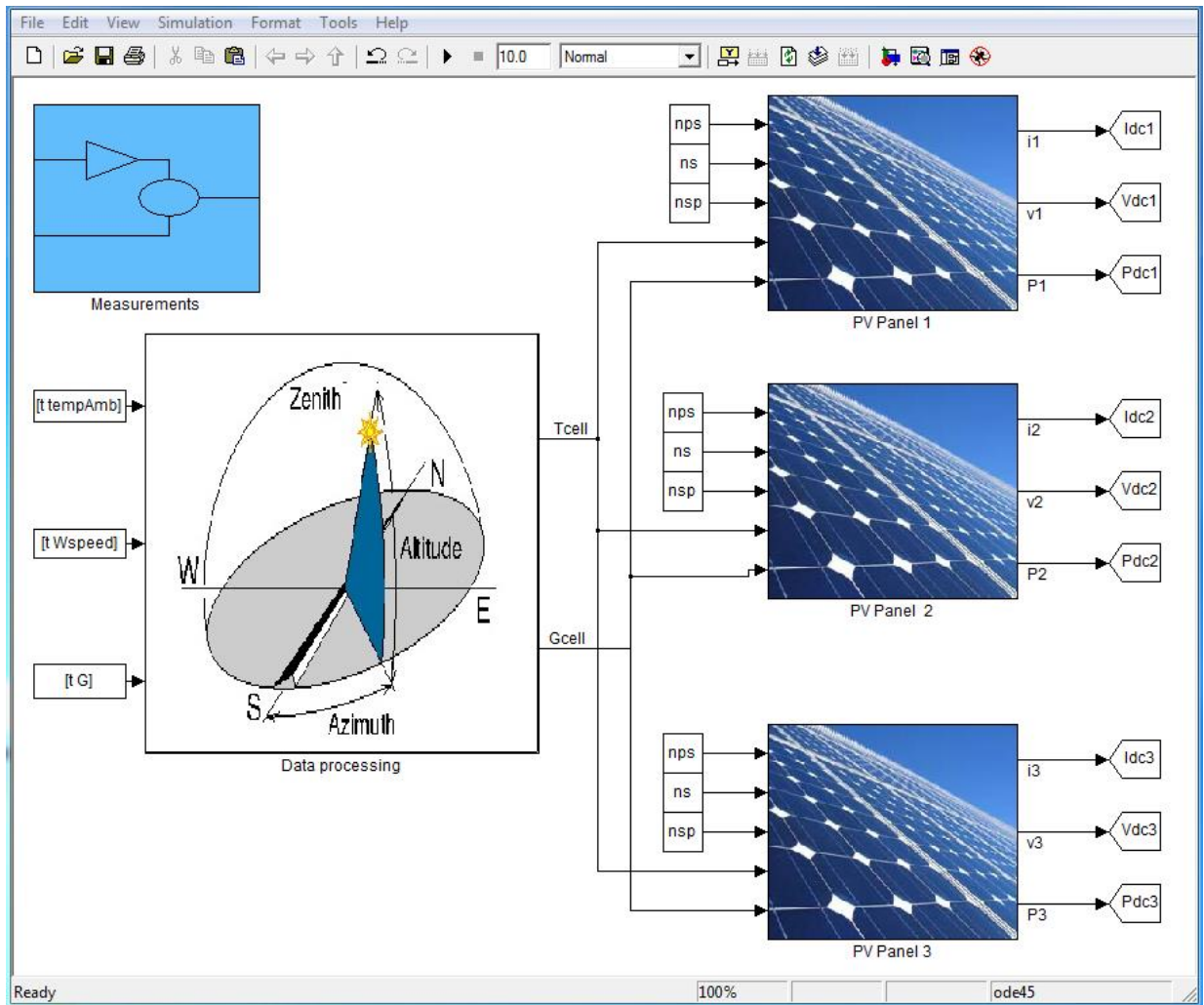


Fig. 2.9. Block diagram of the simulation model for PV array.

The simulation model, developed before for one panel (Fig. 2.10), has been changed adding more parameters as inputs, such as n_{ps} , n_{sp} , as it is shown in Fig. 2.11-2.12. Also, the irradiation, ambient temperature and wind speed are reading from a real data file measured by SCADA system as a function of time and then converted by *Data processing* subsystem in cell temperature and irradiation, parameters used as inputs to PV panels, as shown in Fig. 2.9.

Like in the previous model, regarding the static i-v characteristics on the PV panels, the “Algebraic Constraint” block was used, in this case for computing the voltage value “v” of the panel array using eq. (2.12). An additional assumption was made in this case because the equation also requires the current value, which is computed from the voltage value, in order to break the loop the current value is taken from the last simulation step. This assumption relies on the fact that the electric measurements have a time period of 1 seconds and the environment measurements have a 10 seconds; thus the system changes states each 10 seconds, and only once in this 10 seconds interval the model takes the current value from the previous state.

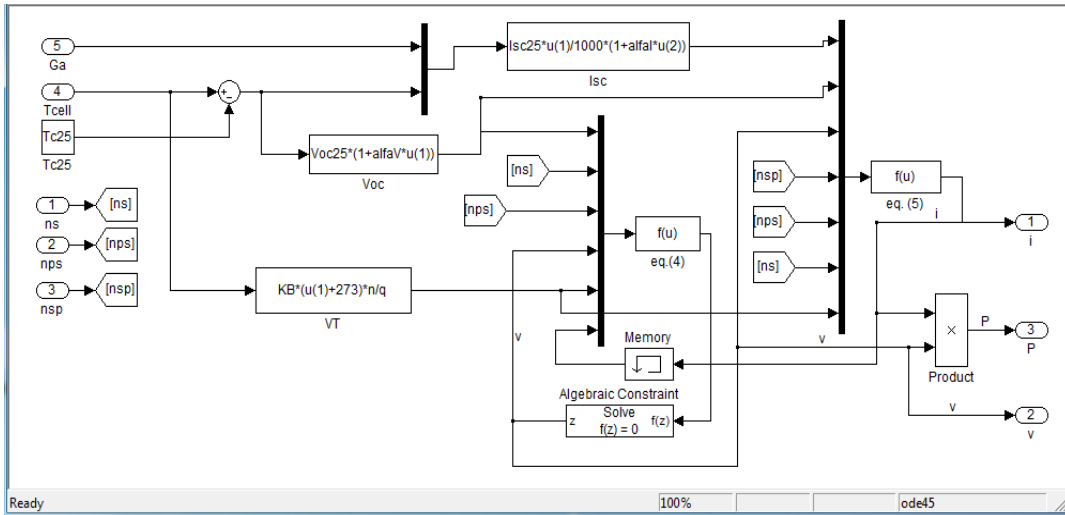
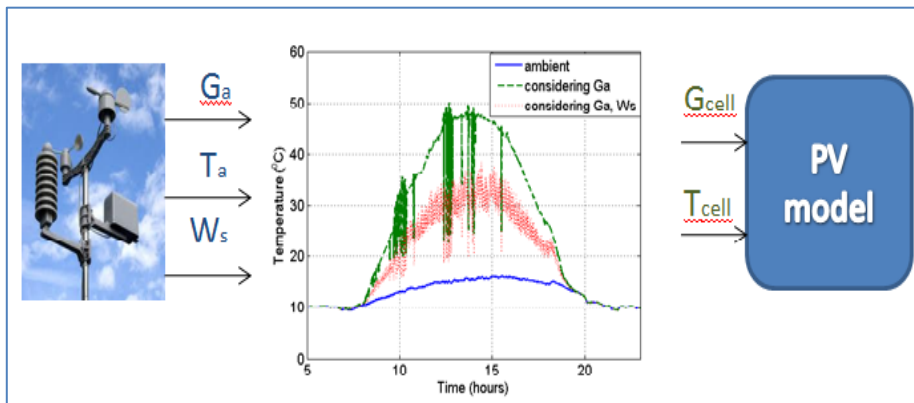
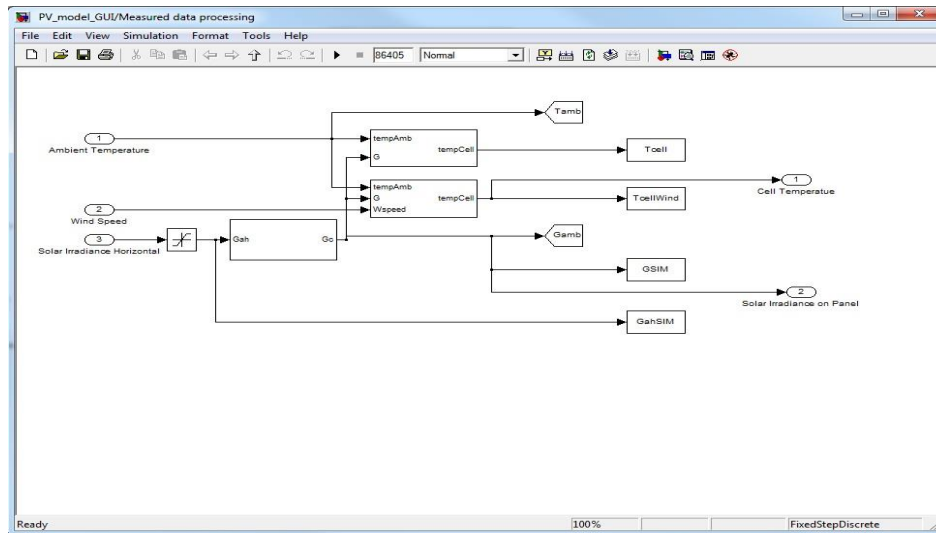


Fig 2.10. PV panel model with irradiance and cell temperature as a function of time.

Input values for the PV system model, measured from the weather station, have to be converted via additional functions, which will be describe in the next subchapter, in order to reproduce the values on the actual PV panel conditions. Figure 2.11 presents the details about the measured data processing subsystem considering the influence of solar irradiance and wind speed on the cell temperature and the block implementation in Simulink.



a)



b)

Fig. 2.11. a) Description of the PV system model input values and b) details about the inputs computation of the simulation model (data processing block in Fig. 2.9).

B) Dependence of the parameters on operating conditions (Input values measurement issues)

The cell temperature dependence

The cell temperature can be very different than the ambient temperature and it depends on the solar irradiation (G_a), ambient temperature (T_a) and also on the wind speed (W_s). Factors like solar irradiation act on increasing (T_c) and factors like the (W_s) have a cooling effect (which can also be seen in Fig. 2.12).

The simplest relation for the steady state operating cell temperature (T_c) and the ambient temperature (T_a), considering the influence of the solar irradiance (G_a) is:

$$T_c = T_a + kG_a \quad (2.17)$$

In this linear expression, which does not consider the wind, the constant k , known as the Ross coefficient [6], expresses the temperature dependence on the solar flux:

$$k = \frac{T_c - T_a}{G_a} \quad (2.18)$$

The values for k are usually in the range of 0.02÷0.04. The value for this coefficient can be obtained from the data sheet, considering the NOCT values:

$$k = \frac{NOCT - T_{aNOCT}}{G_{aNOCT}} \quad (2.19)$$

Usually, in low wind speed areas, the effect of the wind on the PV cells is negligible, the free convection and the radiation term having very small values [6].

If the PV panels are mounted in regions with high wind potential (as in our case), the wind speed must be considered because it has a large influence [6, 23-26]. The forced (wind) convection is large for high wind speeds and the cell temperature (T_c) function takes the following form:

$$T_c = T_a + \omega \left(\frac{0.32}{8.91 + 2 \frac{W_s}{0.67}} \right) G_a \tag{2.20}$$

Where ω is the mounting coefficient, which depends on the mounting conditions of the PV panels and W_s is the wind speed measured on horizontal plane; some values for ω are given in Table 3.

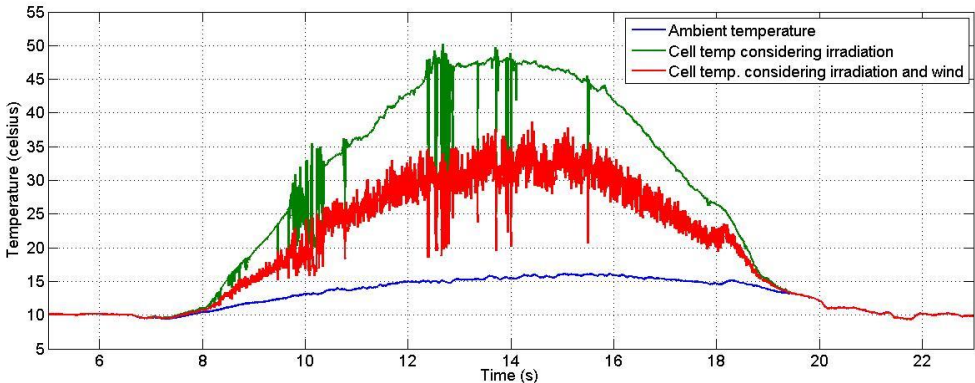
The wind that produces the cooling effect through forced convection is the wind parallel to the panel surface; that is why the transformation $W_{s_parallel} = W_s/0.67$ is used.

Table 3
Values of the mounting coefficient, ω , for various PV array mounting situations

PV array mounting type	ω
Free standing	1.0
Flat roof	1.2
Sloped roof	1.8 (1.0–2.7)
Façade integrated	2.4 (2.2–2.6)

The model uses a “Function” block to compute eq. (13), T_a , G_a , and W_s from the inputs subsystem in Fig. 2.11.

For a better understanding about the influence of solar irradiance and wind speed on the cell temperature, a graphical representation of these values is depicted in Fig. 2.12. For all the model simulations, the effect of both solar irradiance and wind speed are considered.



(a)

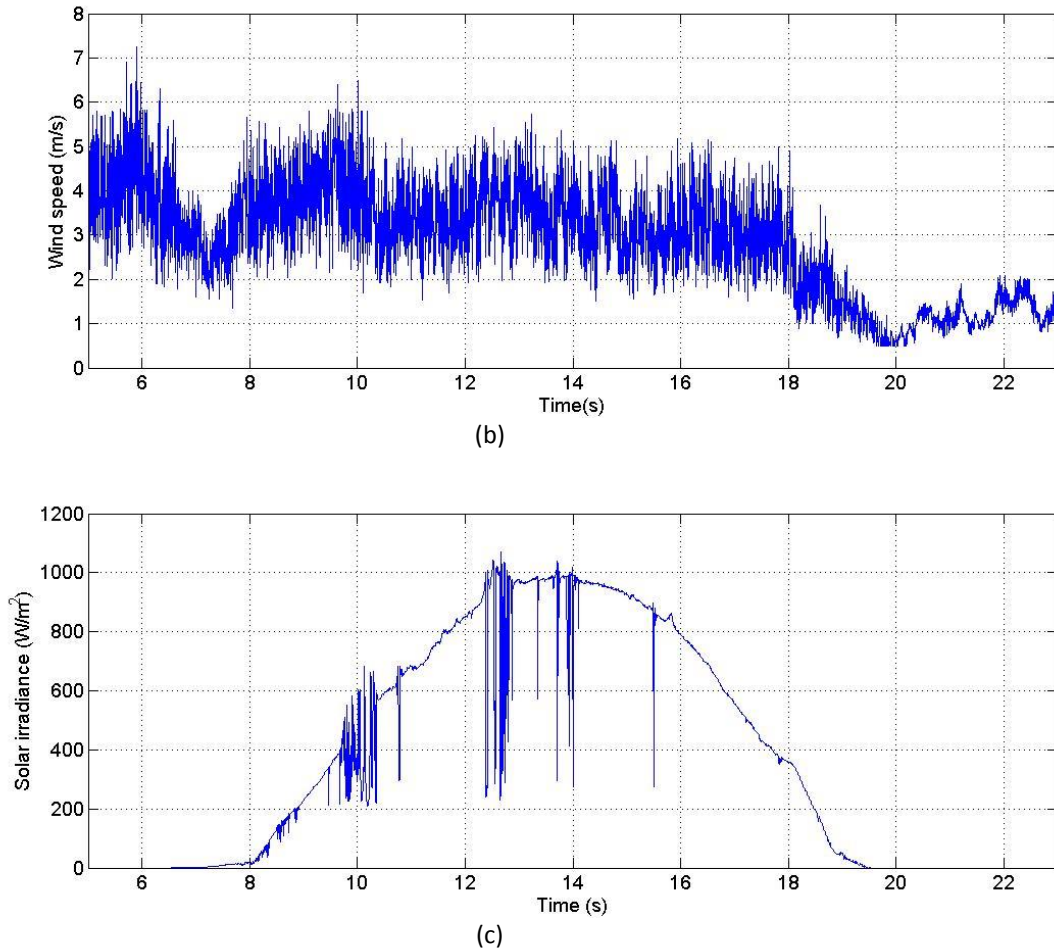


Fig. 2.12. a) Ambient factors influence over cell temperature, b) wind speed and c) solar irradiance on the PV panels as a function of time (h).

The solar irradiance dependence on the panel

In the case when the solar irradiation sensors are not placed on the actual panels and most often are taken from a weather station, like in our case, the solar irradiance is measured on the horizontal plane, in order to be more general and could be used for different applications and purposes.

For the solar irradiance translation, some other phenomenon had to be considered. The subsystem which solves this problem is presented in Fig. 2.13.

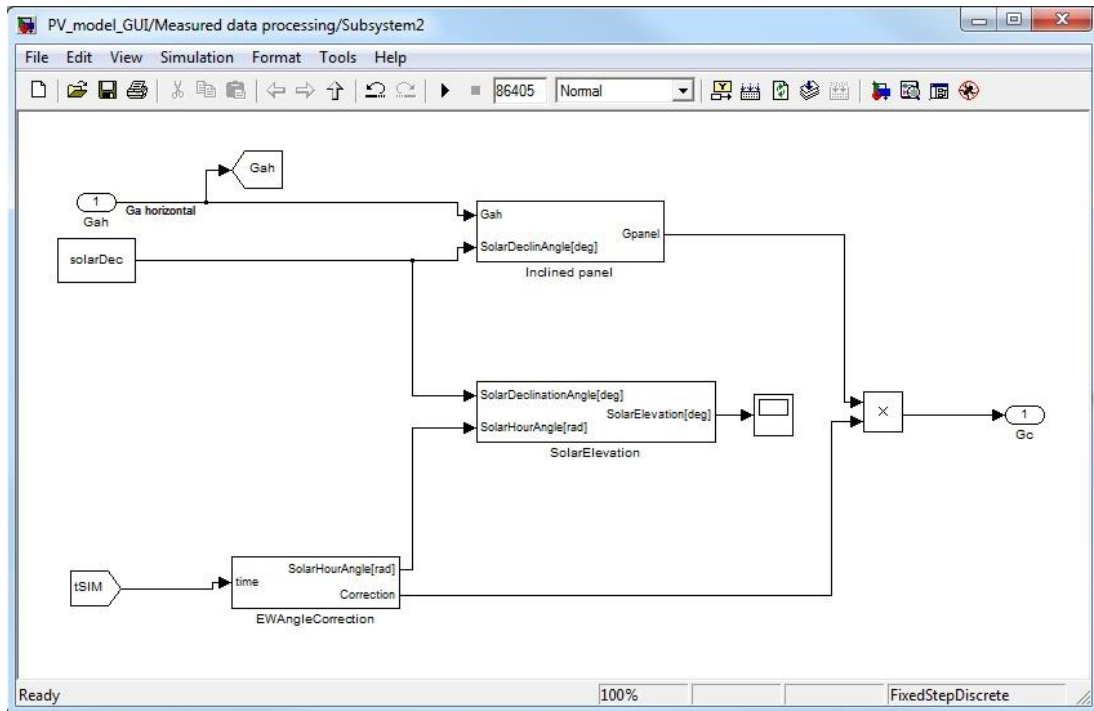


Fig. 2.13. Solar irradiance subsystem taking in consideration tilt angle and solar elevation.

Relationship between the horizontal and the tilted plane solar irradiance

An additional formula is necessary in order to translate this measured horizontal solar irradiance onto the tilted PV panel surface. For this reason, some new parameters have to be introduced into the model:

The declination angle is the angular position of the sun at solar noon with respect to the plane of the equator. Its value is given by:

$$\delta = 23.45 \sin \left(360 \frac{284+n}{365.25} \right) \quad (2.21)$$

Where 23.45 is the Tropic of Cancer latitude, the days are numbered from the spring equinox (day 81) and using the fact that *sin* is a periodic function, 365-81=284.

The relation between solar irradiance on horizontal plane and the solar irradiance on a tilted panel, facing south is:

$$G_{panel} = \frac{G_{horiz} \sin(\alpha+\beta)}{\sin \alpha} \quad (2.22)$$

In which $\alpha = 90-\phi+\delta$, β – panel tilt angle and ϕ represents the location latitude.

From this equation it is clear that the ratio between the solar irradiance on the PV panel and the one on the horizontal changes during the year, as the earth orbits the sun and the declination angle changes with every day.

Figure 2.14 shows the implementation of the tilt angle subsystem using eq. (2.21) and (2.22).

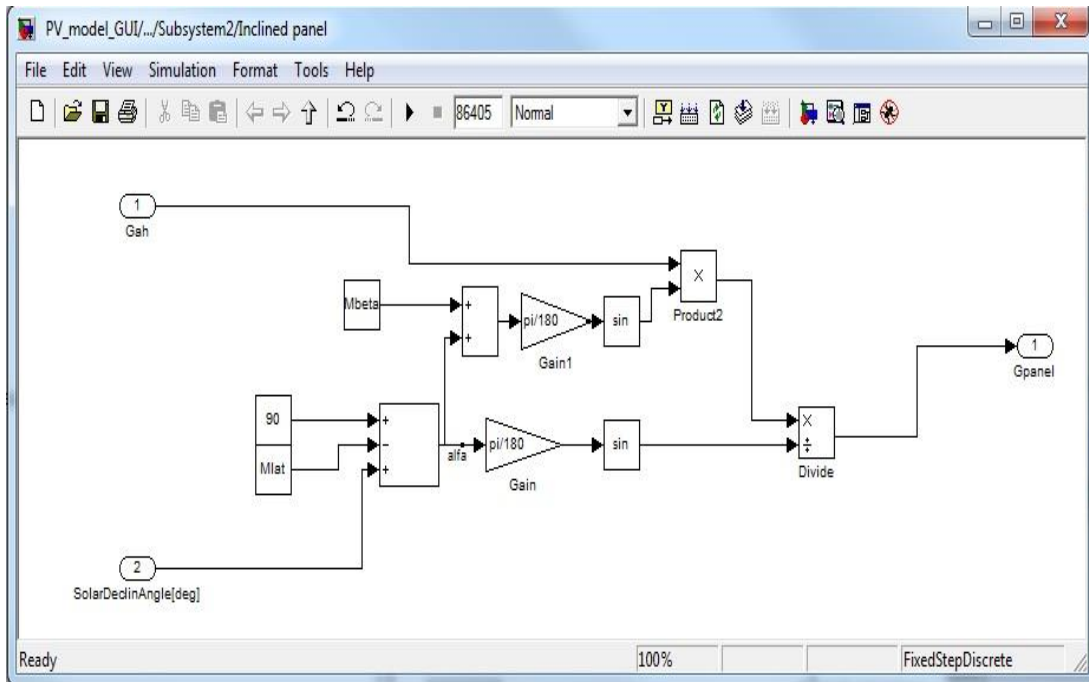


Fig. 2.14. The subsystem block which implement the relationship between the horizontal and the tilted plane solar irradiance angle to obtain the irradiation on the PV panel's surface.

Solar irradiance on tilted and non facing south PV panels

There is an influence on the output power and output power evolution during the day regarding the facing of the PV panels. If they are mounted on the E-W axis, facing directly south, the maximum output power will be at precisely solar noon, when the direct solar beam radiation is at its peak, and the solar azimuth angle is zero. As the panels are deviated from the E-W axis, the output power presents a time characteristic shifted from the time representation of the solar irradiance measured on a horizontal or facing south PV panel.

They present different sunrises, different sunsets and different solar noon. Those points, however, have the same lag in time. For example, if the panel deviation from the E-W axis is of 15° to west, on the deviated panel the sunrise, noon, and sunset will be one hour late that on the one facing south [3, 19].

This phenomenon is clear when the data from the electrical measurements are compared with the results from the model, considering the PV panels on the E-W axis as shown in Fig. 2.15.

The events that appear in Fig. 2.15, like shadows that translate in drop of current / power are synchronized both in the measurement and in the simulation. However the response in amplitude has a different wave form, the one from the simulation has a delay in time of around 50 minutes.

This is due to the deviation of the PV panels from SYSLAB with around 14 degrees to the west, like shown in Fig. 2.15, from National Oceanic & Atmospheric Administration, U.S. Department of Commerce [18].

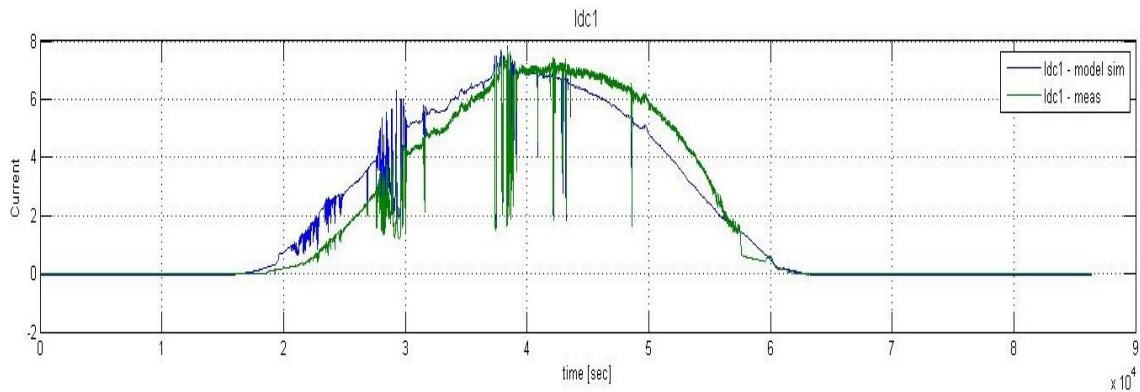


Fig. 2.15. Comparison between measurements and simulations for DC current to point out the solar irradiation effect on tilted PV panels.

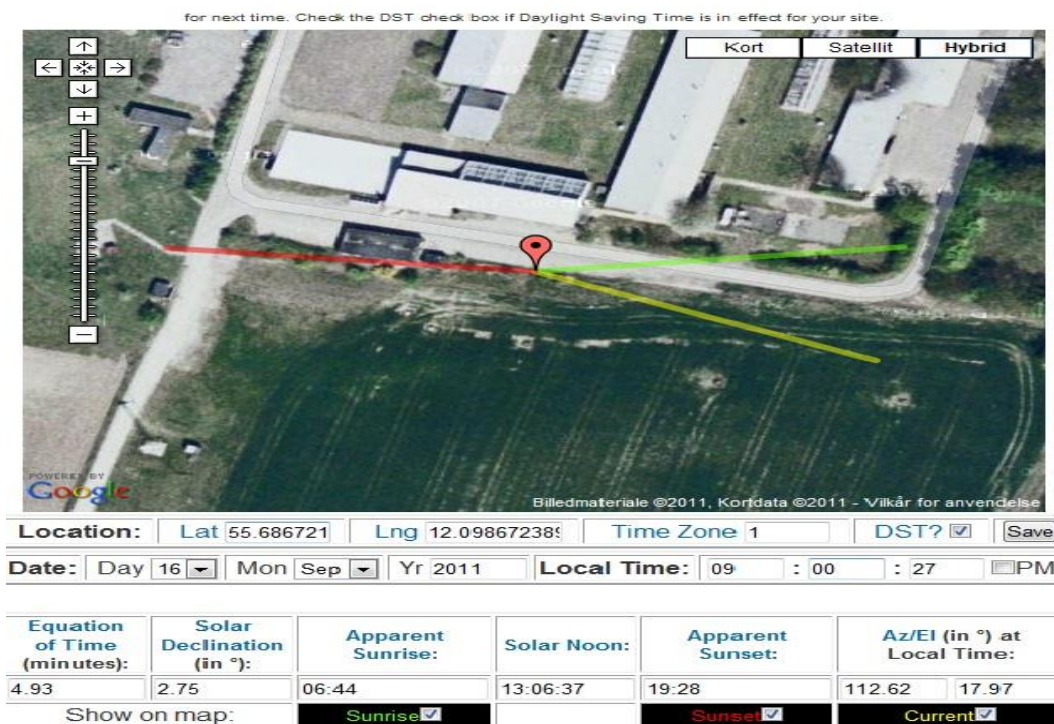


Fig. 2.16. PV panels placement related to solar noon, apparent sunset and sunrise.

In order to translate the horizontally measured solar irradiance on the actual PV panel, some notions have to be understood:

Solar hour angle – the geometrical angle between the sun’s sky position projected on the ground in each moment of the day and the projection at solar noon; each hour, the sun travels 15° on the sky. It has a negative value before solar noon, zero at solar noon and positive after, as can be seen in Fig. 2.23.

$$SolarHourAngle = 15^\circ(SolarNoon - T) \quad (2.23)$$

Equation of time is an astronomical term accounting for changes in the time of solar noon for a given location over the course of a year. Earth's elliptical orbit and Kepler's law of equal areas in equal times are the culprits behind this phenomenon.

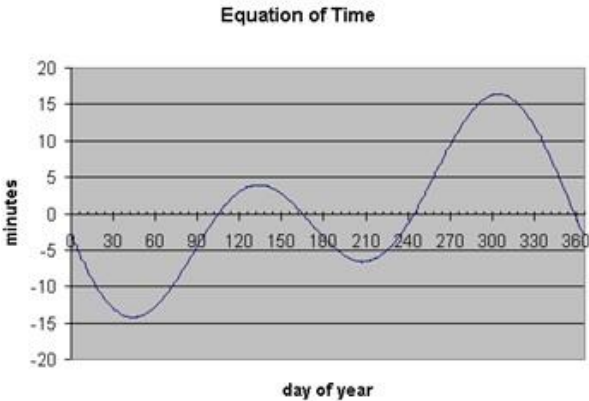


Fig. 2.17. Equation of time [18].

The deviation of 15 minutes has an equivalent of 4° deviation of the panels from the EW axis.

This curve is approximated with a polynomial function (2.24) and implemented in Simulink as it is shown in Fig. 2.17:

$$\begin{aligned}
 MM &= 2 * \pi * Mday / 365.25; \\
 \Delta T_{Noon} &= (-7.657 * \sin(MM) + 9.862 * \sin(2 * MM + 3.599)) * 60; \\
 (2.24) \quad \text{SolarNoon} &= 12 + \Delta T_{Noon}
 \end{aligned}$$

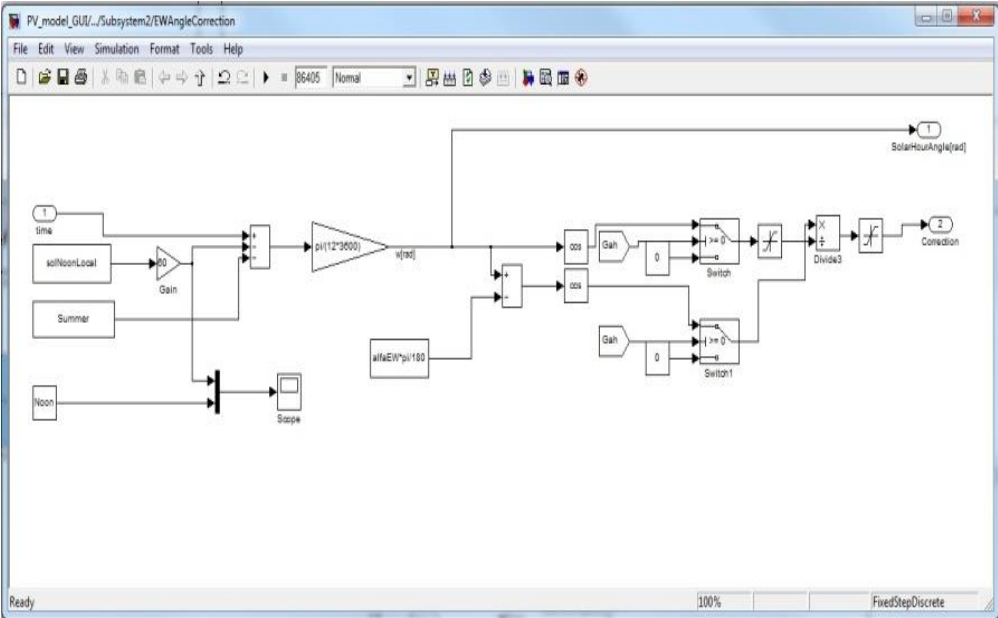


Fig. 2.18. Simulink implementation of the equation of time using a polynomial function.

The solar radiation on the surface on the PV panels I_c , disregarding reflected irradiance, has the time dependent function:

$$G_c = G_{b,h} \frac{\cos i}{\sin \alpha} \quad (2.25)$$

Where i is the incident angle of the direct radiation on the tilted surface, α – solar altitude angle and $\cos i$ can be express as:

$$\cos i = \cos \alpha \cos(\alpha_s - \alpha_w) \sin \beta + \sin \alpha \cos \beta \quad (2.26)$$

Where α_s is the solar azimuth angle, α_w is the azimuth angle and β is the tilt angle of the panels.

$$\sin \alpha = \sin L \sin \delta_s + \cos L \cos \delta_s \cos h_s \quad (2.27)$$

L is the latitude angle, δ_s is the solar declination and h_s is the solar hour angle.

Validation of the simulation model

In order to validate the simulation model for a PV system, developed in the last subchapter, and implemented in MATLAB/Simulink, and to point out the importance of considering the atmospheric conditions, such as irradiation, temperature and wind speed, and also the orientation and tilt angle of the panels, the simulations will be compared with experiments carried out using RISO experimental facility-SYSLAB.

In Fig. 2.19 are presented the simulation results versus measurements at different stages of the modeling. These Figures also shows the importance of several factors that have to be taken in consideration for obtaining a good accuracy of the simulation models.

In Fig. 2.19 a) is shown a comparison between measured and simulated output power (P_{DC}) for a time series of 1 day without considering the wind speed effect or any improvements. As can be seen the difference between both curves is very big that means the simulation model should be improved to fit the measurements.

Fig. 2.19 b) shows the same waveforms for output power of the panels considering the wind cooling effect, with the same peak values and the same changes in power due to shading effect in a synchronous manner. The simulation has a delay of around 50 minutes. This is the effect of the PV panels' orientation, which have a 13° deviation from the E-W axis (as was shown in Fig. 2.18).

Considering the tilt angle and panels' orientation, the influence of solar irradiance and wind speed on the cell temperature the measurements and simulations are almost identically, as can be seen in Fig. 2.19 c).

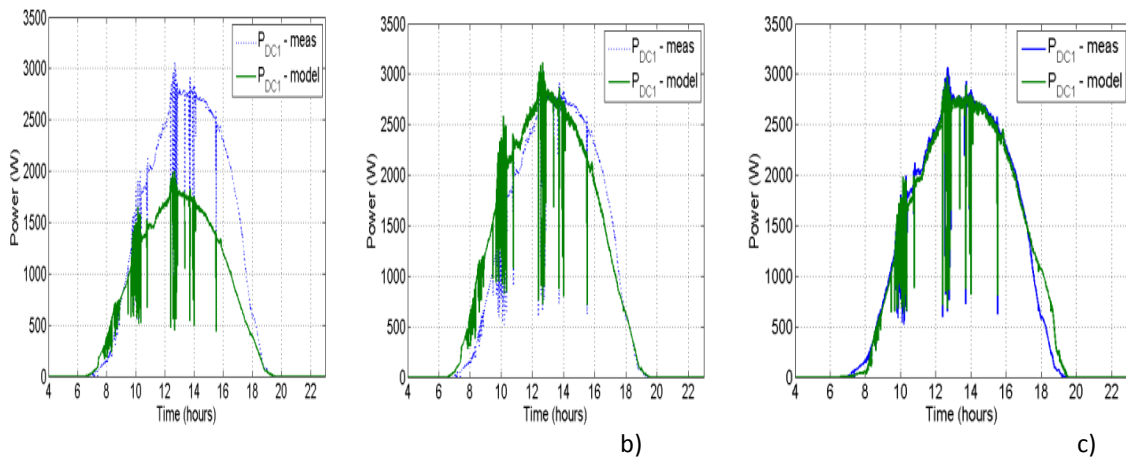


Fig. 2.19. Comparison between simulations and measurements of DC Power at different stages of the modeling.

2.3.3.3 Graphical user interface

A graphical user interface has also been developed in MATLAB/Simulink environment in order to test different types of PV panels and to facilitate the usage of the PV array model of SYSLAB infrastructure for different input data.

The first window, at the opening of the application, allows the possibility of choosing the day or the input data to run the simulation for.

The user can select the day from the PopUp bar. The application automatically displays the environment data selected from that day (Fig. 2.20). If the user chooses to press on with the application, the data are read and the simulation is started.

After the simulation has run, the results are accessible in the next Panels: “Power Output” and “Operation Char”.

In Fig. 2.21 and Fig. 2.22 are presented some simulation results versus measurements for the two types of panels (Schuko 165 and SOLEL 100x, respectively) already installed at RISØ campus.

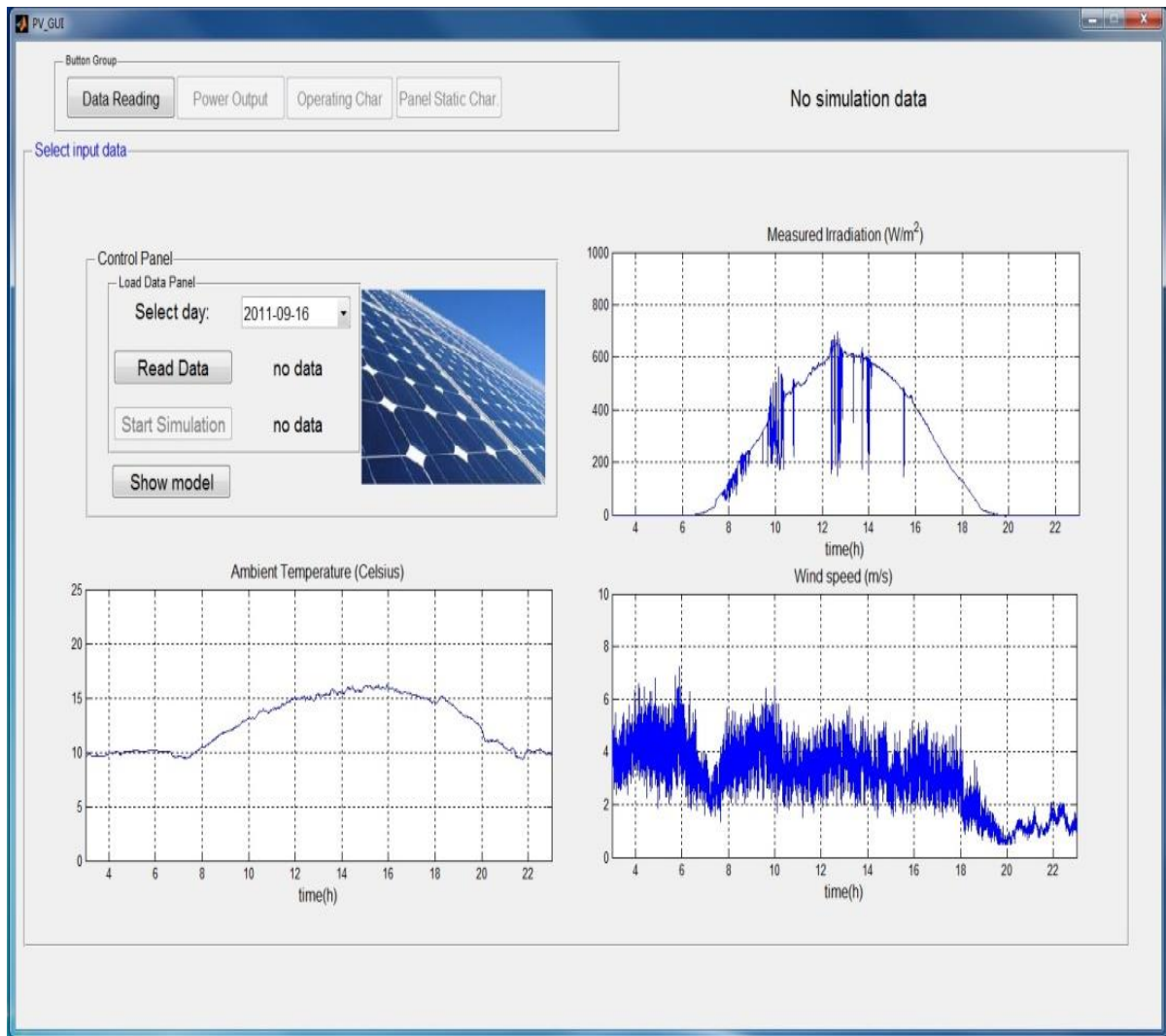


Fig. 2.20. GUI with data measured from weather station used as inputs for PV system simulation model.

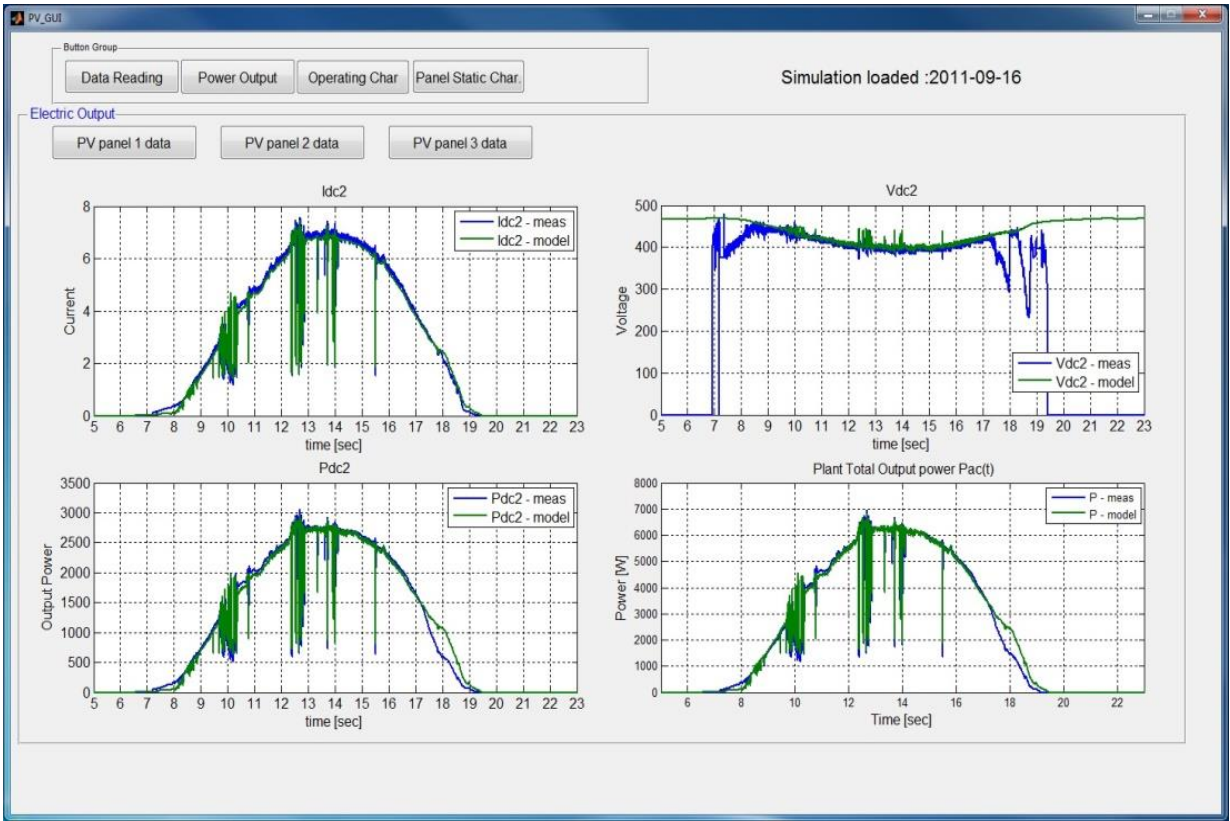


Fig. 2.21. DC current, voltage and power for Schuko165 PV panel and the output power of the inverter (P_{ac}) as a function of time for 24h.

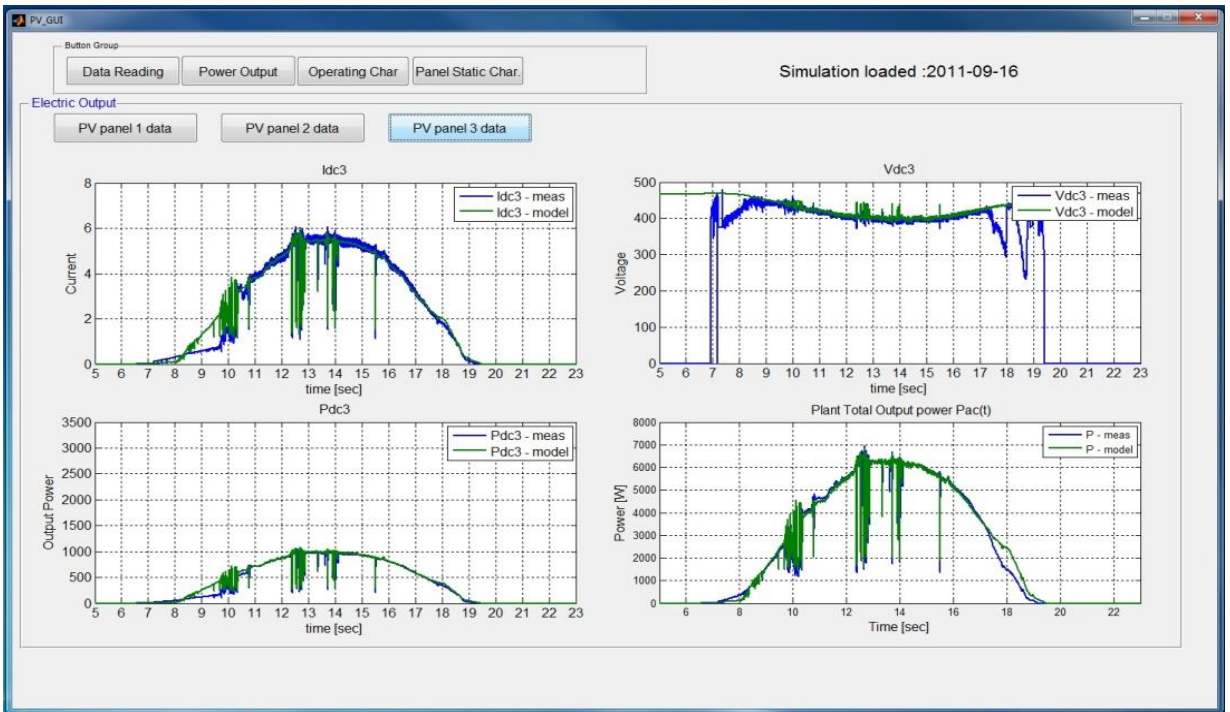


Fig. 2.22. DC current, voltage and power for SOLEL PV panel and the output power of the inverter (P_{ac}) as a function of time for one day.

Some other characteristics important for ensuring a proper model are the current-irradiance, current-voltage, and power-voltage characteristics. In Fig. 2.22, the simulation values are compared with the measurements and a good correspondence was found.

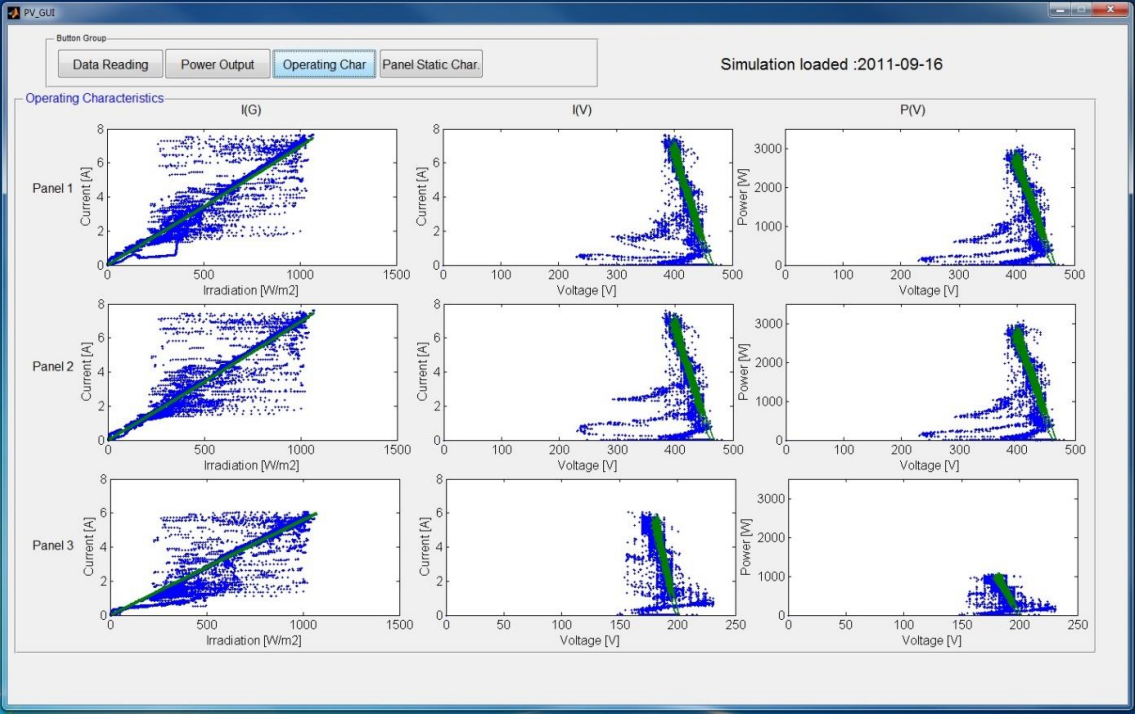


Fig. 2.23. Operating characteristics of the PV panels.

2.3.4 Simulation Model of PV System developed in DigSILENT PowerFactory for distribution networks

In the distribution network a high share of PV may require new approaches for voltage control as the power output of PV system can change rapidly if clouds pass very fast over the PV system. New control approaches may include active P/Q control from the PV system, changed design of the embedded distribution system control as well as active demand-side control.

Simulation models of a single inverter with PV panels are needed for many purposes, such as: Voltage studies with rather distributed sets of single inverter with PV panels, e.g. to determine temporary over voltage within a distribution network or within a PV power plant. Such a model typically only consist of up to 100 busses and requires a high level of details (High bandwidth $f > 10$ kHz);

Integration studies with up to 50,000 busses and $\sim 8,000$ generators. For this purpose simulation models of PV power plants should be rather simple (low bandwidth $f < 100$ Hz), but should reproduce the required behavior needed for the integration study.

Existing models are typically only developed for a single purpose, often focusing on a rather simple representation of a PV system.

The approach in this project follows a slightly different approach: Rather detailed simulation models of PV systems (single inverter/PV panel) will be developed and validated against measurements. For this purpose it is necessary to develop detailed functional

specifications which should be fulfilled by the simulation model and will be tested against specific measurements.

The aim is to use measurements for validation of the simulation models. The simple simulation models for a single inverter/PV model will be validated using the test facilities of the SYSLAB.

The key challenges are:

- Modeling of PV System and validation of the model;
- Modeling the variability of PV System on feeder level and its impact on voltage control;
- Validation of new voltage and protection control strategies for distribution networks;
- Development and validation of the simulation models;
- Integration of additional storage devices into the overall power system operation. The impact on feeders with both PV and controllable loads will be simulated and tested.

2.3.4.1. Description of the PV System Model Implementation

Computer models of power systems are widely used by power system utilities to study load flow, steady-state voltage stability and dynamic and transient behavior of power system.

For this project DigSILENT PowerFactory has been chosen because provides the ability to simulate load flow, RMS fluctuations and transient events in the same software environment. It provides a comprehensive library of models for electrical components in the power system [29].

The models of the PV System are built with standard components/blocks from DigSILENT library. The models of the PV model, DC-Link and controller of the Static Generator have also been implemented in the dynamic simulation language DSL of DigSILENT. DSL allows the user to implement specific models that are not standard in the DigSILENT library and thus to create own developed blocks either as modifications of existing models or as completely new models.

Fig. 2.24 shows the schematic structure of the model, developed for time-domain simulations where a DSL model is required, including Photovoltaic Model, DC-Link Model, PLL block and Static Generator (PV inverter) with its Controller. The PV system frame also contains the measurements blocks used as inputs for different components of the model. The Photovoltaic Model has as inputs irradiation, cell temperature and DC Voltage of the array. Cell temperature and irradiation are taken from a look-up table, obtained from MATLAB/Simulink model presented before, considering the orientation and tilt angle of the panels and the influence of the atmospheric parameters on the cell surface.

The PV System model is implemented in PowerFactory using block diagrams and the internal simulation language DSL [23-25].

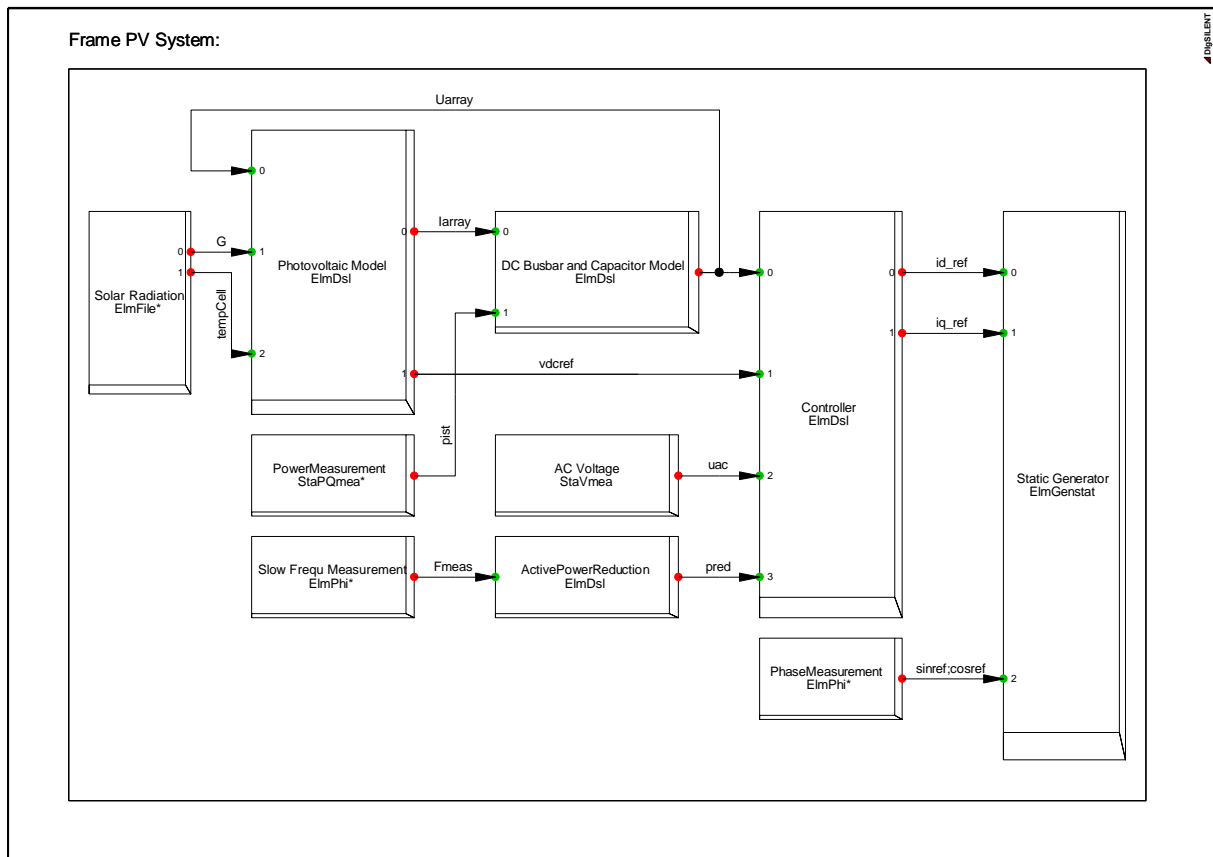


Fig. 2.24. Schematic block diagram of the PV System.

Photovoltaic Model

The PV array model is implemented in PowerFactory using block diagrams to define the PV module and the number of panels in series and the number of strings. The internal simulation language DSL was used to define the PV characteristics and equations, presented in the last subchapter and also implemented in MATLAB/Simulink, and to initialize the parameters and variables of the model.

The model has as inputs the voltage array, irradiation (G) and cell temperature ($tempCell$) and as outputs MPP of the current ($Iarray$) and voltage ($Vmpp_array$) for the PV array. To get the MPP values for I-V characteristics of the array two blocks references have been used.

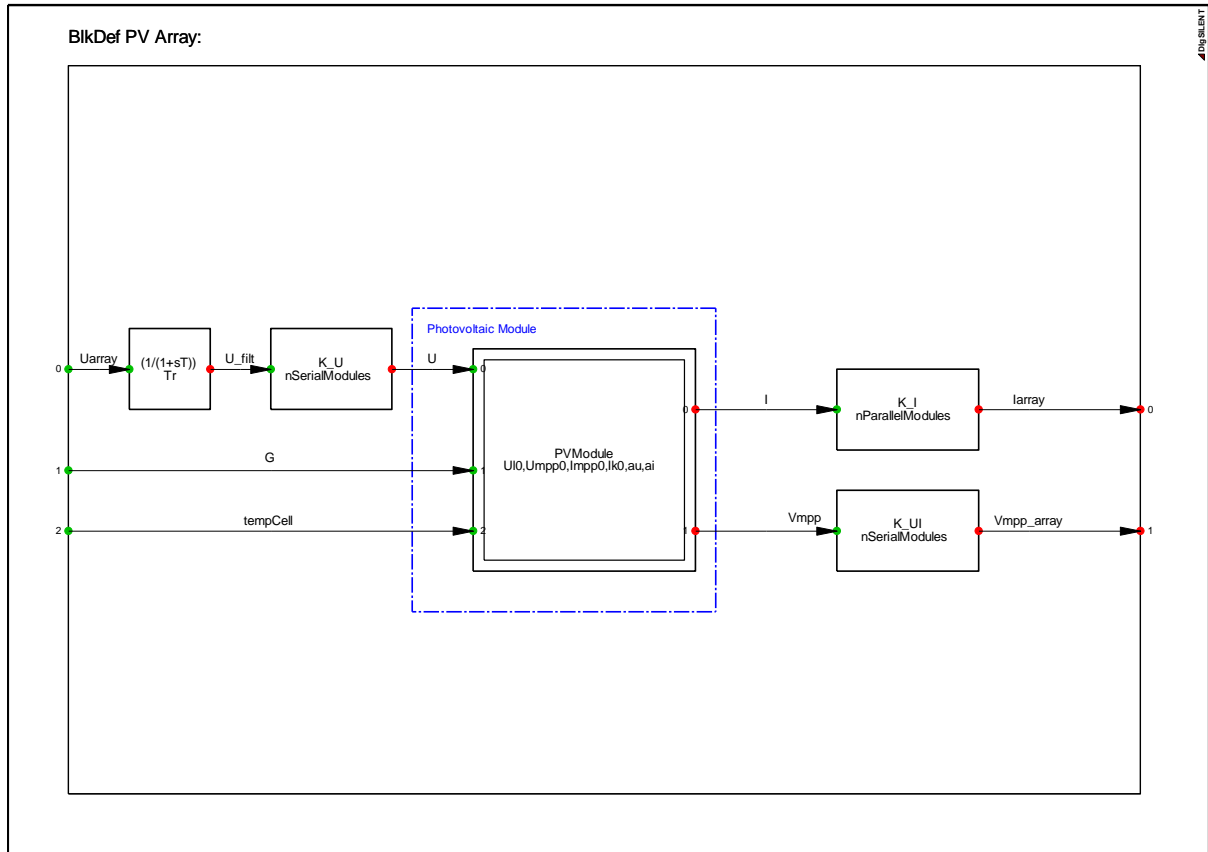


Fig. 2.25. PV array model implemented in PowerFactory.

The equations and variables define in DSL code for these models are presented in appendix A3.

DC-Link Model

The model for DC-Link has as inputs current, that comes from the PV model, and power and as output DC Voltage, which is the input of the PV inverter (Fig. 2.26). It represents the DC bus to which the PV array and the DC side of the inverter are connected. The current enters an integrator in order to calculate the voltage across the capacitor, which is the input of the inverter. The DSL code was also used to define the equation (2.28) and the state variable.

$$i(t) = C \cdot \frac{du_c(t)}{dt} \quad (2.28)$$

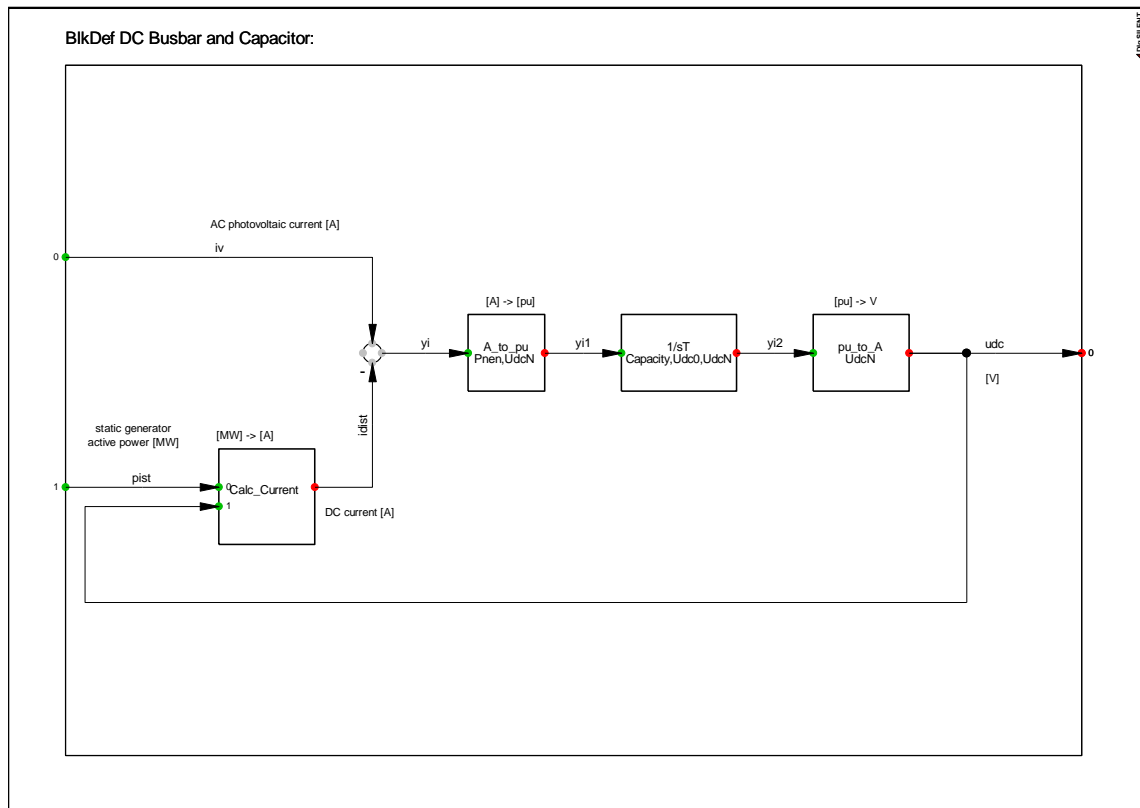


Fig. 2.26. DC Link Model implemented in PowerFactory.

Active and Reactive Power Control

The active power limitation (reduction) block is built using DSL code and uses the frequency deviation measurements to determine whether to trigger the bypass signal or not. If the bypass signal is triggered the frequency deviation is read and the corresponding reduced power output is produced. This slot represents one of the main requirements that the PV inverters should meet according to the GCs.

The output power controller refers to the ability of the generating plant to reduce/adjust its power output as required by the network operator or even disconnect the PV plant in order to avoid potential dangers regarding the stability of the system.

PQ controller is used to provide and limit the i_d and i_q currents used as inputs to the static generator model to control the active and reactive power of the PV generator. The controller also includes the additional capability of reactive power support control in case of voltage dips. The main objective of the reactive power control is to keep the voltage to a specific level by absorbing or inserting reactive power.

The currents are controlled with a build in current controller defined in PowerFactory library as follows:

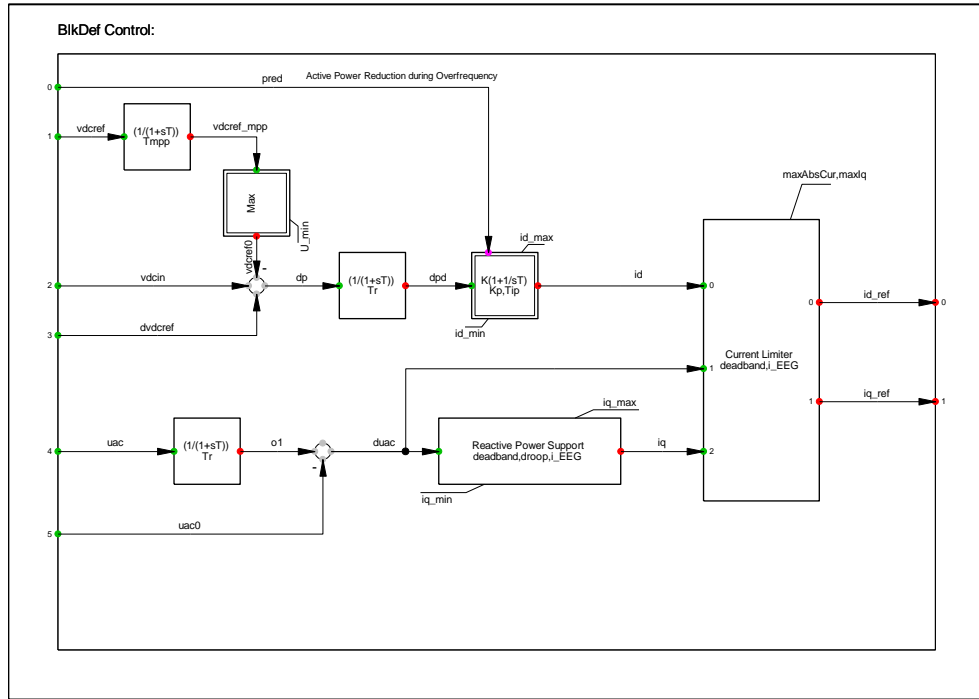


Fig. 2.29. P-Q controller for PV inverter.

Static Generator Model

The Static Generator is an easy to use model of any kind of static (no rotating) generators. Applications are PV Generators, Storage devices, wind generators etc.

For load flow analysis the local voltage controller could be set to three different modes: $\cos\phi$, V and droop. For RMS and EMT simulations the static generator supports two different models: current source and voltage source models.

In our case we use a current source model which has as inputs i_{d_ref} , i_{q_ref} coming from the controller and $\cos ref$ and $\sin ref$ signals from a PLL model.

The current source model is implemented as a voltage source with a controlled current and the current is controlled with a build in current controller. The following equations are used for RMS simulations [2.29]:

$$i_1 = (i_{d_ref} \cdot \cos ref - i_{q_ref} \cdot \sin ref) + j \cdot (i_{d_ref} \cdot \sin ref + i_{q_ref} \cdot \cos ref) \quad (2.29)$$

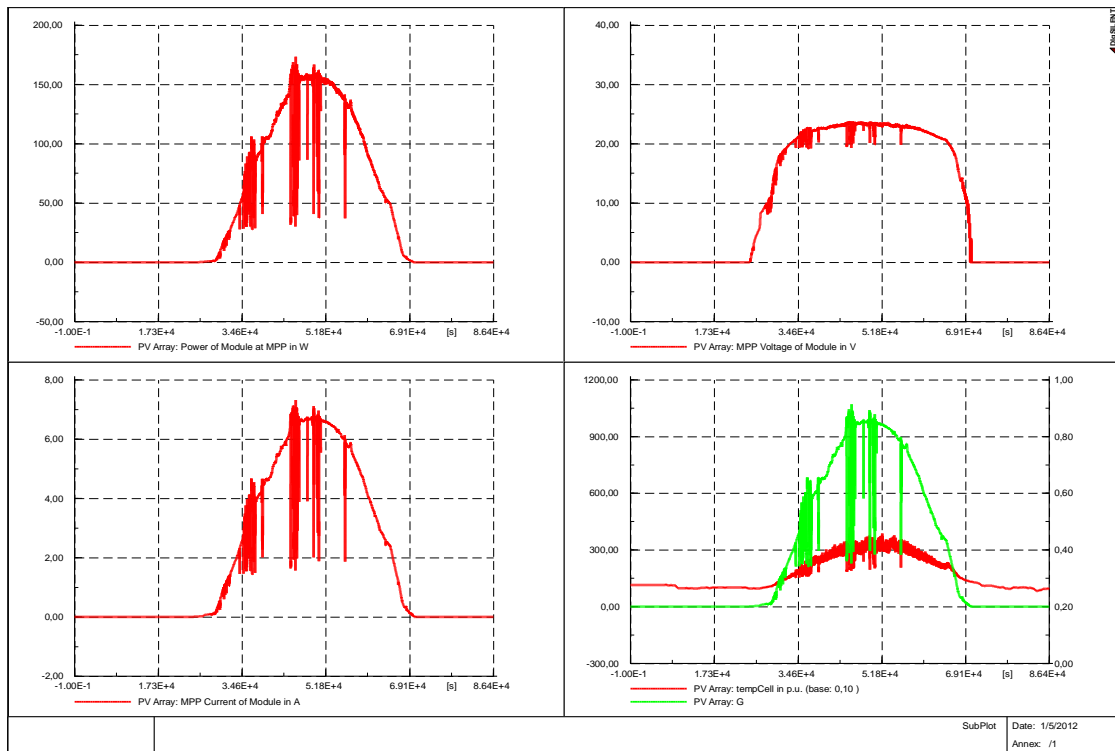
$$\cos ref = \text{Re}(u_1)/|u_1|; \sin ref = \text{Im}(u_1)/|u_1| \quad (2.30)$$

2.3.4.2 Comparison between simulations and measurements

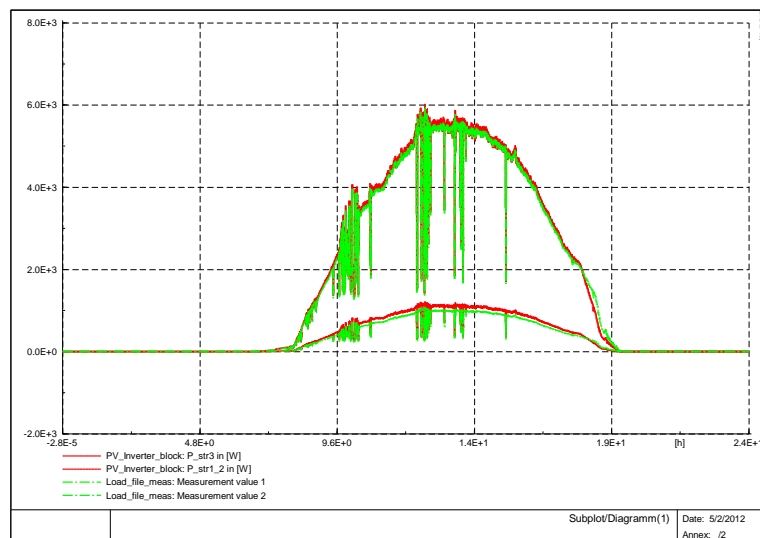
In order to validate the simulation model developed in PowerFactory and to compare the results obtained with MATLAB-Simulink model, the same measurements have been used like in the last section when we compare the results of Simulink model with experiments (Figs. 2.30-2.33).

The Photovoltaic Model has as inputs irradiation G and cell temperature $temp_{Cell}$, obtained from MATLAB-Simulink model considering the tilt angle, orientation and the influence of solar irradiation and wind speed on the cell temperature, implemented as a look-up table, as can be seen in Fig. 2.30 a). Also the MPP of current, power and voltage as a function of time for one module are shown. In

Fig. 2.30 b) is presented a comparison between measurements and simulations of inverter output power for both PV modules (Schuko 165 and SOLEL 100).



a)



b)

Fig. 2.30. a) Simulation results of the PV system model, and b) a comparison between simulations and measurements of the PV inverter output power for both PV modules (Schuko 165 and SOLEL 100).

2.4.Wind Turbine Systems Modeling and Simulation

Abstract-- To optimize the power produced in a wind turbine, the speed of the turbine should vary with the wind speed. A simple control method is proposed that will allow an induction machine to run a turbine at its maximum power coefficient. Various types of power control strategies have been suggested for application in variable speed wind turbines. The usual strategy is to control the power or the torque acting on the wind turbine shafts. This paper presents an alternative control strategy, where the rotational speed is the controlled variable. The paper describes a model, which is being developed to simulate the interaction between a wind turbine and the power system. The model is intended to simulate the behavior of the wind turbine using induction generators both during transient grid fault events and during normal operation. Sample simulation results for two induction generators (2 / 0.5 MW) validate the fundamental issues.

2.4.1. Introduction

One of the simplest methods of running a wind generation system is to use an induction generator connected directly to the power grid, because induction generators are the most cost effective and robust machines for energy conversion. However, induction generators require reactive power for magnetization, particularly during start-up, which can cause voltage collapse after a fault on the grid. To overcome such stability problems, the use of power electronics in wind turbines can be a useful option. [42, 43, 47, 50]

The installation of wind turbines in power systems has developed rapidly in the last 20 years and the national and international growth rates and policies indicate that this development will continue. During 1999, 3920 MW of wind turbine capacity was installed in the world, making up a total accumulated installation of 13932 MW of wind power at the end of 1999 [39].

The system model proposed in this paper is developed in the dedicated power system simulation tools MATLAB-Simulink and DigSILENT PowerFactory, which gives access to an extensive library of grid components, but requires implementation of the relevant wind turbine model. The model also includes wind speed fluctuations and control of soft-starter, enabling simulation of the power quality characteristics of the wind turbine. Finally, the model can be used to study alternative control strategies for wind turbine and additional equipment such as compensation units and storage systems.

2.4.2 Wind Turbine Modeling

The purpose of the model is to simulate the dynamical behavior and the electrical properties of a wind turbine. The modeling of the wind turbine should create a model as simple as possible from a mechanical point of view, but capable of providing a good description of the electrical characteristics of a wind turbine.

The wind turbine is characterized by the non-dimensional curves of the power coefficient C_p as a function of both tip speed ratio, λ , and the blade pitch angle, Θ_{blade} . The tip speed ratio is the ratio of linear speed at the tip of blades to the speed of the wind.

In order to simulate the wind turbine as part of a distribution system, models have been developed and implemented in MATLAB–Simulink and DigSILENT PowerFactory for each element.

The wind turbine model consists of different component models: wind model, aerodynamic model, transmission model and of the electrical components such as induction generator, soft-starter, capacitor bank and transformer model [40].

As shown in Fig. 2.31, the wind model generates an equivalent wind speed u_{eq} , which, together with the blade pitch angle Θ_{blade} and rotor speed ω_{rot} , are input to the aerodynamic block. The output of the aerodynamic model is the aerodynamic torque T_{rot} , which is the input for the transmission system together with the generator speed ω_{gen} . The transmission system has as output the mechanical torque T_{hss} on the high-speed shaft, which is used as an input to the generator model. Finally, the blade angle control block models the active control loop, based on the measured power and the set point.

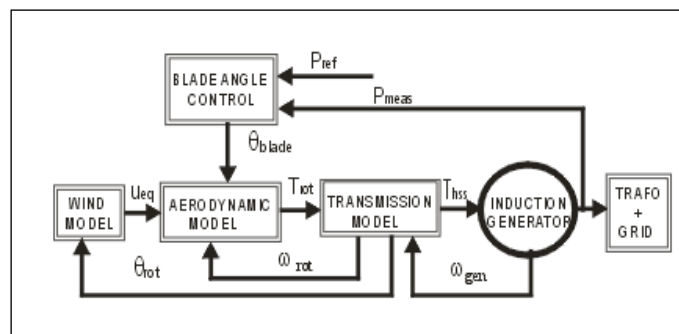


Fig. 2.31. Simplified scheme of wind turbine model.

A. The Wind Model

The wind models describe the fluctuations in the wind speed, which influence the power quality and control characteristics of the wind farm. Thus, the wind speed model simulates the wind speed fluctuations that influence the fluctuations in the power of the wind turbines. The wind acting on the rotor plane of a wind turbine is very complex and includes both deterministic effects (mean wind, tower shadow) and stochastic variations due to turbulence [40].

Fig. 2.32 shows a simulation result of a wind speed as a function of time, based on a look-up table, at an average of a wind speed $u_{eq}=11$ [m/s].

B. The Aerodynamic Model

A wind turbine is essentially a machine that converts the kinetic energy of the moving air (wind) first into mechanical energy at the turbine shaft and then into electrical energy [41].

Fig. 2.33 describes the conversion of wind power (P_{WIND}) into mechanical (P_{MEC}) and thereafter into electrical power (P_{EL}).

The interaction of the turbine with the wind is complex but a reasonably simple representation is possible by modelling the aerodynamic torque or the aerodynamic power as described below.

The force of the wind creates aerodynamic lift and drag forces on the rotor blades, which in turn produce the torque on the wind turbine rotor [41].

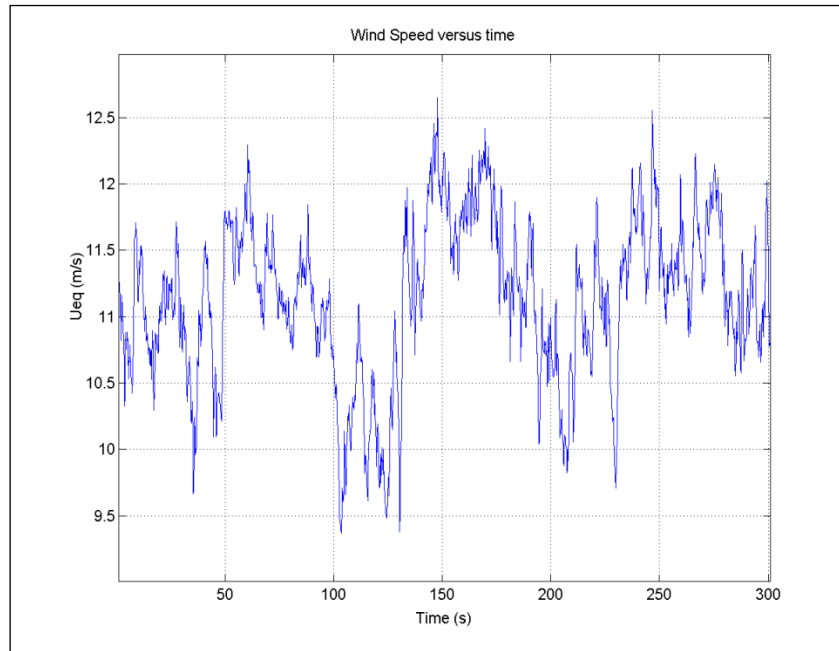


Fig. 2.32. The wind fluctuation (m/s) as a function of time (s).

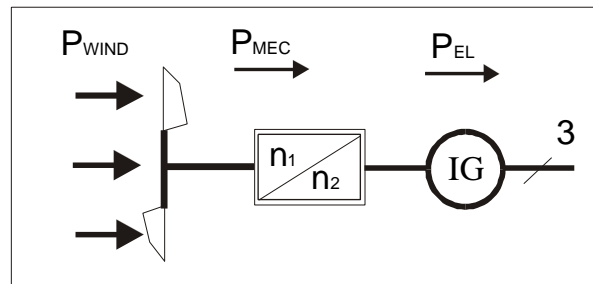


Fig. 2.33. A block diagram of the wind turbine.

The aerodynamic torque is given by:

$$T_{rot} = \frac{P_{aero}}{\omega_{rot}} = \frac{1}{2\lambda} \rho \pi R^3 C_p(\lambda, \theta_{pitch}) \quad (2.31)$$

Where P_{aero} is the aerodynamic power developed on the main shaft of a wind turbine with radius R at a wind speed u_{eq} and air density ρ . It is expressed by:

$$P_{aero} = \frac{1}{2} \rho \pi R^2 u_{eq}^3 C_p(\lambda, \theta_{pitch}) \quad (2.32)$$

The air density is depending on the temperature and on the pressure of the air.

The dimensionless power coefficient $C_p(\lambda, \Theta_{pitch})$ represents the rotor efficiency of the turbine. It is taken from a look-up table, which contains the specific aerodynamic characteristics for the turbine.

This coefficient depends on the tip speed ratio $\lambda = \omega_{rot} \cdot R / u_{eq}$ and on the blade angle Θ_{pitch} , ω_{rot} denotes the rotor speed. For a constant speed turbine, the power coefficient decreases when the wind speed increases (λ small). This fact is used in the passive stall control wind turbine.

The efficiency coefficient (C_p) changes with different negative values of the pitch angle ($0^\circ, -1^\circ, -2^\circ, -3^\circ$) but the best efficiency is obtained for $\Theta_{pitch}=0$.

The aerodynamic model is based on C_p curves for the given rotor blades.

C. Transmission System Model

To describe the impact of the dynamic behavior of the wind turbine, a simple model is considered, where the tower bending mode and the flap-bending mode of the wind turbine are neglected. It is assumed that all the torsion movements are concentrated in the low speed shaft, as T_{lss} . Emphasis is placed on the parts of the dynamic structure of the wind turbine, which contributes to the interaction with the grid, i.e. which influence the power. Therefore only the drive train is considered in the first place because the other parts of the wind turbine structure have less influence on power.

The drive train model is illustrated in Fig. 2.34. The input to the model is the aerodynamic torque. This is converted into the torque on the low speed shaft, which is further scaled down through the gearbox to the torque on the high-speed shaft. The generator inertia is implemented as part of the generator model, not as a part of the transmission system. The output of the model is the torque on the high-speed shaft.

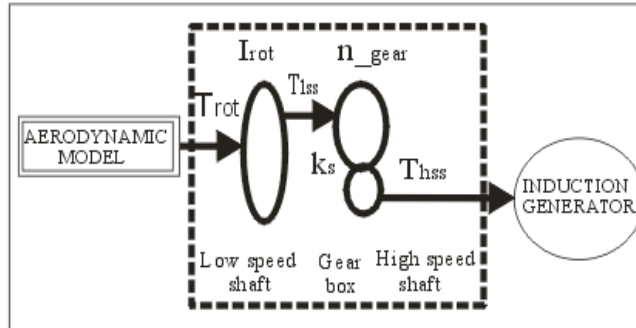


Fig. 2.34. Drive train model in the wind turbine.

The rotor is modelled by inertia I_{rot} , low speed shaft only by a stiffness k_s (the torsion damping is neglected), while the high-speed shaft is assumed to be stiff. Thus the transmission is described by the following equations:

$$I_{rot} \cdot \frac{d\omega_{rot}}{dt} = T_{rot} - T_{lss} \quad (2.33)$$

$$\frac{dT_{lss}}{dt} = k_s \left(\omega_{rot} - \frac{\omega_{gen}}{n_{gear}} \right) \quad (2.34)$$

It is also assumed that the losses in the gearbox are zero, thus the gear transmits ideally from the low speed to high speed. The output of the model is:

$$T_{hss} = \frac{T_{lss}}{n_{gear}} \quad (2.35)$$

where n_{gear} is ratio of the gear box.

D. The Induction Generator Model

The generator model is a combined mechanical and electro-magnetic model. The mechanical model includes the inertia of the generator rotor in the generator model.

The generator wind turbine is of squirrel cage induction type. Based on the existing generator data, a preliminary study has been made in MATLAB using the power system block-set built in induction machine model and a custom d-q model, simulating different dynamic behavior as seen in Fig. 2.35.

The equations used to build up the Matlab-Simulink induction machine d-q model are:

$$\bar{i}_s R_1 - \bar{U}_s = -\frac{d\bar{\psi}_s}{dt} - j\omega_b \bar{\psi}_s \quad (2.36)$$

$$\bar{i}_r R_2' - \bar{U}_r = -\frac{d\bar{\psi}_r}{dt} - j(\omega_b - \omega_r) \bar{\psi}_r \quad (2.37)$$

$$M_e = p_1 \text{Real}[j\bar{\psi}_s \bar{i}_s^*] \quad (2.38)$$

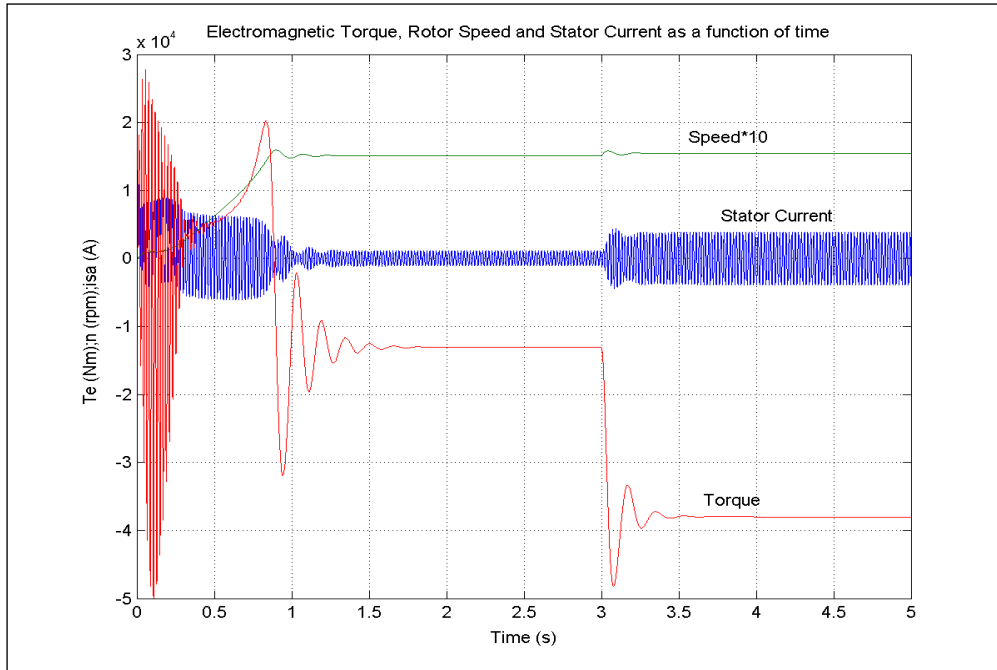


Fig. 2.35. Simulated torque, speed and stator current transients versus time during generator startup. Turbine torque steps up at $t=3$ s, from [full load torque-13.050 Nm] to [pull out torque-38.000 Nm].

Where the stator and the rotor fluxes have the following expression:

$$\bar{\psi}_s = L_{1\sigma} \bar{i}_s + L_m (\bar{i}_s + \bar{i}_r) \quad (2.39)$$

$$\bar{\psi}_r = L_{2\sigma} \bar{i}_r + L_m (\bar{i}_s + \bar{i}_r) \quad (2.40)$$

The parameters in these equations are: R_1, R_2' – stator resistance and rotor resistance;

L_1, L_2' – stator and rotor leakage inductance;

L_m – magnetizing inductance;

ω_b – speed of the reference system;

p_1 – pole pairs of the machine

i_s, i_r – stator and rotor current phasors

(Note: all the rotor quantities are reduced to the stator)

Later the induction generator was defined using the DiGSILENT PowerFactory built in improved induction (asynchronous) machine model [45]. The reasons why the built in DiGSILENT model (squirrel cage with current displacement) has been used are:

1. Different cage rotors can be considered with rotor current displacement;
2. The machine can be defined based on its measured torque – slip curve, short-circuit test and nameplate values;

3. Electrical parameter variations can also be considered;

An eventual implementation of a new d-q model in DiGSILENT PowerFactory can be done by some controlled voltage sources and parameter variation cannot be considered, as there is no measured data for that.

The built-in DiGSILENT model is presented in Fig. 2.36:

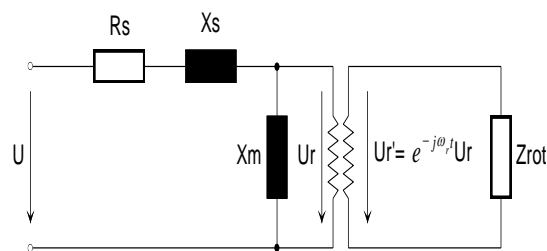


Fig. 2.36. Induction Machine Model built up in DiGSILENT Power Factory [45].

E. The Soft Starter Model

In order to reduce the transient current during connection of generator to the 0.96 kV grid a soft starter is used. When the generator speed increases above the synchronous speed the soft starter is connected and using firing angle control the generator is connected over the grid.

In DiGSILENT the soft starter is a stand-alone element. The commutation devices are 2 thyristors connected in anti-parallel for each phase. A complete control in details of the soft starter using the firing angle as input is possible just in EMT (electromagnetic transient) simulation mode, where every

thyristor switching is modeled in detail, while the RMS simulation uses a simplified model (as a controlled voltage source). The relationship between the firing angle (α) and the resulting amplification of the soft starter is highly non-linear and depends additionally on the power factor of the connected element. In the case of a resistive load φ can vary between 0° (full on) and 90° (full off) degrees. While in the case of a purely inductive load varies between 90° (full on) and 180° (full off) degrees. For any power factor in between, it will be somewhere between these limits [8].

2.4.3 Simulation Results

Simulation results on wind turbines with 2 MW and 0.5 MW induction generators are presented. The scheme also presents a case of load flow simulation, when the wind turbine works at nominal conditions and full power factor compensation is used. In order to limit the starting current transients during the 2 MW generator connections to the grid, a soft starter startup is used. The generators are connected when the generator speed is higher than the synchronous speed.

To simulate the wind turbine, models have been developed for each element and implemented in the dedicated power system simulation tool DigSILENT PowerFactory [45], which provides the ability to simulate load flow, RMS fluctuations and transient events in the same software environment. The DigSILENT PowerFactory simulation tool therefore has a dedicated model for induction generators, which take into account the current displacements in the rotor, the torque – slip and short circuit test curves. Also models of synchronous machines, transformers, bus bars, grid models, static converters etc are provided.

Fig. 2.37 contains the grid representations from 50 kV double bus-bar systems down to the wind turbine. The wind turbine contains the tower cable making the connection to the 0.96 kV/10 kV transformer and the 10 kV cable at the bottom of the tower. The 10 kV cables are modeled using the existing DigSILENT PowerFactory model toolbox.

The power factor compensation units are represented by a capacitor bank on this scheme and a Static Var System (SVS) unit. The switching of capacitors is done as a function of average value of measured reactive power. The generators are full load compensated.

The wind model describes the fluctuations in the wind speed (w_{spoint}), which influences the power quality, and which generates a hub wind speed (w_{sfc}) described in [48].

The simulations shown in Fig. 2.38 illustrate the effect of the rotational sampling. This hub wind speed is used as input to the rotor wind model to produce an equivalent wind speed (u_{eq}), which accounts for the rotational sampling on each of the blades.

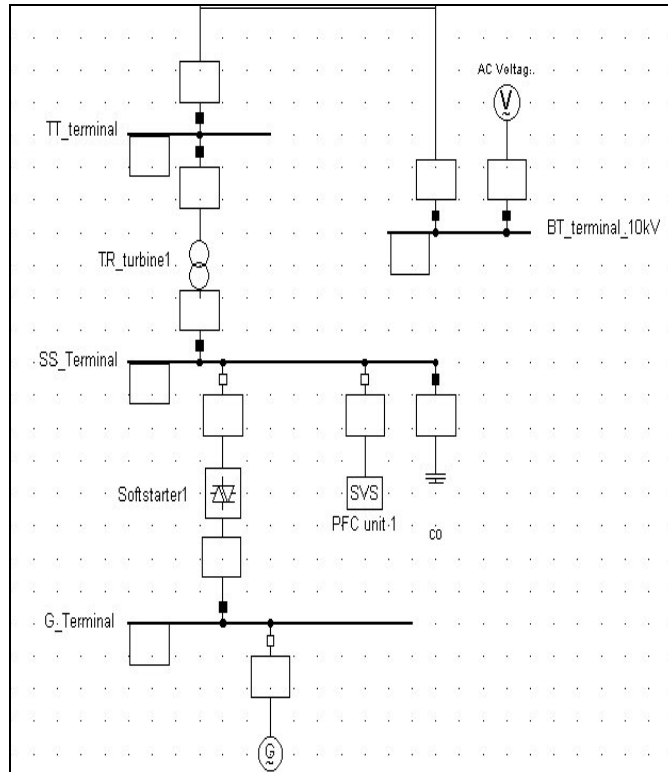


Fig. 2.37. Electrical diagram of 2.0 / 0.5 MW generators.

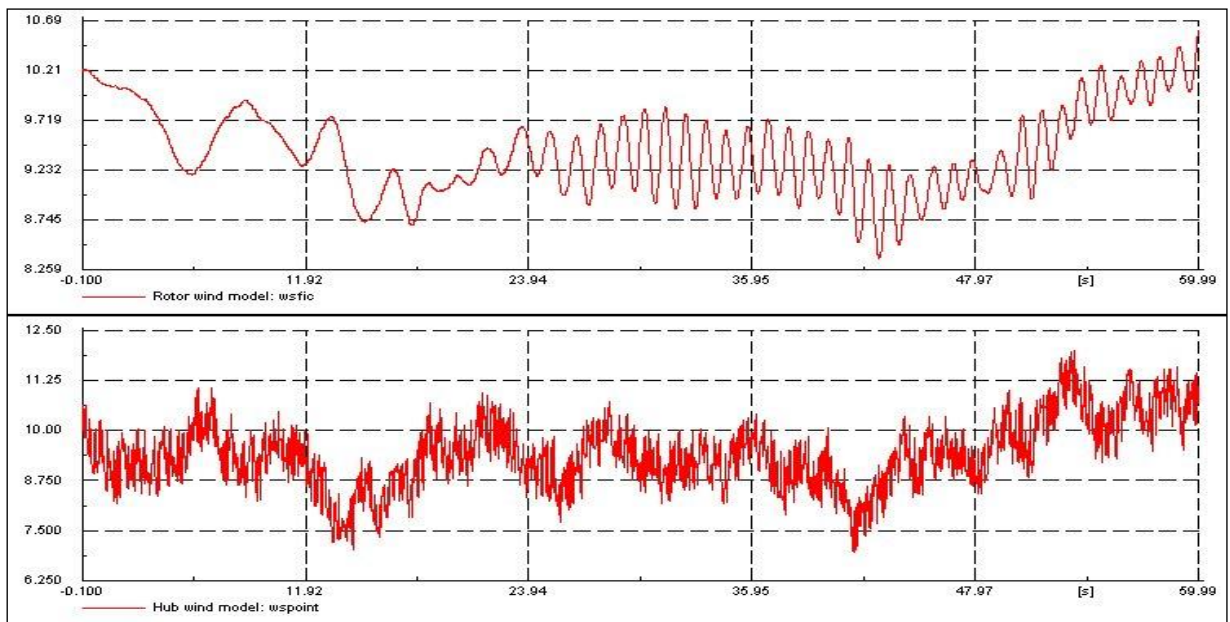


Fig. 2.38. Rotor wind and hub wind model.

The aerodynamic torque (torque_rot-Trot) accelerates the wind turbine rotor, with the generator disconnected from the grid, until the rotor speed (ω_{rot}) is close to its nominal value. Then the generator is connected to the grid as seen in Fig. 2.39. The basic idea is to control the rotational

speed using only measurement of the power (or torque), as it is depicted in Fig. 1 and by equations (2.31) and (2.32) as well.

Results for two induction generators (0.5 and 2 MW) are presented in Fig. 2.40 and Fig. 2.41. These figures contain traces of rotor speed, current magnitude, and total active and reactive power for start-up of the wind turbine with directly connected induction generators at 1505 rpm (1.007 p.u.).

The starting current of 0.5 MW machine is 3 times higher than the rated current, while the starting current of the large induction machine (2 MW) is 8 times higher than its rated value. It is clear that for 2 MW machine it is imperative to reduce the start-up current.

As it can also be seen in Fig.2.40 and Fig. 2.41, the induction generators have a peak consumption of reactive power right after connection to the grid. The reactive power is required to magnetize the generators. The steady state voltage is dependent on the reactive power consumption of induction generator (IG). Therefore it is important to supply the IG with a reactive power compensation unit to provide the reactive power balance and to improve the voltage stability.

In Fig. 2.42 the connection of the 2 MW generator to the grid is realized by a soft-starter. The soft starter limits the current and torque transients and implicitly reduces the reactive power peak value. When the induction machine of 2 MW was connected to the grid through soft-starter, the starting current has been reduced at 1.1 times of rated current, while the reactive power peak became 13.5 times smaller than when the machine was directly connected to the grid.

When the soft-starter is bypassed and thus the 2 MW induction generator is connected, the power factor compensation is performed by the capacitor bank (Fig. 2.43). It is also seen in Fig. 2.43 how the capacitor banks are connected in steps after the 2 MW generator is connected to the grid. The capacitors can be switched on and off individually as a function of average value of reactive power during a certain period of time.

In [50] the use of external resistances in series with the induction machine has been proposed, instead of using the conventional soft-starter, to reduce the grid connection transients of constant-speed wind turbine. Due to the resistor setup is cheaper and the reliability of the resistor arrangement it seems to be on the same level as the reliability of the soft-starter, this alternative method could be used. But it seems that the flexibility brought by the soft-starter capacity to perform the duty of an automatic power switch with corresponding protection means should also be considered.

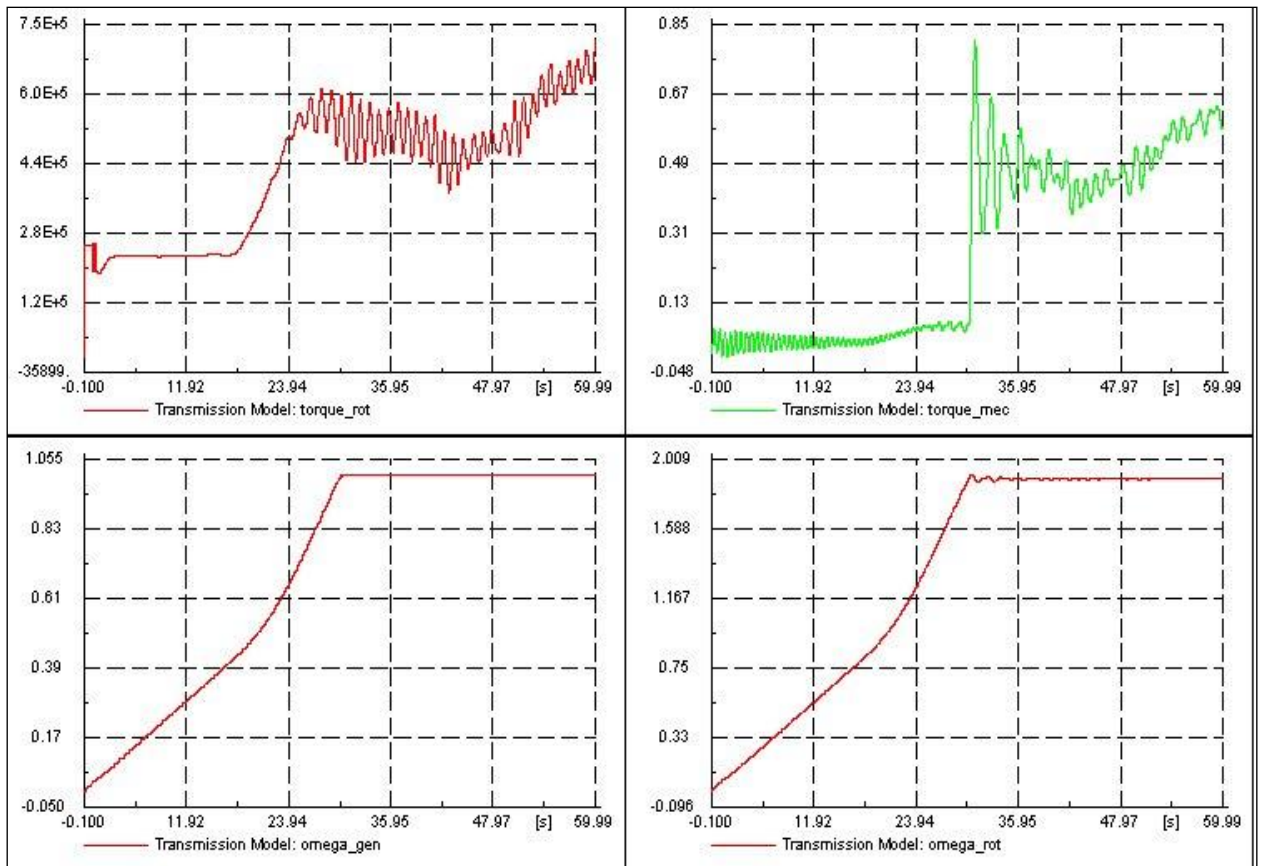


Fig. 2.39. Transmission model during start-up. Aerodynamic torque (**torque_rot**), mechanical torque (**torque_mec**), generator speed (**omega_gen**) and rotor speed (**omega_rot**) of wind turbine system.

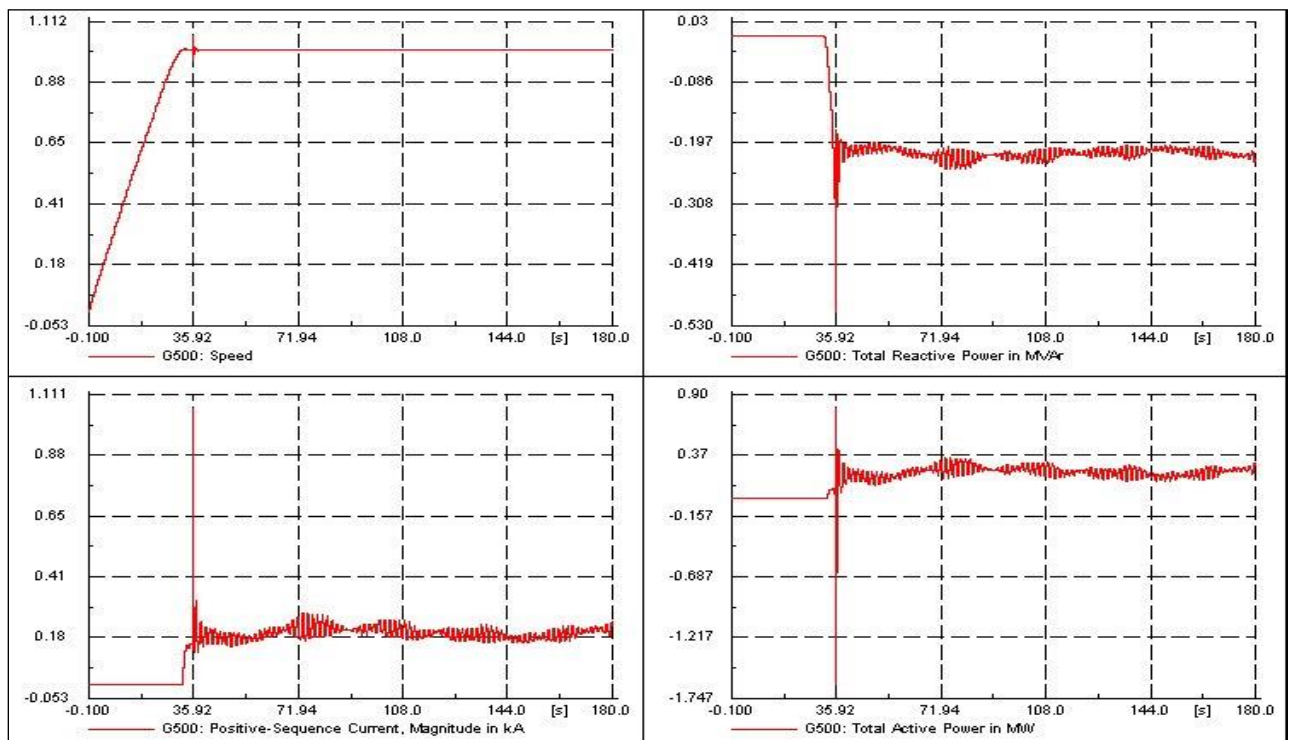


Fig. 2.40. Start-up with directly connected and operation of 0.5 MW induction generator. Speed, reactive power, current and active power of the generator.

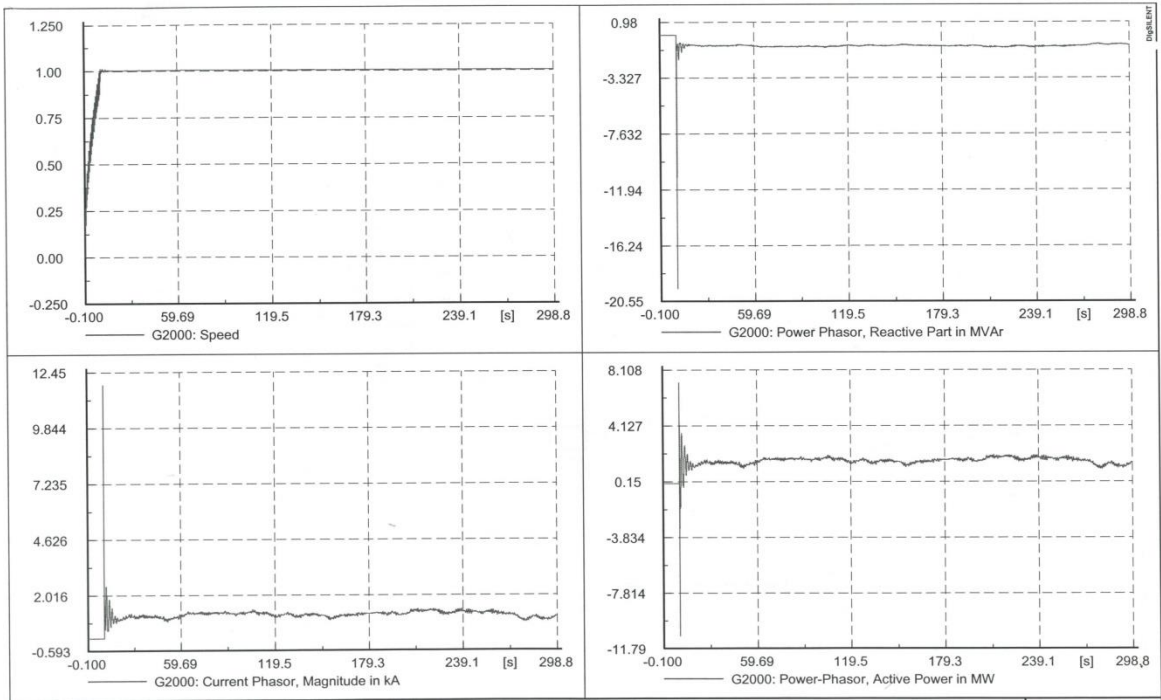


Fig. 2.41. Start-up with directly connected and operation of 2 MW induction generator. Speed, reactive power, current and active power of the generator.

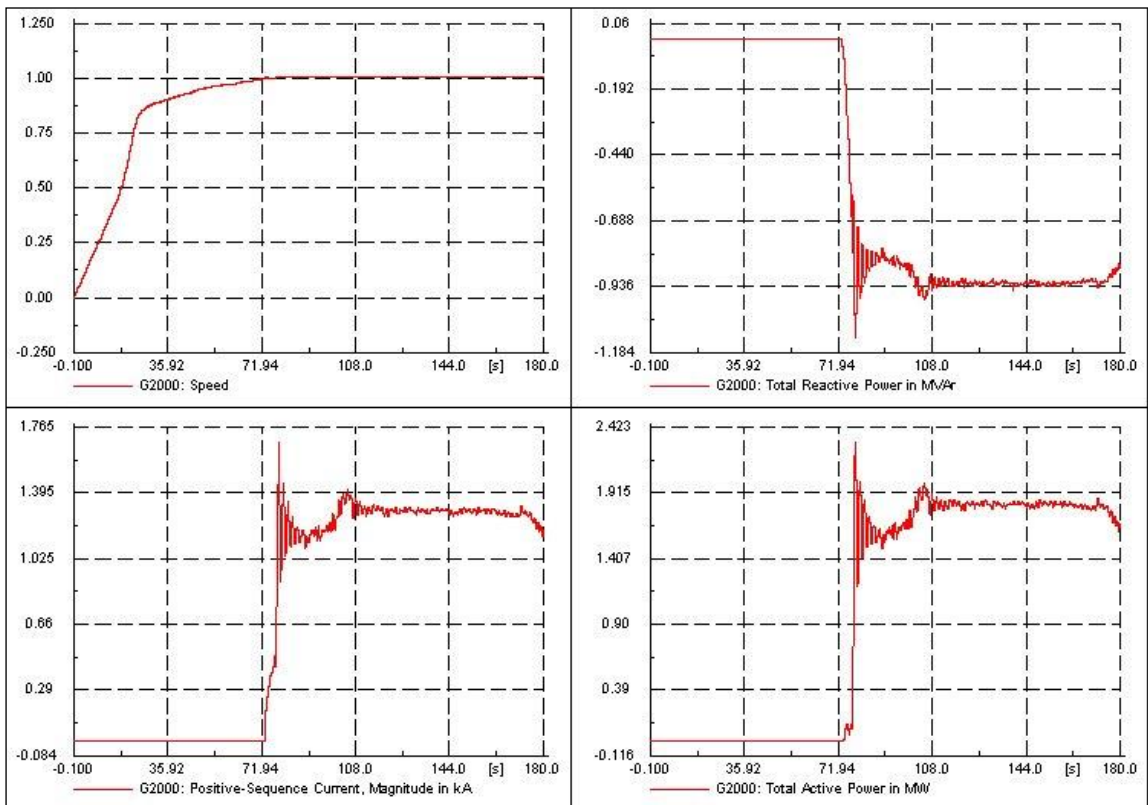


Fig. 2.42. Start-up with soft-starter and operation of 2 MW induction generator. Speed, reactive power, current and active power of the generator.

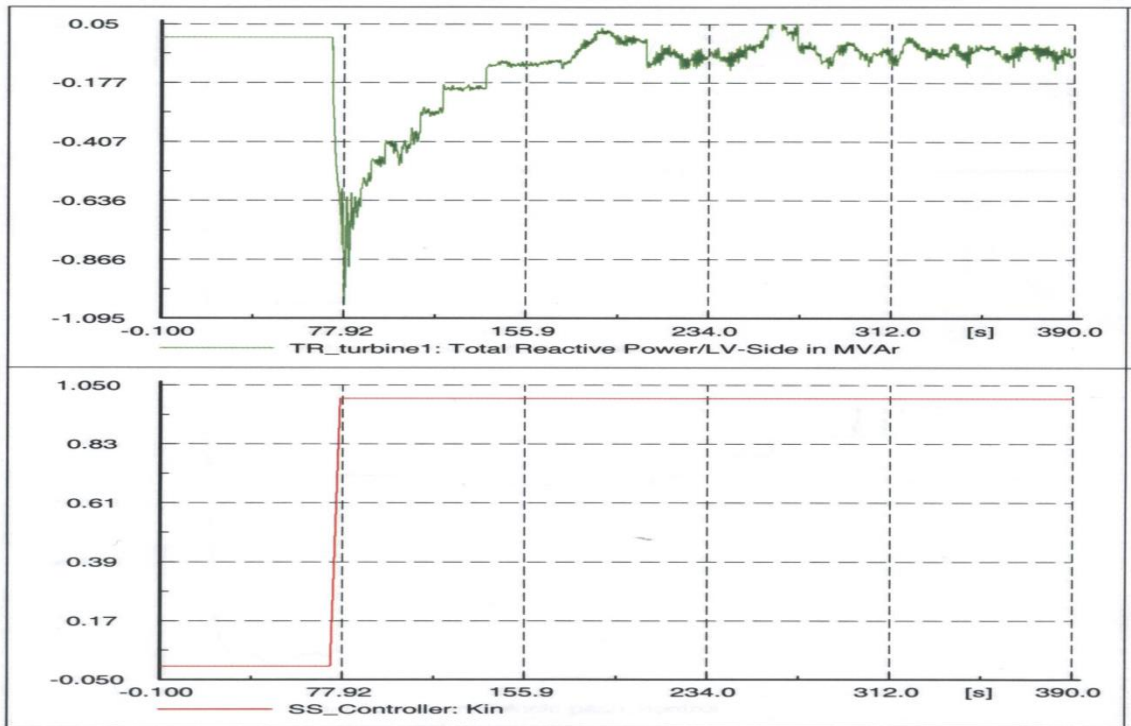


Fig. 2.43. Reactive power compensation with capacitors connected in steps and the soft-starter by-passed controller (SS_controller: K_{IN}).

2.5 Energy Storage Systems in a Distribution Network

The electrical power system is facing an evolution from the traditional concept of energy generation by few localized power plants interconnected together through a meshed system to distributed medium and small scale generators. Some topologies of these generators embedded into the distribution network are fed by renewable sources like wind and sunlight. Their main drawback is their hardly predictable behavior and uncontrollable output. The presence of energy storage system may allow a better management of the electric system allowing the full exploitation of renewable energy sources. Distribution companies start to recognize that storage has the unique ability to act as a buffer between the grid and generation that is either intermittent or not controlled by the utility [5, 9-12, 34].

The vanadium battery system installed in SYSLAB is connected to the grid via a four quadrant power converter and can deliver 15 kW on the AC side and the nominal storage capacity is 180 kWh. Figure 2.44 shows a picture of the system during installation and a list with the main system components. The battery can operate in two modes: P-Q mode (where the active and reactive power of the battery is set by the user) and U-f-mode where the power is set according to the grid voltage and frequency and the pre-defined droop-curves.

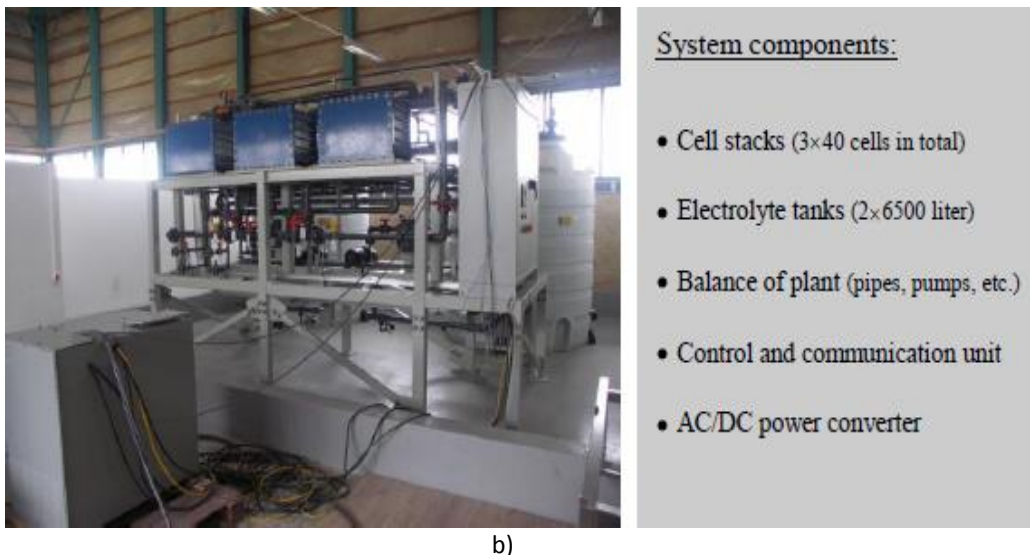


Fig. 2.44 The Vanadium Redox Battery in SYSLAB during installation a) and its system components b).

The current installation is shown in Fig. 2.45. The area of the installation is 7m x 7m.



Fig. 2.45. Vanadium battery installation seen from above: electrolyte tanks in the back and 3 cell stacks at the front [8].

A vanadium battery stores energy in two electrolytes. The capacity of the battery is determined by the size of the tanks and its power is determined by the size of the cell stack. The Vanadium Redox Battery (VRB) uses different ionic forms of Vanadium in a dilute sulphuric acid for both half cells, eliminating the possibility of cross contamination. The two acid electrolytes are separated from each other by a PEM (Proton Exchange Membrane). The different redox couples are V_{5+} (VO_{2+}) and V_{4+} (VO_{2+}) for the positive half-cell and V_{3+} and V_{2+} ions for the negative half-cell. At discharge the negative half-cell V_{2+} is oxidized to V_{3+} . The freed electron passes through the circuit and participates in the reduction of VO_{2+} to VO_{2+} . During charge the reaction occurs in the opposite direction [8, 32-33].

The open cell voltage is 1.4 V at 50% SOC (state of charge) and 1.6 V at 100% SOC. By power electronics the DC Voltage is transformed to 400 V_{AC}. The supplier of the vanadium battery specifies high efficiencies (>70%) and long cycle life (more than 13000 cycles for the battery). Also, it should not degrade under prolonged periods of discharge [8].

The battery package is an interesting option for storing excess energy from the hybrid grid (wind intermittency) for later use. It may also act as a peak shaving unit and thereby contribute to a stronger grid [11-13].

The propose of the energy storage system is to be coupled with a PV/wind generation system in order to realize different tasks, such as: to have the generation output power smoothed and to grant no power transfer, for a certain period on distribution system operator request, at a point of common coupling (PCC) in any battery state of charge condition. The idea is to control the battery charging and discharging in order to control the whole power plant.

2.5.1 Analytical model of the VRB

The VRB model is based on the power balance between the input and the stored power considering the efficiency of different components, such as: cell stacks, electrolytes, pumps and power converter and the power losses.

Figure 2.46 shows a schematic picture of the sources of losses of the battery system. In this depiction, the system has four parts: the power converter, the cell stacks, the storage and the auxiliaries. The following four subsections will describe the characteristics of these four parts.

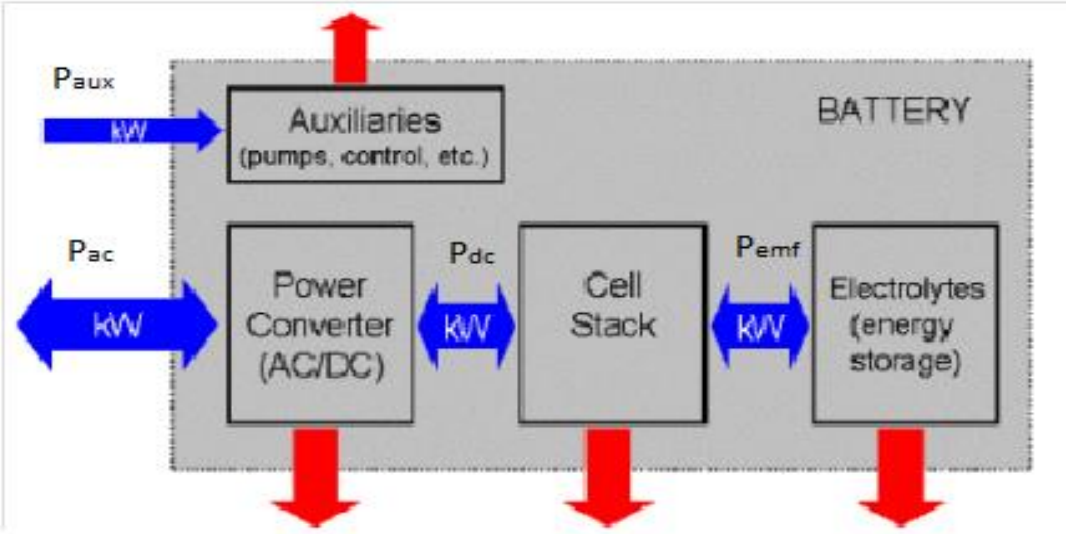


Fig. 2.46 Schematic drawing of the battery system. The red arrows indicate losses from the different parts of the system.

The reference power that is given by the system to the battery’s converter in order to operate in charge/discharge mode, is the value of P_{ac_ref} . Due to the efficiencies of different components, the actual charge/discharge power that supplies the electrolyte has a different value: in charge mode $P_{ac} > P_{dc} > P_{emf}$ and in discharge mode $P_{ac} < P_{dc} < P_{emf}$.

The actual energy stored in the battery has the following equation:

$$E_{Batt} = E_{Batt0} + \int [P_{emf} dt] \tag{2.41}$$

Where: E_{Batt0} - initial energy stored in the battery and P_{emf} - charge/discharge power at the electrolyte side.

The state of charge (SOC) is defined as the amount of energy stored in the battery (in percent)

$$SOC = E_{Batt} / E_T \tag{2.42}$$

Where E_{Batt} – the energy stored in the battery and E_T – the total energy capacity of the battery

AC-DC converter efficiency

The power converter efficiency has been estimated from the measured power on both the AC and the DC side. There is a slight difference between the AC to DC efficiency and the DC to AC efficiency: At maximum power in discharge mode is approximately 93% where in charge mode is approximately 91%. In both modes the characteristic of the efficiency has a relative large range where it is flat. The

absolute efficiency is not very high for a modern power converter. The efficiency curve is presented in the chapter describing the simulation model.

Cell stacks efficiency

The power delivered to the stack is $P=V_{DC} I$, while the power delivered to the electrolytes is $P = V_{EMF} I$. This means that the stack efficiency is V_{EMF}/ V_{DC} in charge mode (when $I<0$) and V_{DC}/V_{EMF} in discharge mode (when $I>0$). Figure 42 shows the efficiency of the cell stacks as function of DC power at different SOC levels, when the battery is running in stable conditions. The figure illustrates how the relative deviation from the EMF grows with the power, leading to a decrease in the cell stack efficiency. There should also be a slight efficiency dependence on temperature, but this is expected to be insignificant in the temperature range that the battery is operated in and it has been disregarded in this study. There is also a dependency on SOC since the open circuit voltage is higher when the SOC is higher and thus the current is smaller for the same power resulting in a decrease in the losses and a higher efficiency.

During the testing of the battery it has been put through a number of different charge and discharge cycles. The charging/discharging pattern including faster cycling does not have a significant impact on the efficiency and are covered by the efficiency results in Figure 42.

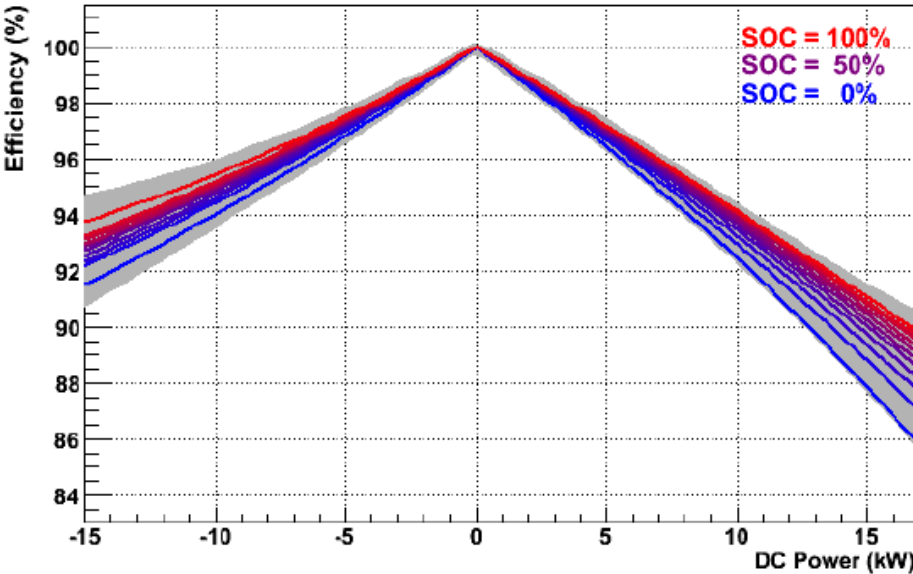


Fig. 2.47. Efficiency of the cell stacks as function of DC power. The different colors indicate the different SOC's. The grey area indicates the variations in the efficiency [8].

Other storage losses

As a part of the normal operation of the battery, water will diffuse through the cell membranes when the ionic composition in the two electrolytes differs (due to the osmotic pressure). This results in a difference in the level of the electrolyte in the two tanks. In order to avoid a too large difference in the level an equalization process is carried out every 24 hours. A valve between the two tanks is simply opened for about half an hour allowing electrolyte to flow from the tank with the highest electrolyte level to one with the lowest level. The energy loss during equalization depends on the current SOC and of course the difference in electrolyte level. The loss has been measured to be 1.5% SOC (2.7 kWh) on average during the measurement period. This corresponds to a constant energy

use of about 110 Watts. The losses during equalization are the only observed energy losses in the electrolyte.

Auxiliary power consumption

For a vanadium battery the auxiliary power consumption is significant since the electrolyte has to be circulated for the battery to be operational. The power of the auxiliaries (control system, pumps, etc.) can be derived from the measured AC power of the battery and the total power flow over the bus (when only the battery is connected). When the battery is off, the power consumption (for the control PC and the displays) is 235W. When the battery is on and the pumps are running the power consumption is between 1.1 and 1.6 kW depending on the AC power. This is illustrated in Figure 2.48. At low power ($|P_{AC}| < 4 \text{ kW}$) a high flow speed of the electrolyte is not required and the pumps speed is reduced, which can be seen in the auxiliary power consumption. At high power ($|P_{AC}| > 4 \text{ kW}$), the pumps are running at higher speed and the auxiliary power is about 1.5 kW. The slight AC power dependence observed in the charge mode (and why a similar dependence is not observed in the discharge mode) has not been understood. The fraction of the auxiliary losses will probably decrease with size of the battery e.g. by introducing stages in the battery so only stages that are necessary are in operation. Further might the control of the pumps be more sophisticated and depend more on the current operating conditions.

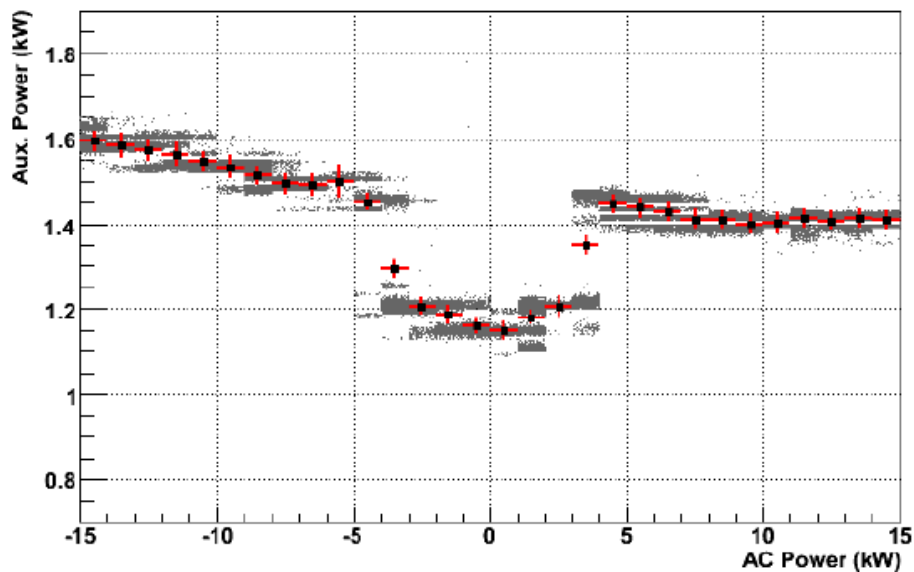


Fig. 2.48. Auxiliary power as a function of AC power. The grey regions show data (5 second averages) taken when operating the battery half an hour on each integer AC power (from -15 to 15kW). The red crosses indicate the average value [8].

2.5.2 VRB model implemented in Matlab/Simulink

The model for the VRB was developed in Matlab/Simulink and is based on the power equilibrium between the input and the stored power considering the efficiencies of different components and the power losses. These efficiencies were computed through experiments by measuring different electric values at different locations [23-25].

Initial conditions: The model needs one initial condition at the start of the simulation- the state of charge (SOC).

Input variable: The model considers one input value AC Power of the inverter. This input power is measured from the point of view of the electric system, since for the charging process of the battery the input power has negative values, and for discharging mode it has positive values. The operation of the ac-dc converter in both charge-discharge mode, and also the physical electric limitation that manifest at low and high SOC of the battery are reproduced in the model.

State variables the state variables of the simulation model are:

- E_{bat} – the amount of energy stored in the battery
- P_{pump} – power needed for the pumps to move the electrolyte inside the battery
- V_{emf} – dc voltage of the electrolyte
- V_{dc} – dc voltage at the ac-dc convertor side
- P_{ac_in} – the actual power that is at the ac side of the converter (at higher SOC, even if the battery is requested to charge at a certain amount of power, the physical electric limitations makes the actual input ac power less than requested)
- P_{dc} – power at the dc side of the converter
- P_{emf} – dc power of the cell stack, on the electrolyte side.

Output variable: The model has the SOC as output.

In Fig. 2.49 is presented the VRB block diagram implemented in Matlab/Simulink using blocks from standard library of Simulink. The blocks are detailed and explained in the followings. Basically, the model reproduces the power flow in the battery, considering the efficiency and losses of each component presented in [8]. These characteristics of the battery have been computed based on experiments by measuring different electric values at different loads and SOC levels. The simulation model of the battery system contains five subsystems: the power converter, the cell stacks, the energy storage, voltage limitation and the auxiliaries, as it is depicted in Fig. 2.49.

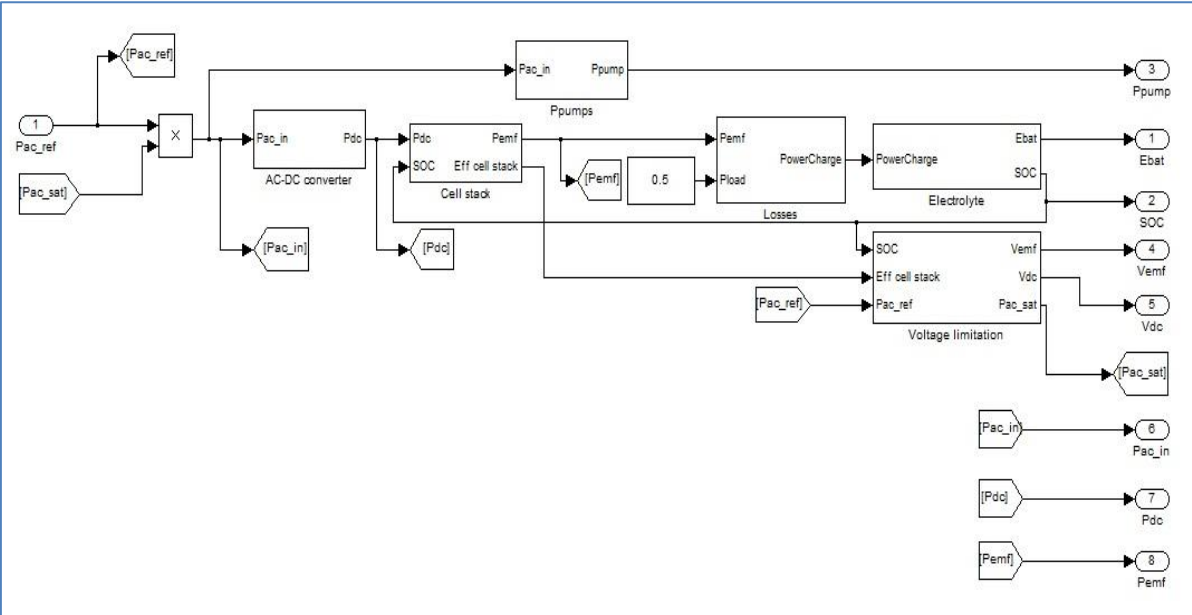


Fig. 2.49. VRB block diagram implemented in Simulink.

Each component has different behavior, regarding the mode of operation of the battery: charge/discharge. The model implemented these behaviors in a component base manner, like shown in Figure 2.50, the operation mode is considered by each particularly component, rather than having two large blocks, one for charge mode and the other for discharge mode.

In Figure 2.50 is presented the block for the AC-DC converter. The efficiency of the converter is implemented using a look-up table with the values presented in Figure 2.48.

As stated in [8], in charge mode $P_{ac_in} > P_{dc}$ and $Eff_{ACDC} = P_{DC} / P_{AC_IN}$. In discharge mode $P_{DC} > P_{AC_in}$ and $Eff_{ACDC} = P_{AC_IN} / P_{DC}$.

In Figure 2.50, the efficiency of the AC-DC converter is shown for both operation modes. In charge mode (AC Power with negative values) the efficiency is 91% where in discharge mode is 93%.

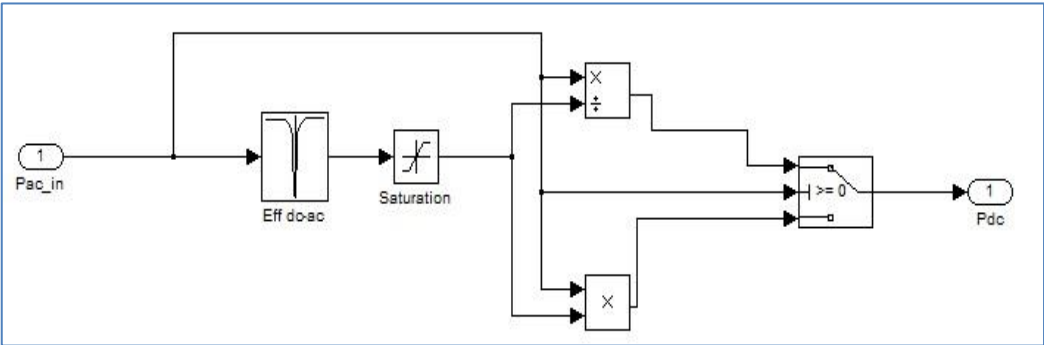


Fig. 2.50. Simulation model for the AC-DC converter.

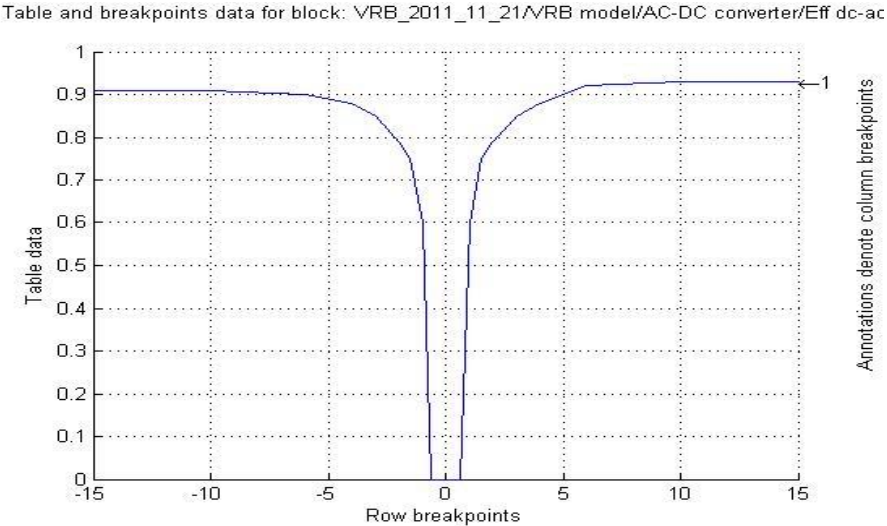


Fig. 2.51. Look-up table with the efficiency of the AC-DC converter implemented in Simulink.

The efficiency of the cell stacks depend both on charge/discharge power and also on SOC, as shown in Figure 2.49.

In order to consider these factors, two formulas were developed for each operation mode. The formula considers the efficiency at $P_{DC}=15$ kW and SOC= 0 as eff_{SOC0} , and $P_{DC}=15$ kW and SOC=100 % as eff_{SOC100} .

First, the slope at the higher characteristic (at SOC=100 %) is calculated:

0... P_{DC} (known)...15 kW

1...eff (unknown)... eff_{SOC100}

The value for efficiency in this case, for constant SOC=100%, considering a known P_{DC} is:

$$eff = \left(1 + \frac{(eff_{SOC100}-1)}{15} P_{DC} \right) \quad (2.43)$$

In order to model also the dependence of SOC, an additional term has to be used. At 0 power has to have no effect, and at 15 kW and SOC=0 has to produce a deviation of $\frac{eff_{SOC0}}{eff_{SOC100}}$.

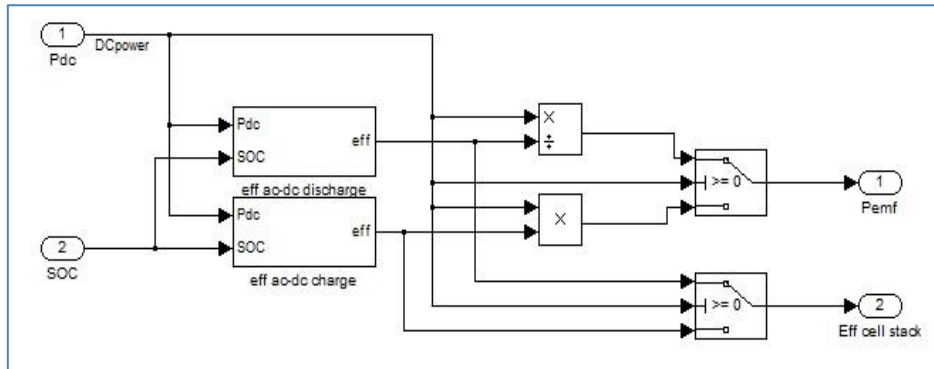


Fig. 2.52. Simulation model for the cell stacks.

Because in charge mode the input power has negative values, in the developed formula the minus sign has to be used. The obtained two formulas are:

Charge mode:

$$eff = \left(1 + \frac{(eff_{SOC100}-1)}{15} (-P_{DC}) \right) \left(1 - \left(1 - \frac{eff_{SOC0}}{eff_{SOC100}} \right) (1 - SOC) \right) \quad (2.44)$$

Discharge mode:

$$eff = \left(1 + \frac{(eff_{SOC100}-1)}{15} P_{DC} \right) \left(1 - \left(1 - \frac{eff_{SOC0}}{eff_{SOC100}} \right) (1 - SOC) \right) \quad (2.45)$$

Other losses

Other losses refer at operation losses like PC and display supply, and also at the energy loss during equalization. They are modeled as a constant 0.5 kW loss.

Pump losses

The power pumps (auxiliary power) consumption is modeled with a look up table, considering the experimental data shown in Figure 2.51. However, it does not influence the power flow from AC side to the battery because it consumes power from a different source, as shown in Figure 2.52.

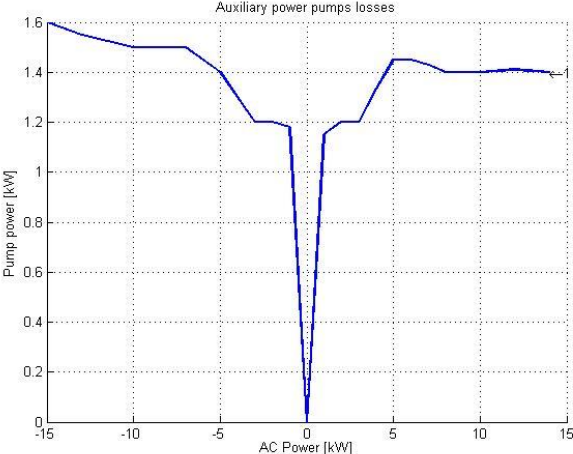


Fig. 2.53. Auxiliary power as function of AC power

Electrolyte block

In Figure 2.54 is presented the energy storage block that uses equation (2.44) in order to compute the stored energy and the SOC level of the battery.

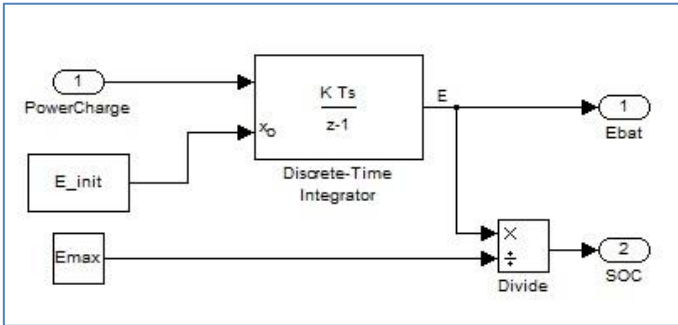


Fig. 2.54. Energy storage model subsystem.

Voltage limitation block

This block has two functionalities: to calculate the DC side voltage of the converter and to calculate the AC limit power according to the SOC. As explained before, the power input is physically limited and at high SOC values, the converter is not able to receive the prescribed power, but a limited one. The MATLAB/Simulink model is depicted in Figure 2.55.

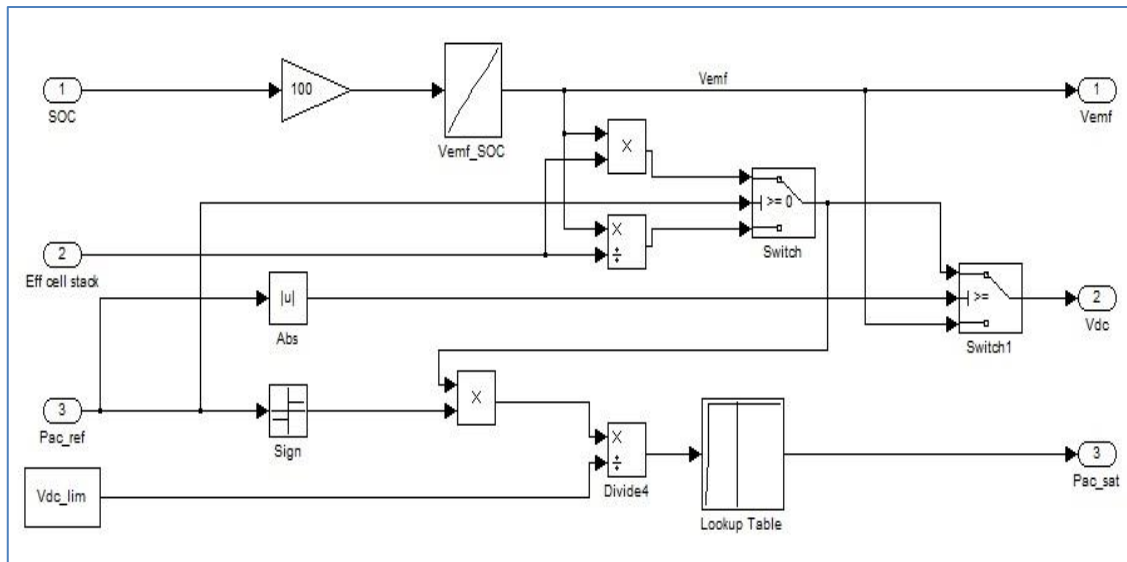


Fig. 2.56. Voltage limitation block implemented in Simulink.

An empirical relation between the SOC and the voltage across the electrolyte (V_{EMF}) is plotted after numerous experiments.

Figure 2.57 shows the open circuit voltage (V_{EMF}) as function of the SOC. The axis on the upper edge of the plot shows the theoretical state of charge (see Appendix B). The dotted curve shows a fit to the data points. Due to the resolution of the measurement of the reference cell (V_{EMF}) measurement the SOC fluctuates 2-3 %. The SOC used in most of the analysis presented here is the average over 60 consecutive SOC measurements (one each second).

Considering the cell stacks efficiency and this relation between V_{EMF} and SOC, the voltage over the DC side of the converter can be calculated.

According to the mode of operation, there can be considered three cases:

1. Battery is in charge mode, $P_{AC} < 0$

$$V_{DC} = V_{EMF} * \text{Eff}_{\text{cellstack}}$$
2. Battery is in standby mode $P_{AC} = 0$

$$V_{DC} = V_{EMF}$$
3. Battery is in discharge mode $P_{AC} > 0$

$$V_{DC} = V_{EMF} / \text{Eff}_{\text{cellstack}}$$

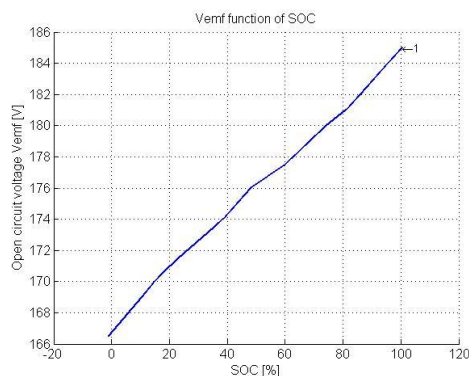


Fig. 2.57. Open circuit voltage (V_{EMF}) as function of the SOC implemented in Simulink as a look-up table.

2.5.3 Validation of the simulation model

In order to validate the simulation model, measurements were taken from the DAQ board of the VRB, fed into the model and verifying the output values of the battery and of the model.

The following experiment for a time scale of 36 hours was considered: starting from a SOC=93.5 % the battery was discharged with a constant $P_{AC}=15$ kW, until SOC=18 %. Then a charge sequence from SOC=14 % until SOC=87 % at $P_{AC}=10$ kW was considered, as can be seen in Fig. 2.58. A comparison between simulations and measurements is presented in Fig. 2.59 and Fig. 2.60.

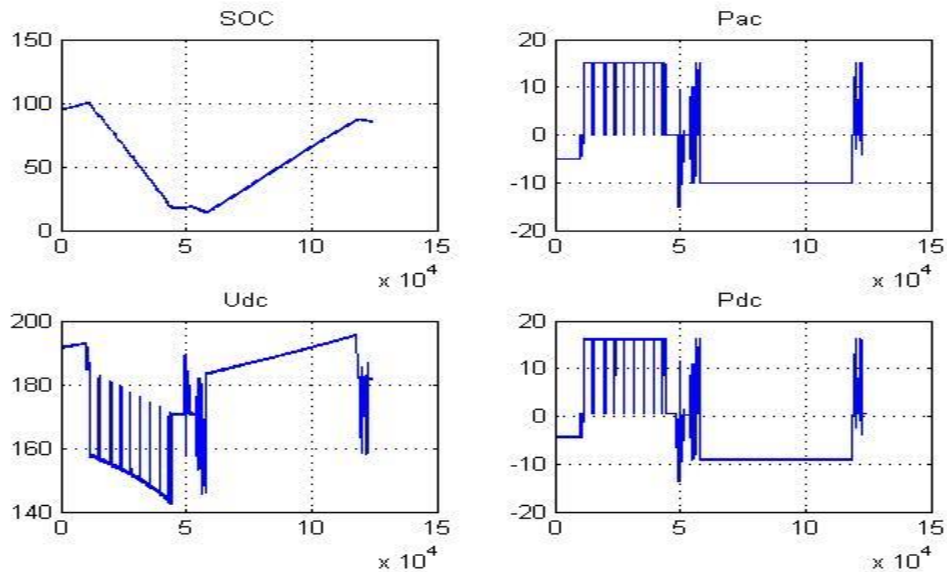


Fig. 2.58. Measured data from the DAQ board of VRB acquired and process by MATLAB.

After running the simulation with P_{AC} read from the VRB data acquisition board as input, the output simulation model parameter SOC was plotted against the measured SOC, as seen in Figure 2.59. In Figure 2.60 is shown a comparison between measured and simulated DC-Voltage (V_{DC}) as a function of time.

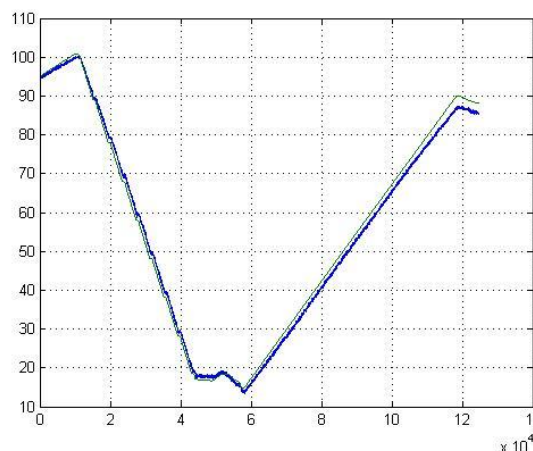


Fig. 2.59. Comparison between measurements and simulations values of SOC:
blue – measured; green – simulated.

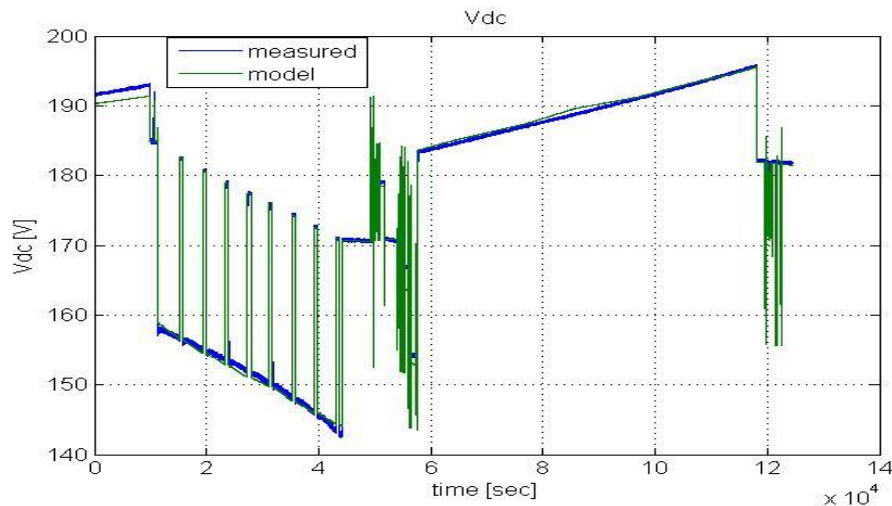


Fig. 2.60. Compared values of V_{DC} : blue – measured; green – simulated.

2.5.4 Simulation Model of VRB System developed in DigSILENT PowerFactory for distribution networks

The battery package is an interesting option for storing excess energy from the hybrid grid (wind intermittency) for later use. It may also act as a peak shaving unit and thereby contribute to a stronger grid.

In the distribution network a high share of PV may require new approaches for voltage control as the power output of PV system can change rapidly if clouds pass very fast over the PV system. New control approaches may include active P/Q control from the PV system, changed design of the embedded distribution system control as well as active demand-side control.

Simulation models of a battery system are needed for many purposes, such as:

- 1) Voltage studies with rather distributed sets of single inverter with PV panels, e.g. to determine temporary over voltage within a distribution network or within a PV power plant. Such a model typically only consist of up to 100 busses and requires a high level of details (High bandwidth $f > 10$ kHz);
- 2) Integration studies with different types of generators. For this purpose simulation models of PV power plants should be rather simple (low bandwidth $f < 100$ Hz), but should reproduce the required behavior needed for the integration study.

Existing models are typically only developed for a single purpose, often focusing on a rather simple representation of a battery system.

The approach in this project follows a slightly different approach:

Rather detailed simulation models of battery systems (battery and inverter) will be developed and validated against measurements. For this purpose it is necessary to develop detailed functional specifications which should be fulfilled by the simulation model and will be tested against specific measurements.

The aim is to use measurements for validation of the simulation models. The simple simulation models for a battery inverter model will be validated using the test facilities of the SYSLAB.

The key challenges are:

- Modeling of the VRB model and validation of the model;
- Modeling the Battery Management System and its impact on voltage and frequency control;
- Validation of new voltage and protection control strategies for distribution networks;
- Development and validation of the simulation models;
- Integration of additional storage devices into the overall power system operation. The impact on feeders with both PV and controllable loads will be simulated and tested.

2.5.4.1 Description of the Battery System Simulation Model Implementation

Computer models of power systems are widely used by power system utilities to study load flow, steady-state voltage stability and dynamic and transient behavior of power system.

For this project DigSILENT PowerFactory has been chosen because provides the ability to simulate load flow, RMS fluctuations and transient events in the same software environment. It provides a comprehensive library of models for electrical components in the power system.

The model of the VRB System is built with standard components from DigSILENT library. The models of the battery model, charge/discharge controller and P-Q controller of the Static Generator are implemented in the dynamic simulation language DSL of DigSILENT. DSL allows the user to implement specific models that are not standard in the DigSILENT library and thus to create own developed blocks either as modifications of existing models or as completely new models [29].

Fig. 2.61 shows the schematic structure of the model including Battery Model, charge/discharge controller, PLL block and Static Generator with its Controller. The VRB system frame also contains the measurements blocks, such as voltage, active & reactive power and frequency, used as inputs for different components of the model. The VRB Model has as outputs cell current and voltage and SOC level, which are the inputs for charge/discharge controller.

The VRB System model is implemented in PowerFactory using block diagrams and the internal simulation language DSL.

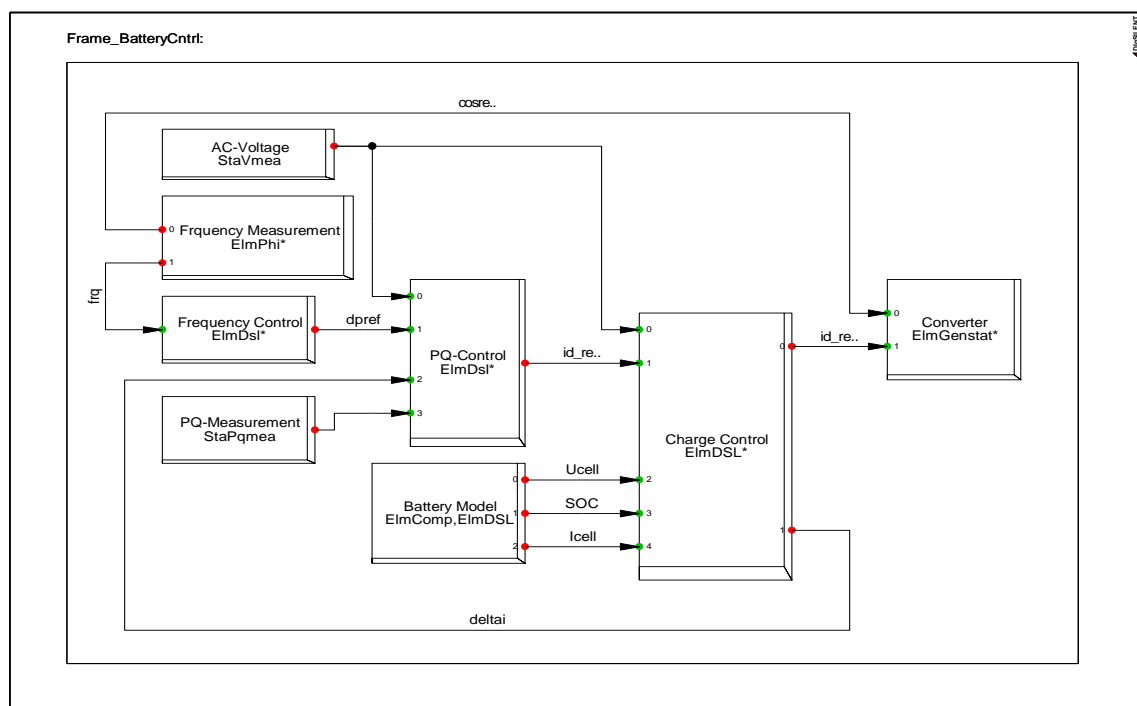


Fig. 2.61. Schematic block diagram of the Battery System.

Battery Frame Model

The battery model is implemented in PowerFactory using block diagrams to define the battery components and characteristics using the same approach as for MATLAB/Simulink implementation described in the last subchapter. The internal simulation language DSL was used to define the characteristics and to initialize the parameters and variables of the model. The model includes DC Side Calculation block and Battery Model and has as input the active power measured from the bus-bar at which the battery is connected and was implemented as a look-up table and the frame block has as outputs Ucell, SOC and ICell (Fig. 2.62).

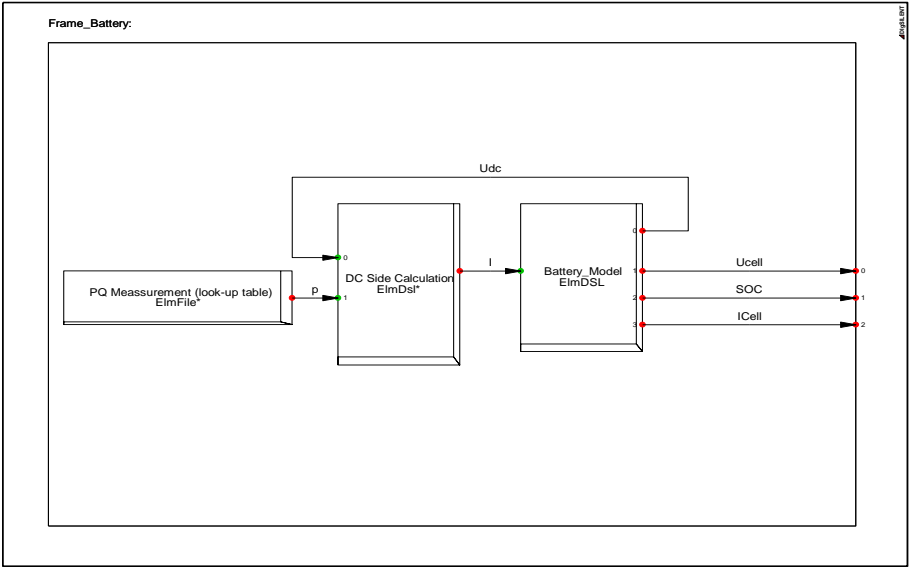


Fig. 2.62. The frame model of the battery implemented in PowerFactory.

Frequency Controller

The Frequency Controller is used in connection with PQ controller and it works only when the frequency will goes up after the limit. The model for Frequency Control has as inputs frequency reference and frequency measured from the bus bar where the battery is connected (Fig. 2.63) and contains a droop factor and a dead band which is added preventing excessive charging and discharging of the battery. This is desirable for improving the life time of the battery.

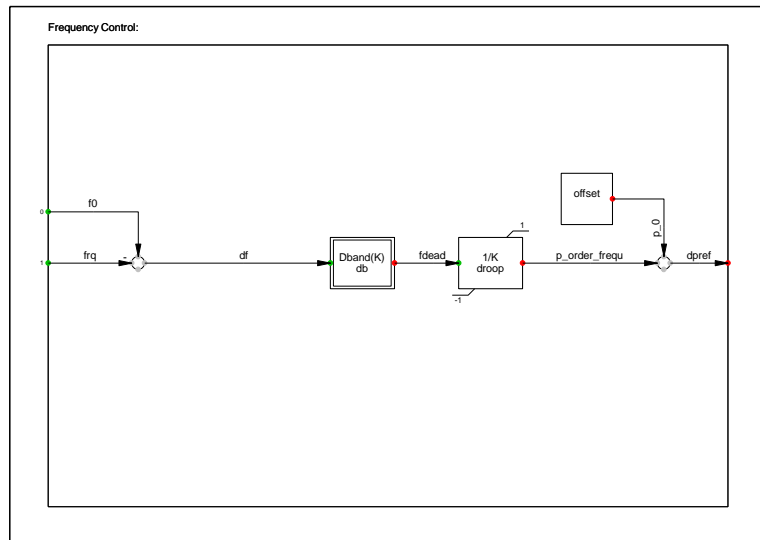


Fig. 2.63. Frequency controller with dead-band and droop factor.

Charge Controller

The charge/discharge controller is able to control the state of charge of the battery by controlling the currents. A current limiter block is used to limit the battery power within its maximum charging and discharging capabilities, as can be seen in Fig. 2.64.

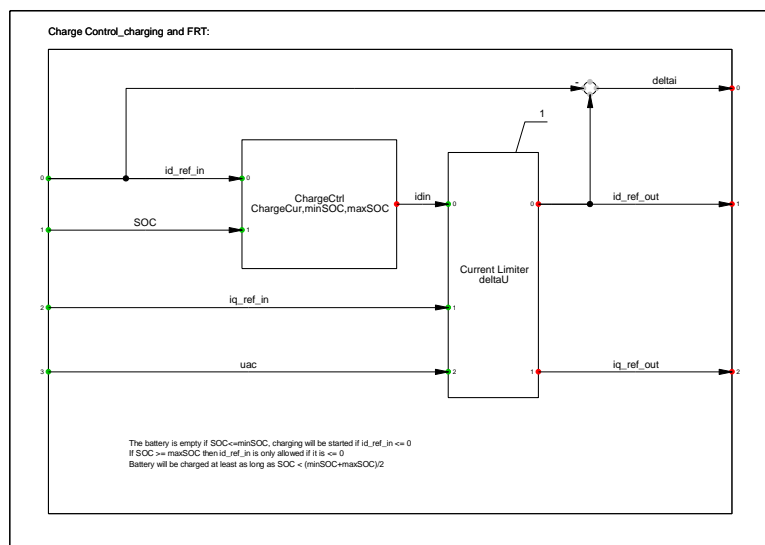


Fig. 2.64. Charging/Discharging controller with current limitation.

P-Q Controller

P-Q controller is used to provide and limit the i_d and i_q currents used as inputs to the static generator model to control the active and reactive power of the battery system.

The currents are controlled with a build in current controller defined in PowerFactory library, as it is depicted in Fig. 2.65.

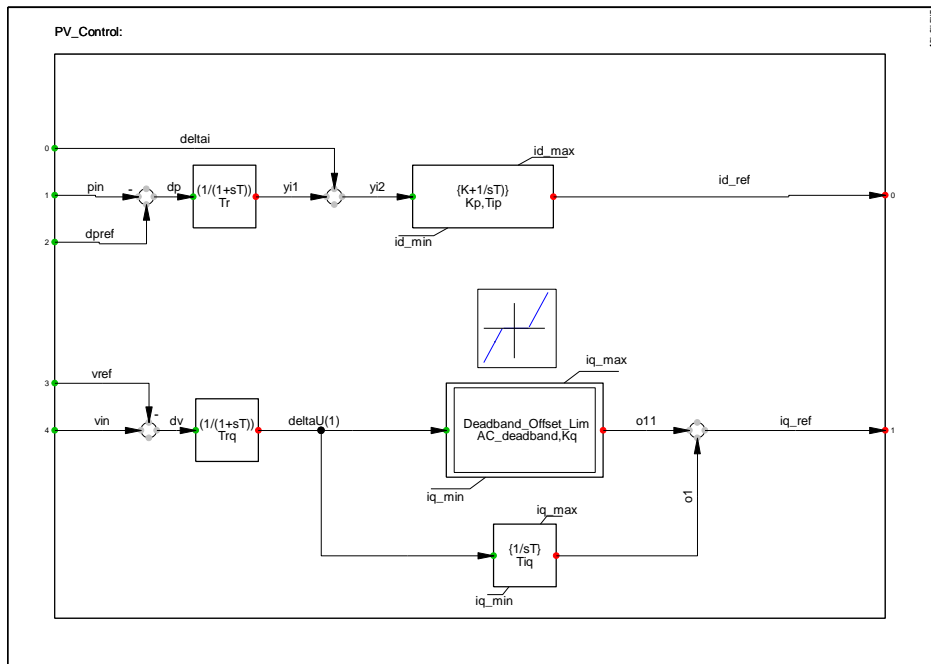


Fig. 2.66. P-Q controller used to regulate the currents.

Static Generator Model

The Static Generator is an easy to use model of any kind of static (no rotating) generators. Applications are PV Generators, Storage devices, wind generators etc.

For load flow analysis the local voltage controller could be set to three different modes: $\cos\phi$, V and droop. For RMS and EMT simulations the static generator supports two different models: current source and voltage source models.

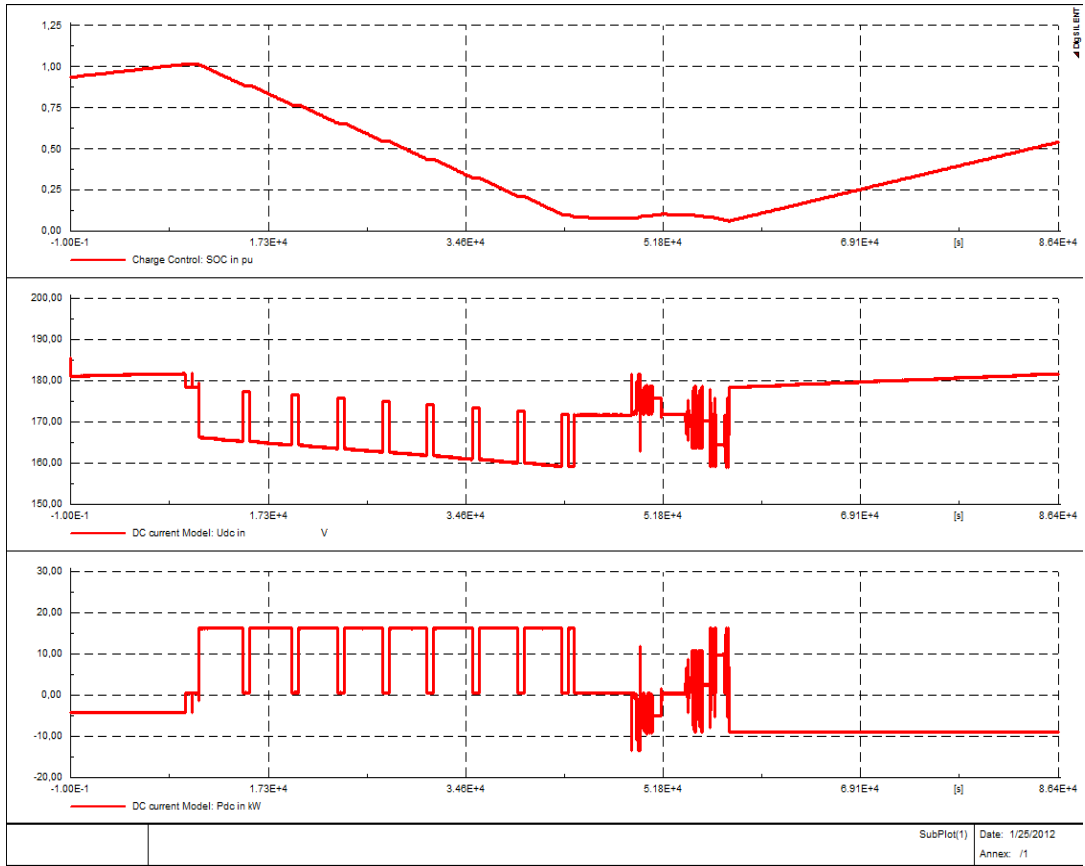
The static generator is equivalent with an ideal PWM converter able to control active and reactive power independently.

2.5.2 Simulation Results and Model Validation

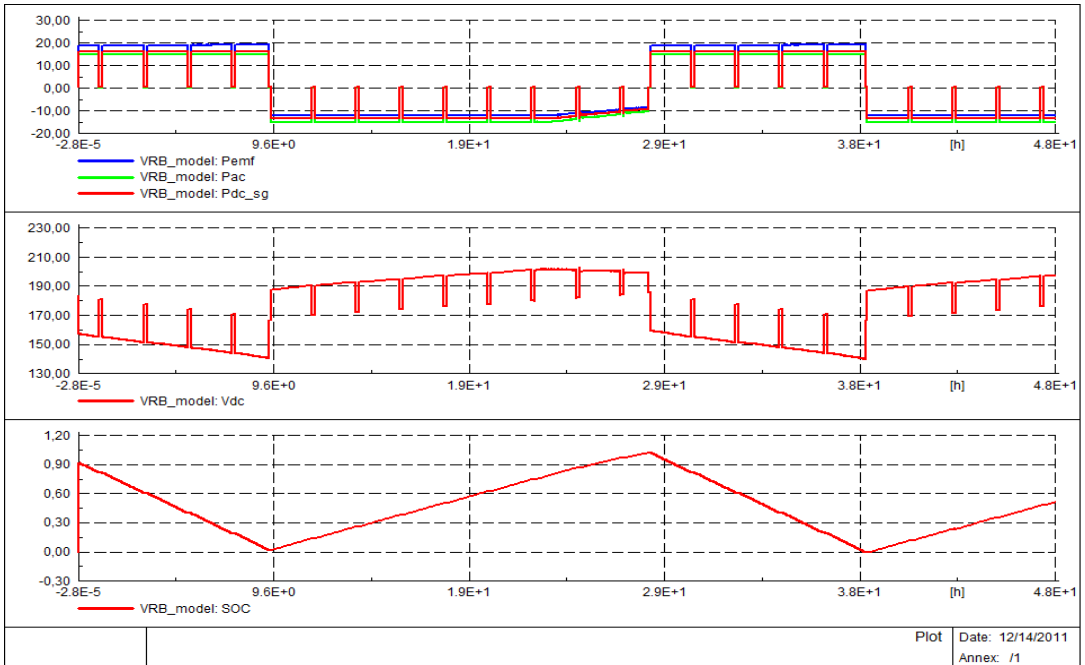
In order to validate the simulation model developed in PowerFactory and to compare the results with MATLAB-Simulink model, the same measurements have been used like in the last section when we compare the results of Simulink model with experiments (Figs. 2.67-2.68).

In Fig. 2.67 a set of simulations are presented pointing out the DC Voltage and Power of the battery (Fig. 2.67 a), and a comparison between DC and AC powers (Fig. 2.67 b), at different SOC levels. Also, comparing the simulation results, obtained with PowerFactory model (Figs. 2.68) and with MATLAB/Simulink model (Figs. 2.59-2.60), for different SOC levels, the results are similar.

To point out the accuracy of the simulation model developed in PowerFactory and to validate it in Fig. 2.68 is depicted a comparison between simulated and measured SOC level.



a)



b)

Fig. 2.67. Simulation results of the VRB system model during a few cycles of charging and discharging.

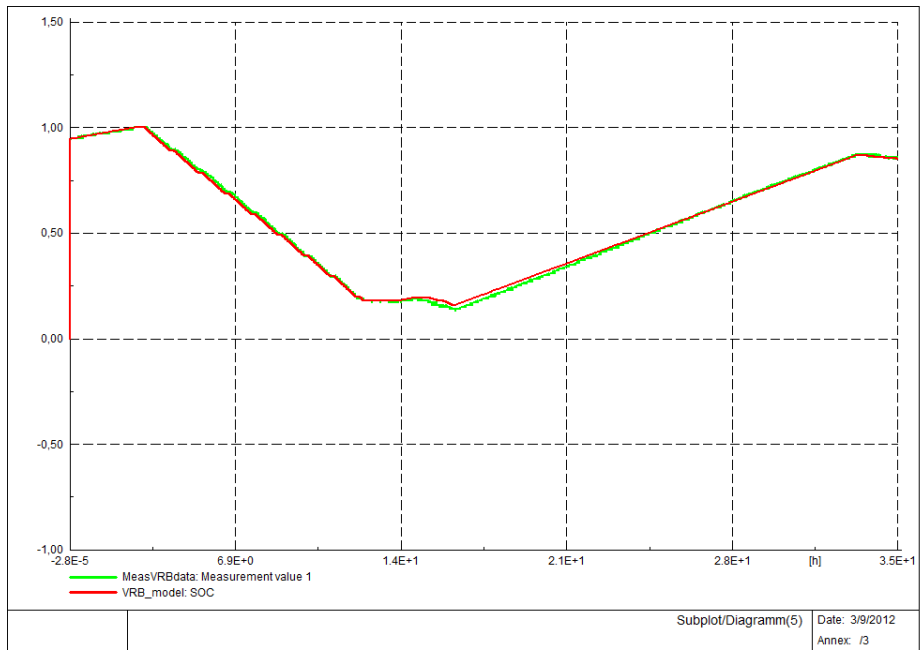


Fig. 2.68. Comparison between simulated and measured of SOC level.

2.6 Modeling, simulation and validation of an office building model

One of the components on the SYSLAB grid is a small, intelligent office building, Flex House. It contains seven offices, a meeting room and a kitchen. Each room is equipped with a motion detector, temperature sensors, light switches, window and door contacts and actuators. A weather station outside of the building supplies local environmental measurements of ambient temperature, wind speed, wind direction, and solar irradiation. The electrical load of the building consists of heating, lighting, air-conditioning, a hot-water supply and various household appliances, such as a refrigerator and a coffee machine. The combined peak load of the building is close to 20kW. All individual loads in the building are remote-controllable from a central building controller. The controller software runs on a Linux-based PC. It is also written in Java (TM) and is based on the SYSLAB software stack. The controller software consists of several modules, which are always working together. The hardware module collects data from the sensors and sends commands to the actuators. It does this via serial port (communication with the weather station), mod bus (switchboard instruments), and wireless transceivers (Enocean and infrared). The database module collects all sensor measurements and all commands sent to the actuators for further analysis. Another module collects data from external sources: the Nord Pool power price, the local weather forecast data, and some state information from the Danish power system. Finally, the controller module supports the development of any kind of controller algorithm for the Flex House. The controller can communicate with the SYSLAB grid through its own node computer (See Fig. 2.69). Information can also flow in the other direction, for example providing the power system supervisor controller with the expected near-future behavior of the building loads [26].

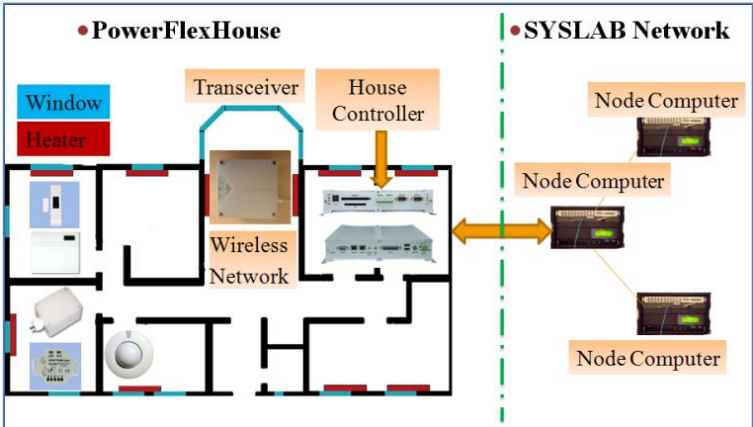


Fig. 2.69. Communication between Flex House and SYSLAB.

2.6.1 Flex House Modeling & Implementation

Flex House is an office building, operating as an active load in the SYSLAB distribution system. The building is heated by ten 1 kW electrical heaters which can be used as a controllable load in the system. The building is also rather old and has poor isolation which means that on sunny days it heats up more than in a modern building and on cold days it will lose heat quicker.

The heaters in the building are all connected to controllable relays which enable a central computer in the building to control the heaters. The central computer can be programmed with various control

strategies such as controlling the load after a price signal or by following local electricity production from the renewable energy sources in SYSLAB.

Mathematical model

The model for Flex house is formulated as a lumped RC-model in accordance with the commonly used thermal-electrical analogy. Figure 2.70 shows the heat flow diagram for the building and the equivalent RC-circuit.

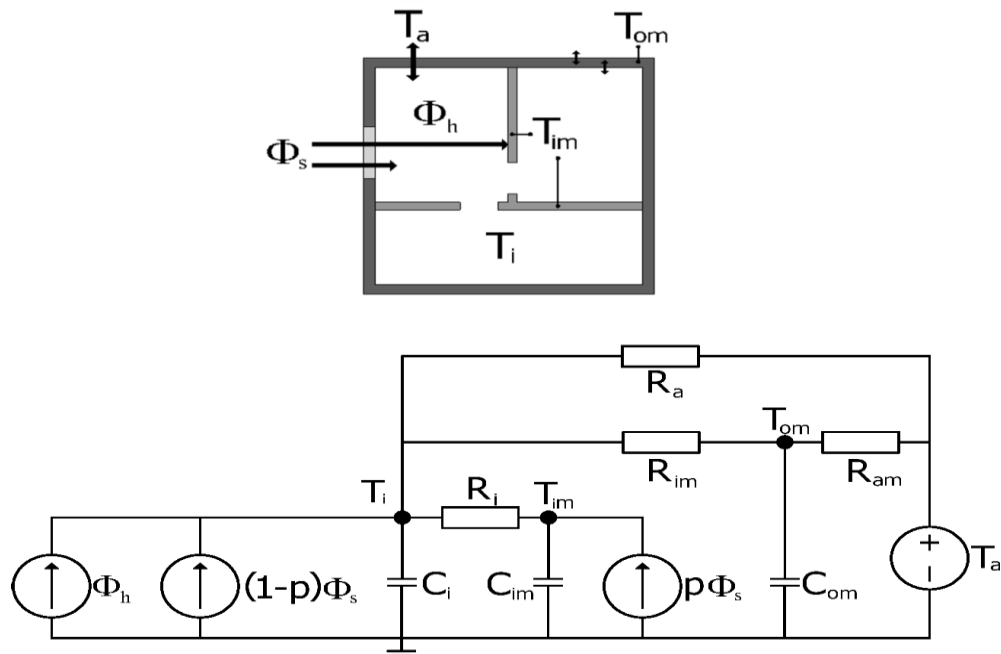


Fig. 2.70. FlexHouse single room RC-circuit model [36].

The model parameters are then derived from physical knowledge and experimental data is then used statistically to estimate the parameters in the model. Detailed description of the modeling work is found in [36].

Due to complexity of the heat flow in the building, approximations of the heat dynamics of the building have to be formulated:

The heat capacity of the house envelope, i.e. walls and floor, is concentrated in a thin layer inside the walls;

The heat capacity of the inner wall is concentrated in a thin layer inside the walls;

The toilet is assumed to be a part in the main room;

The temperature of the air is homogeneously distributed in the house;

The surface temperature of the walls is the same as in the heat accumulating layer;

The air-conditioners are assumed to be turned off;

Doors and windows are assumed to be closed;

The heat input from the heaters only affects the indoor air temperature;

The model parameters do not vary in time.

The model of heat dynamics of the building is formulated as one large room exchanging heat with an ambient environment.

Three time constants are needed to describe the heat flow in the building. Therefore three states are used to describe the development of the indoor temperature in the building. The first state is the indoor air temperature, T_i , the second state is the temperature of heat accumulating layer in the building envelope, T_{om} and the third state is the temperature in the heat accumulating layer in the inner walls and floor, T_{im} .

From [36] the following equation for the buildings stochastic linear state space model in discrete time is given as:

$$T(t+1) = \Phi T(t) + \Gamma U(t) \quad (2.46)$$

Where T is the state vector and U is the thermal input vector. The matrix Φ defines how the current state affects future states and the Γ matrix defines how thermal inputs influence the system.

To separate ambient inputs from the input from the heaters in the building the equation is rewritten to:

$$T(t+1) = \Phi T(t) + \Gamma_1 Z_A(t) + \Gamma_2 Z_B(t) + \Gamma_3 U(t) \quad (2.47)$$

The Γ matrix defining the thermal input influence is now split up so that the ambient inputs, T_A and G_s , can be separated from the input from the heaters in the building, U , T_A and G_s represent ambient input from outdoor temperature and solar radiation.

The matrices Φ and Γ are expressed like in [36]:

$$\Phi = \begin{bmatrix} 9,9288 \cdot 10^{-1} & 1,8661 \cdot 10^{-4} & 5,6429 \cdot 10^{-3} \\ 7,2489 \cdot 10^{-1} & 8,1923 \cdot 10^{-4} & 1,5641 \cdot 10^{-4} \\ 9,9649 \cdot 10^{-1} & 0 & 0 \end{bmatrix} \quad (2.48)$$

$$\Gamma_1 = \begin{bmatrix} 1,2844 \cdot 10^{-3} \\ 1,8592 \cdot 10^{-4} \\ 3,3551 \cdot 10^{-3} \end{bmatrix} \quad (2.49)$$

$$\Gamma_2 = \begin{bmatrix} 2,9990 \cdot 10^{-2} \\ 2,6053 \cdot 10^2 \\ 1,6128 \cdot 10^{-6} \end{bmatrix} \quad (2.50)$$

$$\Gamma_3 = \begin{bmatrix} 1,0226 \cdot 10^{-2} \\ 1,4838 \cdot 10^{-3} \\ 8,0402 \cdot 10^{-7} \end{bmatrix} \quad (2.51)$$

Equation (2.47) and the parameter matrices (2.48) – (2.51) make up the blocks needed to implement a model of Flex house in MATLAB/Simulink and Power Factory.

Implementation of the Flex House model in MATLAB/Simulink

The model contains 2 subsystems, a thermal model of the building, described by a Discrete State-Space System, and a controller model implemented using a state-flow chart, which is an interactive graphical design tool of Simulink for developing and simulating event driven system based on finite-state machine theory. A block diagram of the model implementation is presented in Fig. 2.71.

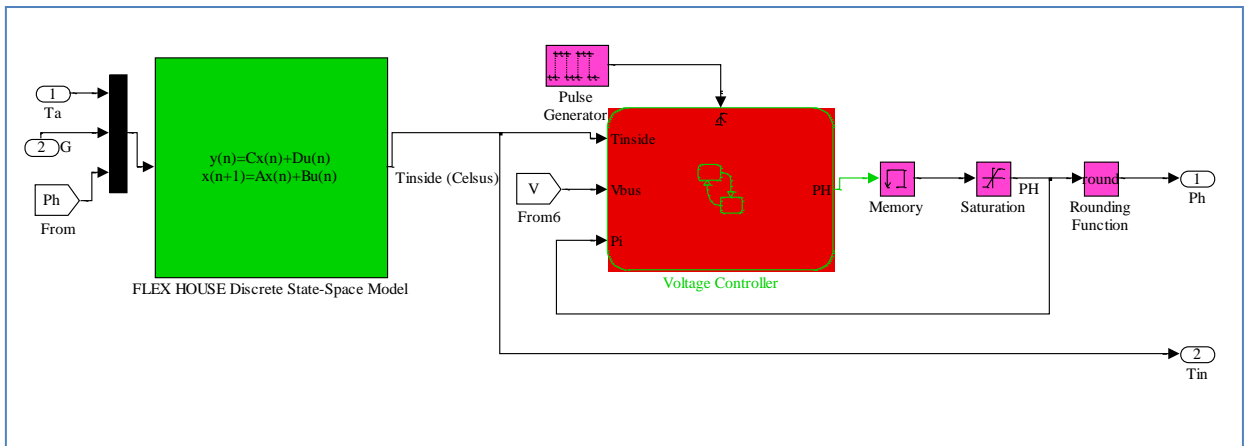


Fig. 2.71. Implementation of the Flex House model in Simulink.

The thermal model of the house is based on equation (2.47) and has as inputs ambient temperature (T_a), irradiation (G) and the power of the heaters (P_h), which is also an output parameter of the model. The voltage controller is based on equations (2.48)-(2.51) presented in the last subchapter and has as inputs the inside temperature, the power of the heaters and the voltage from the bus bar at which the active load is connected. The loads are represented only by the heaters and 1 kW modifies the voltage with $\pm 0.5\%$.

The voltage controller is a thermostatic control for the building, so that when the temperature inside the building is below a certain set point the heaters in the building turn on, and when the temperature is above another set point the heaters turn off. The controller was developed using a GUI of Simulink library called state flow chart, as can be seen in Fig. 2.72.

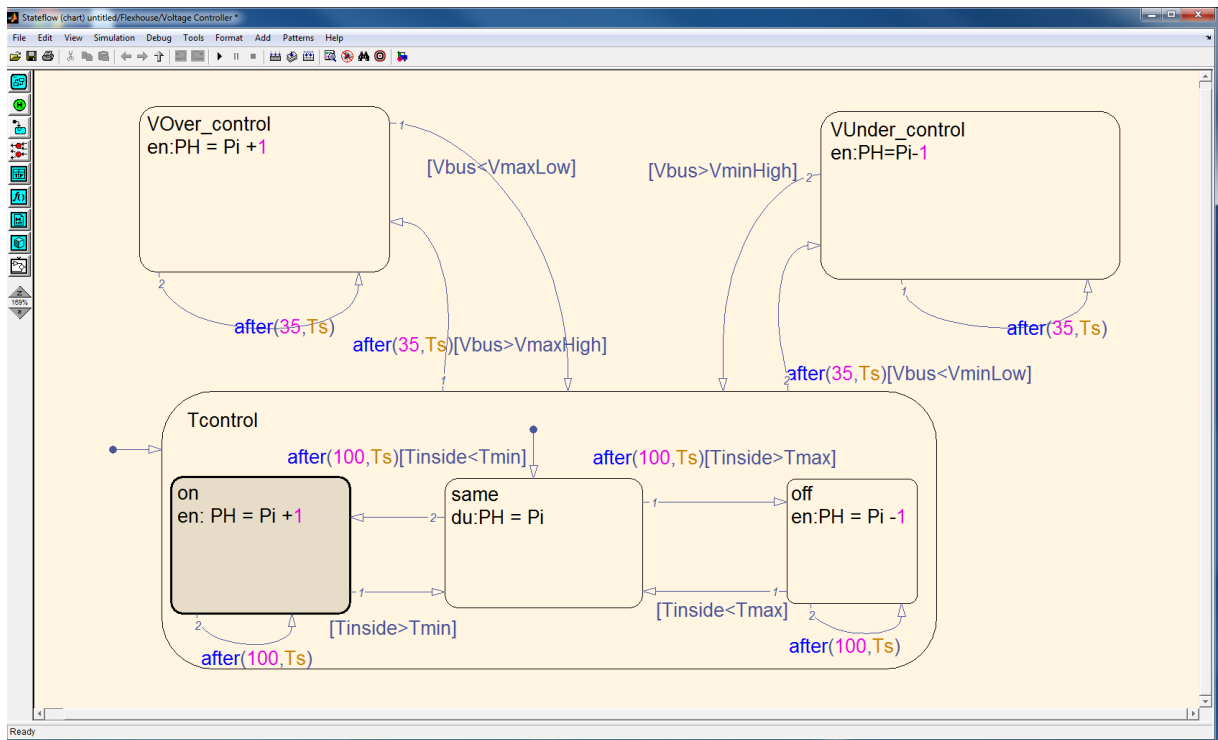


Fig. 2.72. Stateflow chart of the Flex House Voltage Controller.

DigSILENT PowerFactory implementation

The model is divided into four separate parts, a thermal model of the building, a controller model, a module to read input data and a load connected to a power system. The input values are measured ambient temperature and solar radiation. Figure 2.73 shows the block diagram of the building model. From the right the blocks are: input data reader, thermal model of the building, the building temperature controller and the power system load model.

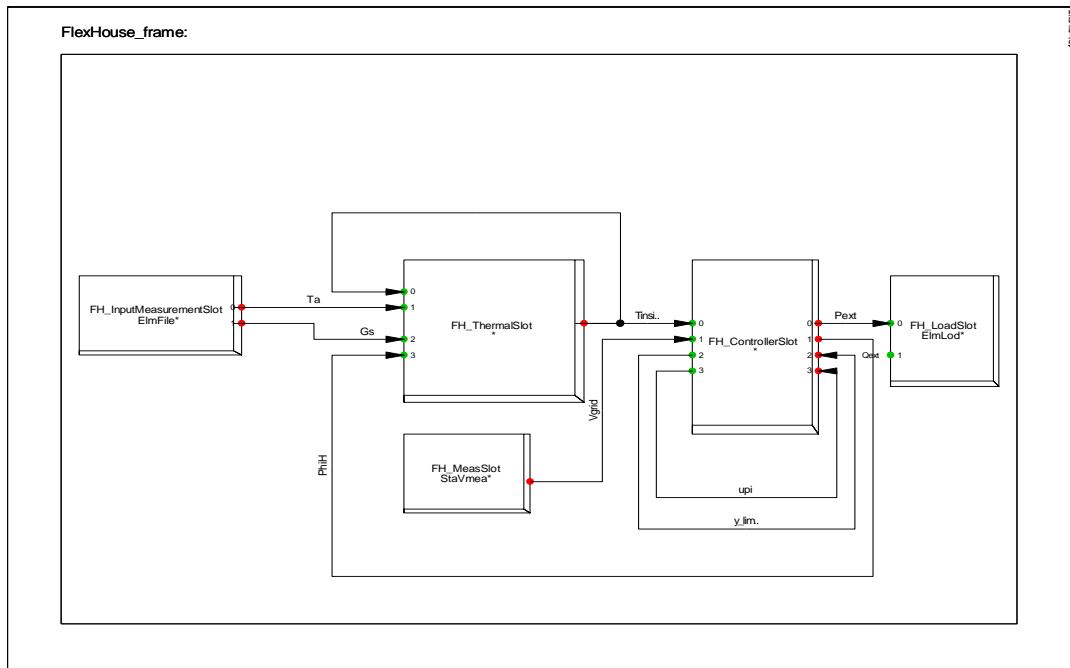


Fig. 2.73. PowerFactory implementation of the Flex House model.

The thermal model is based on equation (2) which in PowerFactory's DSL code becomes:

! OUTPUT SIGNALS: T_{1p} , T_{2p} , T_{3p}

! INPUT SIGNALS: T_1 , T_2 , T_3 , T_a , G_s , U

inc(T_{1p})=-2.3649+22; inc(T_{2p})=-14.2950+20; inc(T_{3p})=-4.2696+20

inc(T_1)=-2.3649+22; inc(T_2)=-14.2950; inc(T_3)=-4.2696; inc(U)=-2.6583

Phi11=0.99288613320715036; Phi12=0.00018660843264863363;

Phi13=0.0056429031579034094; Phi21=0.27410487038045089

Phi22=0.72488998040530539; Phi23=0.00081922792233383578

Phi31=0.00015641214518686284; Phi32=0.000000015459204224112224

Phi33=0.99648848346014673

GammaA11=0.0012843552018051694; GammaA12=0.029989926257748430

GammaA21=0.00018592127423841003; GammaA22=260.52940916962297

GammaA31=0.0033550889360424731; GammaA32=0.0000016127564591163370

GammaB11=0.010226000365209639; GammaB21=0.0014837683681845294

GammaB31=0.00000080402475834812924

$$T1p=Phi11*T1+Phi12*T2+Phi13*T3+GammaA11*(Ta+15)+GammaA12*(Gs+0)+GammaB11*U$$

$$T2p=Phi21*T1+Phi22*T2+Phi23*T3+GammaA21*(Ta+15)+GammaA22*(Gs+0)+GammaB21*U$$

$$T3p=Phi31*T1+Phi32*T2+Phi33*T3+GammaA31*(Ta+15)+GammaA32*(Gs+0)+GammaB31*U$$

The temperature control for the building is a simple thermostatic controller, so that when the temperature inside the building is below a certain set point the heaters in the building turn on, and when the temperature is above another set point the heaters turn off.

This controller is modelled in PowerFactory with the following DSL code:

```
inc(P_set)=0; T_max=21; T_min=19
X=flipflop(T_inside<T_min, T_inside>T_max)
Theater=select(X=1, 10, 0); P_set=select(X=1, 0.01, 0)
```

2.6.1.2 Simulation Results

Figure 2.74 shows a simulation of the temperature inside the building and the power consumption of the heaters for one day using measured temperature and solar radiation from SYSLAB as inputs of the model.

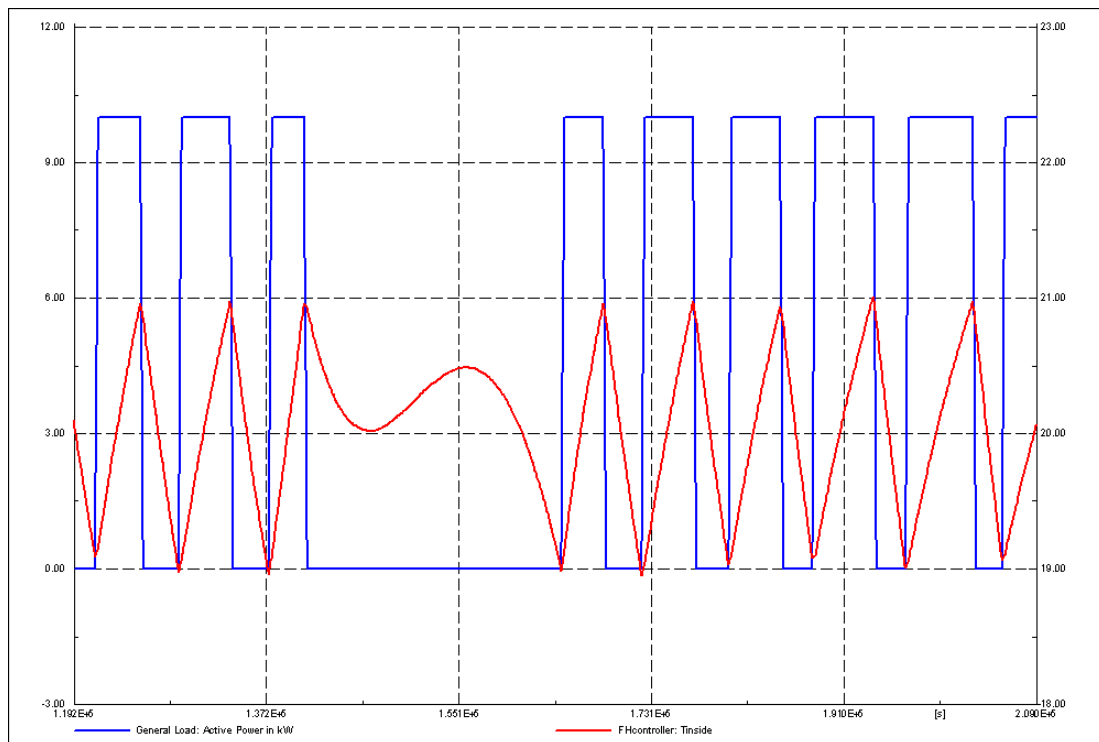


Fig. 2.74. Simulation results of the temperature inside the building (T_{inside}) and the power consumption of the heaters (Active Power) for one day.

2.7 Conclusion

This chapter was focus on development of tools for simulation components and systems that include PV panels and systems, Wind Turbine Systems, an electricity storage system - Vanadium Redox Flow Battery including its inverter system and a small office building with actively controllable loads.

The simulation models have been implemented in MATLAB/Simulink and DigSILENT PowerFactory and validated using experimental facilities of SYSLAB. The results show good alignment between simulations and measurements.

The second subchapter proposes a four-parameter model of a PV panel and a PV system, implemented in MATLAB/Simulink, using data provided by the manufacturer with semi-empirical equations to predict the PV characteristics for any condition. PV characteristics are modeled according to a single diode four parameter equivalent circuit and PV parameters values taken from the manufacturer technical data.

This subchapter also proposes a model that relies on ambient data from a local weather station, like most common in a real situation, not from sensors mounted on the PV panels. The model calculates the cell temperature and the solar irradiance on the PV panels considering, among others, the tilt angle, the orientation of the panels, and the wind cooling effect. The paper shows that these factors significantly influence the power output from the PV panels.

A PV system model, using the same equations and parameters as in MATLAB/Simulink to define the PV module and characteristics, has also been developed and implemented in PowerFactory to study load flow, steady-state voltage stability and dynamic behavior of a distributed power system. Comparing the simulation results developed and implemented in both tools we obtained the same results.

The models have also been validated against measurements using SYSLAB facilities. Comparison with experimental data, acquired by SCADA system and processed by MATLAB, and with the characteristics of the PV panels, provided by manufacturers, has shown that the models implemented in MATLAB/Simulink and PowerFactory can be an accurate tool for the analyses and the prediction of energy production.

In subchapter 3 a wind turbine model has been built to simulate the influence on the transient stability of power systems. The model of the wind turbine includes the wind fluctuation model, which will make the model useful also to simulate the power quality and to study control strategies of a wind turbine. The control scheme has been developed for turbine control including soft starter start-up, and power factor compensation.

The constant speed wind turbine has to be operated at the optimum tip speed ratio, which gives the maximum power transfer.

The comparative results between MATLAB-Simulink and DigSILENT show a good similarity during generator start-up and steady state performance. The computer simulations prove to be a valuable tool in predicting the system behavior.

The above-presented model can be a useful tool for wind power industry to study the behavior and influence of big wind turbines on power distribution networks.

In subchapter 5 has been presented the development of simulation tools for Vanadium Redox Flow Battery System. The models are based on the efficiency of different components and the power losses and have been implemented in MATLAB/Simulink and PowerFactory.

The simulation models were validated using experimental facilities of SYSLAB.

A voltage controller of the VRB system for overvoltage control has also been developed using a state flow chart and a PI controller. The main idea was to control the voltage at the local bus-bar, to maintain it under a maximum value due to the PV production, changing the battery mode of operation. Simulation results have shown that the controller has been designed and implemented successfully.

In this chapter/subchapter 6 a model of Flex House has also been presented and implemented in MATLAB/Simulink and PowerFactory. The house model contains 2 subsystems, a thermal model of the building, described by a Discrete State-Space System, and a controller model implemented using finite-state machine theory. The indoor temperature model of Flex House is given as a stochastic discrete-time linear state-space model, which was directly obtained from the reference [35]. The heat flow in Flex House is modeled by using physical knowledge about heat transfer together with statistical methods to estimate model parameters.

The voltage controller is a thermostatic control for the building, so that when the temperature inside the building is below a certain set point the heaters in the building turn on, and when the temperature is above another set point the heaters turn off. The idea was to keep the voltage under a certain level when the PV production increases, increasing the power of the heaters and the inside temperature of the house. Simulation results have shown that the controller has been designed, implemented and tested successfully.

Appendix

A1) OPERATIONAL DATA FOR PV PANEL FROM DATA SHEET

Parameter (unit)	Value	Description
for STC – solar irradiance (G_a)=1000W/m ² , cell temperature(T_c)=25°C, wind speed 1m/s		
P_{mpp} (W)	165	Rated output power
V_{mpp} (V)	24.2	Nominal voltage
I_{mpp} (A)	6.83	Nominal current
V_{oc25} (V)	30.4	Open circuit voltage
I_{sc25} (A)	7.36	Short circuit current
α (%/°C)	-0.478	Temperature coefficient for change in (P_{mpp})
β (%/°C)	0.057	Temperature coefficient for change in (I_{sc})
χ (%/°C)	-0.346	Temperature coefficient for change in (U_{oc})
δ (%/°C)	-0.004	Temperature coefficient for change in (I_{mpp})
ϵ (%/°C)	50	Temperature coefficient for change in (U_{mpp})
for NOCT – solar irradiance(G_{aNOCT})=800W/m ² , ambient air temperature(T_{aNOCT})=20°C, wind speed 1m/s		
NOCT (°C)	46.2	Cell temperature on the above mentioned conditions

A2) PV panel parameters from data sheet

Parameter name [unit]	Schuco S 165-SP Photovoltaic module	SOLEL SE100x Photovoltaic module
--------------------------	--	-------------------------------------

for STC – solar irradiance (G_a)=1000W/m², cell temperature(T_c)=25°C, wind speed 1m/s

P_{mpp} [W]	165	100
V_{mpp} [V]	24.20	16.90
I_{mpp} [A]	6.83	6.13
V_{oc} [V]	30.40	21.10
I_{sc} [A]	7.36	6.60
α (P_{mpp}) [%/°C]	-0.478	
β (I_{sc}) [%/°C]	+0.057	
χ (V_{oc}) [%/°C]	-0.346	
δ (I_{mpp}) [%/°C]	-0.004	
ϵ (V_{mpp}) [%/°C]	-0.474	
Number of cells	50	70

for nominal operation conditions (NOCT) – solar irradiance(G_{aNOCT})=800W/m², ambient air temperature(T_{aNOCT})=20°C, wind speed 1m/s

NOCT [°C]	46.2
-----------	------

A3) The equations and variables defined in PowerFactory using DSL code for PV array model:

```
!-----!
! Model of a Photovoltaic Module      !
! - Current Voltage Characteristic    !
! - Dependency of Solar Radiation,    !
```

! - Dependency of Module Temperature and irradiation !
!-----!

ModelI,Vmpp='PVModule'(U,G,tempCell;;U10,Umpp0,Imp0,Ik0,au,ai;U1,Ik,P,Umpp,Imp,Pmpp,c1,c2,c3,c4,tempCorrU,tempCorrI,lnEstc,lnEquot,E_help,ImpIk)

!vardef(U10) = 'V'; 'Open-circuit Voltage (STC)'
!vardef(Ik0) = 'A'; 'Short-circuit Current (STC)'
!vardef(Umpp0) = 'V'; 'MPP Voltage (STC)'
!vardef(Imp0) = 'A'; 'MPP Current (STC)'
!vardef(au) = '1/K'; 'Temperature correction factor (voltage)'
!vardef(ai) = '1/K'; 'Temperature correction factor (current)'

!vardef(U1) = 'V'; 'Open-circuit Voltage'
!vardef(Ik) = 'A'; 'Short-circuit Current'

!vardef(Umpp) = 'V'; 'MPP Voltage'
!vardef(Imp) = 'A'; 'MPP Current'
!vardef(Pmpp) = 'W'; 'Power at MPP'

!vardef(U) = 'V'; 'Voltage'
!vardef(I) = 'A'; 'Current'
!vardef(P) = 'W'; 'Power'

inc(G)=1000

! Constants

inc(lnEstc) = ln(1000) ! ln of E at STC

inc(ImpIk) = ln(1-Imp0/Ik0)

!-----

! Equations

! Temperature Dependency:

tempCorrU = 1+au*(tempCell-25) ! Voltage Correction Factor

tempCorrI = 1+ai*(tempCell-25) ! Current Correction Factor

! Open-circuit voltage:

E_help = max(G, 1.0) ! to avoid ln(0) in next equation

lnEquot = select(G>1.0, ln(E_help)/lnEstc, 0.0) ! ln(E)/ln(1000W/m²), if E > 1W/m²

U1 = U10*lnEquot*tempCorrU ! Open-circuit voltage dependent from E and theta

! Short-circuit current:

!Ik = Ik0*E/1000*tempCorrI ! Short-circuit current dependent from E and theta

Ik = select(G>1, Ik0*G/1000*tempCorrI, 0.0) ! Current generation only if E>1 (limitation of model)

! Maximum Power Point:

Umpp = Umpp0*lnEquot*tempCorrU ! MPP voltage dependent from E and theta

!Imp = Imp0*E/1000*tempCorrI ! MPP current dependent from E and theta

Imp = select(G>1, Imp0*G/1000*tempCorrI, 0.0) ! Current generation only if E>1 (limitation of model)

Pmpp = Umpp * Imp

! Voltage of MPP (output signal)

Vmpp = Umpp

! Current output and power calculation and internal variables:

c3 = 0.0

c4 = select(U1>0, Umpp - U1, 1.0) ! to avoid division by 0 in equation for c2

c2 = select(U1>0, select(c4<0, ImpIk/c4, 0.0), 0.0)

c1 = min(max(c2*(U-U1),-13),3)

! Current output (output signal)

I = max(Ik*(1-exp(c1)),0.0)

! Power: P = U * I

! Limits /

limits(U10) = (0,]; limits(Umpp0) = (0,]; limits(Imp0) = (0,]

limits(Ik0) = (0,]; limits(G) = [0,]

B1) VRB MODEL PARAMETERS

PARAMETER	VALUE
SERIES RESISTANCE, $R_s[\Omega]$	0.25
DC NOMINAL CURRENT, $I_{DC}[A]$	136
AC NOMINAL CURRENT, $I_{AC}[A]$	30
DC VOLTAGE(OPERATING RANGE), $V_{DC}[V]$	130-190
AC VOLTAGE(OPERATING RANGE), $V_{AC}[V]$	360-440
MAXIMUM OPERATING APARENT POWER, $S[kVA]$	20
MAXIMUM OPERATING ACTIVE POWER, $P[kW]$	20
MAXIMUM REACTIVE POWER, $Q[kVAR]$	12

Chapter 3:
Control Strategies Developed for
Renewable Energy Systems

Contents of the Chapter 3:

Control Strategies Developed for Renewable Energy Systems

Contents

Chapter 3:.....	94
Control Strategies Developed for.....	94
Renewable Energy Systems.....	94
3. Control Strategies developed for Renewable Energy Systems	96
3.1. Introduction.....	96
3.2. Dynamics of Control Strategies for Wind Turbine Systems	98
3.2.1. Control Strategies for Wind Turbines.....	98
3.2.2. Active Stall Constant-Speed Wind Turbines using Cage-Rotor Induction Generators.....	101
3.2.3. Control Design for a Variable-Speed Wind Turbine	103
3.2.4 Simulation Results	106
3.3. Control Strategies developed for Variable-Speed Wind Turbine Generators.....	110
3.3.1. Control Strategy of the DFIG based Wind Turbines	110
3.3.2. Control Strategies developed for Variable-Speed Wind Turbines with CRIG and implemented using a real-time digital platform	117
3.4. Control Strategies of DER Components in a Distribution Network.....	122
3.4.1. Voltage control by active power	122
3.4.1.1. Voltage Control by Load Shifting.....	123
3.4.1.2. Voltage Control using BESS	127
3.5. Discussion and Conclusion	132
5.5. Discussion and Conclusion	198

3. Control Strategies developed for Renewable Energy Systems

3.1. Introduction

Renewable energy systems are growing up due to not only environmental aspect but also due to social, economic and political interest. One of the main goals today in Europe energy policy is to increase the amount of renewable energy. For instance in Denmark the goal is to increase the amount of renewable energy to 30% of the total energy production in 2025 [18]. Last year, the Danish parliament approved an even more ambitious target: to have renewable supply 35 % of the country's total energy needs-not just electricity but also heating and transportation-by 2020, and an incredible 100 % by 2050 [19].

The European Union is aiming at a specific CO₂ reduction in the electricity sector in the near future (20 % reduction by 2020). This will involve a significant growth of PV installations all over Europe resulting in a few Giga watts of capacity [18-19].

Due to variable nature of power generation from Wind Turbines (WT) and Photo Voltaic (PV) Systems, storage systems and Demand-Side Management (DSM) and response as flexibility options gain particular importance for the secure and cost-efficient operation of power systems and best utilization of available WT and PV resources. These both options provide the shift in time which would help accommodate high penetration levels of PV in the system.

The wind energy industry has developed rapidly through the last 20 years. The development has been concentrated in main for grid connected wind turbines (wind farms) and their control strategies.

Small efficient wind turbines can also be used to supply private houses or farms in remote locations in developing countries where low-cost access to the electrical power grid is impractical [1, 5].

Due to the latest developments in power and digital electronics, the market for small distributed power generation systems connected to the domestic grid is increasing rapidly. Increased energy production at low wind speed (6-8 m/s), elimination of the capacitor bank necessary for magnetization, and the possibility for grid-connected and stand-alone operation modes can thus be achieved at the expense of a back-to-back converter with a flexible control [2-3].

The trend is that these systems should be able to work in stand-alone mode but also connected to isolated local loads/grid in parallel with others generators, such as other wind turbines, photovoltaic or diesel generators [1].

The variable speed wind turbines represent a new technology within wind power for large-scale applications and their models have to be set up for making power stability investigations. Therefore, this concept will be analyzed as follows.

An efficient way of controlling the voltage in a distribution network is to control the local power consumption at the bus-bar. The consumption can be influence by shifting load or using energy storage. The ability to control active units can reduce the stress on the low-voltage grid by consuming the PV/Wind production locally.

It is anticipated that new home appliances (e.g., Electric Vehicles (EVs) and Heat Pumps (HPs)), and embedded generations will be introduced to the power system. In addition, control strategies of various energy resources are going to be implemented in the current power system. To capture the behaviors of such elements, and to handle the correlation of behaviors in time, time series simulation is one of the key function that should be implemented in the future grid design. Moreover, it is of interest that how Smart Grid control strategies can be represented and how concurrent control of units is handled in the simulation tools.

This chapter, in the first part, gives an overview of the state of the art control strategies for large wind turbines using induction generators. An active stall constant speed wind turbine controller with its actuator system for variable pitch angle and a control strategy for a pitch controlled variable speed wind turbine are described. The simulation results of a 2 MW constant speed wind turbine using cage rotor induction generator (CRIG) with both passive stall control and an active stall control strategy are modelled, digitally simulated and compared. To evaluate the performance for an active stall constant speed wind turbine using CRIG versus a pitch controlled variable speed wind turbine using Doubly fed induction generator (DFIG), a set of simulations are performed for wind gusts at an average wind speed higher than the rated value.

Afterwards two different control strategies developed for variable-speed wind turbines using induction generators are described and implemented on a real-time digital platform. A doubly-fed induction generator of 11 kW fed by a vector controlled back-to-back PWM-VSI inverter on the rotor side and a cage rotor induction generator of 11 kW rating with a vector controlled back-to-back PWM-VSI inverter on the stator side have been tested and the results compared with digital simulations. The variable-speed wind turbine generator system with a vector controlled back-to-back PWM-VSI on the stator side has also been modeled, designed and simulated to study its steady state and dynamic behavior. The grid connection control mode of a wind turbine based on a flexible dSPACE digital signal processor system that allows user-friendly code development, monitoring and online tuning is used.

In the last part of this chapter two different types of voltage controllers in a distribution grid using active loads/office building appliances and battery energy storage systems have been implemented and tested successfully. Using the model of the office building a controller for load shifting has been developed. The controller uses the electrical heaters in the office building to either reduce or increase the local grid voltage turning the heaters on or off respectively. The thermal capacity of the building is used to buffer the energy and the indoor temperature is the restraint limiting the durations of the voltage control actions. Two types of controllers for voltage regulation using battery energy systems have been developed and implemented in MATLAB/Simulink and DigSILENT PowerFactory based on finite state machine for controlling the bus-bar voltage at the connecting point. One controller is able to control the voltage at the bus-bar charging the battery when an overvoltage is detected. Another method of controlling the voltage with the help of storage energy systems is to set the battery (VRB) to run in schedule mode. That means the battery is scheduled to operate during the day in function of the weather conditions (PV penetration) and the voltage measurements. In the end, the experiences are discussed and summarized in the last section.

This work made in chapter 3 has been funded by 3 international EU grant/projects: "Smart Modelling of Optimal Integration of High Penetration of PV-Smooth PV", PV ERA NET and partial by the ForskEL "Smart Plan" project 55807 and by POS_CCE-SEE-RO 018, „Improvement of the structures and

efficiency of small horizontal axis wind generators with non-regulated blades". Also, this chapter is based on our papers, developed in national and international partnerships and collaborations, and published in International Journals and Conference Proceedings highlighted in Part III of this thesis, to the end of each reference list.

3.2. Dynamics of Control Strategies for Wind Turbine Systems

Conventional stall wind turbines are equipped with cage rotor induction generators [1-2], in which the speed is almost constant, while the variable speed and variable pitch wind turbines use doubly-fed induction generators or synchronous generators in connection with a power converter (partial rate or full rate) [1-4]. The variable speed wind turbine has a more complicated electrical system than the fixed-speed wind turbine [3], but it is able to achieve maximum power coefficient over a wide range of wind speeds and about 5-10 % gain in the energy capture can be obtained.

The aim of a wind turbine controller is to ensure that the wind turbine is able to produce energy at the lowest possible cost (minimum price per kWh) [1-4]. The cost of wind-generated electricity has declined about 90 % over the last 20 years. Today, large new wind farms at excellent wind sites generate electricity at a cost of 0.04 to 0.06 US dollars / kWh [5]. That places the cost of power from the most efficient wind farms in a range that is competitive with that of electricity from new conventional power plants.

The goal of this subchapter is to give an overview over the state of art in wind turbines control strategies and to evaluate their performance using two different software packages, MATLAB/Simulink and DIgSILENT PowerFactory.

3.2.1. Control Strategies for Wind Turbines

A) Pitch Controlled Wind Turbines

On a pitch controlled wind turbine the electronic controller checks the output power of the turbine several times per second. When the output power becomes too high, it sends an order to the blade pitch mechanism which immediately pitches (turns) the rotor blades slightly out of the wind [12]. Conversely, the blades are turned back into the wind whenever the wind drops again. The rotor blades thus have to be able to turn around their longitudinal axis (to pitch). During normal operation the blades will pitch a fraction of a degree at a time - and the rotor will be turning at the same time. Designing a pitch controlled wind turbine requires some clever engineering to make sure that the rotor blades pitch exactly the amount required.

The pitch mechanism is usually operated using hydraulics or electric stepper motors [1, 2 and 4]. As with pitch control it is largely an economic question whether it is worthwhile to pay for the added complexity of the machine, when the blade pitch mechanism is added.

B) Stall Controlled Wind Turbines

Stall controlled (passive stall controlled) wind turbines have the rotor blades bolted onto the hub at a fixed angle. The geometry of the rotor blade profile however has been aerodynamically designed to ensure that the moment when the wind speed becomes too high [2, 6]; it creates turbulence on the side of the rotor blade which is not facing the wind. This stall prevents the lifting force of the rotor blade from acting on the rotor. As the actual wind speed in the area increases, the angle of attack of the rotor blade will increase, until at some point it starts to stall. If you look closely at a rotor blade for a stall controlled wind turbine you will notice that the blade is twisted slightly as you move along its longitudinal axis. This is partly done in order to ensure that the rotor blade stalls gradually rather than abruptly when the wind speed reaches its critical value [12].

The basic advantage of stall control is that one avoids moving parts in the rotor itself, and a complex control system. A normal passive stall controlled wind turbine will usually have a drop in the electrical power output for higher wind speeds, as the rotor blades go into deeper stall. On the other hand, stall control represents a very complex aerodynamic design problem, and related design challenges in the structural dynamics of the whole wind turbine, e.g. to avoid stall-induced vibrations.

C) Active-Stall Controlled Wind Turbines

An increasing number of larger wind turbines (1 MW and more) are developed with an active stall power control mechanism. Technically the active stall turbines resemble pitch controlled turbines, since they have pitch able blades. In order to get a reasonably large torque (turning force) at low wind speeds, the wind turbines will usually be programmed to pitch their blades much like a pitch controlled wind turbine at low wind speeds [4]. (Often they use only a few fixed steps depending upon the wind speed).

When the turbine reaches its rated power, however, it will notice an important difference from the pitch controlled wind turbines: If the generator is about to be overloaded, the turbine will pitch its blades in the opposite direction from what a pitch controlled wind turbine does. In other words, it will increase the angle of attack of the rotor blades in order to make the blades go into a deeper stall, thus wasting the excess energy in the wind.

One of the advantages of active stall is that one can control the power output more accurately than with passive stall, so as to avoid overshooting the rated power of the turbine at the beginning of a gust of wind [4, 6]. Another advantage is that the wind generator can be run almost exactly at rated power at all high wind speeds.

D) Rotor Efficiency under Stall and Pitch Controlled Wind Turbines

The output power of wind turbines varies with wind speed, but is not proportional to it, as the energy that the wind contains increases with the cube of the wind speed. At low wind speeds (1-3 m/s), wind turbines are shut down, as they would be able to generate little or no power (Fig. 1). Wind turbines only start up at wind speeds between 2.5 and 5 m/s, known as the “cut-in” wind speed. “Nominal” or “rated” wind speed, at which nominal output power is reached, is normally between 12 and 15 m/s.

The precise value depends on the ratio of generator capacity to rotor surface area, and is a design variable. Finally, any wind turbine has a “cut-out wind speed”: this is the wind speed at which

the turbine is shut down to avoid structural overload. Its value is around 25 m/s for IEC Wind class I and II turbines [4]. For IEC Wind Class III turbines, which generate maximum output power at lower wind speeds, the cut-out value is in the range of 17-20 m/s. Wind turbines are shut down if the 10-minute average of the wind speed is above this design value. Below nominal wind speed, the aim is to maximize rotor efficiency (Fig. 3.1).

The rotor efficiency depends on the ratio of the rotor blade tip speed and wind speed, known as the “tip speed ratio” (λ), described by:

$$\lambda = \omega_{rot} \cdot R / u_{eq} \dots\dots\dots(3.1)$$

Where R represents the radius of wind turbine rotor blades, u_{eq} -equivalent wind speed and ω_{rot} denotes the turbine rotor speed.

The tip speed ratio of a fixed speed wind turbine cannot be controlled, as the rotor speed (and thus the blade tip speed) is fixed. Nevertheless, the tip speed ratio varies with wind speed, and thus reaches the optimum value at one wind speed only in case of fixed speed designs (or at two speeds if the wind turbine can operate at two different, but constant, rotor speeds), [4, 6, 7].

With a variable speed wind turbine, the tip speed ratio varies, and depends both on wind speed and rotor speed. For maximum rotor efficiency, the tip speed ratio must be maintained at the value that corresponds to optimum rotor efficiency (usually 6-9) at all times. This is achieved by controlling the rotor speed accordingly. The higher aerodynamic efficiency that is thus achieved explains why a variable speed turbine generates more energy for the same wind speed regime.

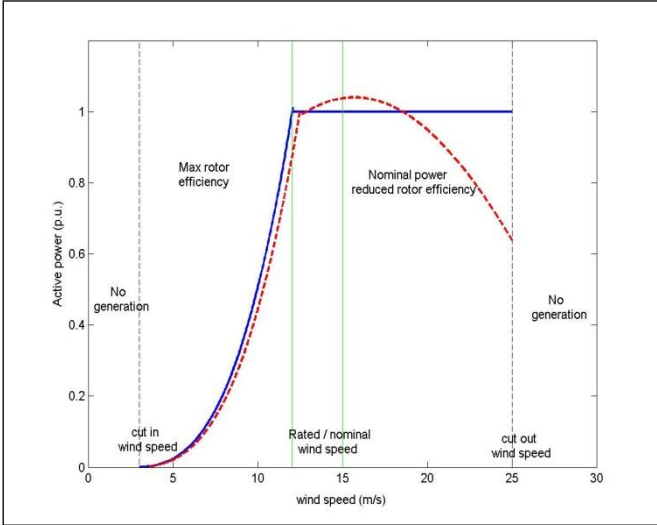


Fig. 3.1. Typical power curves and operation areas of a stall (dashed line) and pitch controlled (solid line) wind turbines [7].

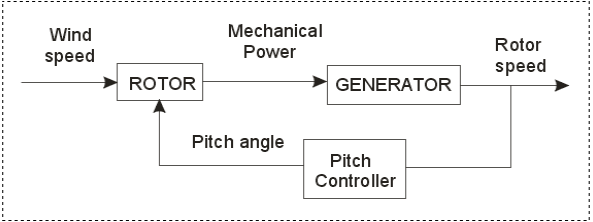


Fig. 3.2. Rotor speed control principle for wind speeds above nominal.

At wind speeds below nominal, the aim is to extract energy from the wind as efficiently as possible; however, this ceases to apply above nominal wind speed, as this would overload the generator and/or the converter system. Above nominal wind speed, therefore, the mechanical power extracted from the wind must remain constant. To achieve this, the aerodynamic rotor efficiency must be reduced when the wind speed increases, as can also be seen in Fig. 3.1.

In a stall controlled wind turbine, the blades are designed such that the rotor efficiency “collapses” at high wind speeds. Due to the blade design, this behavior is intrinsic, and no active control systems are required to achieve the aerodynamic efficiency reduction. In a pitch controlled wind turbine, the blades are gradually turned out of the wind, so the wind impact angle changes and the aerodynamic efficiency is reduced. In this case active stall control is applied, by means of hydraulics or an electric drive system. The input variable for the pitch controller is the rotor speed, as it is depicted in Fig. 3.2. The higher the rotor speed, the more the blades are turned out of the wind. The blades are turned back into the wind when the rotor speed falls. In general, fixed speed turbines use stall control for technical reasons, while variable speed turbines are usually equipped with pitch control [7, 9].

A relatively recent innovation in 2000 was the active-stall concept. This is similar to normal stall power limitation, except that the whole blade can be rotated backwards (in the opposite direction as is the case with pitch control) by a few (3-5) degrees at the nominal speed range in order to give better rotor control. The application of this concept is more or less restricted to fixed speed turbines. Typical active-stall representatives are the Danish manufacturers Bonus (1 MW and over) and NEG Micon (now Vestas) (1.5, 2 MW and over) [4-5, 10-11].

The difference from active pitch control is not only that the range of blade angle variation is less, but also that the direction of the variation is opposite.

All what follows refers basically to two 2 MW wind generator systems using induction generators with the data in appendix.

3.2.2. Active Stall Constant-Speed Wind Turbines using Cage-Rotor Induction Generators

A common control concept for new megawatt-size wind turbines/wind farms without power electronic converters is the active stall regulation. An active stall wind turbine is a stall controlled turbine with variable pitch angle. At high wind speeds, the pitch angle is adjusted to obtain the desired rated power level. When connecting the wind generator to the grid, the pitch angle is also adjusted in order to obtain a smooth connection. The use of active stall control also facilitates the emergency stopping of the turbine.

The control strategy called active stall constant speed involves the combined interaction between wind model, pitch control and the aerodynamics of the wind turbine [4], as can be seen in Fig. 3.3.

The blade angle control block models the active stall control of the wind turbine, based on the measured power and the set point, where rotational speed is the controlled variable [4, 10 & 11].

The most used electrical generator of an active stall constant speed turbine is a cage rotor induction generator connected to the grid through a soft starter, as can be seen in Fig. 3.3.

A clear difference between stall and active stall controlled wind turbines is a pitch actuator system for variable pitch angles, which allows the stall effect to be controlled, as can be seen in Fig. 3.4.

The model of the pitch control system [4], is based on the measured generator power (P_m) and the aerodynamic power of wind turbine as a function of measured wind speed (v_{wind}) at different pitch angles.

The measured power is compared with its reference (P_{ref}) and the error signal (P_{err}) multiplied by pitch angle of power control ($f_1(v_{av})$) is sent to the PI-controller producing the pitch angle demand (θ_{dp}), which together with maximum pitch angle-upper limit (θ_{max}) are sent to the pitch limitation non-linear block producing the reference value of the pitch angle (θ_{ref}).

The reference value is in the range between the optimized pitch (θ_{dp}) and the maximal pitch angle ($\theta_{max}=90^\circ$). The maximum value is defined as a function of average wind speed ($f_2(v_{av})$). The reference value is, further, compared to the actual pitch angle (θ_{pitch}) and the error signal (θ_{e2}) is corrected by the pitch hydraulics.

This control strategy takes its origin in the power coefficient curves $C_p(\theta, u)$ [4], typical for a 2 MW constant speed wind turbine, as it is shown in Fig. 3.5.

C_p represents the rotor efficiency of the wind turbine and depends on the pitch angle ϑ and on the tip speed ratio λ . For a constant speed wind turbine, the power coefficient C_p decreases when the wind speed increases (λ small), as can also be seen in Fig. 3.5.

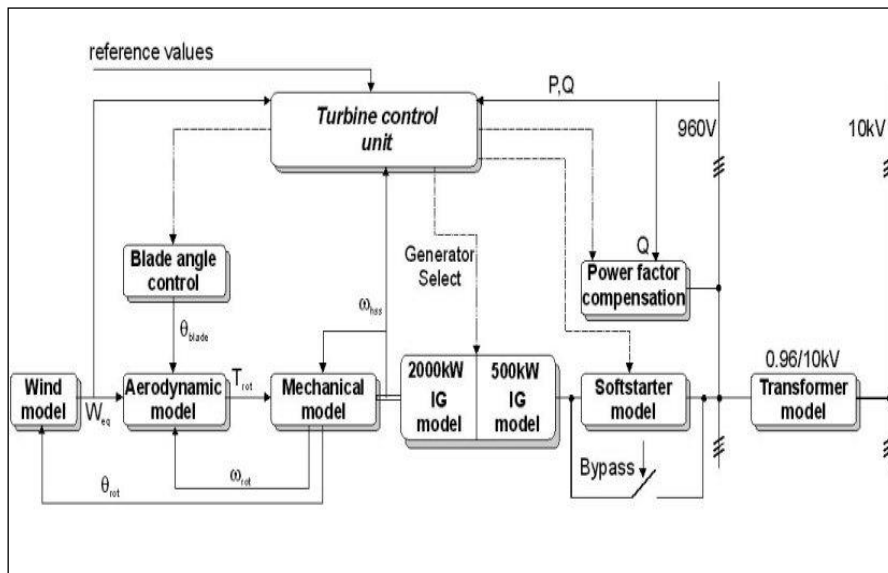


Fig. 3. 3. Block diagram of an active stall constant speed wind turbine.

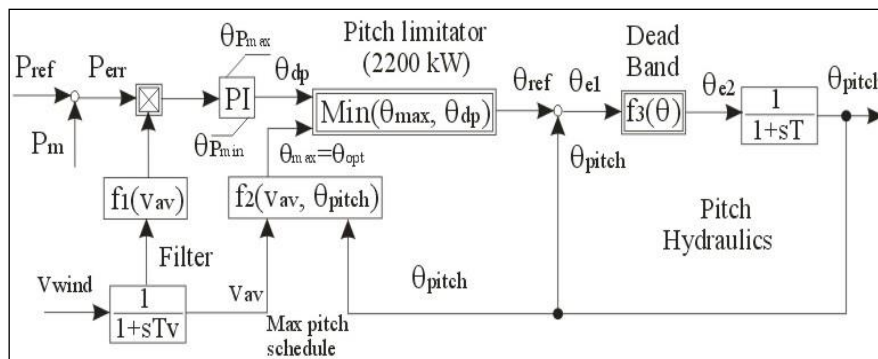


Fig. 3.4. The block diagram of blade pitch angle control system.

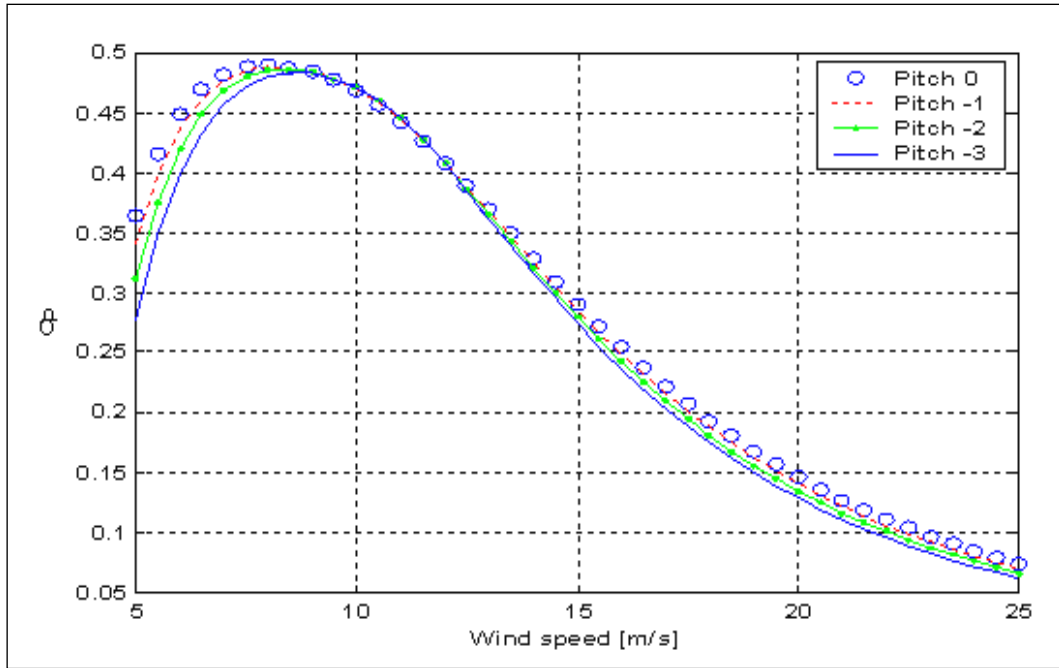


Fig. 3.5. Power coefficient (C_p) of a 2MW constant speed wind turbine versus wind speed for different pitch angles, used in the blade pitch angle control system.

The aerodynamic power is calculated according to:

$$P_{aero} = \frac{1}{2} \rho \pi R^2 u_{eq}^3 C_p(\lambda, \theta_{pitch}) \dots (3.2)$$

In order to achieve maximum power yield for each wind speed the maximal C_p and the corresponding ϑ has to be found. In fact, the control strategy is characterized by two terms: the optimal region and the power limiting region. In the optimal region (between start-up wind speed and nominal wind speed), the output power is designed to fulfil the criterion of maximal C_p , which corresponds to the optimal energy capture, by keeping the tip speed ratio (λ) constant. In the power limiting region (between nominal wind speed and cut-out wind speed), the output power is kept constant, while the wind turbine will pitch the blades a few degrees every time when the wind changes in order to keep the rotor blades at the optimum angle. When the wind turbine reaches its rated power, and the generator is about to be overloaded, the turbine will pitch its blades in the opposite direction. In this way, it will increase the angle of attack of the rotor blades in order to make the blades go into a deeper stall, thus wasting the excess energy in the wind.

3.2.3. Control Design for a Variable-Speed Wind Turbine

Figure 6 presents the control system of a variable-speed wind turbine with DFIG. The control system contains two control levels: the DFIG control level, with a fast dynamic response, and the wind turbine control level, with a slow dynamic response.

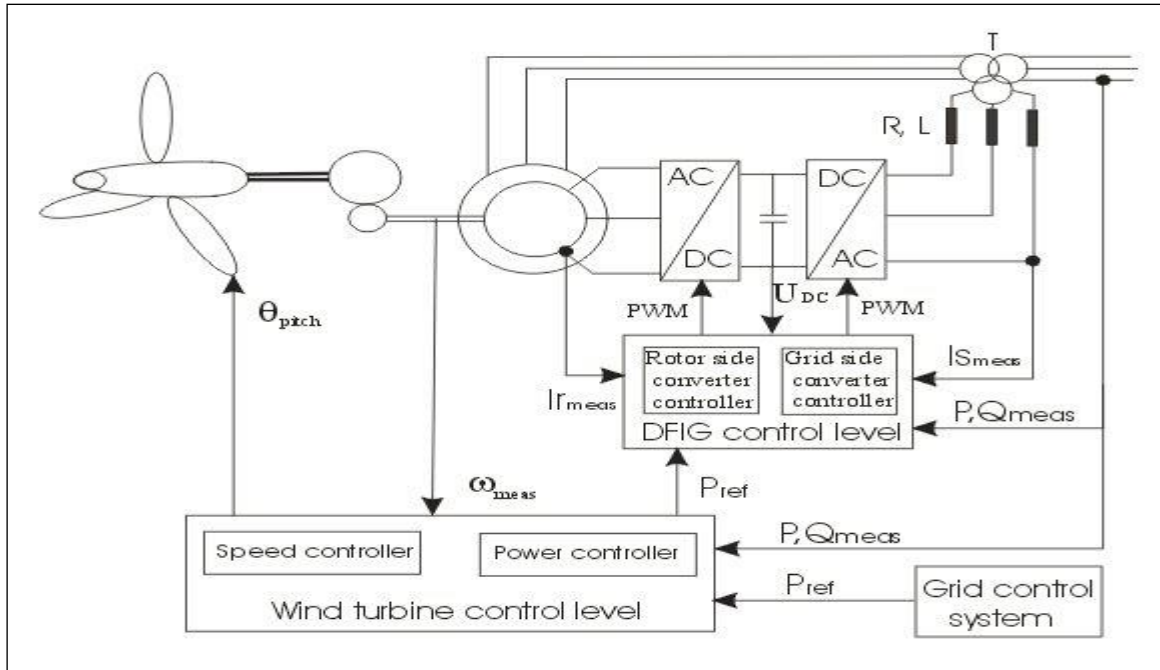


Fig. 3.6. The block diagram of the Controls' system of a variable-speed wind turbine with DFIG fed by a back-to-back VSI.

A doubly-fed induction generator (DFIG) is a standard wound-rotor induction machine with the stator windings directly connected to the grid and with the rotor windings connected to a back-to-back partial scale frequency converter. The frequency converter consists of two independent converters connected to a common dc-bus. The behavior of the generator is governed by these converters and their controllers. The DFIG control level contains two controllers: the rotor side converter controller, which controls independently the active and reactive power on the grid and the grid side converter controller, which controls the DC link voltage and maintains unity power factor. The rotor side converter controller contains an independent cascade control branches, one for active power control and the other for reactive power control, controlled indirectly by controlling the impressed rotor currents [3, 4, 6]. The DFIG model is expressed in the rotor reference frame and the rotor side converter controller is expressed in the stator flux reference frame. The control of rotor side converter is based on the stator flux oriented rotor current control approach, where the rotor current is split into a parallel and orthogonal component to the stator flux. It contains two control loops in cascade: a slower (outer) power control loop and a fast (inner) rotor current control loop [4]. The parameters of the PI controllers in the rotor side converter, for the 2 MW machine investigated are: $K_p=0.1$ and $T_i=0.1$ (for the power controller) and $K_p=1$ and $T_i=0.01$ (for the current controller). The control of the grid side converter also contains two control loops in cascade, a slower (outer) dc-voltage control loop, which regulates the dc link voltage to a predefined value, and a fast (inner) converter current control, which regulates the converter current to the reference value specified by the slower dc-voltage controller [3]. Similarly to the rotor side converter, the grid side converter is current regulated. The dc-voltage and the reactive power are controlled indirectly by controlling the grid side converter current. The parameters of DC-link voltage controller are $K_p=0.35$ and $T_i=0.02$, while the parameters of converter current controller are $K_p=4.8$ and $T_i=0.08$.

The wind turbine control provides reference signals both to the pitch system of the blades and to the DFIG control level. It contains two controllers: speed controller, which controls the generator speed at high wind speeds and maximum power tracking controller, which generates the active power reference signal for the active power control loop.

This reference signal is determined from the electrical power versus generator speed characteristic (Fig. 3.7), taken from a look-up table. This characteristic is based on aerodynamic data of the wind turbine’s rotor and its points correspond to the maximum aerodynamic efficiency. Up to 8.5 m/s with a tip speed ratio of around 8.7 (optimum), the rotor speed is proportional to the wind speed (lower part of the curve up to 800 kW/1500 rpm-Fig. 3.7).

From 8.5 m/s to 12 m/s (rated) the rotor speed is controlled until the rated power of 2 MW at 1580 rpm is reached. If the turbine accelerates to above 1580 rpm, due to the wind speed above rated value, the generator power is kept constant at the rated value (2 MW) by the power limitation controller, while the speed controller it takes no action (there is no longer any control of the generator speed). Both the speed controller and the maximum power-tracking controller are active in the power limitation strategy, while only maximum power tracking controller is active in the optimization power strategy.

Figure 3.8 shows the speed controller, the maximum power tracking one and the rotor side and grid side converter controllers. All these controllers, except maximum power tracking controller, contains PI-controllers with anti-windup. Both the speed controller and the maximum power tracking have as input the filtered measured generator speed. The generator speed is measured and then a low-pass filter is used. The pitch angle controller is also developed, as a part of the power controller in order to compensate the non-linear aerodynamic characteristics. The error between the filtered measured generator speed and the rated value is sent to the PI speed controller. The output of this controller is used as reference pitch signal ϑ_{ref} to the pitch system.

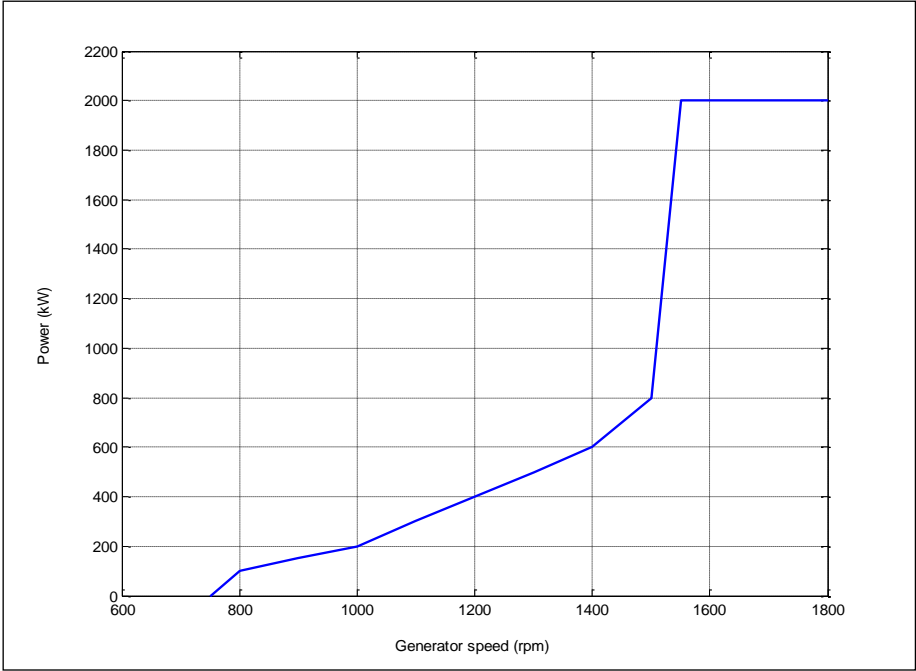


Fig. 3.7. Electrical power versus generator speed characteristic used in the maximum power tracking controller.

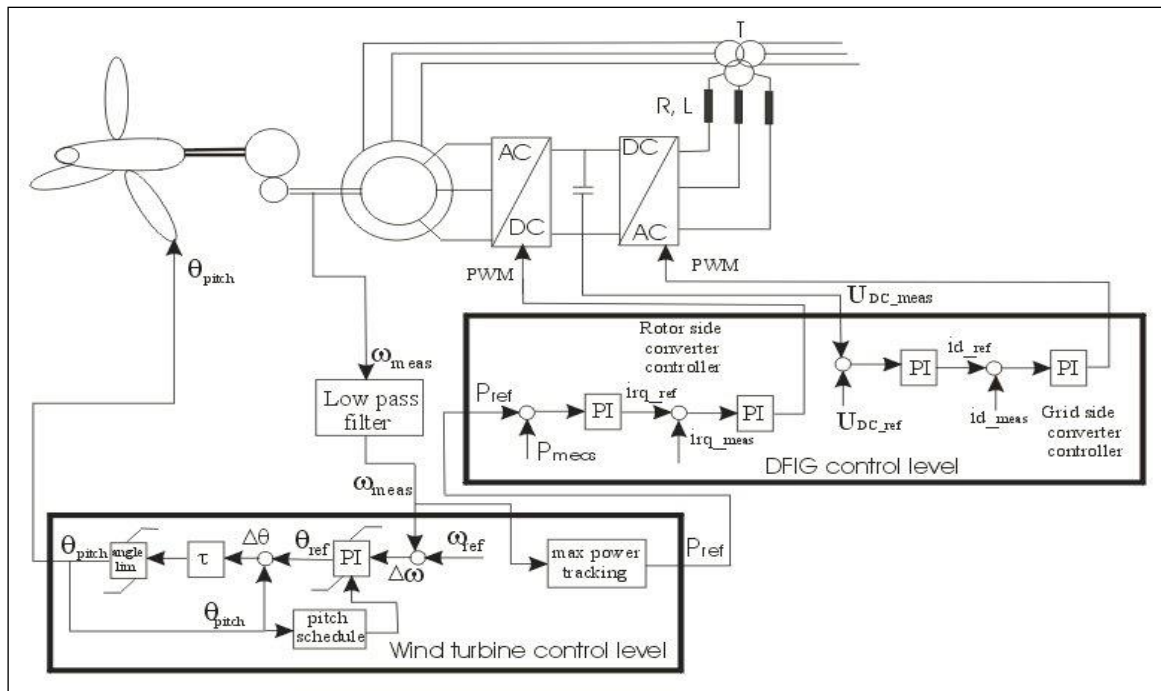


Fig. 3.8. An overview of the variable-speed wind turbine control strategy.

The reference is compared to the actual pitch angle θ and then the error $\Delta\theta$ is corrected by the servomechanism, as can also be seen in Fig. 3.8.

Assuming that the dynamic behavior of the speed controller can be approximated with a second order system behavior, the parameter design of the PI speed controller can be based on the transient response analysis. The parameters of the PI speed controller are: $K_p=850$ and $T_I=2.2$, where the integral time it was directly determined based on design parameters (damping ratio and natural frequency) while the proportional gain has a proportional variation with the aerodynamic sensitivity $dP/d\theta$.

3.2.4 Simulation Results

To evaluate the performance of both wind turbine control systems presented before and implemented in MATLAB-Simulink and DigSILENT software packages, a set of simulations are performed. More details about wind turbine models and software's implementation are described in [3] and [4].

A) Comparison between Active-Stall and Passive-Stall

Figure 3.9 shows a comparison between active stall and passive stall of a 2 MW constant speed wind turbine at a mean wind speed (18 m/s) higher than rated wind speed (12 m/s). One of the advantages of the active stall control, point out in Fig. 3.9, is that it can control the power output more accurately than with passive stall, so as to avoid overshooting the rated power of the induction generator of the beginning of a gust of wind.

Another advantage is that the machine can be run almost exactly at the rated power at all high wind speeds. In a stall controlled wind turbine the pitch angle is fixed and the output power cannot be held constant, while the maximum output power of an active stall turbine can be controlled to a

constant value (nominal rated value). In Fig. 3.9 the pitch angle control is only used during active stall control strategy.

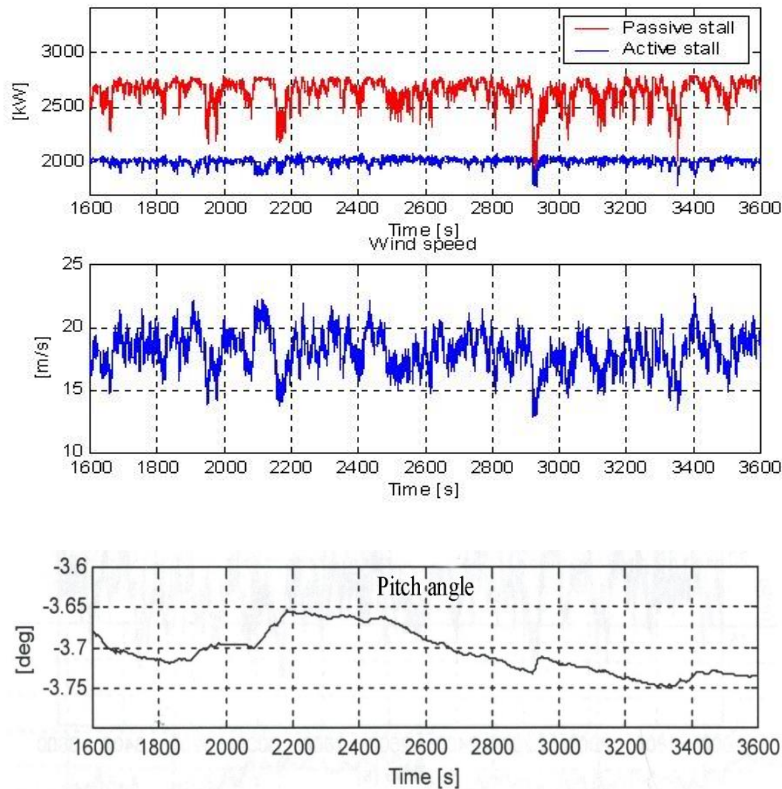


Fig. 3.9. Comparison between simulated active power with active stall control and passive stall control at an average wind speed $u_{eq}=18$ (m/s) and at turbulence intensity of $ti=0.12$.

B) Active Stall Constant Speed Wind Turbines versus Pitch-Controlled Variable-Speed Wind Turbines

Both Fig. 3.10 and Fig. 3.11 show how a 2 MW wind turbine, with variable speed (Fig. 3.10) and constant speed (Fig. 3.11), works during different operation conditions, such as sudden changes in wind speed (wind gusts) with a turbulence intensity of 12 %, at high wind speed.

Figure 3.10 presents the simulation results of 2MW variable speed wind turbine that works at a mean wind speed higher than rated one ($16 \text{ m/s} > 12 \text{ m/s}$) corresponding to the power limitation strategy, in which both the speed controller and the power limitation controller are active.

The power limitation controller sets the blade angle to keep the rated power, while the speed controller permits a dynamic variation of the generator speed, in a predefined speed range (in the speed range allowed by the size of the power converter), in order to avoid mechanical stress in the gearbox and the rotor shaft.

To illustrate the elasticity of the variable speed DFIG wind turbine and to test the power controller performance, some wind gusts of 6 m/s up and down, are introduced in wind speed at each 150 seconds (at 150 s, 300 s and 450 s).

For instance, at $t=150$ s the mean wind speed suddenly reaches from 16 m/s to 22 m/s. In the same time the generator speed and the electrical power increases too. The power limitation control loop is

strong and fast and the generator speed follows very well the generator speed reference in order to be able to absorb the maximum energy from the wind.

The pitch controller also reacts modifying the pitch angle, while the wind gusts are absorbed as variation in the generator speed, as can also be seen in Fig. 3.10.

The rotational speed of the wind turbine rotor is thus allowed to increase storing energy into the wind turbine’s inertia.

The control strategy of active stall constant speed wind turbine contains three modes of operation: acceleration control (speed control), power control (power limiting region) and direct pitch control (blade angle control).

The acceleration and pitch control modes are used during start-up, shut down and emergency conditions, while the power control mode is only used during normal operations.

In Fig. 3.11 the 2 MW induction generator was connected to the grid through a soft-starter (in order to reduce the transient current), at t=73 seconds and then the soft-starter was by-passed at t=77 seconds.

In the same time the power factor compensation unit started to work using capacitor switching, as a function of average value of measured reactive power [4, 8, 10].

The mean wind speed was 12 m/s. At t=100 seconds the mean wind speed was modified to 18 (m/s) and at t=170 seconds mean wind speed was modified again at 11 (m/s) to simulate sudden changes in wind speed and to test the system performance and implemented control strategy. The active and reactive powers have been able to follow these changes in all situations. It is concluded that the wind turbine absorbed the transients very fast and the control strategy offers a good stability of the system during transition of dynamic changes.

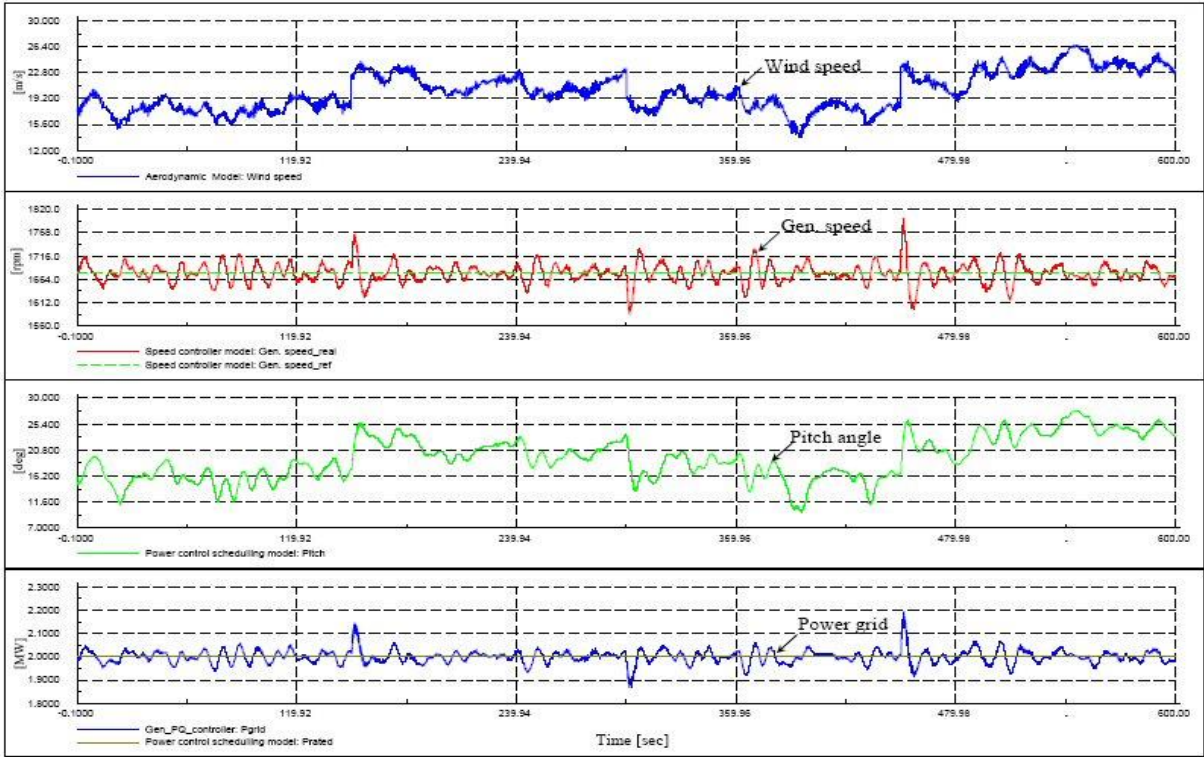


Fig. 3.10. Simulation results for a 2MW pitch controlled variable-speed wind turbine using DFIG with power control strategy implemented.

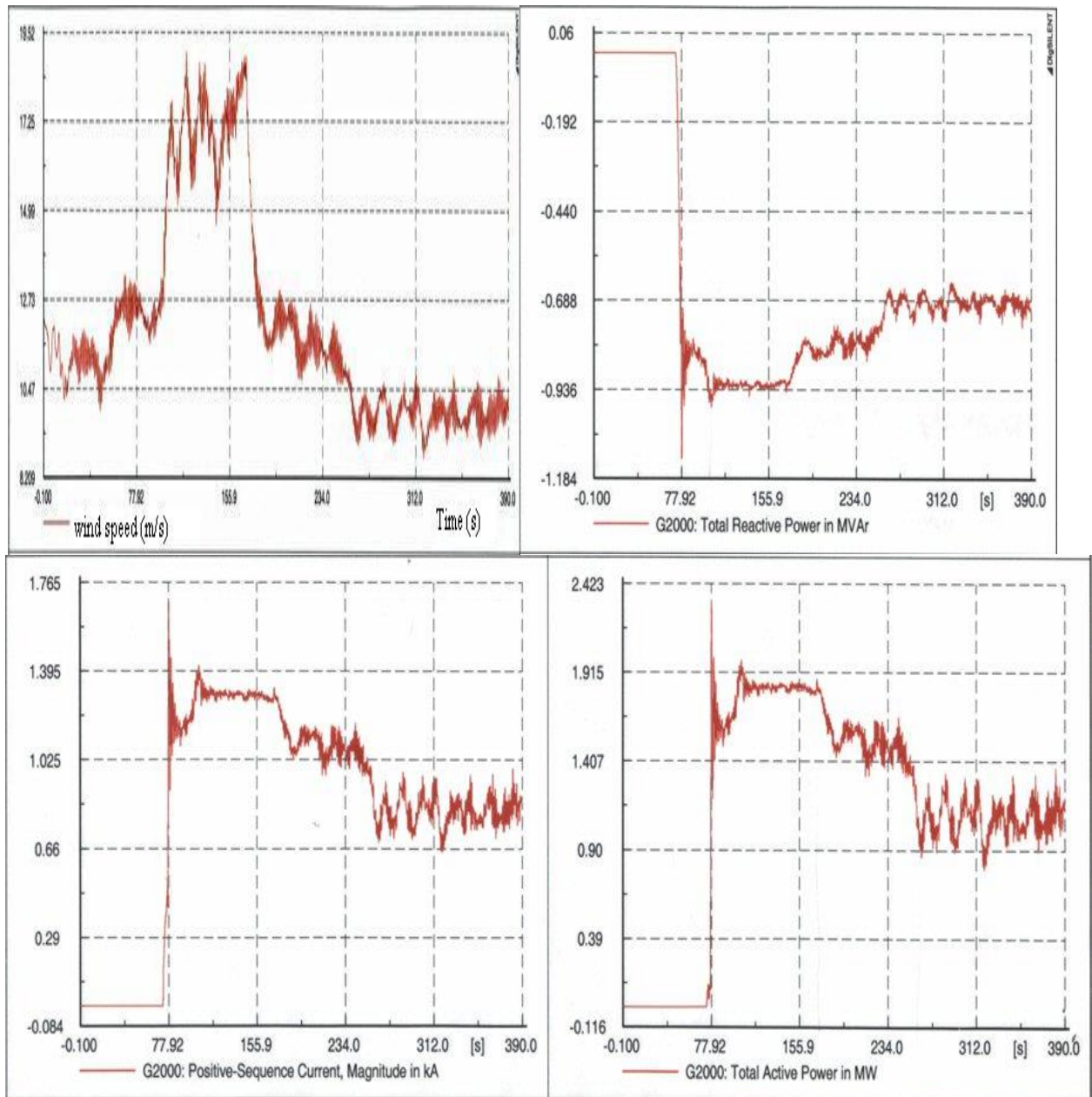


Fig. 3.11. Simulation results for a 2MW active stall constant-speed wind turbine using CRIG.

3.3. Control Strategies developed for Variable-Speed Wind Turbine Generators

In this subchapter, the performance of two variable-speed wind turbine concepts with induction generators connected to the grid is investigated.

Variable-speed wind turbine generator systems have been modelled and simulated to study their steady state and dynamic behavior.

A doubly-fed induction generator of 11 kW fed by a vector controlled back-to-back PWM-VSI inverter on the rotor side and a cage rotor induction generator of 11 kW rating with a vector controlled back-to-back PWM-VSI inverter on the stator side have been tested and the results compared with digital simulations.

It is shown by both modelling and laboratory tests that a doubly-fed induction machine can be used as a variable speed wind generator over a large speed range ($\pm 40\%$). The cage rotor induction machine also allows good speed range and it should be used in low-power variable-speed systems, replacing the classical direct grid connected fixed speed wind generator systems. Its capacity to deliver reactive power is remarkable.

3.3.1. Control Strategy of the DFIG based Wind Turbines

The Doubly Fed Induction Generator (DFIG) is an induction machine with a wound slip ring rotor. This provides the machine with an additional power port, giving additional control opportunities that may be exploited in the wind power generating systems.

The doubly fed induction generator can supply power at constant voltage and constant frequency while the rotor speed varies. This makes it suitable for variable speed wind energy applications. Additionally, when a bidirectional AC-AC converter is used in the rotor circuit, the speed range can be extended above synchronous speed and power can be generated both from the stator and the rotor. Various types of power control strategies have been suggested for application in variable speed wind turbines [1-2, 13-17]. One possible implementation scheme of adjustable speed generators consist of a synchronous generator and a power converter. The power converter, which has to be rated at 1 p.u. total system power, is expensive. Compared to direct-in-line systems, the doubly fed induction generator (DFIG) systems offer the following advantages [1-3, 13]:

- reduced inverter cost, because inverter rating is typically 25 % of total system power, while the speed range is $\pm(20-25)\%$ around the synchronous speed;
- improved system efficiency;
- power factor control can be implemented at lower cost, because the DFIG system basically operates similar to a synchronous generator.

DFIG is implemented as a variable speed, constant frequency scheme, by applying a converter to the rotor terminals of DFIG. The wind rotor determines the rotor speed, and controlling the rotor currents may control the stator power of the DFIG. If the stator flux is chosen as a reference, the q-rotor current (I_{qr}) controls the stator reactive power (Q_s), and the rotor d-current (I_{dr}) controls the stator active power (P_s). Controlling the rotor q- and d-currents respectively may control the stator active and reactive power. The ability to supply/subtract power to/from the rotor makes it possible to operate the DFIG at sub- and super-synchronous speed, having constant voltage and frequency on

the stator terminals. Furthermore it is possible to recover slip power in the rotor and supply it back into the power grid, through which the efficiency of the machine may be increased.

A) Development and implementation

The control strategy is developed in the stator flux fixed reference frame. The input from the stator is in the stator fixed reference frame and rotor input in the rotor fixed reference frame. Rotor voltage output is in the rotor fixed reference frame. The control strategy for controlling the stator active and reactive power is based on the power decoupling. It means that the stator active and reactive power feedback loops are required, as can be seen in Fig. 3.12.

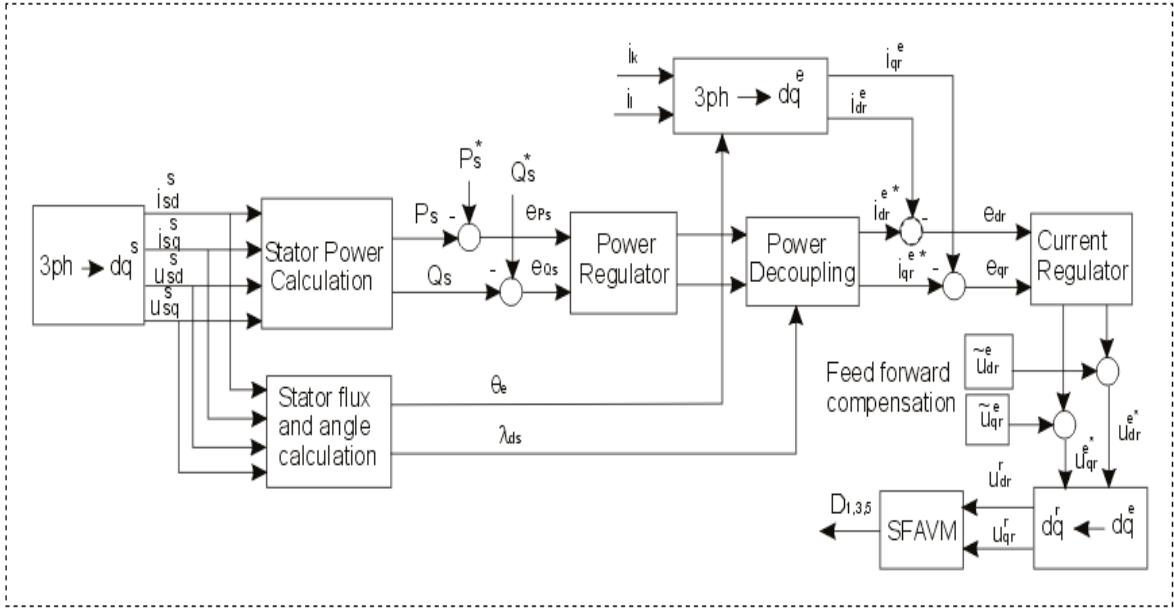


Fig. 3.12. Control scheme of DFIG with measurement of stator voltage and stator and rotor currents, implemented in Matlab-Simulink. The rotor d- and q- axis are compensated by use of feed-forward loop.

The control scheme consists of two control loops: an inner loop for controlling the rotor current, and an outer loop for controlling the stator active and reactive power.

The stator voltages and currents are measured in the stator fixed reference frame. In addition, the stator active and reactive power is calculated in the stator fixed reference frame. From the stator quantities, the stator flux is calculated, and the amplitude and angle of the resulting stator flux is found. The measured stator power (P_s, Q_s) is compared to the power references (P_s^*, Q_s^*), and the errors (e_{P_s}, e_{Q_s}) are fed to the power regulator. From the power regulator the reference values of rotor d- and q-currents are calculated using power decoupling. The reference values of rotor currents are compared to the rotor currents measured in the rotor fixed reference frame and transformed to the stator flux fixed reference frame, and the errors are fed to the current regulators. After the current regulator, feed forward compensation is used for decoupling rotor voltages and currents and then the reference values of rotor voltages are transferred to the rotor fixed reference frame and fed to the stator flux asynchronous vector modulation (SFAVM).

Since the power is independent of the choice of reference frame, the calculation of stator power may be performed in any reference frame. If the stator power is calculated in the stator fixed reference frame, the number of transformations to be performed may be minimized. The stator power is calculated using equations (3.3) and (3.4):

$$P_s = \frac{3}{2} * (u_{ds}^s i_{ds}^s + u_{qs}^s i_{qs}^s) \dots\dots\dots(3.3)$$

$$Q_s = \frac{3}{2} * (u_{ds}^s i_{qs}^s - u_{qs}^s i_{ds}^s) \dots\dots\dots(3.4)$$

The measured stator power is compared to the reference values of Ps and Qs, and the error signals are fed to the power regulator.

If the stator flux fixed reference frame, the d-axis stator flux is equal with zero and the stator active and reactive power may be expressed as in equations (3.5) and (3.6):

$$P_s = -\frac{3}{2} \cdot \frac{P}{2} \cdot \omega_e \cdot \lambda_{qs}^e \cdot i_{dr}^e \dots\dots\dots(3.5)$$

$$Q_s = \frac{3}{2} \cdot \frac{P}{2} \cdot \omega_e \cdot \lambda_{qs}^e \cdot \frac{\lambda_{qs}^e - M \cdot i_{qr}^e}{L_s} \dots\dots(3.6)$$

As can be seen in (3.5) and (3.6) power decoupling may be obtained by controlling the rotor d- and q-currents. This means that power decoupling is obtained by simply applying to the power rotor regulator output as a reference to the rotor current loop. The output from the power decoupling is the rotor d- and q-current references, as shown in Fig. 3.13.

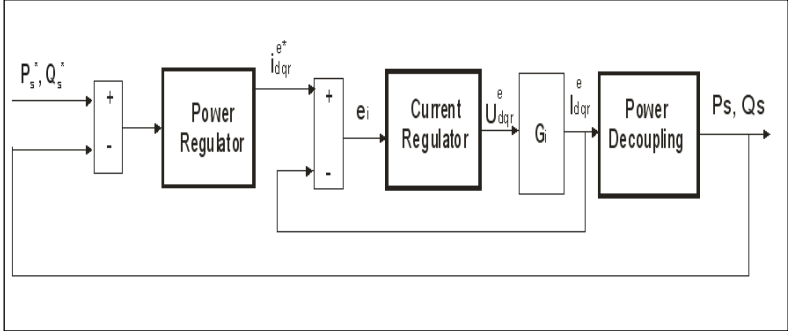


Fig. 3.13. Simplified control scheme with an inner rotor current control loop, and an outer power control loop. Full decoupling between rotor currents is assumed.

The control scheme is implemented as shown in Fig. 3.13. The current regulator is designed and the closed loop transfer function (Gi) for the current loop is found. The power regulator is also designed and the closed loop performance of the power loop is evaluated.

The control scheme (Fig. 3.12) and the regulators are implemented in a complete simulation model also including the DFIG model, rotor converter model and the control program developed in Ansi C and converted in Matlab-Simulink function and the C-file may be executed in Simulink by means of

the Matlab MEX-function., more details can be found in [8]. The model of the DSP implemented in Simulink is shown in Fig. 3.14:

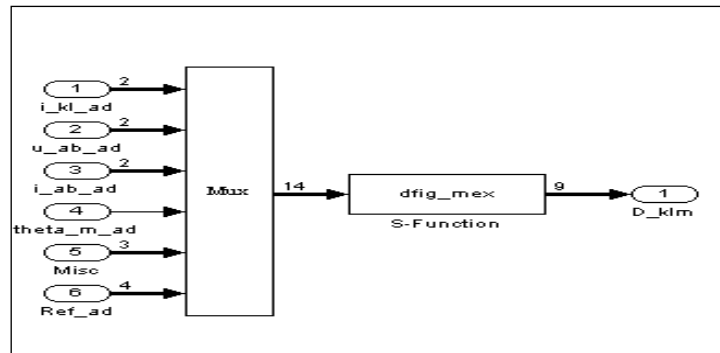
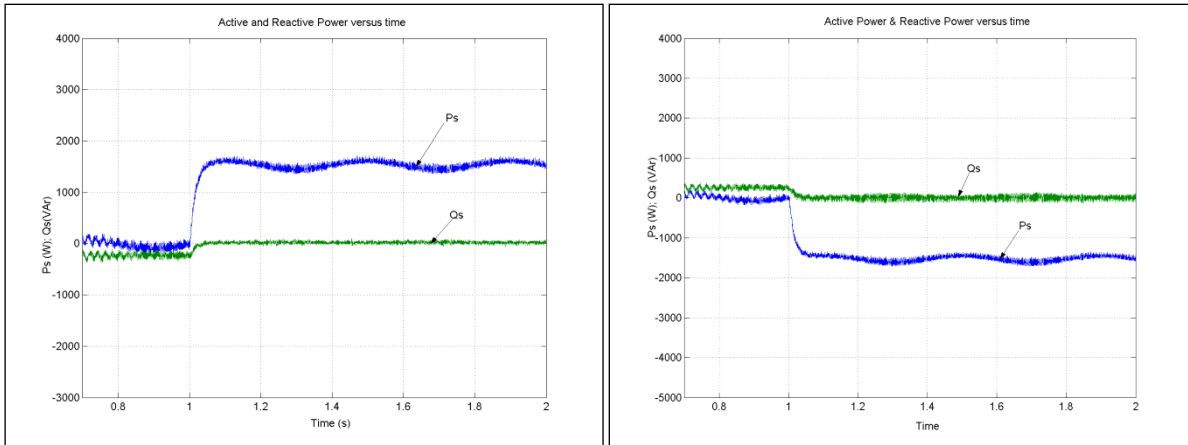


Fig. 3.14. Model of the TMS320C32 – DSP developed in Simulink. The control algorithms written in the Ansi-C language executed using the Matlab mex S-function.

The advantage of implementing the Ansi-C file in Simulink is the direct connection to the implementation in DSP, and decrease in simulation time.

B) Simulation results.

In order to evaluate the performance of implemented control strategy presented before and to analyze system response in steady state and transients the DFIG was subject to step changes in active and reactive load power with the machine driven at both sub- and super-synchronous speeds. The transient response due to a step change in reference active power control is shown in Fig. 3.15. The Fig. 3.15 a) shows the response to a step change in the active load power from 0 to 1.5 kW, while the reference of reactive power is maintained at 0 and the corresponding stator active and reactive power of the machine are monitored. Similar transient response for generating condition is given in Fig. 3.15 b). When a step in active power is applied ($t=1\text{sec}$), the reactive power shows small additional oscillations. It is also observed that (P_s) reaches its set value in approximately 10 ms. The simulation results indicate that the generator follows the reference very fast and is dynamically stable. It may be noted from these waveforms, that the transient responses in (P_s) and (Q_s) are perfectly decoupled. The DFIG was driven by the drive system at 1125 rpm (75% of synchronous speed-sub synchronous speed operation mode).



a)

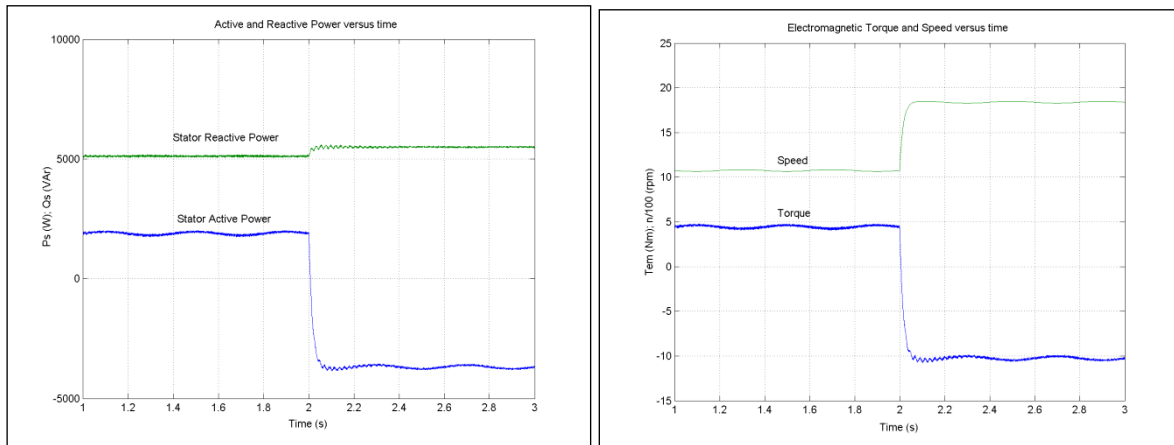
b)

Fig. 3.15. Simulated stator active and reactive power at 1125 rpm with a step change in active power command from 0 to 1500 W (a) and with a step change in active power reference from 0 to -1500 W at $t=1s$, b).

The validity of the model presented before is also verified by simulating a step in rotor speed and sample the stator active and reactive power, electromagnetic torque and stator and rotor currents. All simulations are performed with constant DFIG parameters.

The DFIG is driven by the drive system at 1125 rpm (sub-synchronous mode-75 % of synchronous speed), and the reference speed is changed at $t=2s$ to 1875 rpm (super-synchronous operation mode-125 % of synchronous speed).

The speed and torque response are shown in Fig. 3.16 b). The mechanical system is modelled using a first order approximation, where the time constant is determined from a step in rotor speed.



a)

b)

Fig. 3.16. Simulation of the stator active and reactive power (a) and electromagnetic torque and speed (b) as a function of time. The speed reference of the drive system is changed at $t=2s$ from 1125 rpm to 1875 rpm.

Figures 3.16 a) illustrates the simulated stator active and reactive power of the DFIG as a function of time. The stator active power and stator reactive power are controlled independently, by controlling the rotor currents.

If the speed increases so that the machine is operating in generating mode at super-synchronous speed, the stator active power and electromagnetic torque change direction from the sub-synchronous operation (Fig. 3.16).

C) Description of the experimental set-up and Results

The experimental system is a scaled model of a 2MW variable speed wind generator system. It is composed of four main components: a DFIG with a four quadrant ac-to-ac converter connected to the rotor windings, a drive system and a control processor unit. The generator is a wound rotor induction generator (Doubly Fed Induction Generator - DFIG), with slip rings, rated at 11 kW provided with a gearbox. The wind turbine rotor is emulated by use of a drive system scaled for driving the DFIG; the drive system is composed of a 15 kW induction motor and a 22-kVA-frequency converter. Two back-to-back PWM-VSI converters with a standard control system, with a DC-link including a DC capacitor filter are used to control the rotor currents, active and reactive power flow. The grid converter is designed to give unity power factor and is controlled by the Control Processor (CP) – board via a PC. It works as an active rectifier supplying the rotor converter with a constant DC voltage. The measurement and control system is composed of a PC with a digital signal processor (TMS320C32 DSP), interfaces and transducers for measuring stator and rotor currents, stator voltages, and rotor speed, as can be seen in Fig. 3.17.

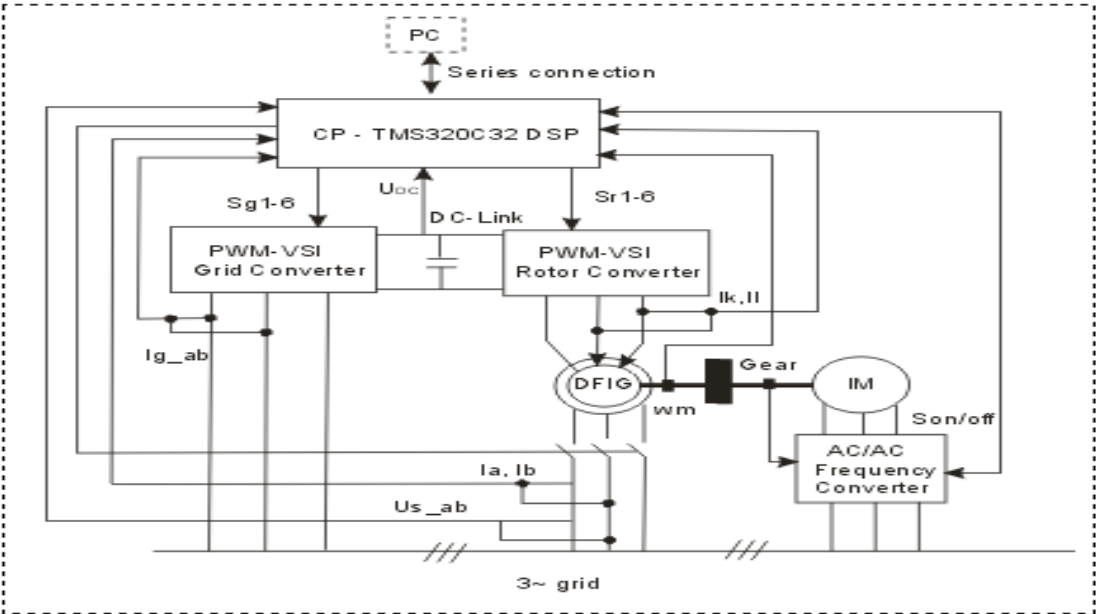


Fig. 3.17. Schematic diagram of the experimental set-up.

D) Comparison between Simulations and Experimental Results

The equipment used to obtain the test data was described in the previous sub-section. Tests and simulations were performed to examine the system performance in steady-state and to validate the Matlab-Simulink implemented system developed for a variable speed wind turbine with DFIG.

Fig. 3.18 and Fig. 3.19 shows the steady-state waveforms of stator currents and stator voltages of the DFIG running at 1475 rpm (sub-synchronous speed operation mode) and stator power of 4 kW. The Fig. 3.18 shows a comparison between simulated and measured stator currents of DFIG, while in Fig. 9 is presented a comparison between simulated (b) and measured (a) stator voltages of DFIG. The measured data were acquired by an Oscilloscope, while the simulation results were performed by MATLAB/Simulink. The correspondence between simulation and experiments is very good as can be seen in Fig. 3.18 and Fig. 3.19.

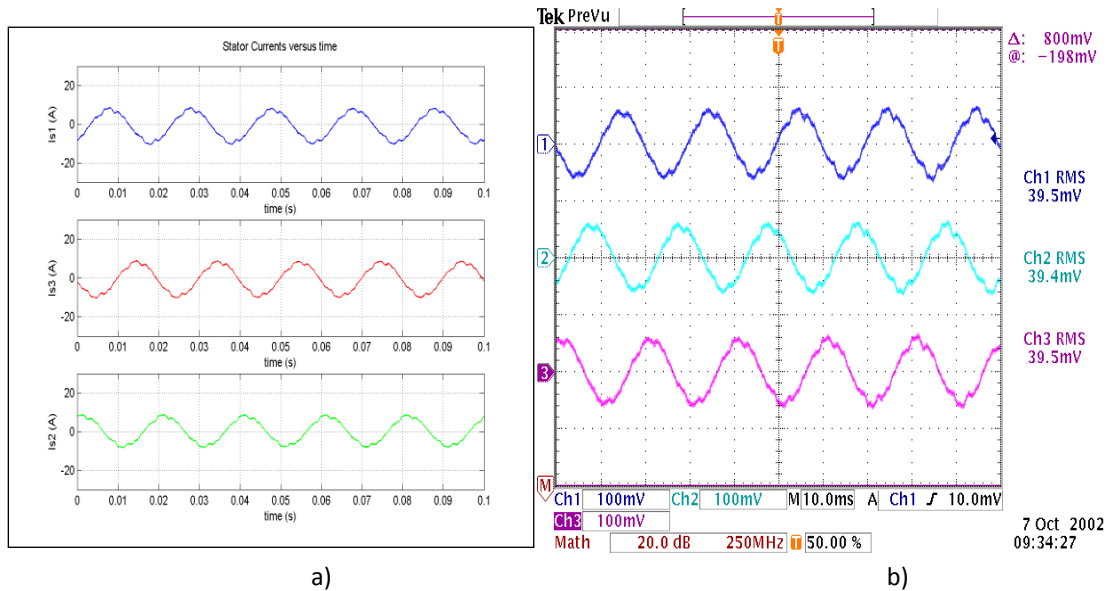


Fig. 3.18. The simulated stator currents of DFIG (a) using Matlab-Simulink and measured stator currents (b) by an Oscilloscope in steady-state at $P=4$ kW and $n=1475$ rpm (sub-synchronous operation mode). Scaling factor of measured stator currents is 4 (mV/A).

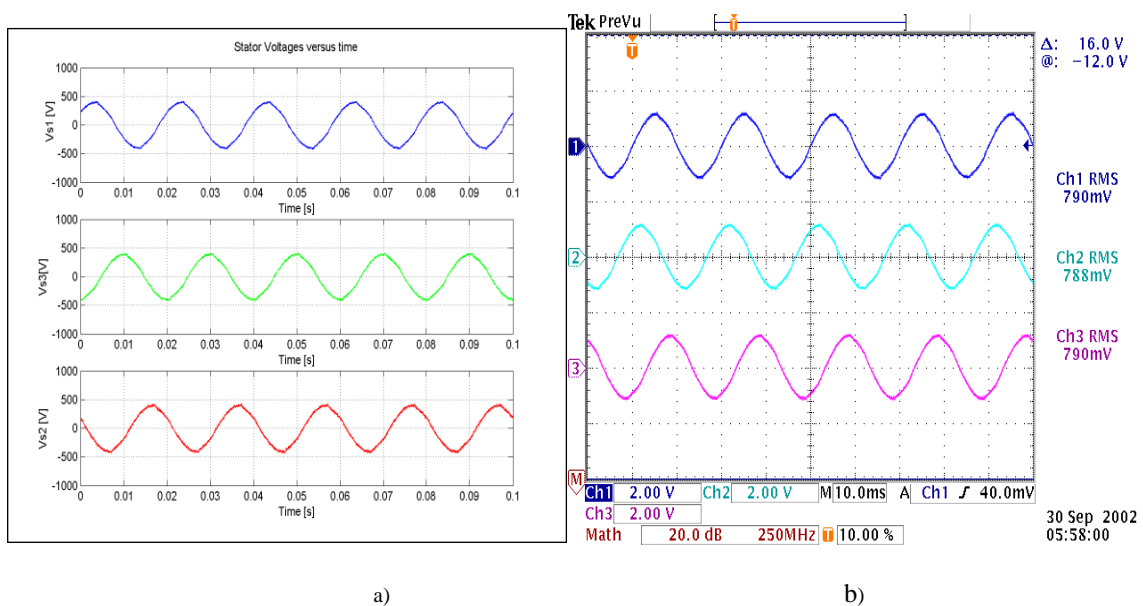


Fig. 3.19. The Simulation of stator voltages in steady-state (a) and measured line – line stator voltages of DFIG acquired by an Oscilloscope TDS 540. Scaling factor of measured stator voltages is 2 (mV/V).

3.3.2. Control Strategies developed for Variable-Speed Wind Turbines with CRIG and implemented using a real-time digital platform

The adjustable speed generators systems with Cage Rotor Induction Generator (CRIG) are commonly used in low power variable-speed wind turbines replacing the classical direct grid connected fixed speed drives. The goals that can be achieved by using this topology are to increase the energy production especially in the low wind range, eliminate the capacitor bank for reactive power compensation and allow both grid-connection and stand-alone operation modes.

There is an increase demand on the market for low-power variable speed wind turbines that can be used in remote places. To achieve this goal a relatively complex control strategy need to be developed using power converters to process the power flow.

A) Experimental arrangements

In this subchapter a flexible real-time development platform using dSPACE DS1103 digital controller was used in order to control the power converters for an 11 kW wind generator system.

The power converter is a back-to-back voltage source converter (VLT 5022), which is a bi-directional power converter consisting of two conventional voltage source inverters rated at 18.5 kW/400 V, as shown in Fig. 3.20.

One frequency inverter is connected to the induction generator and uses the standard vector flux control to regulate the speed and to provide magnetizing flux. The second one is connected to the grid through an LCL filter and is working as an active rectifier. Both inverters are controlled via dSPACE 1103 real-time system connected to a PC.

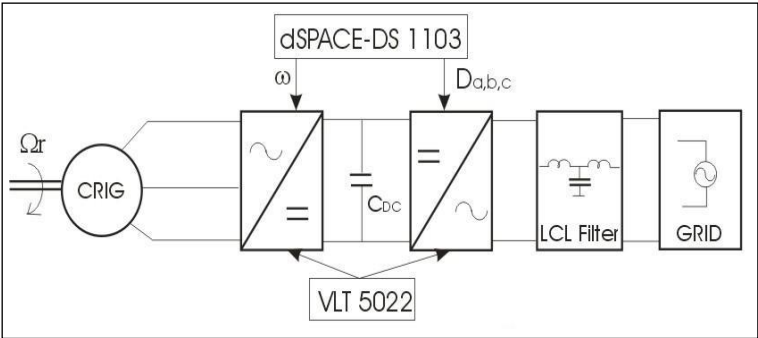


Fig. 3.20. Block diagram of the variable-speed wind turbine using cage rotor induction machine test system.

To achieve full control of the output, the DC-link voltage must be boosted to a level higher than the amplitude of the grid voltage. The power flow of the grid side converter is controlled in order to keep the DC-link voltage constant.

A technical advantage of this topology is the capacitor decoupling between the grid converter and the generator converter. This decoupling offers separate control of the two converters.

The complete grid-side controller including DC-link, grid inverter, Space Vector Modulator (SVM) and grid is shown in Fig. 3.21.

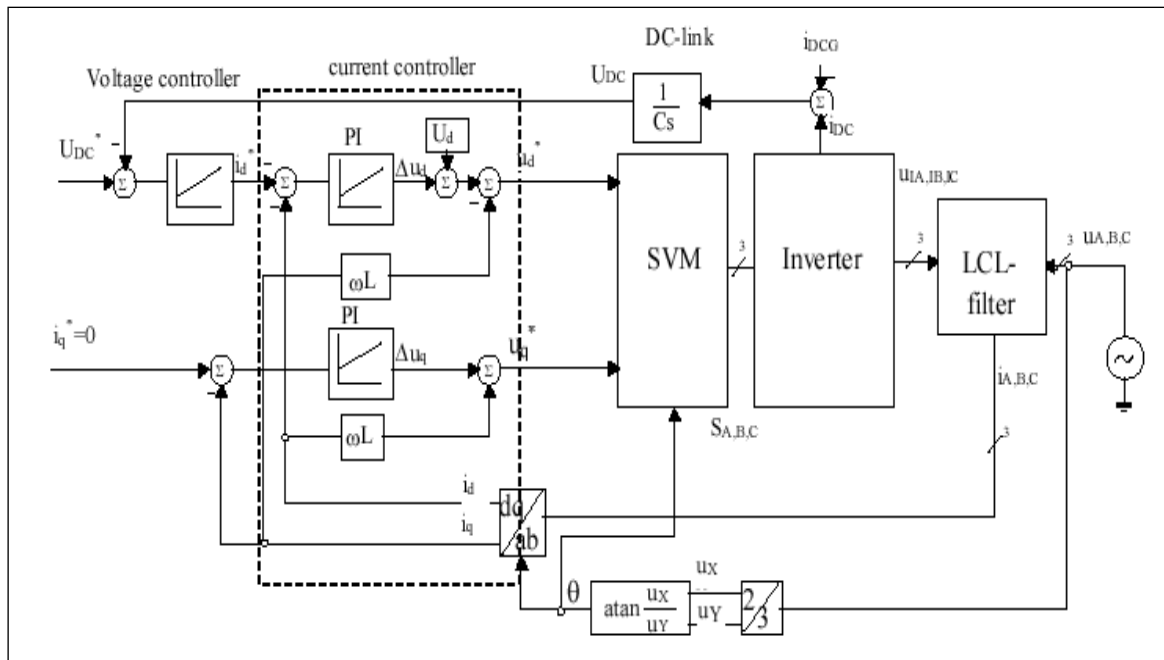


Fig. 3.21. A schematic block diagram of grid converter side controller.

The current controller is designed in d-q synchronous reference frame using two PI regulators for each component. Grid voltages are measured and feed-forward to compensate grid voltages. Cross couplings are compensated with (ωL) terms, assuming that $(d\omega/dt) = \text{constant}$. PI regulators are used to determine appropriate voltages for the reference currents. The reference current (i_q^*) in the q-branch of the current loop is set to zero in order to achieve 0 phase angle between voltage and current and therefore unity power factor.

The wind emulator is composed of a cage rotor induction machine (15 kW) supplied by a speed-regulated standard commercial frequency converter (VLT 5022-scalar control) used to control the mechanical power ($P_M = T_M \cdot \Omega_r$) on the generator shaft.

The cage – rotor induction motor is mechanically coupled with the induction generator. The desired torque from the maximum power tracking algorithm is setting the torque reference for the generator converter which has internal torque regulator.

B) Experimental real-time platform and Results

In order to verify the performance of the wind generator system the whole control strategy, including the generator control and the grid converter control, is implemented using DS1103 prototype.

A virtual control panel interface has been developed in Control Desk [4] in order to monitor the parameters of the wind generator system, as shown Fig. 3.22.

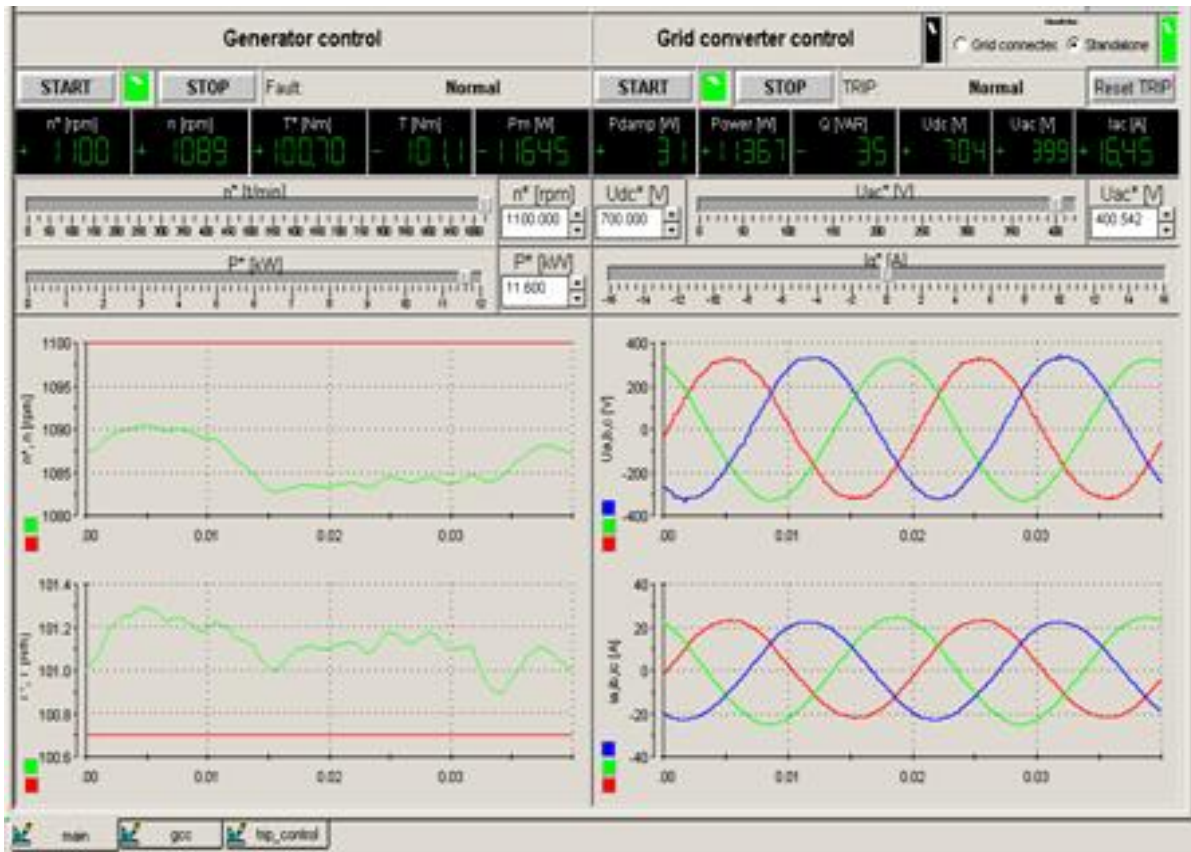
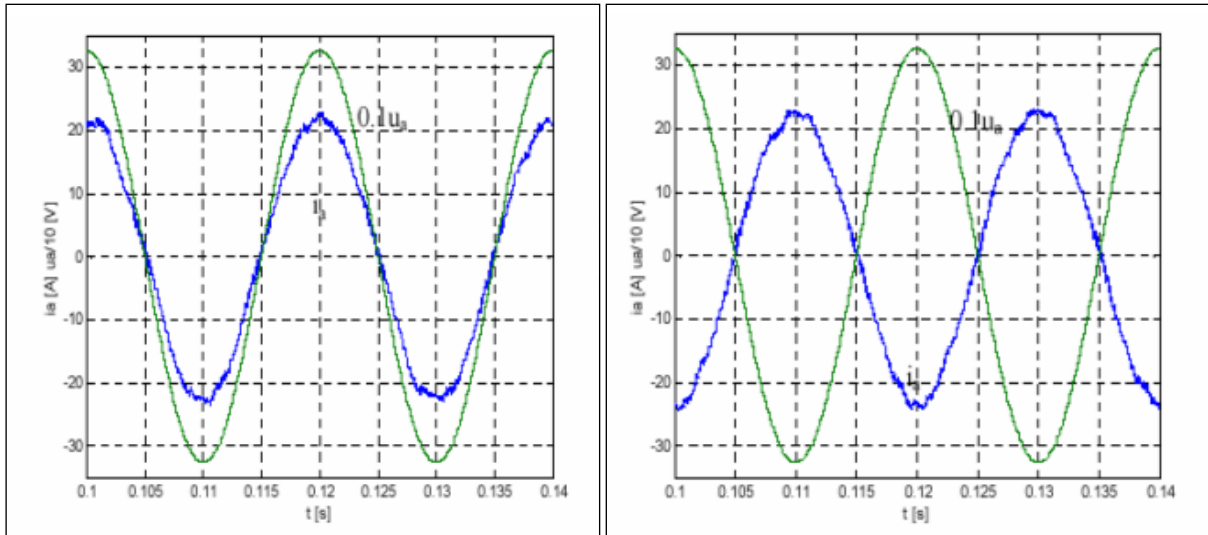


Fig. 3.22. The control desk panel interface to monitor online the parameters of the 11 kW wind generator system.

Using the control desk panel interface the parameters of the wind generator system can be shown in both representations, numerically and graphically, as can be seen in Fig. 3.23. Reference values and parameters of the experimental system can be changed online during the operation mode.

Fig. 3.24 illustrates an acquisition of data in steady-state using the control desk panel interface, presented before in Fig. 3.23, at nominal load (11 kW) in generating mode (Fig. 3.24 a) and in motoring mode (Fig. 3.24 b). In rectifying mode phase voltage (u_a) is in phase with phase current (i_a), while the difference in generating mode has 90 degrees. The DC-link voltage controller (regulator) maintains the DC-link voltage almost constant when applying disturbance of nominal load (DC-link voltage drop is under 4 %).

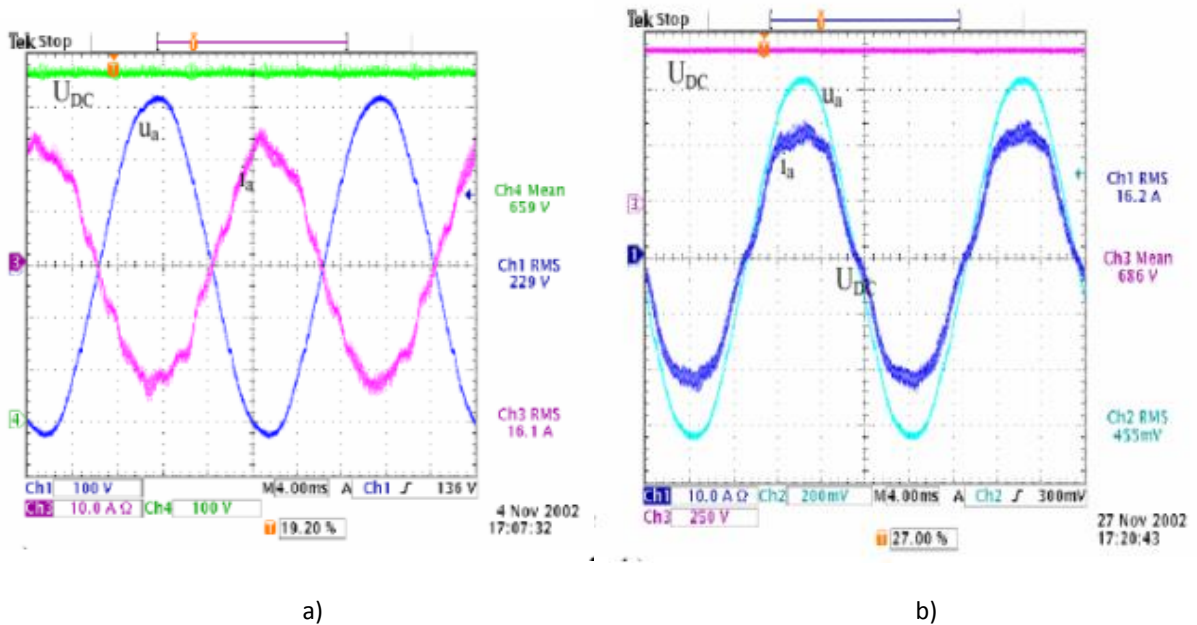


a) b)

Fig. 3.23. Grid phase current and voltage at nominal power (11 kW) in rectifying mode (a) and generating mode (b), acquired by a PC via dSPACE card.

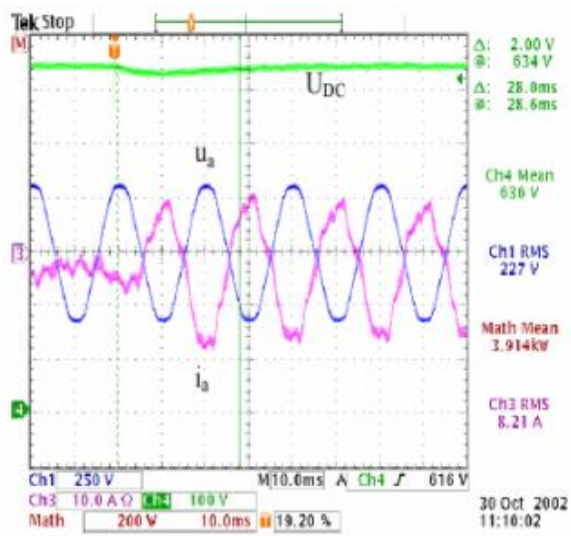
Fig. 3.24 illustrates an acquisition of data in steady-state using an Oscilloscope (TDS 3014) at nominal load (11 kW) in generating mode (Fig. 3.24 a) and in motoring mode (Fig. 3.24 b). In rectifying mode phase voltage is in phase with phase current, while the difference in generating mode has 90 degrees.

The performances of the system are shown in Fig. 3.25, under sudden changes in load. It shows that the DC voltage is maintained almost constant during transient conditions. DC-link voltage drop was under 4 % when applying disturbance of nominal load and disturbance rejection time was less than 60 ms, as can also be seen in Fig. 3.25.

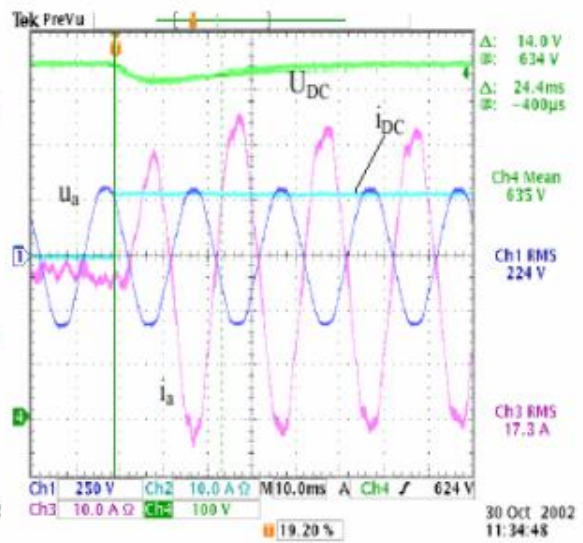


a) b)

Fig. 3.24. Phase current (i_a), phase voltage (u_a) and DC voltage (U_{DC}) at nominal load in generating mode, (a), and in rectifying mode (b), acquired by an Oscilloscope.



a)



b)

Fig. 3.25. a) Step load changed from no load to 40 % of nominal load (11 kW), and b) from no load to nominal load.

3.4. Control Strategies of DER Components in a Distribution Network

3.4.1. Voltage control by active power

As a part of the power system, the low voltage distribution grid has the objective to provide energy to the end consumers.

The voltage control is a major objective in a distribution network due to a large number of factors, such as different load profiles and load types or different number of phases (asymmetrical distribution of DERs in the grid).

An efficient way of controlling the voltage in a distribution network is to control the local power consumption at the bus-bar. The consumption can be influenced by shifting load or using energy storage. The ability to control active units can reduce the stress on the low-voltage grid by consuming the PV/Wind production locally.

In Fig. 3.26 a) is presented the consumer configuration along a feeder in a low-voltage distribution grid with a voltage profile increasing or decreasing in function of the number of loads (including EVs) and PV systems connected to the grid along the feeders. The length of the cables is also an important factor. Due to the PV penetration the voltage along the feeders could increase over the admissible limits defined by standards. Also, due to the EVs connected along the feeders the voltages can decrease exceeding the minimum level.

In this case a local voltage controller using distributed energy storage and/or a local voltage controller by load shifting could be an option.

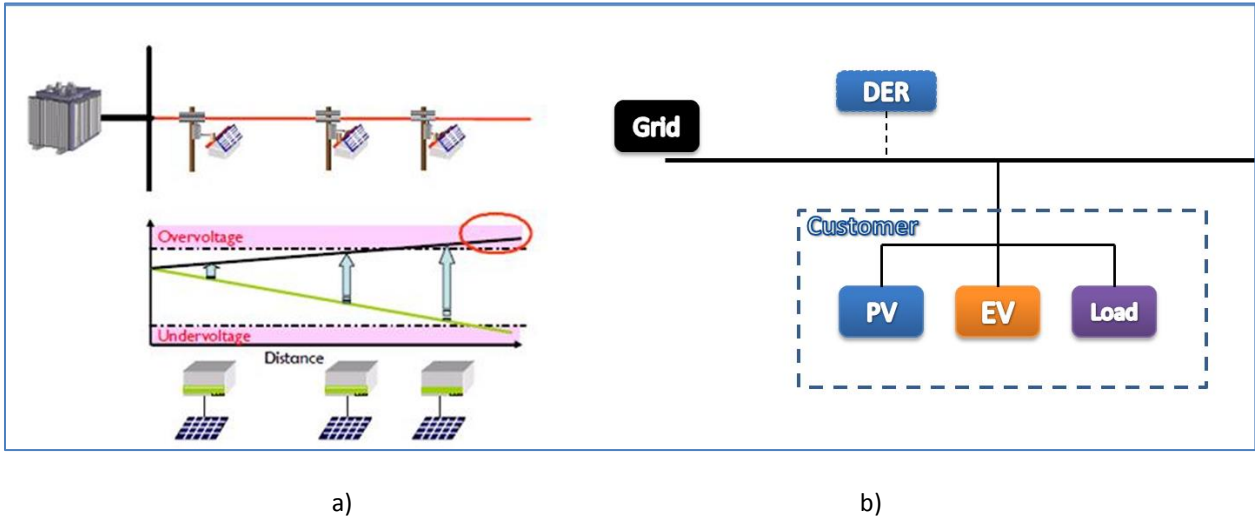


Fig. 3.26. a) Voltage profiles in a low-voltage distribution grid with b) DER components used in this study.

Two types of controllers for voltage regulation have been developed and implemented in MATLAB/Simulink and DigSILENT PowerFactory for controlling the bus-bar voltage at the connecting points.

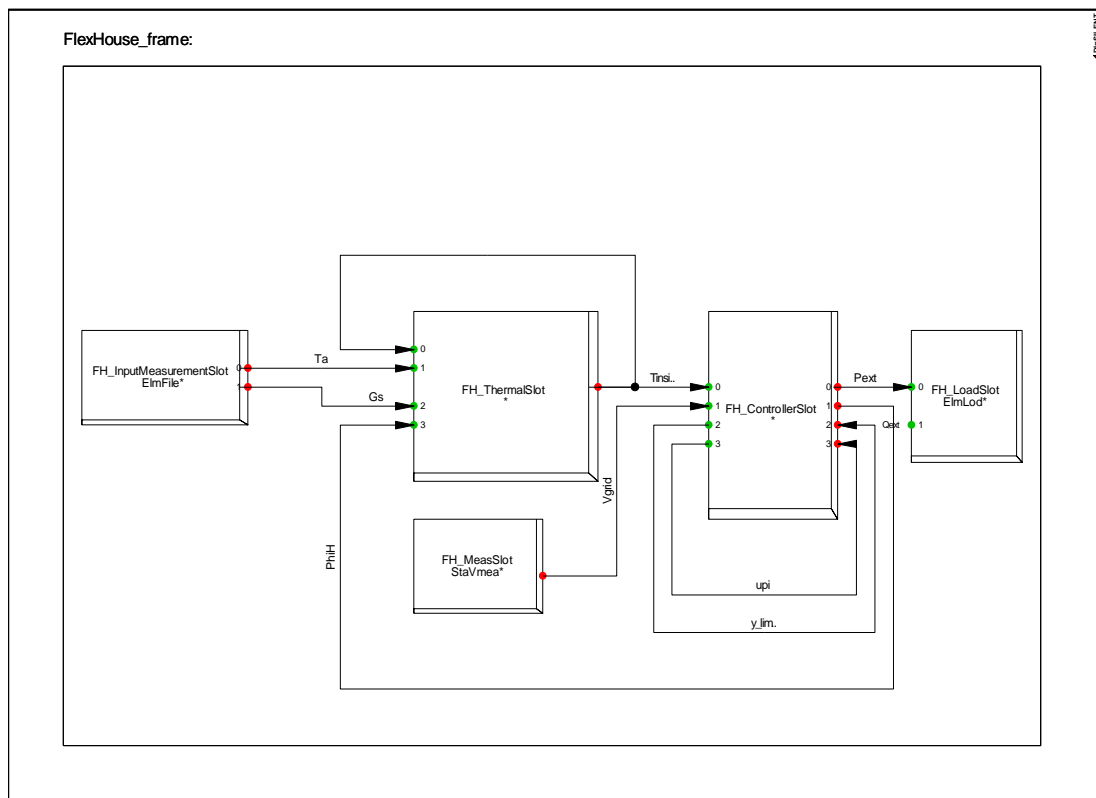
One of them is based on local control by load shifting; another one is controlling the voltage with the help of energy storage systems.

3.4.1.1. Voltage Control by Load Shifting

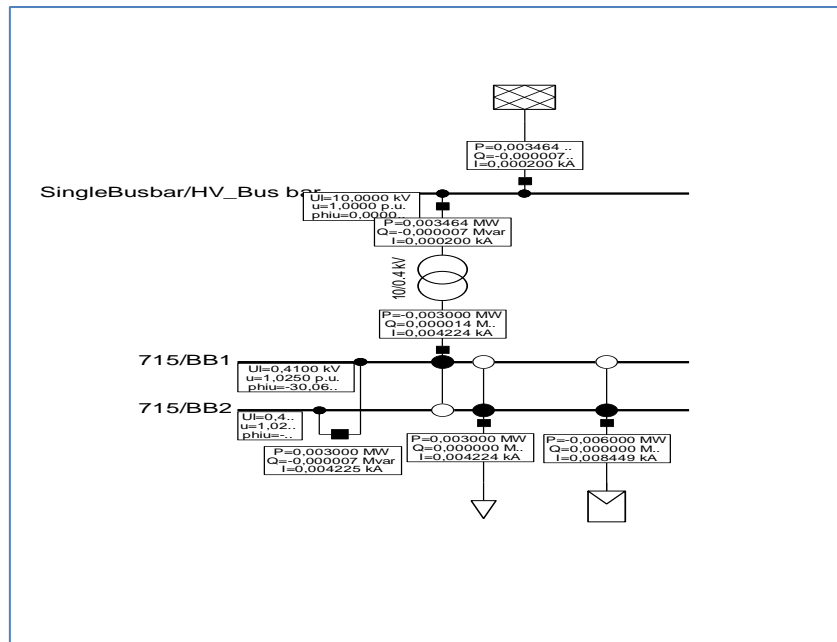
A) Implementation

The ability to control active units (Flex House heaters in our case) will reduce the stress on the low-voltage grid by consuming the PV energy production locally. Home energy management system, such as the SMA Sunny Home Manager [30], can increase the share of PV energy being consumed at the distribution customer's site. Thus decentralized consumption is increased and the stress and losses in the grid are reduced.

To test the voltage controller, developed and implemented in Power Factory (as can be seen Fig. 3.27 a), the Flex House has only been connected with the PV system at the same bus-bar (Fig. 3.27 b). Also a power flow calculation has been shown for the case when PV production was 6 kW and the Flex House heaters consumed 3 kW.



a)

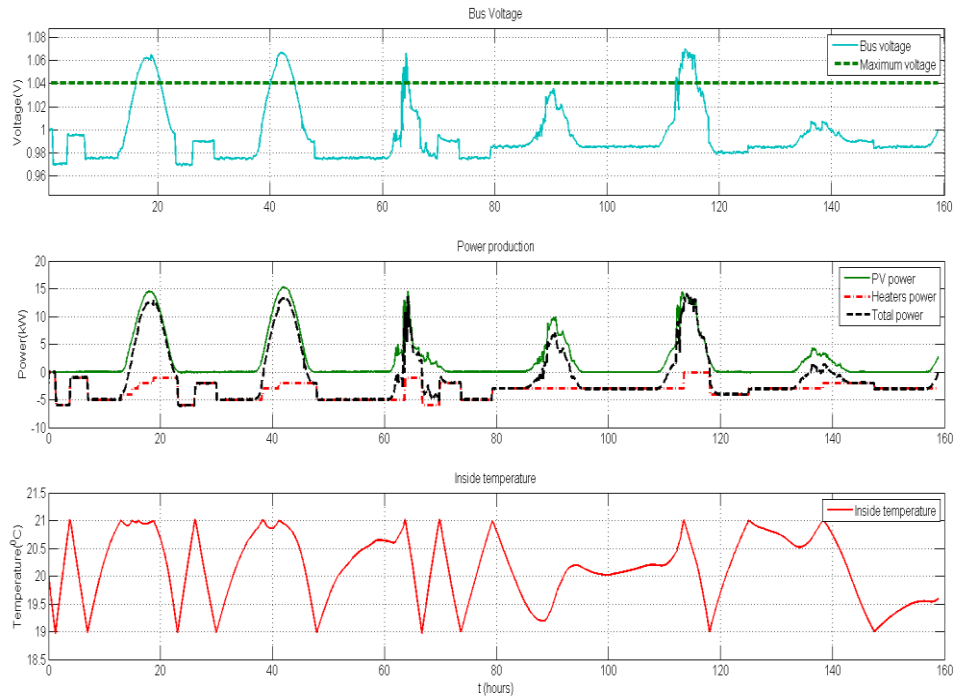


b)

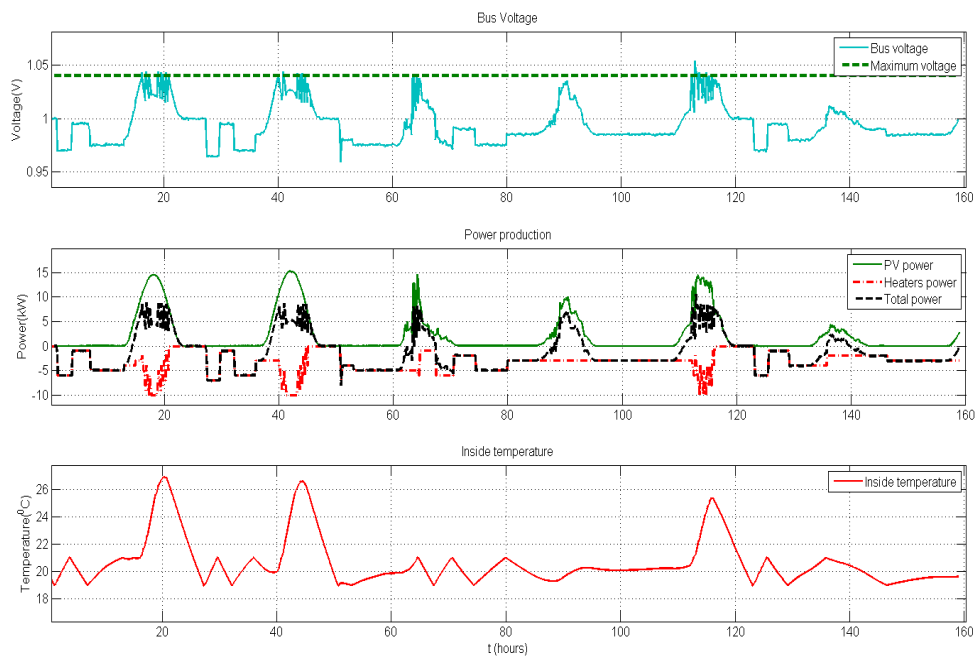
Fig. 3.27. a) DigSILENT PowerFactory implementation of the Flex House frame model with voltage control and b) grid diagram with Flex House and PV Generator connected to the same bus-bar.

C) Simulation Results

Fig. 3.28 point out the difference between normal operation (Fig. 3.28 a), without any voltage control to the local bus-bar at which the PV generator is connected together with the Flex House, and the situation when the voltage is controlled using load shifting (Fig. 3.28 b) by consuming the PV energy production [25-26, 35]. The idea was to keep the voltage under a certain level (set-up at 1.04 in our case) when the PV production increases, increasing the power of the heaters and the inside temperature of the house. As can be seen on the right graph when the power production increased more heaters were switched on by the controller and the inside temperature was increased from 21 °C to 27 °C keeping the voltage under the set point value. The high increase in the indoor temperature is allowed to show the functionality of the controller, in actual use the indoor temperature would also limit the control action.



a)



b)

Fig. 3.28. a) Normal operation without any control versus b) local voltage control by load shifting.

D) Voltage Controller Validated by Measurements

To validate the local voltage controller using load shifting an experimental test is performed using SYSLAB research lab (see chapter 2). The parameters monitored are heaters output power, inside temperature of the house and the voltage measured at the bus-bar where the Flex House was connected, the measurements for these values are shown in **Error! Reference source not found.** The third plot points out all four voltage limits: the maximum and the minimum set voltage for the current bus-bar as well as the two limits defining the dead-bands responsible for stabilizing the system.

The events that trigger state transitions are marked with coloured circles. The marks in the first plot correspond to the controller reactions and are the effect of the voltage limit intersection with the voltage at the bus-bar, which is presented in the third plot. The red circles represent events when the bus-bar voltage is reaching the upper limit, the blue circles represent events when safe voltage limits are reached and the controller turns back to the control state, and the green circles represent events when the lower voltage boundary is reached (Fig. 3.29).

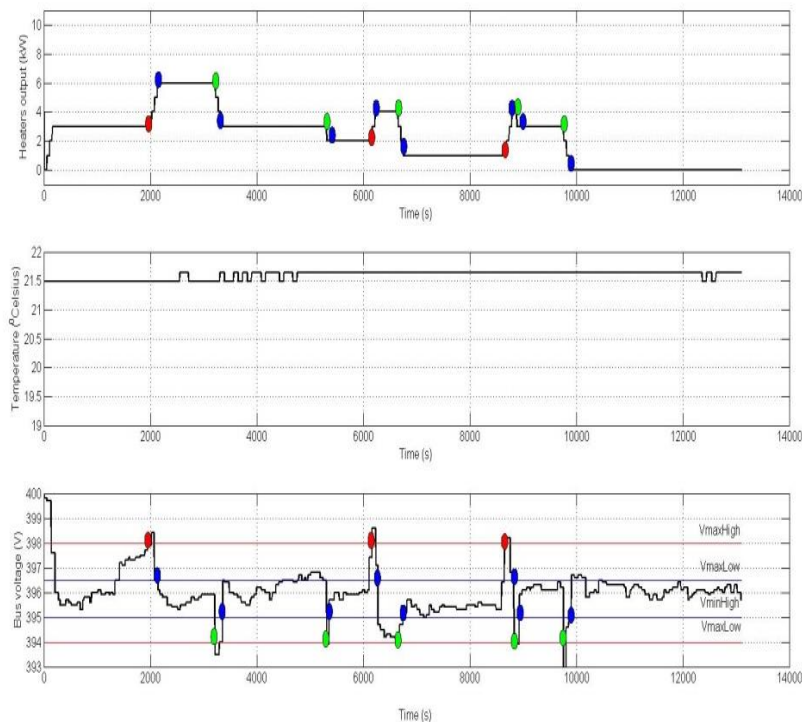


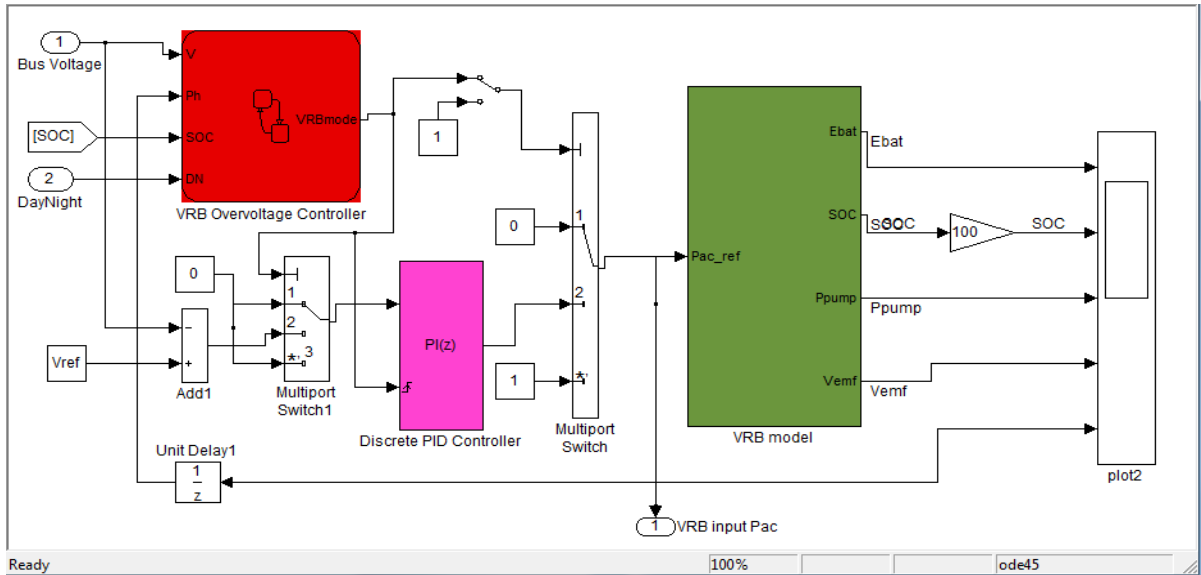
Figure 3.29: Voltage controller using load shifting validated by measurements.

As can also be seen in Fig. 3.29 when the voltage exceeded the maximum value set to 398 V the controller reacts by changing the power of the heaters. By doing that the inside temperature of the house increased, as in simulations presented before.

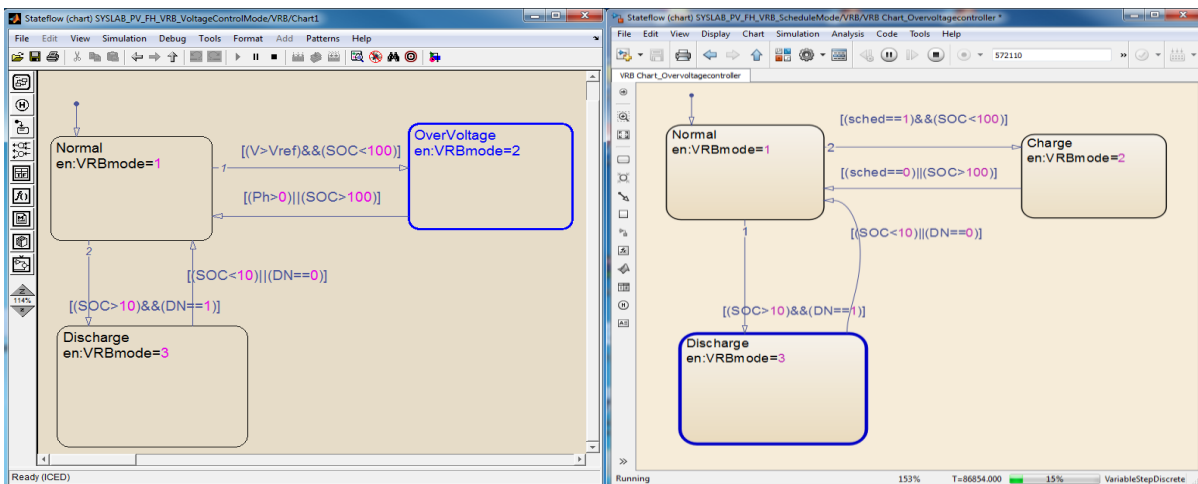
3.4.1.2. Voltage Control using BESS

A) Implementation

Two voltage controllers have been developed and implemented in MATLAB/Simulink (Fig. 3.30) and DigSILENT Power Factory (Fig. 3.31). An overvoltage controller, able to charge the battery when the bus-bar voltage exceeds the limits, and a voltage controller able to set-up the battery to run in schedule mode [35].



a)



b)

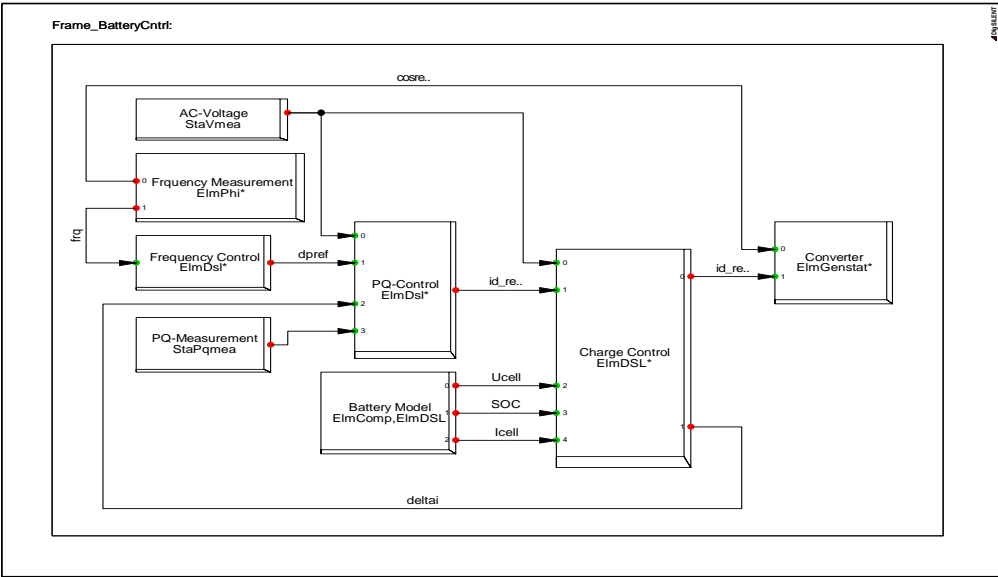
c)

Fig. 3.30. a) Implementation of the EV model with the voltage controller, b) voltage controller developed in state flow for over-voltage control and c) EV controller implementation using schedule mode.

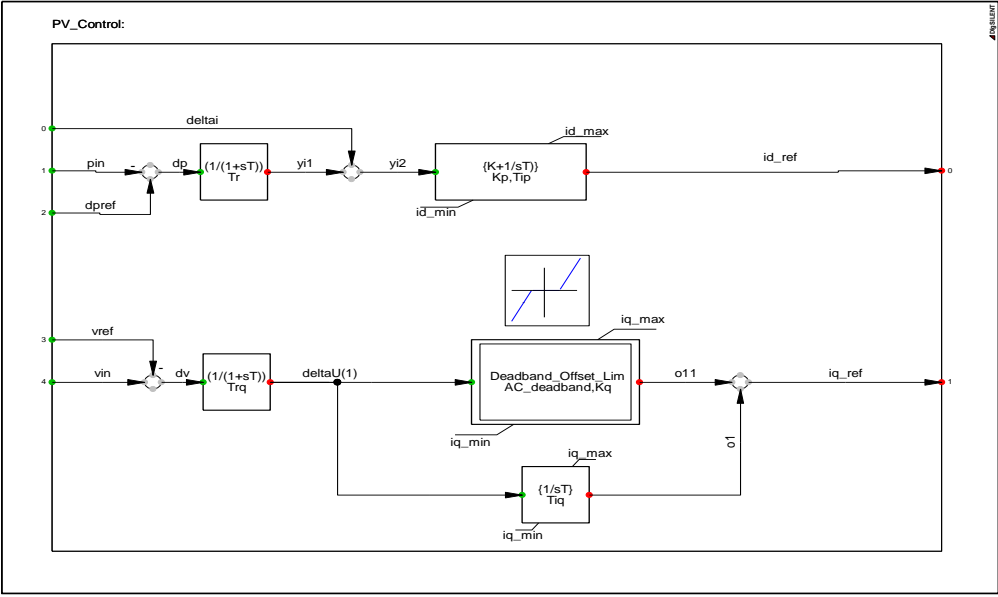
The voltage controller of the VRB system for overvoltage control implemented in MATLAB/Simulink was developed using a stateflow chart and a PI controller, (Fig. 3.30 a). The stateflow chart is an interactive graphical design tool of Simulink for developing and simulating event-driven systems

based on finite-state machine theory. Details about stateflow chart controllers are shown in Fig. 3.30 b) and 3.30 c).

The implementation of the model in DigSILENT PowerFactory is presented in Fig. 3.31



a)



b)

Fig. 3.31. a) The frame model of the battery energy storage system and b) details about the voltage and power controllers, implemented in PowerFactory.

The first controller is able to control the voltage at the bus-bar charging the battery when an overvoltage is detected. The idea was to control the voltage at the bus bar when exceeds the maximum value ($1.1 U_n$), due to the PV production, changing the battery mode of operation (discharging/charging).

Another method of controlling the voltage with the help of storage energy systems it is to set the EV to run in schedule mode. That means the battery is scheduled to operate during the day in function of the weather conditions, such as PV penetration.

In the case of the former, the BESS is connected only when an over voltage occurs and consumes the excess power until the power injected into the grid is not causing the bus voltage to exceed the limit. It means that the battery requires fewer charging/discharging cycles, leading to increased battery life.

The advantage of the second controller is that doesn't require any sensors to measure the voltage but requires a very precisely estimation of the PV production.

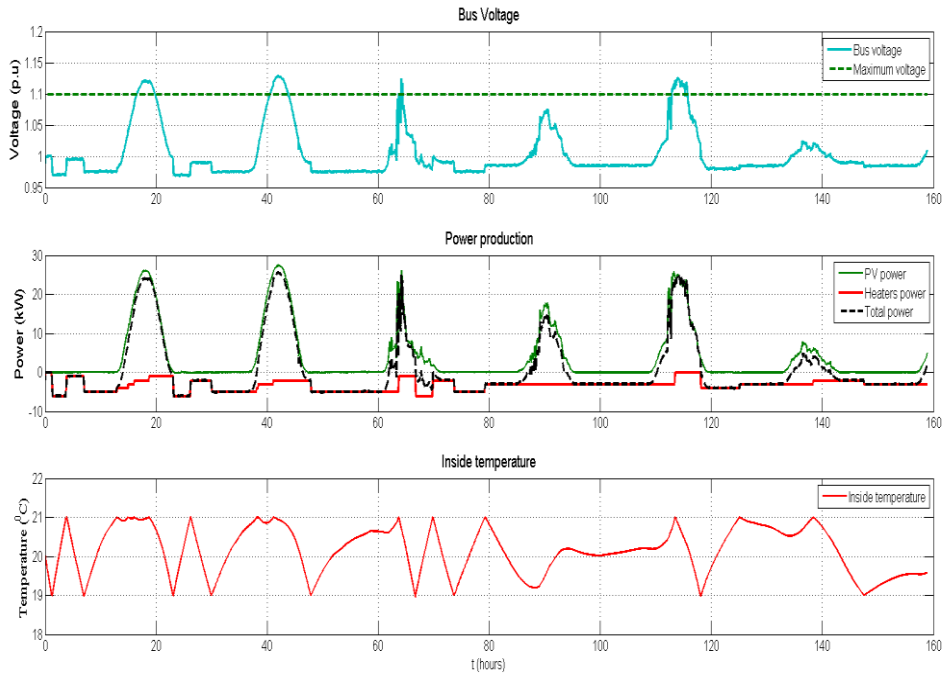
C) Simulation results

This section presents three study cases with PV production for 6 days during a summer week. The PV system is connected together with the Flex-House and the EV at the same bus-bar (last cabinet of the designed distribution grid in Fig. 3.32).

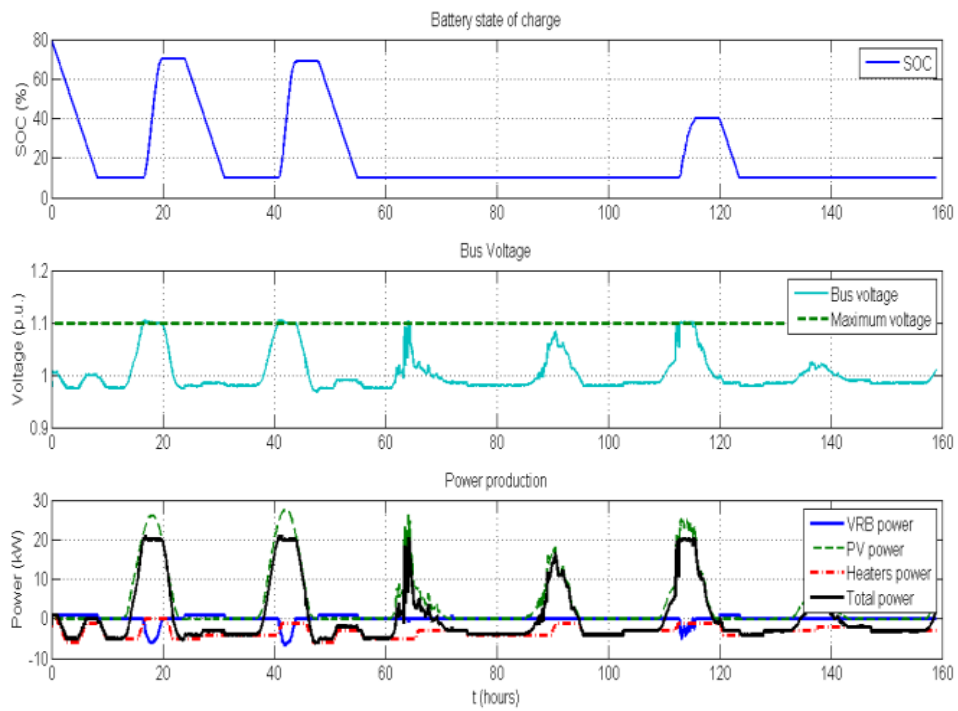
In Fig. 3.32 a) is shown a comparison between voltage at the bus-bar and the maximum voltage, set-up at 1.1 p.u., power production with PV power, Flex-House (Heater) power and the total power injected into the grid, and the temperature inside the house, during normal operation when no controller is implemented. Due to the PV penetration voltage at the bus-bar exceeds the maximum value.

Fig. 3.32 b) shows the case when the voltage controller (presented in Fig. 3.31)) is used. In this case the EV's battery operation is defined as using the voltage control mode during the day, when the PV system is able to produce power, while the battery was discharged during the night. The EV is connected when an over voltage occurs and it consumes the excess power until the power injected into the grid is not affecting the bus voltage to exceed the voltage limit, as can also be seen in Fig. 3.32 b).

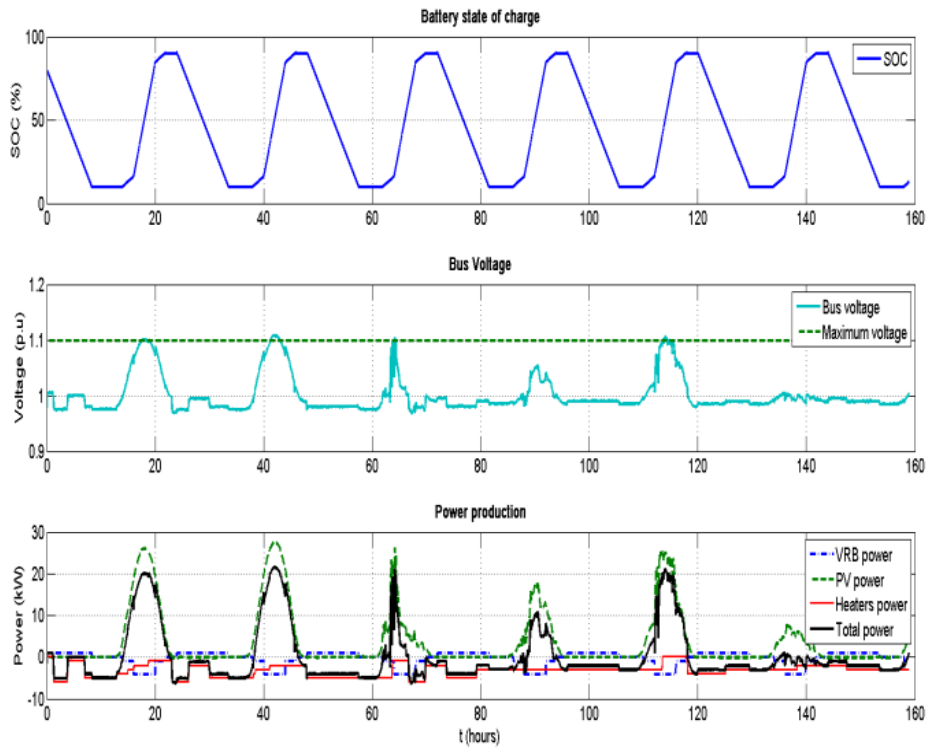
In Fig. 3.32 c) is presented the simulation results for another method to control the voltage using the battery storage system setting the EV battery to work in scheduling mode. The battery was scheduled to operate (charged) between 10-18 o'clock during the day, when the PV systems inject the power into the grid, and was discharged during the night. In order to operate in an efficient way in this case the EV battery has to be appropriated scheduled of charging itself with the right amount of energy in the middle of the day.



a)



b)



c)

Fig. 3.32. a) Simulation results for normal operation, b) simulation results with SOC, comparison between bus-bar and maximum voltage and power production for 6 days with voltage control and c) with EV battery control in schedule mode.

3.5. Discussion and Conclusion

The state of the art of wind turbines seen from electrical point of view includes old and new potential concepts of generators and power electronics based on technical aspects and market trends.

Several generic types of generator are possible candidates in wind turbines. The squirrel cage induction generator has been frequently applied commercially. The most dominating type, especially in the last ten years, is the induction generator with wound rotor, while the third is the current excited synchronous generator.

A large number of alternative wind turbine designs exist but the state of the art wind turbine may be summarized as a 3-bladed upwind turbine using active stall control with constant speed using cage rotor asynchronous generator or pitch control combined with variable speed using DFIG.

Active stall constant speed combines the advantages of passive stall, namely simplicity due to the absence of a pitch mechanism, with the advantages of pitch control, namely controllability.

Simulation results of a 2 MW active stall constant speed wind turbine had shown a good stability of the system during normal operation and also during transition of dynamic changes in wind speed.

The overall control of the variable speed pitch controlled wind turbine with DFIG has as goal to track the optimum operation point, to limit the power in the case of high wind speeds and to control the reactive power interchanged between the wind turbine generator and the grid.

The control strategy contains two control levels: DFIG control level (control of active and reactive power using vector control approach) and wind turbine control level (speed controller and power limitation controller).

The variable speed wind turbine has a more complicated electrical system than the fixed-speed wind turbine, but it is able to achieve maximum power coefficient over a wide range of wind speeds and about 5-10 % gain in the energy capture can be obtained.

The simulation results showed that the implemented control strategy for a 2 MW variable speed pitch controlled wind turbine is able to control efficiently the DFIG parameters during normal operation and during sudden changes in wind speed.

An important difference between an active stall controlled wind turbine and a pitch controlled wind turbine, when they reach rated power, is that the active stall wind turbine pitch the blades in the opposite direction (negative direction) from what a pitch controlled wind turbine does.

Both wind turbine control strategies implemented are an important step towards the long term objective of developing tools for study and improvement of the dynamic interaction between wind turbines and power systems.

In subchapter 3 two control strategies regarding induction generators connected to the grid were developed, implemented and tested for two variable speed wind turbines concepts.

The simulation shows good dynamic performance regarding power control when the rotor speed is varied. Measurements obtained confirm the theoretical results and validate the simulation program of the variable-speed constant frequency system with the DFIG for wind power generation applications.

A control scheme was developed for decoupled control of active and reactive stator power of the DFIG. The control strategy is a cascade control, has two control loops. An inner rotor current control loop and an outer stator power control loop. The two-phase d-q reference system with the q-axis aligned along the stator flux is chosen for implementation to realize decoupling of active and reactive power. The simulations developed in MATLAB-Simulink show that full power decoupling is obtained

in the complete operating range between 60 % and 140 % (± 40 %) of nominal speed. The doubly fed induction generator system presented in this paper offers many advantages to reduce cost and has the potential to be built economically at power levels above 1.5 MW, e.g. for off-shore applications. Additionally, when a bidirectional AC-AC converter is used in the rotor circuit, the speed range can be extended above synchronous speed and power can be generated both from the stator and the rotor. The two back-to-back PWM converters in the rotor circuit result in low distortion currents, reactive power control and both sub- and super-synchronous operations. Another advantage of this type of DFIG drive is that the rotor converter need only be rated for a fraction of the total output power (20-25 % of the total generator power), the fraction depending on the allowable sub- and super-synchronous speed range.

In the last part of subchapter 3 a flexible development platform with dSPACE-DS1103 was used to implement and test a control strategy for 11 kW variable-speed wind turbines with a cage-rotor induction generator. Using this configuration is possible to increase the energy production especially in the low wind range, up to 1 MW per unit that can be used in remote places.

In the last subchapter two types of controllers for voltage regulation in a distribution network have been successfully developed and implemented in MATLAB/Simulink and DigSILENT PowerFactory for controlling the bus-bar voltage at the connecting point. One type is based on local control by load shifting; another one is controlling the voltage with the help of storage energy system.

The comparison between both simulation tools has shown a good alignment and the possibility to use them for further developments, regarding the integration of smart-grid technologies. It means that this work could be used for development and improvements of the models for different components placed along the feeders in a future Smart-Grid distribution network.

Chapter 4

Testing of DER Components with Storage Devices and Actively Controlled Loads in a Smart Grid

Content of the Chapter 4

Contents

- Chapter 4..... 134
- Testing of DER Components with Storage Devices 134
- and Actively Controlled Loads in a Smart Grid..... 134
- 4.1. Introduction 136**
- 4.2. Experimental Testing for Stability Analysis of D E R Components with Storage Devices and Loads 138**
 - 4.2.1. DER Components with Storage Devices and (Controllable) Loads 138**
 - 4.2.2. Components Testing under different Modes of Operation..... 141**
- 4.3. Electric Vehicle Batteries Testing in a Smart Grid using Renewable Energy 147**
 - 4.3.1. Smart Grid Energy System Infrastructure 147**
 - 4.3.1.1. Battery Management System Test Platform..... 147**
 - 4.3.2. Experimental Tests and Results 149**
- 4.4. Discussion and Conclusions..... 161**
- Appendix 163**

4.1. Introduction

The distributed energy resources (DER) contains several technologies, such as diesel engines, small wind turbines, photovoltaic inverters, etc. The control of DER components with storage devices and (controllable) loads, such as batteries (Electric Vehicle (EV) batteries, Vanadium Redox Battery (VRB)), capacitors/supercapacitors, dump loads, smart houses are central to the concept of the Micro Grids or Smart Grids.

EV technologies are still relatively new and under strong development. Many different designs and choices of technologies have been pursued by the automotive OEMs, battery industry and EV research centers. Although some standardized solutions are being promoted and becoming a new trend, there is an outstanding need for common platforms and sharing of knowledge and core technologies.

Advanced energy storage devices and converters are introduced and tested in the last time for the next generation of EV for the smart grids [1]-[3].

The different types of EV batteries have different characteristics regarding cost, energy density, safety, energy efficiency, degradation etc. making them suitable for different EV applications, such as PHEV (many small cycles), full EV (many full cycles), fast charging or V2G (cycles at high SOC) [4]-[6].

Today, batteries are still a critical component in the EV industrialization due to their high price, technical complexity, limited records of long term operational data, etc. One of the most commonly selected Li-ion battery types for commercial electric vehicles is Li-ion manganese oxide based due to its overall balanced performance in energy/power densities, lifetime, cost and safety. At the same time new Li-ion battery types started to show competitive key feature. Lithium-iron phosphate type was becoming a promising choice for PHEV's due to its high power/energy ratio favorable for HEV and PHEV as well as improved safety and cycle life. On the other hand, mixed oxide based Li-ion types such as NMC (Ni, Mn and Co based) showed high energy density, which is crucial for the driving range of pure EVs and started to be an interesting choice for EV's [4], [7]-[11].

Battery management system (BMS) functionalities are very important for the optimal use and handling of batteries. The functionalities of the BMS could play a critical role to make an EV battery robust and vulnerable towards charging tests [12]-[16].

Smart charging is one of the main challenges in EV mobility development. It is seen as indispensable to facilitate the optimal integration of EV to power system in order to avoid technical bottlenecks and corresponding unnecessary investments in electricity network [4], [17]-[19].

Vehicle-to-grid (V2G) allows using EVs to provide ancillary services to the electrical power grid. Additional grid services contribute to the optimization of energy use, for example, by the management of energy and power balance. Interaction with power grid needs bi-directional communication between electric vehicles and charging spots and bi-directional power flow. Therefore, the focus is on issues such as: reverse energy flow, control, communication and safety, which are the key issues in the future smart city concepts [20]-[22].

Fast charging should be able to charge a significant amount of energy (25÷75 % of the battery's capacity) into the battery within 5÷15 minutes, depending on the actual application. As the capacity of the batteries for the EVs required fast charging are expected to be in the range of 25÷50 kWh and the charging power should be in the range of 100÷200 kW [4-5].

The change of the load profile depends on the penetration level of EVs as well as on the used charging strategies. Several smart charging strategies as well as charger topologies are presented and assessed in [24]-[28].

This chapter is focus on testing of DER components with storage devices and actively controlled loads and also on electric vehicle batteries testing to study the impact of smart charging and fast charging on the power system and on the battery degradation. Two different types of EV battery packs have been tested: a 16 kWh Lithium-Ferro type, optimized for hybrid EV applications, and a 26 kWh Lithium polymer type, optimized for full EV applications. The objectives of the smart charging tests are to address not only the charging needs specified by the user, but also to address the needs for power regulation in the power system. The objectives of the fast charging tests are to test different charging profiles and to study the impact on the charging efficiency and on the batteries.

Also the chapter provides description of the battery management systems with details about monitoring, protection and control of the battery pack systems. The experimental tests and results are presented including performance testing, for smart charging and fast charging, as well. Finally, concluding remarks are presented in the last section.

4.2. Experimental Testing for Stability Analysis of D E R Components with Storage Devices and Loads

The electrical power system is facing an evolution from the traditional concept of energy generation by few localized power plants interconnected together through a meshed system to distributed medium and small scale generators. Some topologies of these generators embedded into the distribution network are fed by renewable sources like wind and sunlight. Their main drawback is their hardly predictable behavior and uncontrollable output.

The presence of energy storage system may allow a better management of the electric system allowing the full exploitation of renewable energy sources. Distribution companies start to recognize that storage has the unique ability to act as a buffer between the grid and generation that is either intermittent or not controlled by the utility [32-35].

The distributed generation is taking importance pointing out that the future utility line will be formed by distributed energy resources and micro-grids. The flexible micro-grid has to be able to import/export energy from/to the grid, control the active and reactive power flows and manage of the storage energy [36].

With the publication of IEEE Standard for Interconnecting Distributed Resources with Electric Power Systems, the electric power industry has a need to develop tests and procedures for verifying that DER components meet the technical requirements [37].

A Micro Grid/Smart Grid can operate interconnected to the main distribution grid or in islanded mode.

This subchapter presents experimental tests for static and dynamic stability analysis carried out in a dedicated laboratory for research in distributed control and Smart Grid with a high share of renewable energy production. Moreover to point out, on a laboratory scale, the coupling between Distributed Resources and storage and to effectively compensate wind fluctuations a number of tests have been done. In order to find out the parameters of various types of DER components for dynamic simulation models a number of tests are required under different operation modes and loads. The testing reporting here includes three modes of operation: stand alone, parallel/hybrid and grid connection.

Dynamic and transient events (wind variation, connecting/disconnecting sequence etc.) are studied as a basis for further activities in which the dynamic simulation models of DER components and other DG units and the related control systems capable of performing a coordinated management will be implemented. Also, in order to find out the differences between DER components in power systems and to study the impact on bus bar voltage and frequency the system will be tested for different wind speeds and loads.

4.2.1. DER Components with Storage Devices and (Controllable) Loads

The system under tests was presented in chapter 2/2.2 and contains a Diesel Gen-set of 60 kVA/48 kW, a GAIA Wind Turbine of 11 kW, a Dump-Load of 75 kW, a Vanadium-Redox Battery (VRB) of 15 kW/180 kWh, and a local grid.

All units on the grid – generators, loads, storage systems, switchgear – are automates and remote-controllable. Each unit is supervised locally by a dedicated controller node. The node design combines an industrial PC, data storage, measurement and I/O interfaces, backup power and an Ethernet switch inside a compact, portable container. All nodes are interconnected via redundant

high speed Ethernet, in a flexible setup permitting on-line changes of topology and the simulation of communication faults.

A) Wind Turbine

The GAIA Wind Turbine has 11 KW rated power, 2 bladed horizontal axis, stall controlled; Rotor diameter has 13 m, rotor speed is keep constant at 56 rpm with a gear box ratio of 1:18. Starting wind speed is 2.5 m/s, cut in wind speed is 3.5 m/s, rated wind speed is 9.5 m/s and cut out wind speed is 25 m/s [40]. The machine driven by wind turbine is a cage rotor induction generator with rated power of 11 KW, rated speed of 970 rpm, rated voltage of 400V and rated current of 21.8/12.7 A; It has also a capacitor bank of 10 kVAR for self-excitation and no-load compensation. The consumption of reactive power at no load is 6.32 kVAR and at full load is 9.7 kVAR.

It has a soft starter in order to reduce the inrush current during connection. The maximum cut-in current controlled via soft starter is 22 A, and also max starting current is 30 A;

B) Diesel GenSet

Diesel Gen-set contains a diesel engine with 6 cylinders, a speed governor and a synchronous generator with an AVR (automatic voltage regulator) and an AGC (automatic gen-set controller).

The governor and the diesel engine system control the generator speed and provide mechanical power as an input to the generator. Speed governing is dedicated to generator response to load changes.

The synchronous machine is a four pole machine with salient-pole design. It uses brushless excitation and a digital automatic voltage regulator (AVR controller). The AVR controller regulates the parameters of exciter field to provide a constant terminal voltage. AVR acts upon the DC Voltage that supplies the excitation winding of SGs. The variation of field current in the SGs increases or decreases the emf (no load voltage) and thus for given load the generator voltage is controlled.

C) PV Inverter

48th PV panels of around 8 kW are connected to the SYSLAB grid through a three-phase PV inverter (SMA Sunny Tripower). The PV inverter has the ability to provide active and reactive power regulation.

PV controller can be programmed to automatically regulate the active power at frequency deviations and the reactive power at line voltage deviations when SYSLAB is operated in isolated mode and also grid connected one.

D) Data Acquisition and Control System

The data acquisition and control system (hardware and software) is responsible for the supervision and control of the research platform for distributed intelligent energy systems with a high penetration of renewable energy. The supervisory software code was written in Java and is able to manage the data acquisition, processes the data and executes the control loop and outputs the control variables. The sensors outputs are connected to a signal conditioning board, which in turn is connected to the data acquisition (DAQ) board based on a PC (SCADA System).

Some loads can be controlled by the central building controller which receives data and events from wireless switches and sensors. In one room, a small touch-screen user interface can be used to influence the controller policy (Fig. 4.1). Through its own grid control node, the building controller

4.2.2. Components Testing under different Modes of Operation

The testing reported here include three modes of operation: stand alone, parallel/hybrid and grid connected.

In order to find out the differences between DER components in power systems and to study the impact on bus bar voltage and frequency the system will be tested for different wind speeds and loads.

To test the static and dynamic characteristics of a VRB a set of charge/discharge tests and a step response tests at different SOC levels have been done. The proposed tests have been carried out to characterize the battery from a power system point of view and to assess it with respect to integration of wind energy in power system and to evaluate its potential role in the future energy systems. Also the tests have been done to find the main parameters of the battery and to test the system response for parameter tuning of the controller.

A) Stand Alone Operation

In this mode of operation the Diesel Gen-set is connected together only with a dump load, as can be seen in Fig. 4.2.

The voltage and frequency are controlled by the gen-set and the load is provided by diesel generator. The ability of the diesel generator to respond to frequency changes is affected by the inertia of the Diesel Gen-set, the sensitivity of governor and the power capability of the Diesel Engine and Synchronous Generator. The response time of AVR and excitation system will show the ability of the machine to control the voltage.

The objective of the test is to investigate static and dynamic stability that means the property of the synchronous generator to remain in synchronism at a very slow and quick variation of load and to test the system response for parameter tuning of the AVR and governor controllers.

In Fig. 4.3 the diesel gen-set was running and at $t=1$ sec has been applied a large step in load (about 80% of nominal load) from zero to 40 kW and back to zero at $t=7$ sec. The droop voltage was about 10-12 V and the settling time around 3 sec.

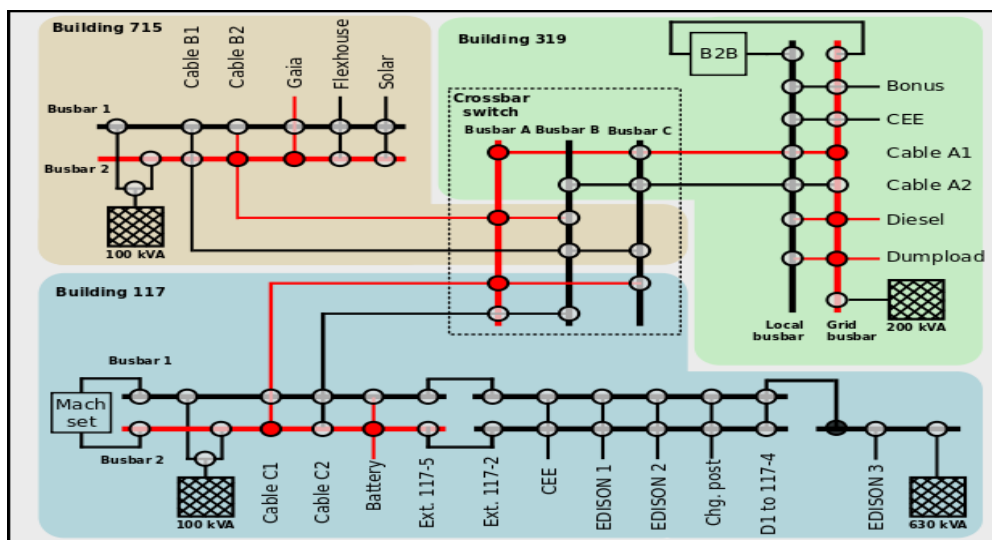


Fig. 4.2. Details about SYSLAB Micro-Grid architecture (plant components) in islanding mode.

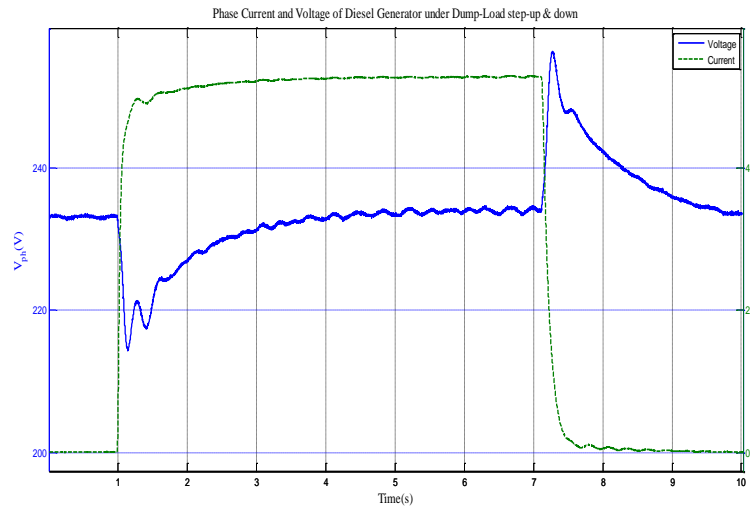


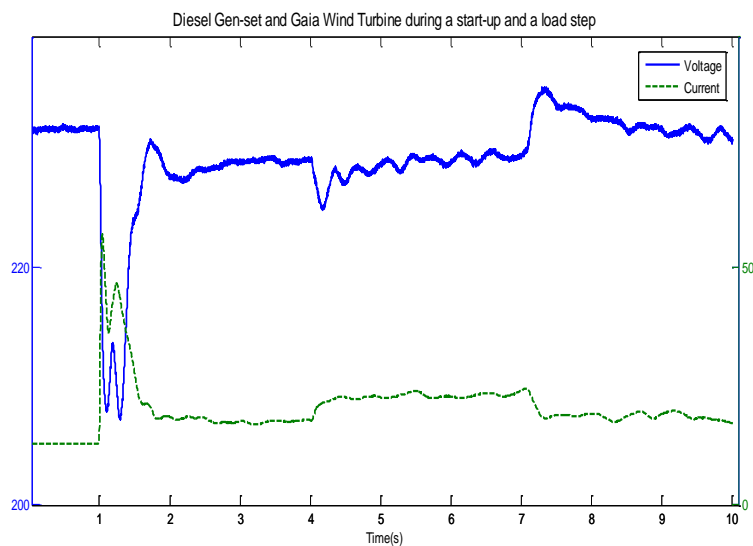
Fig. 4.3. Phase Voltage and Current as a function of time during switch-on and off of a large step in load. The data was acquired by an Oscilloscope with a sampling frequency of 1 kHz.

B) Hybrid/Parallel Mode

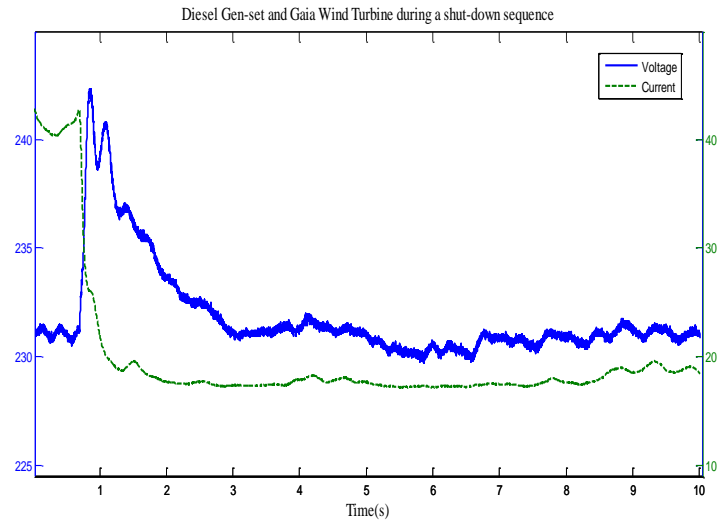
In this mode of operation the Diesel Gen-set is connected together with GAIA Wind Turbine, a dump load and a battery. The voltage and frequency are controlled by the gen-set and the load is shared between DG and Gen-set.

The main objective of the tests has been to study the voltage, active and reactive power and frequency and speed variations during variable wind conditions and during start-up and shut-down of the wind turbine and during changes in load.

Another objective was to investigate if the Gen-set unit maintains synchronism during these transients. This includes the dynamic performance (Fig. 4.4) and the long term conditions, too (Fig. 4.5).

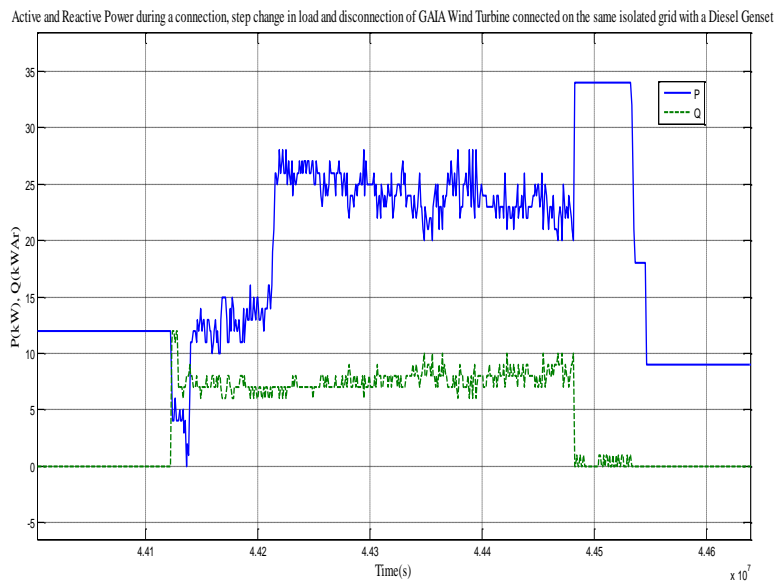


a)

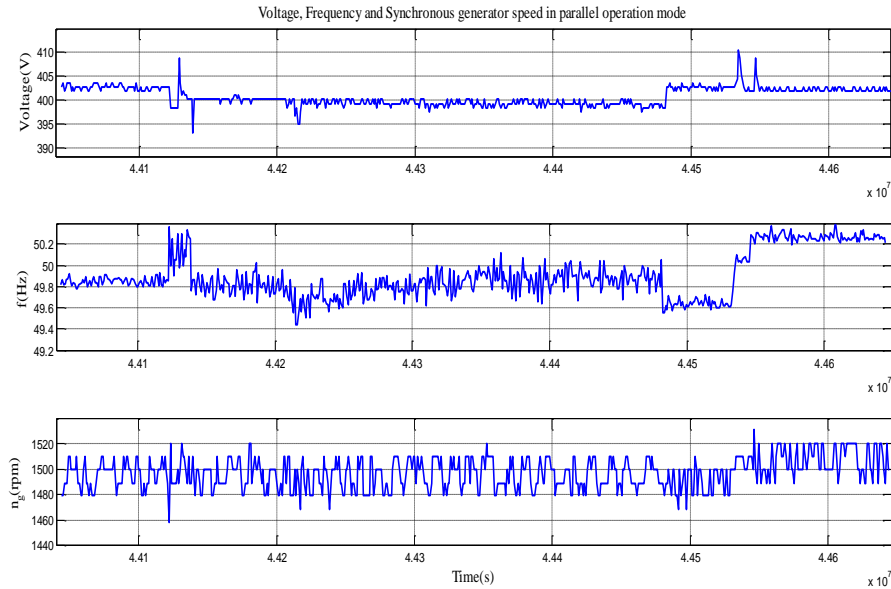


b)

Fig. 4.4. Phase current and voltage acquired by an Oscilloscope a) when the wind turbine was connected at 1 sec and an increase and a decrease step in load was applied at 4 and 7 sec. respectively, and b) during a shut-down sequence. The GAIA was connected together with the Diesel Gen-set and a dump load.



a)



b)

Fig. 4.5. a) Active and reactive power and b) voltage, frequency and speed as a function of time when the Gaia WT was connected together with Diesel Gen-Set and a battery ($t=4.41$ sec), then a step in load was applied at $t=4.42$ sec and the GAIA was disconnected at around $t=4.45$ sec.

In Fig. 4.4 is depicted a start-up sequence of GAIA Wind Turbine at a wind speed higher than nominal ($w_s=12$ m/s $>$ $w_{sN}=9.5$ m/s), with the Diesel Gen-set and a load of 12 kW already connected (see Fig. 4.2). The GAIA WT was connected at $t=1$ sec, then a step-up in load was applied at $t=4$ sec and a step-down at $t=7$ sec from 15kW to 20kW. During these changes in load the voltage response of the synchronous generator controller was very fast. The droop voltage was the same as in standalone operation when we applied a large step in load but the settling time in this case was larger (about 4 sec). Also the current has risen from 18 A to 42 A.

In Fig. 4.4 b) is shown the voltage response when the GAIA Wind Turbine was disconnected with Diesel Generator and a load of around 12 kW still connected.

The Figures 4.5-4.6 presents the dynamic performance of the system in terms of active and reactive power distribution between the components and voltage, frequency and speed response of the system during different transient, such as connection and disconnection of the wind turbine, and during a large step in load.

The variations in wind turbine output are compensated by diesel gen-set. The voltage and frequency variations are very small during dynamic changes due to the automatic voltage regulator (AVR) of the synchronous machine exciter and speed governor of the diesel engine. The frequency variations are between (49÷51) Hz and speed variations are between (1480÷1520) rpm, as can also be seen in Fig. 4.5.

In Fig. 4.6 the battery was used as a load with GAIA wind turbine and Diesel Gen-set connected together.

Frequency band of AVR controller is within 2-3 Hz and of speed governor control is less than 2 Hz, in general. SGs operating in a power system have speed droop controllers to allow for power sharing between various units. Speed droop is typically (4-5) % [9].

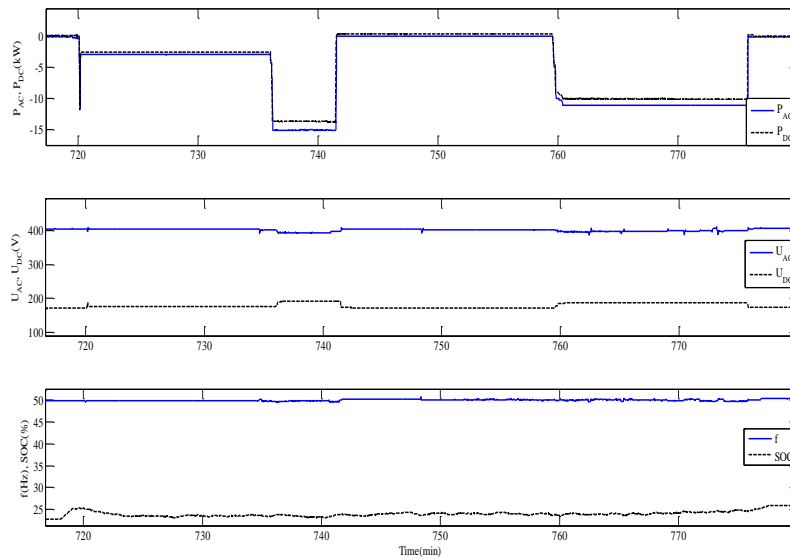


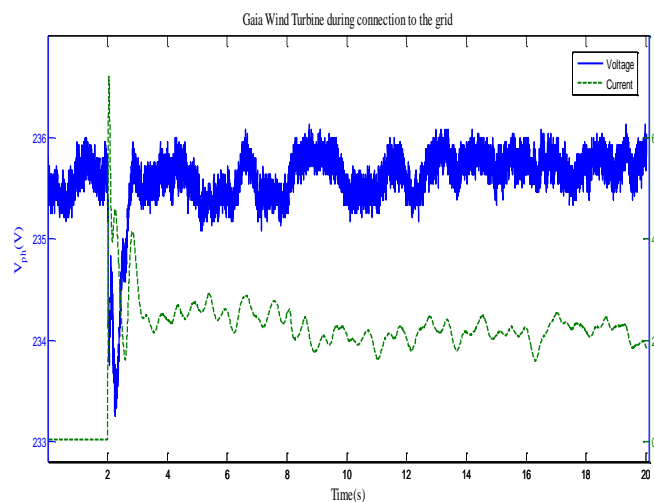
Fig. 4.6. AC and DC Power and Voltage, SOC level and Frequency of the battery terminals when the GAIA Wind Turbine was connected ($t=720$ min)/disconnected ($t=775$ min) to/from the hybrid system and a step in load was applied at 738 min and again at 760 min.

C) Grid Connection

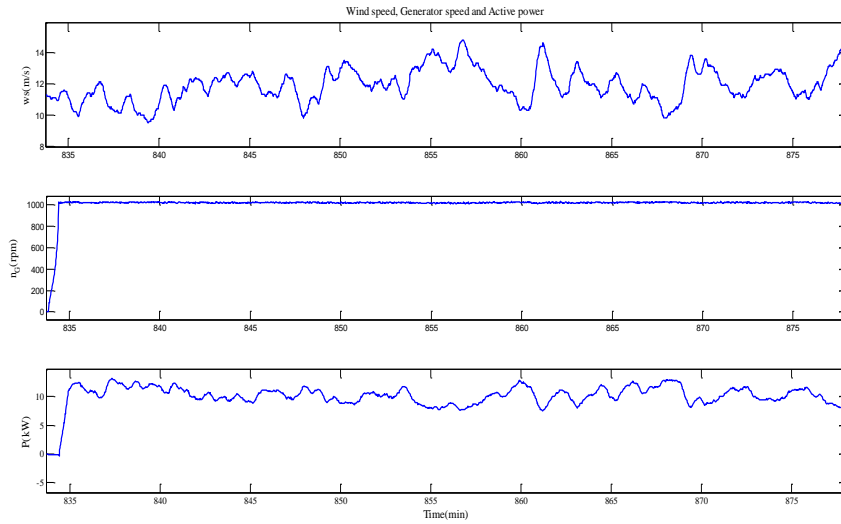
In this mode of operation the GAIA Wind Turbine was connected to the local grid together with a Vanadium Battery. The main objective of the tests has been to study the active power and generator speed variations during variable wind conditions and during start-up and shut-down of the wind turbine.

During the start-up sequence the current of the induction generator increased 3 times more than nominal current ($i_N=22$ A) and the start-up time was around 2 second, as shown in Fig. 4.7 a). The wind speed was between 10-15 m/s and the active power produced by wind turbine between 9-12 kW, as can also be seen in Fig. 4.7 b).

In Fig. 4.8 is shown a dynamic response test of VRB during charge/discharge cycle and a step response test at different SOC levels. The battery-inverter system can function as a power source when it is discharging energy, and as a load as it is storing energy.



a)



b)

Fig. 4.7. a) Generator Phase Voltage and Current during a start-up sequence to the local grid, acquired by an Oscilloscope and b) Wind, Generator Speed and Active Power, acquired by SCADA system with a sampling frequency of 1Hz.

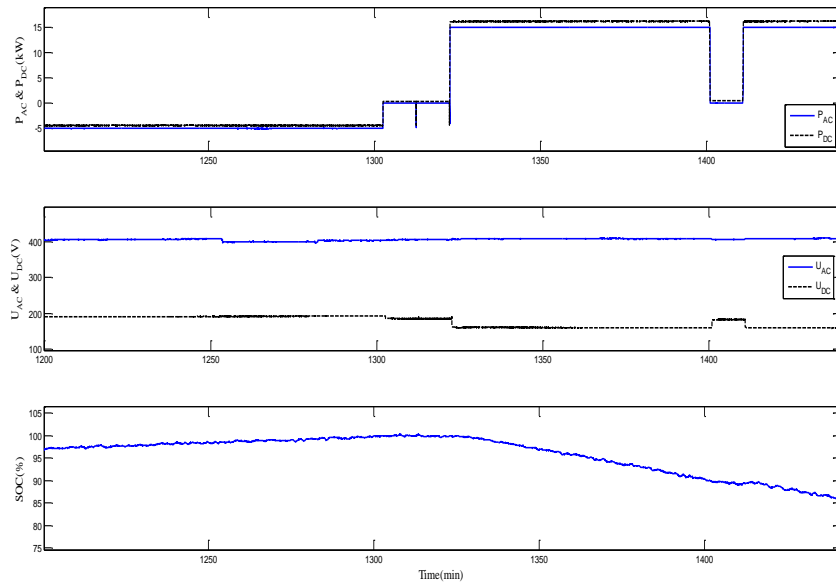


Fig. 4.8. AC and DC Power and AC and DC Voltage during a charge/discharge cycle at different SOC levels. The data was acquired by SCADA System at battery terminals.

4.3. Electric Vehicle Batteries Testing in a Smart Grid using Renewable Energy

4.3.1. Smart Grid Energy System Infrastructure

The architecture of the Smart Grid system, used for the experimental test of this chapter, is called SYSLAB and was presented in chapter 2/subchapter 2. It is a laboratory for research in distributed control and smart grids with a high share of renewable energy production. Its experimental facility is a Wind/PV/Diesel Hybrid Mini-Grid with local storage and a novel control infrastructure.

Under the tests reported in this subchapter the SYSLAB power system has been operated as a micro-grid connected to the national grid, emulating a local part of a larger power system. In addition to the EV batteries, the micro-grid includes wind power, solar power and flexible loads representing future consumers. The batteries can switch between being connected either to the micro-grid or direct to the national grid through dedicated grid connections, emulating grid connected state or driving state, respectively, as can also be seen in Fig. 4.9.

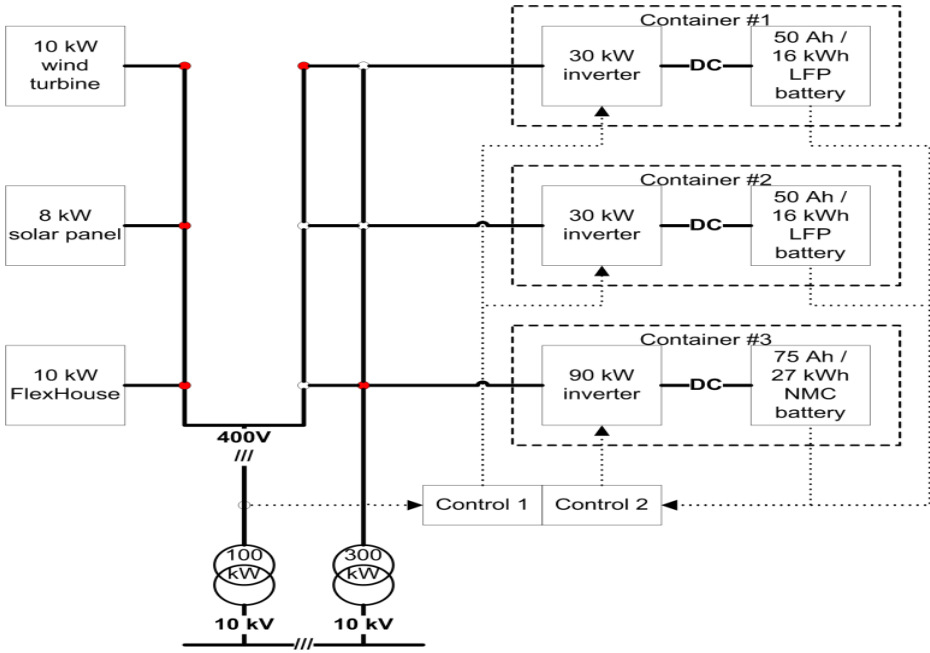


Fig. 4.9. The power grid connection options of the EV batteries and their inverters to the SYSLAB power systems.

4.3.1.1. Battery Management System Test Platform

This section covers the description of the battery management systems with details about monitoring and protection of the battery, communication technologies and interfaces to enable open network communication and interoperability. Also, a block diagram of the BESS topology, including the bi-directional Voltage Source Converter (VSC) is presented.

The EV batteries packs are equipped with a dedicated battery management unit/system (BMU/BMS), monitoring the states of the individual cells in terms of voltage, current and temperature. The

battery management system covers an individual BMU, CAN-CAN converter and a bidirectional power converter and protects the battery from being overloaded by external load requests, as it is shown in Fig. 4.10.

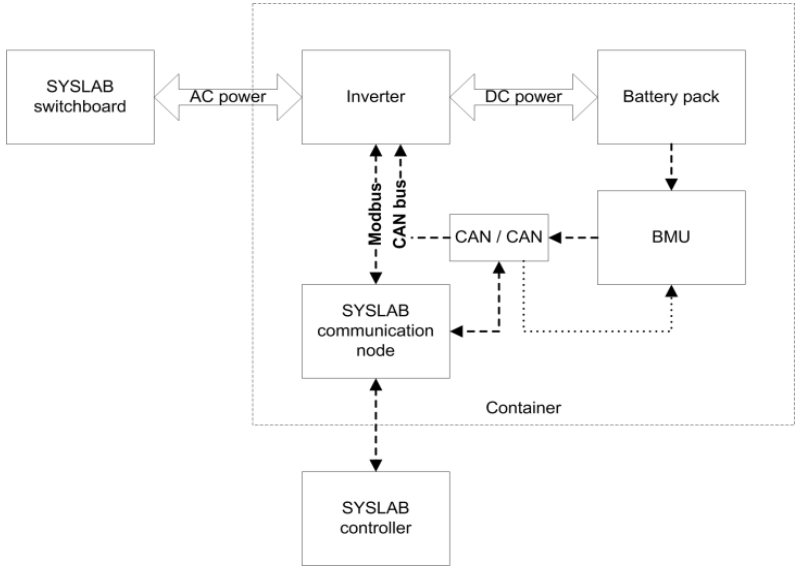


Fig. 4.10. Details about the communication and control of the test platform including EV pack and bidirectional converter.

The BMU (BMS) monitors the state of the individual cells and send a request to the inverter to reduce the power, controlling the power flow to and from the battery, in order to protect the battery from being overloaded by an external load request.

Individual CAN-CAN converter has been developed and inserted between the BMU (BMS) and the inverters (bi-directional power converter), monitoring the communication between them and converting the communication between different protocols.

The bidirectional inverter is able to control the power flow to and from the battery within the specified limitations using its integrated control panel and also by external communications. The block diagram of the BESS topology, including the bidirectional power converter is shown in Fig. 4.11 The power converter contains a DC-DC bidirectional buck-boost converter and a pulse with modulation (PWM) VSC. A current-controlled voltage source, using active and reactive power loops with PI-regulators, is used. The active current component is used to control the DC link voltage and, consequently, the inverter active power output, in order to balance the EV battery and inverter active output power. The reactive current component controls the inverter’s reactive output power.

The bidirectional inverter is able to control the power flow to and from the battery within the specified limitations using its integrated control panel and also by external communications.

The inverter communication ports are: an Ethernet port for communication with the SYSLAB communication node (Mod bus TCP) and a CAN port for communication with the BMU, as can also be seen in Fig. 4.10.

The various test load patterns are controlled from dedicated controllers implemented in the SYSLAB controller. From the SYSLAB controller the power flow to/from the batteries can be controlled in either current or power control mode independent of the sign of the control parameter. The power flows to and from the batteries are fully controlled by the SYSLAB controller.

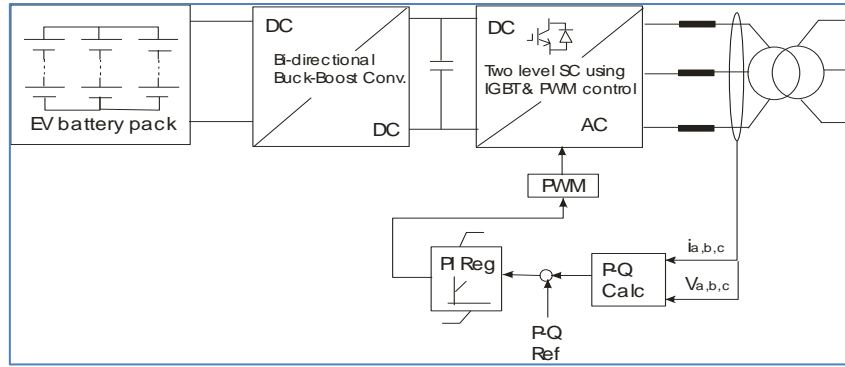


Fig. 4.11. Block diagram of the BESS topology with its two-level bidirectional power converter.

4.3.2. Experimental Tests and Results

The test platform includes three test benches in individual containers (for safety), each with an EV battery pack and a bidirectional converter to control the power flow to and from the battery, as it was shown in Fig. 4.10.

Two of the inverters have capacities of 80 A and the 3rd one has a capacity of 210 A, used for fast charging testing.

Two types of batteries were tested: a BYD 50 Ah/16 kWh Lithium-Ferro-Phosphate [22], suitable for hybrid EV applications, and a Kokam 75 Ah/26 kWh Lithium-Polymer (NMC) [23], suitable for EV applications. More details can be found out in the appendix. Each battery pack is equipped with a dedicated battery management unit (BMU) to monitor the voltages, currents and temperatures of the individual cells, and, if necessary, sending requests to the inverters to reduce the current in order to protect the battery against overloading.

It is very important to implement standardized and compatible communication and control interfaces (ICT) platforms for charging infrastructure to support intelligent and controllable charging in an open network for optimal socio-economic impact. We used IEC 62196 standard for setting the electrical connectors and charging modes for EVs and IEC 61851 for communication and control interface platform for charging infrastructure.

A) Performance Testing

The irreversible or permanent degradation of the battery's electrical performances over time is very critical to the operation of the battery in terms of the cell voltage, current and temperature. These parameters are typically monitored by a dedicated Battery Monitoring/Management Unit (BMU), controlling the power flow in the battery, and thereby protecting the battery from overloading.

A specific objective of the work has been to develop, calibrate and evaluate a general battery degradation model for Li-ion batteries.

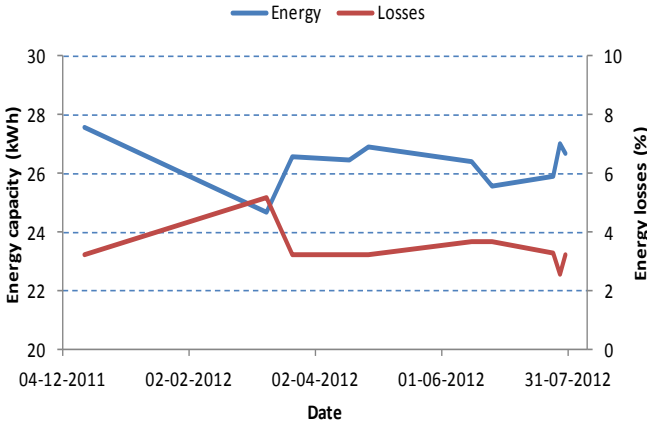
Two performance parameters, the energy capacity- E_{bat} and the energy losses- E_{loss} of the battery, are considered for this test. The energy capacity is provided by the energy of the battery from fully charged to fully discharged and the energy losses are given by the energy efficiency (η) as the losses for a full discharge-charge cycle relative to the discharged energy:

$$\eta = \frac{E_{loss}}{E_{batt}} = \frac{E_{char} - E_{disch}}{E_{disch}} \quad (4.1)$$

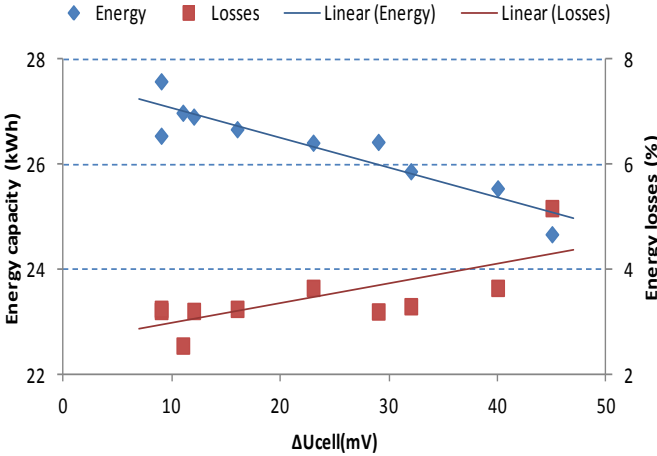
Where E_{char} is the full charge energy and E_{disch} is the full discharge energy. The fully charged and discharged levels are defined by the maximum and minimum cell voltages, as specified by the manufacturer (see the appendix).

The two performance indicators (the energy capacity and the energy losses) were measured in the same way on regular basis. Before the performance measurements, the cells have been balanced, using their dedicated BMUs. Also, the battery was discharged and charged with constant and relative low current (0.3 C) in order to keep the temperature relative constant.

The development over time (8 months) of the two measured performance indicators is illustrated in Fig. 4.12 a), while in Fig. 4.12 b) is shown a linear approximation between the cell voltage balancing level and the performance indicators.



a)



b)

Fig. 4.12 a) The measured development over time of the energy capacity and the energy losses for the Kokam battery and b) the two performance indicators measured at different time as function of cell balancing.

To get a better understanding of the losses the internal resistance was also measured at different SOC, current levels and temperatures using pulse current discharging/charging. The internal resistance shows much stronger dependence on temperature than on SOC increasing at low temperature and decreasing at high temperature. More details can be found in [29], where is also presented the development of dynamic electro-thermal model of the battery, based on equivalent

circuit modeling including the lifetime electrical battery model and nonlinear open-circuit voltage, one RC parallel network and a series resistor as a function of SOC, current and temperature. A graphical user interface, generated by the battery degradation model, developed and integrated in our simulation model, is presented in Fig. 4.13.

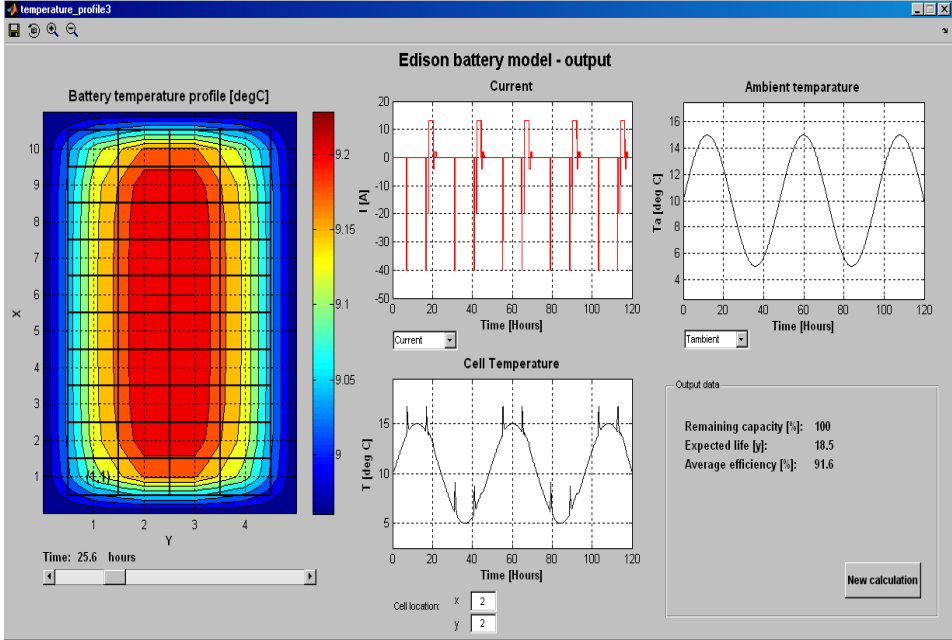


Fig. 4.13. The graphical user interface of the battery degradation model having as input the electrical and heat exchange specifications and the charge/discharge current and ambient temperature profiles and as output the electrical performance, lifetime, degradation effects and efficiency of the battery.

B) Fast Charging Tests

The objectives of the fast charging tests are to test different charging profiles impact on the charging efficiency and on the battery. This method has been tested with many cycles of fast charging and slow discharging at different power levels, SOC levels and charging energy. The battery’s SOC is defined as the remaining usable energy in the battery at the given load level and temperature relative to the battery capacity at the actual load level and temperature. The SOC is therefore 100% at fully charged and 0% at fully discharged.

Fig. 4.14 presents a block diagram of the set-up with the high power inverter and EV battery used for the fast charging tests.

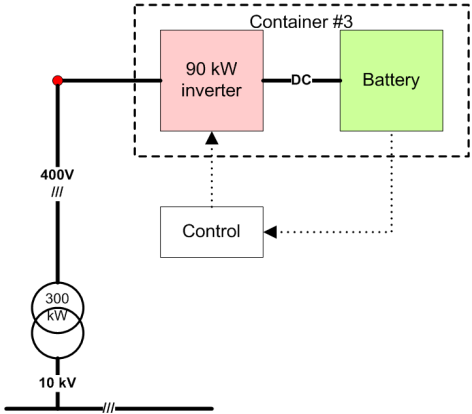


Fig. 4.14. The power connection of the EV battery and its inverter for fast charging tests.

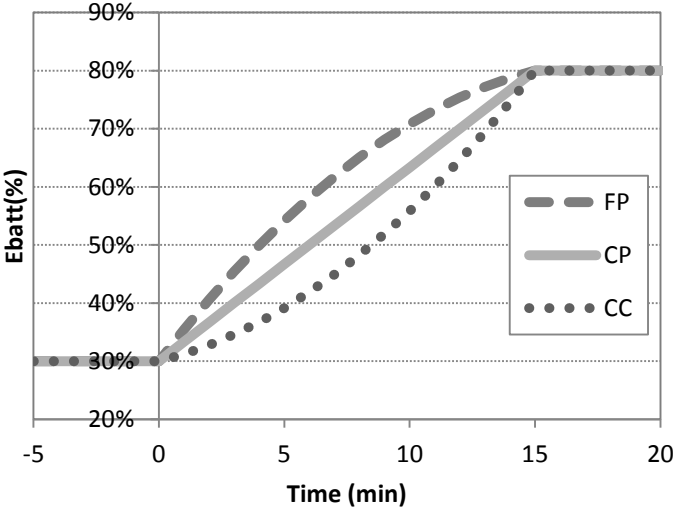
Different charging profiles have been tested. An overview of these profiles is given in Table 4.1, including constant current (CC), constant power (CP), and forced power (FP).

TABLE 4.1: An overview of the different charging profiles tested

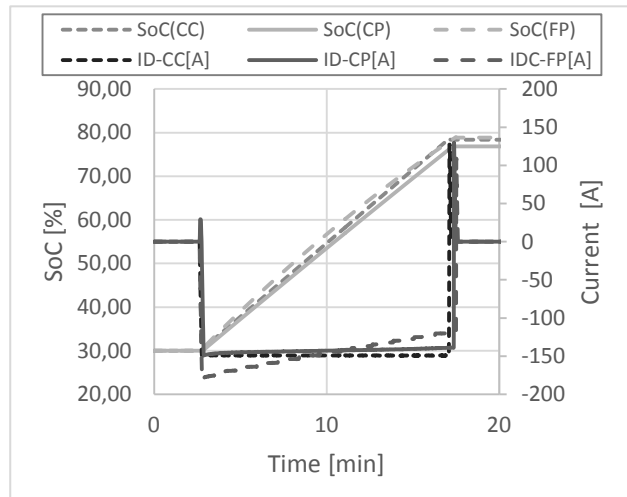
Profile	Charging characteristics
Constant Current-CC	The battery is charged with CC until the required energy has been charged or the charging power is limited by battery constrains
Constant Power-CP	The battery is charged with constant power until the required energy has been charged or the charging power is limited by the battery constrains
Forced Power-FP	The charging power is gradually reduced until the required energy has been charged or the charging power is limited by the battery constrains

To point out the difference between charging profiles a comparison is shown in Fig. 4.15 a). The different charging profiles reach a given amount of charged energy within a given time, 15 minutes in Fig. 4.15 b), and independent of the profile. As can also be seen in Fig. 4.15, during the CC charging, the SOC increased linearly with time, while during CP charging, the battery current decreases with time as the voltage increases.

With the limited cooling of the batteries in the tests, there were found very little differences between the different charging profiles.



a)



b)

Fig. 4.15 a) The estimated stored energy in the battery during the planned fast charging strategies and b) Battery's SOC & current as a function of time for 50% energy charged in 15 minutes for three charging profiles: CC, CP and FP.

An example of the repeated fast charging tests cycles with a constant power is presented in Fig. 4.16. The temperature increases very fast from around 25 °C to around 40 °C and as the voltage increases with the SOC level the charging current decreases during the fast charging.

Since the voltage of the Kokam battery increases constantly with the SOC over the full range this makes possible to use it in combination with temperature to estimate the SOC, and allows identifying the fully charged/discharged states by checking the specified maximum/minimum cells voltage. It means that the current must be limited when is close to fully charged/discharged.

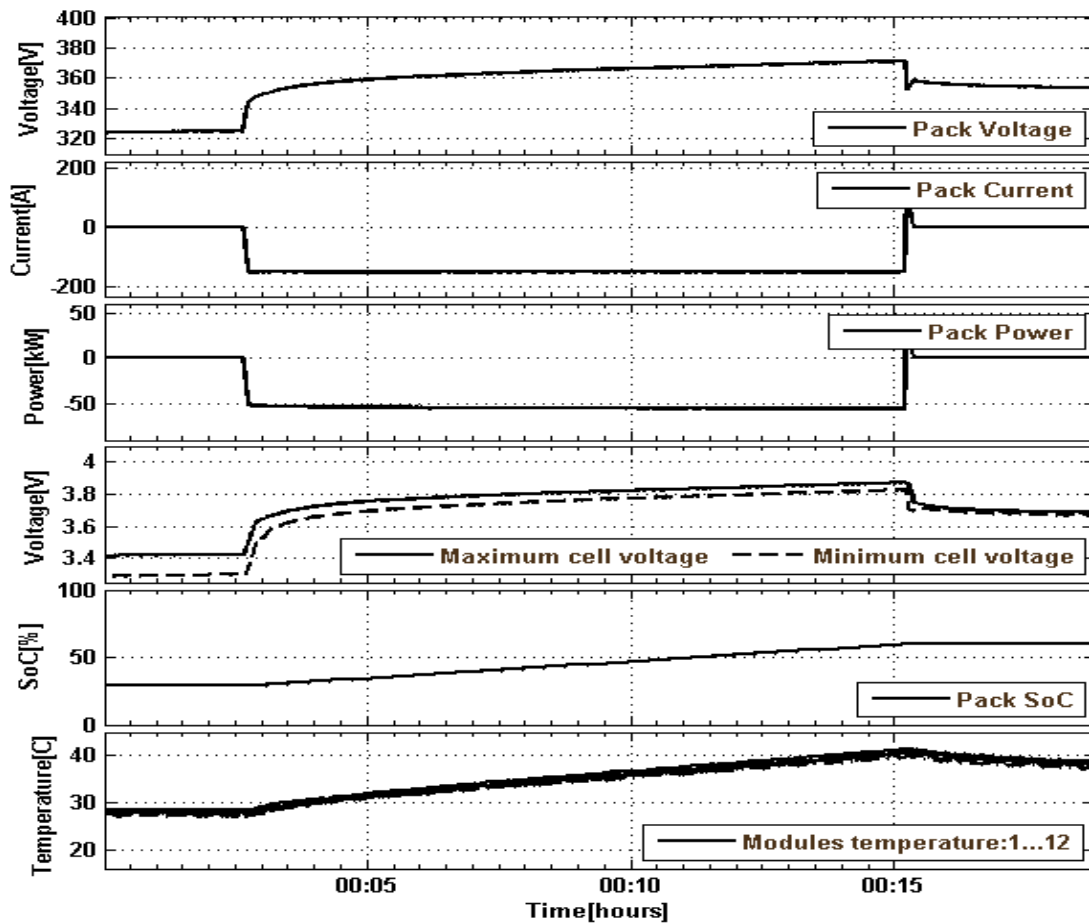


Fig. 4.16. Example of a repeated fast charging test cycling of the Kokam battery with a charge energy of 13 kWh (50 % of SOC) at constant current of 2C (150A) & discharging with C/3(25A).

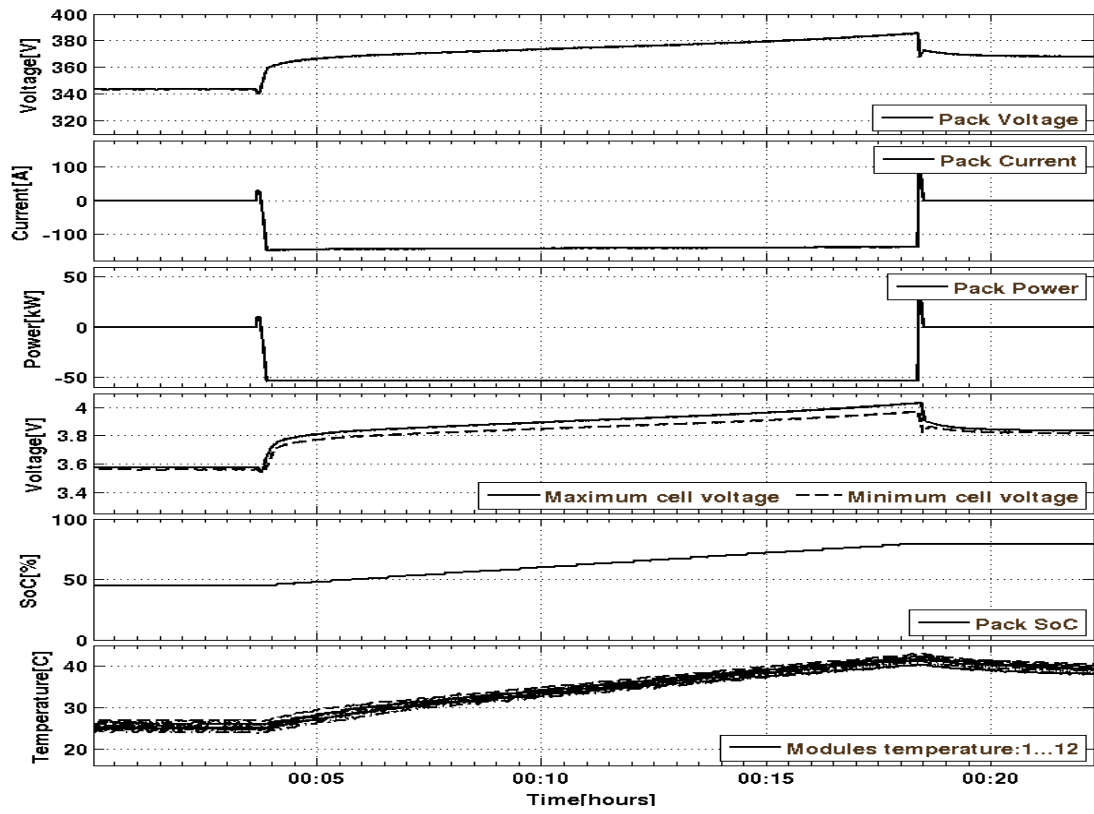
Fig. 4.17 presents a detail with a comparison between CC, CP and FP profiles during fast charging tests of the Kokam battery. The SOC is difficult to be estimated under normal operation and because of that cannot be used as an accurate measure, but only as an indicator.

The SOC will decrease/increase linearly when the battery is discharged/charged with constant current, but not when the battery is discharged/charged with constant power (and variable voltage). As can also be seen in Figs. 9 the charging power to the EV battery is not only limited by the capacity of the charging unit, but also by the battery's maximum charging current, the temperature and by the SOC. As the internal cell temperature cannot be measured directly, and therefore not correctly, the charging current is gradually reduced by the BMU when the temperature reaches the given maximum temperature.

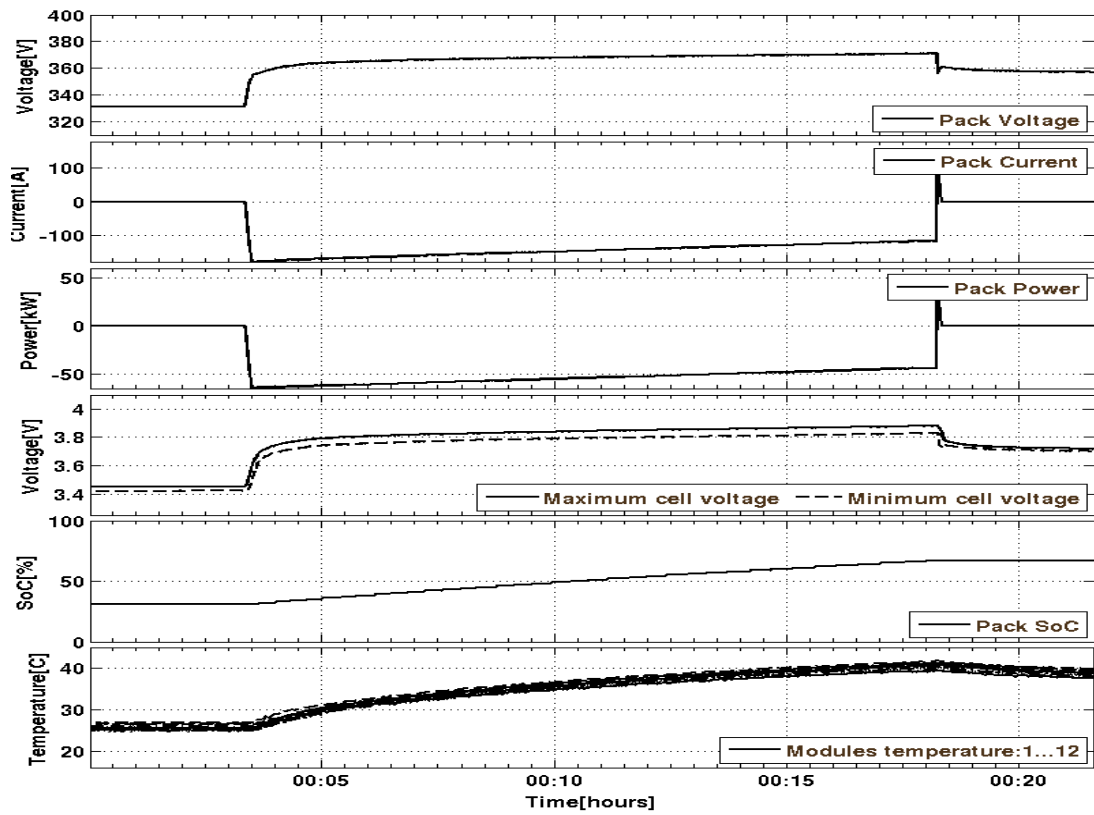
As a comparison between CC (Fig. 4.17 a) and CP (Fig. 4.17 b): when the voltage increases with the SOC during the CC profile, the charging power will also increase, whereas during the CP profile when the voltage increases, the charging current decreases. During the FP profile (Fig. 4.17 c) as the voltage is lowest to the beginning of the charging, the charging current is very high, as well.



a)



b)



c)

Fig. 4.17. Details of the fast charging with a charge energy of 13 kWh (50 % of SOC) for a) constant current at 2C (150A), b) constant power at 52 kW, and c) forced power from 60 kW to 44 kW.

C) Smart Charging Tests

Smart charging tests cover all types of regulated charging with an additional objective to the simple charging with maximum power until fully charged. The objective of this test is to address not only the charging needs specified by the user but also the needs for power regulation in the power system. The “smart” control of the charging ensures full charging of the battery within a given period, but schedules the charging within the period relative to the local power balance.

This test is made with the real components of the SYSLAB, including a 10 kW wind turbine, a 8 kW PV system and the consumption from a 10 kW office building, as can be seen in Fig. 4.18.

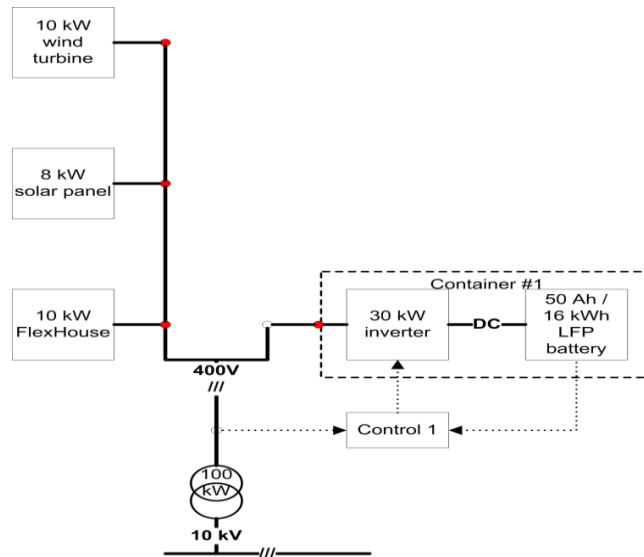


Fig. 4.18. The set-up for smart charging tests.

The tests emulate that the EV (battery) alternates between driving and being connected to the grid for charging. While “driving” (discharging the battery), the inverter is connected directly to the national grid and while “charging” the inverter is connected to the local power system.

The tests have been performed with a series of 6 hours driving-charging tests cycles with the driving loads emulating real driving patterns (based on vehicle driving data recorded in the Copenhagen area by GPS loggers, as part of the AKTA project [30]), as can be seen in Fig. 4.19.

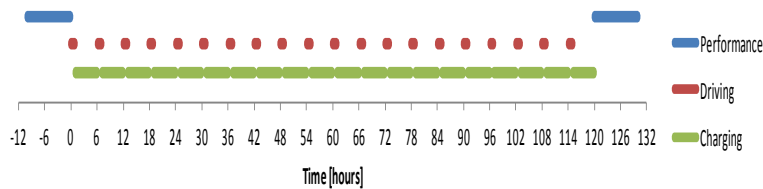


Fig. 4.19. The “smart” charging tests alternate between one hour driving (time in which a single driving day is performed) and six hours charge modes and performance test at regular intervals.

Fig. 4.20 presents an example of the smart charging test cycling of the BYD battery with a driving load based on AKTA driving pattern.

As can also be seen in Fig. 4.20 are shown the BYD battery parameters which have been monitored during the smart charging test, such as the battery pack DC power, current and voltage (from the

top), the maximum and minimum cell voltage and a comparison between the battery temperature, the maximum and minimum cell temperature during the test.

The tested smart charging strategy focuses on fulfilling the charging needs and constrains of EV owner (in this case the battery must be fully charged in maximum 6 hours) and also focus on supplying power system services such as power regulation and load shifting.

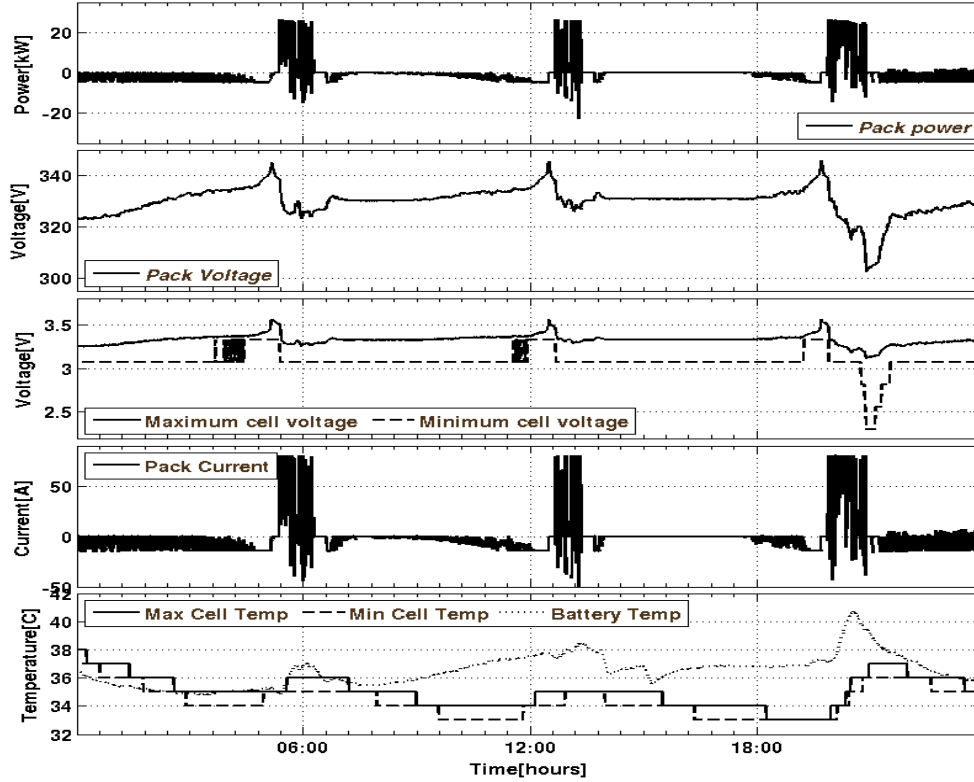


Fig. 4.20. Driving load based on AKTA driving pattern and the EV battery load model.

Additionally, the battery constrains are taken into account, so that a maximum charging current is set to a limit of $C/3$ according to the IEC 62196 standard. Hence, the charge process is accomplished by fully charging the battery within the specified time and scheduling the charge according to the power balance of the local grid ($P_{\text{generation}}=P_{\text{consumption}}+P_{\text{losses}}$, in which $P_{\text{generation}}=P_{\text{wind}}+P_{\text{PV}}$ and $P_{\text{consumption}}=P_{\text{Flex-house}}$)

The tested control algorithm for smart charging, implemented as SYSLAB controller block (see Fig. 4.10), is based on: the higher local aggregated excess power, P_x , and the less charging flexibility, C_x , the higher charging power, P_c . The local aggregated excess power, P_x , is defined as:

$$P_x = P_w + P_s + P_h \quad (4.2)$$

Where P_w is the wind turbine power, P_s is the PV solar power and P_h is the Flex-house power.

The charging flexibility, C_x , which represents a number between $[0 \div 1]$, where 0 means no flexibility and 1 means full flexibility, could be defined as:

$$C_x = 1 - T_{c_min} / T_c \quad (4.3)$$

Where T_c is the remaining charging time and its minimum value could be express as:

$$T_{c_min} = E_c / P_{c_max} \quad (4.4)$$

In which E_c represents the remaining required charging energy and P_{c_max} is the maximum charging power.

In charging mode the charging power is giving by:

$$P_c = k_p \cdot (P_x - P_{x,e}) - k_c \cdot \log(T_c \cdot P_{c_max} / E_c - 1) \quad (4.5)$$

Where $P_{x,e}$ is the “expected” aggregated excess power at the actual time of the day and k_p and k_c are weighting constants. Since the first terms from (4.5) represent the power system needs k_p expresses the deviation of the actual aggregated excess power (positive when the actual aggregated excess power is higher than expected and negative otherwise). Also, because the second part of (4.5) represents the charging needs, negative when the charging flexibility is high and positive when flexibility is low, k_c can be set up accordingly.

A flow diagram of the active power control algorithm for smart charging, based on the equations (1)-(4) and the assumptions presented in this section, is shows in Fig. 4.21.

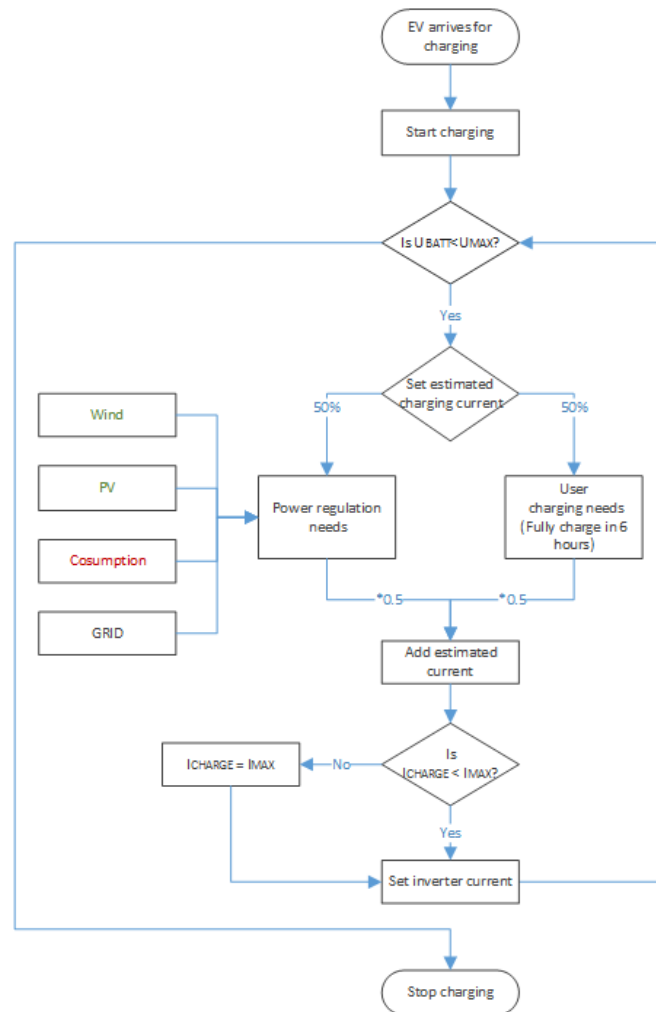


Fig. 4.21. A flow chart diagram of the active power control algorithm for the smart charging strategy.

An example of the smart charging is presented in Fig. 4.23, monitoring the current and the voltage of the battery pack. It can also be seen how the charging current is controlled according to the defined algorithm, based on (4.2) ÷ (4.5).

The impact of the tested smart charging strategy on the power exchange to the public grid is illustrated in Figs. 4.22 Fig. 4.22 a) presents the output power during the battery charging (for around 6 hours) for each component-power production (wind power and solar power), power consumption (representing here by Flex-House) and the charging power of the battery (P_c). Fig. 4.22 b) presents a comparison between local aggregated excess power (P_x) exchange to the public grid with and without considering charging power of the battery (P_c).

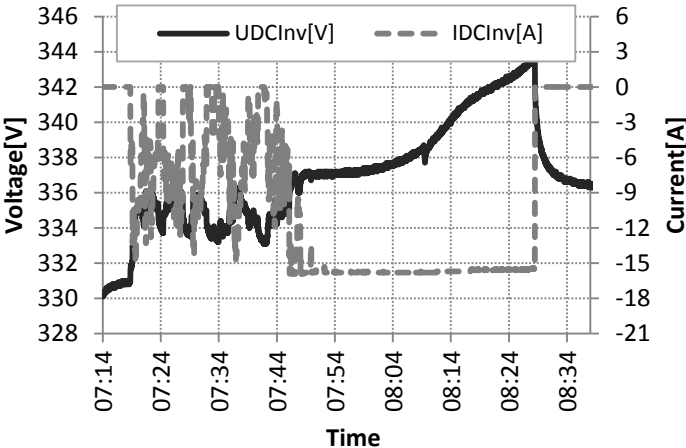
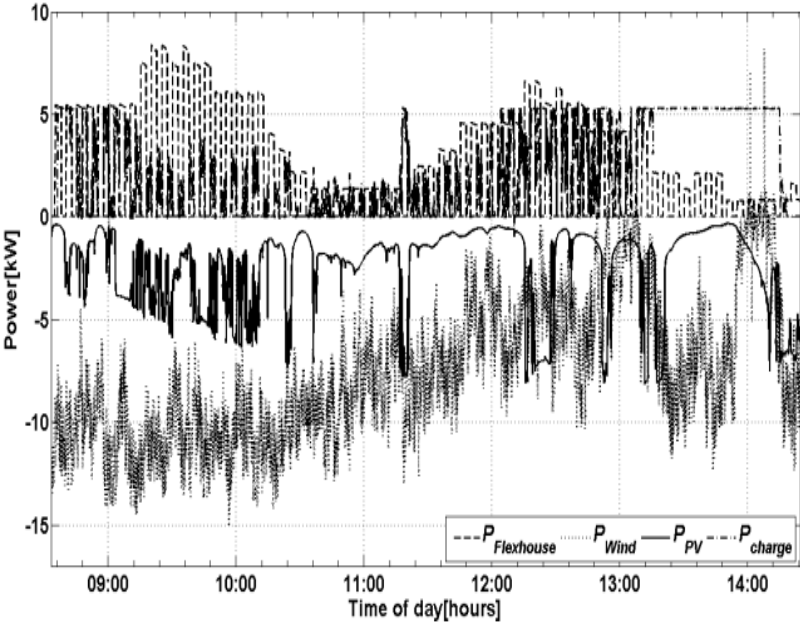
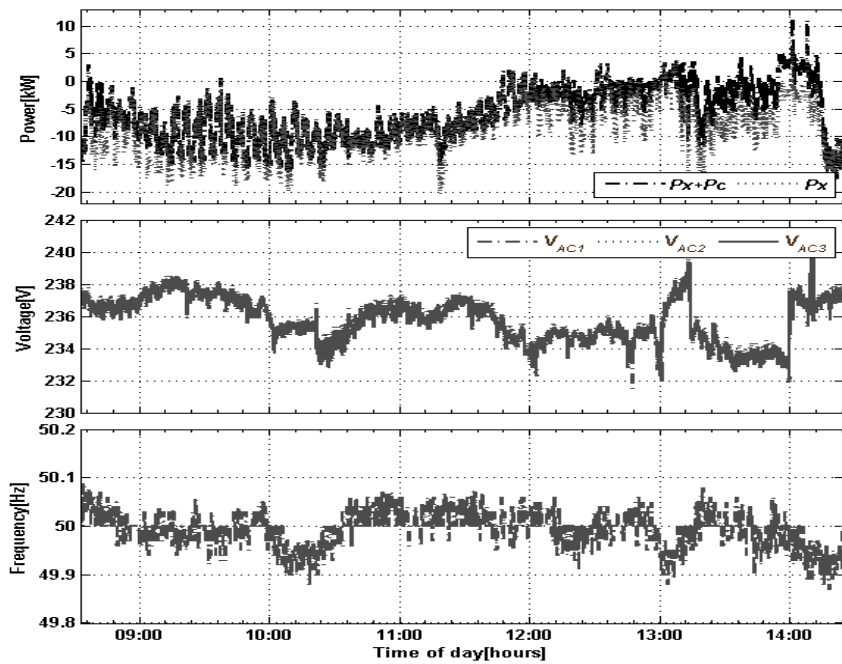


Fig. 4.22. The battery pack current and voltage during a smart charging cycle.



a)



b)

Fig. 4.23 a) Power exchange to the public grid of the individual components, and b) a comparison of the power exchange to the power grid with $(P_x + P_c)$ and without (P_x) the smart charging power (from the top), phase voltage and frequency versus time.

The influence of the charging power of the EV on the total power of DER components, in order to balance the grid power, is also pointed out in Fig. 4.23 b). When the battery was connected to the grid the power fluctuations have been reduced from 8.053 kW to 5.932 kW, which means 26 %. Voltage and frequency deviation in normal operation for LV grid interface, regarding EU Standard EN 50438 and IEC 61727, is $\pm 10\%$ for voltage and ± 1 Hz for frequency. Regarding the Fig. 4.23 b) the voltage oscillations were $\pm 2\%$ and 0.1 Hz, respectively.

4.4. Discussion and Conclusions

The modeling of DER components in power systems and the relative control architecture are an important part for the introduction of relevant quantity of renewable energy in the future smart grid. Therefore it is a strong necessity to have proper validated models to help operators to perform better studies and to be more confident with the results.

In order to find out the parameters of various types of DER components for dynamic simulation models a number of tests are required under different operation modes and loads. It is essential to find generic parameters and the approach to obtain their values in order to facilitate the modeling of a system. Effects of static and dynamic stability, effects of disturbances on power system equipment and network should be analyzed.

AC power system satisfactory operation is obtained when frequency and voltage remain nearly constant or vary in a limited and controlled manner when active and reactive loads vary. Active power flow is related to prime mover's energy input and thus to the speed of synchronous generator. On the other hand, reactive power control is related to terminal voltage. When a generator acts alone on a load, or it is by far the strongest in an area of a power system, its frequency may be controlled via generator speed, to remain constant with load. Integration of a diesel gen-set in an isolated power system can improve the system behavior during large changes in load.

Automatic generation control (AGC) distributes the generation task between AVR controller and speed governor. Speed (frequency) control quality depends on the speed control of the SG but also on the other induced influences, besides the load dependence on frequency. SG voltage control quality depends on the SG parameters and excitation power source dynamics.

The battery package is an interesting option for storing excess energy from the hybrid grid (wind intermittency) for later use. It may also act as a peak shaving unit and thereby contribute to a stronger grid.

A series of tests has been done, in subchapter 2, for different operational scenarios and during several modes of operations to find out the parameters for dynamic modeling of DER components in power systems and also to implement and test different control strategies for the combined system. Moreover to point out, on a laboratory scale, the coupling between wind generation and storage and to effectively compensate wind fluctuations a number of tests have been done during charge/discharge cycles.

A suitable model for SYSLAB Micro-Grid has been developed and implemented in the dedicated simulation tool PowerFactory and the parameters used for DER components were based on the measurements and tests reporting in this chapter.

In the last subchapter was presented the development of a test platform, including three Lithium-ion batteries, designed for EV applications, for testing impacts on different advanced loadings of EV batteries.

The aim of the tests was to study the impact of smart charging and fast charging on the power system, on the battery state of health and degradation, and to find out the limitation of the batteries for a future smart grid.

The test results we have obtained from the performance characterization of the batteries in general confirm the performance characteristics specified by the suppliers and reported in the literature. The main confirmations of such characteristics are:

- a high DC roundtrip efficiency of above 95% was normally obtained in different test conditions, including fast charging;

- the NMC battery pack has shown negligible capacity degradation since the battery was assembled 2 years ago, during which different tests have been conducted, including repeated fast charging cycles. This indicates a good capacity retention during cycle life;
- the LFP battery has shown a capacity loss during the 2 years in the range of (10-15)%, indicating a less impressive life time;
- temperature is a critical parameter for the performance and lifetime of the battery, and cooling/heating management is an important factor to secure optimal operation of the batteries. The NMC battery has shown a higher increase of temperature during charging and discharging cycles and required stronger cooling, especially during fast charging tests. In contrast, the LFP battery has shown minor temperature changes during cycling under comparable cooling conditions and current rates;
- with respect to battery aging, the clearest indicator seems to be the cell voltage, for both types of batteries.

One of the main conclusions is that the smart charging can turn electric vehicles from grid congestion threats to flexibility resources. However, to realize the potential of smart charging, we need to address not only the needs for power regulation in the power system but also the charging needs specified by the user. The smart charging tests performed have demonstrated that even with a simple control algorithm it is possible to provide a required charging energy within a given period of time and to provide power system services in terms of regulation of the aggregated local power, reducing the peak power (reducing the power capacity of the power connection) and the total energy exchange (reducing the energy losses in the power connection line) of the power exchange with the national grid. This shows the potential to use EV batteries to successfully deliver power balancing services to the grid, when the communication interfaces between the battery, BMS, charging inverter and the control room of the grid are standardized for interoperability.

EV fast charging infrastructure is expected to be required for specific EV applications in the urban areas and along the highways to compensate for the limited driving range, provided by a fully charged battery (typically 150-200 km). Fast charging should be able to charge a significant amount of energy (25-75% of the battery capacity) into the battery within 10-15 minutes. Fast charging tests have been performed with constant power, constant current and forced power at charging rates corresponding to a double (2C) and triple (3C) capacity. The constant power gives the lowest impact on the grid and the main limitation of the Kokan battery seems to be the increase of the temperature. The charging rate of the battery is not only limited by the power capacity of the charger, but also by constraints of the battery in terms of max current, max temperature and SOC. For future battery design, this could be addressed through build-in cooling systems and/or through increased thermal capacity of the cells.

As a future work we will build a simulation model based on the tests reported in this paper which will describe the dynamic behavior of the batteries packs as a function of SOC and cell temperature to be used in a power system analysis tool to design different scenarios for a future smart grid.

Appendix

TABLE II
Main specification of the battery packs tested in this paper

Manufacturer	BYD	Kokam
Model	FV 50 F3DM Fe	SLPB 75
Type	Lithium-Ferro-Phosphate	Lithium Polymer
Typical application	PHEV	EV
Nr. of modules	10(each with 10)	12(each with 8)
Nr. of cells	100	96
Nominal voltage	320 V	350 V
Capacity	50 Ah/16 kWh	75 Ah/26 kWh
Max cell voltage	3.6 V	4.15 V
Min cell voltage	2 V	3 V
Max charging current	100(300) A	225 A
Max discharging current	300(600) A	450 A
Max temperature	55 °C	45/55 °C
Nr. of battery packs	2	1

Chapter 5

Modeling and implementation of different scenarios designed to identify critical cases in a future Smart Grid

Contents of the Chapter 5

Contents

Chapter 5	164
Modeling and implementation of different scenarios designed to identify critical cases in a future Smart Grid	164
Chapter 5. Modeling and implementation of different scenarios	166
Designed to identify critical cases in a future Smart Grid	166
5.1. Introduction.....	166
5.2. Grid model components and implementation.....	167
5.2.1. Description of the grid models and scenarios.....	167
5.2.2. Grid model implementation in NEPLAN and DigSILENT PowerFactory	169
5.3. Steady-state simulation results. Power flow calculation analysis.....	174
5.4. Time-series simulation results.....	178
5.4.1. Steady-state simulations	178
5.4.2. Time-series simulations using dynamic models	187
5.4.2.1. PV system modeling	187
5.4.2.2. Active and Dynamic Loads Modeling	191
5.4.2.3. EV battery modeling and implementation	193
5.4.2.4. Simulation Results	196
5.5. Discussion and Conclusion	198
Appendix:	199

Chapter 5. Modeling and implementation of different scenarios

Designed to identify critical cases in a future Smart Grid

5.1. Introduction

One of the main goals in the Danish energy policy is to increase the amount of renewable energy in the energy mix to 30% of the energy in 2025 [1]. Last year, the Danish parliament approved an even more ambitious target: to have renewable supply 35 % of the country's total energy needs-not just electricity but also heating and transportation-by 2020, and an incredible 100 % by 2050 [2].

It is anticipated that new home appliances (e.g., Electric Vehicles (EVs) and Heat Pumps (HPs)), and embedded generations will be introduced to the power system. In addition, control strategies of various energy resources are going to be implemented in the current power system. To capture the behaviors of such elements, and to handle the correlation of behaviors in time, time series simulation is one of the key function that should be implemented in the future grid design. Moreover, it is of interest that how Smart Grid control strategies can be represented and how concurrent control of units is handled in the simulation tools.

This chapter has been prepared in connection with the International Project "Distribution System Planning for Smart Grids-Smart Plan", ForskEL ID no. 10680, 2012-2013.

The purpose of the Smart Plan project was to design a distribution network with different DER Components connected along the feeders and to identify limitations of existing simulation and planning tools for distribution networks, with a particular focus on the challenges imposed by the introduction of Smart Grid technologies.

Based on the survey of tools, the project was also trying to identify the existing tools with the highest potential able to implement the grid model and the scenarios developed. The commonly used simulation tools are identified by a survey to distribution system operators (DSOs) in Denmark. Based on the survey of tools, the project has also been tried to find out the limitations and the user experience of them during the implementation of smart grid solutions and corresponding functions. The simulations are made using the smart grid model, which was designed based on measurements and a future estimation of production and consumption with the highest potential able to implement the grid model and the worst case scenarios.

Applying these tools, two of them also used in the previously chapters, a network simulation model for the base case is implemented and verified. The simulation tools were used to model the different future scenarios and to record limitations, lack of functionality and inefficiencies of the tools encountered. The particular questions of interest are how Smart Grid control strategies can be represented and how concurrent control of units is handled in the simulation tools. Another important output of the chapter 5 is to identify critical load cases and voltage variations for the defined scenarios.

The structure of this chapter is as follows. The grid model and different scenarios will be described and implemented in subchapter 3.2 with the further simulations and study in next Sections. Afterwards, two approaches will be described to build up the simulation platforms in order to achieve the aforementioned function in Subchapter 3.3 and 3.4. Having the existing simulation platforms, different control strategies are applied in the platform to identify further limitations and

barriers to implement smart grid solutions in the simulation software's. In the end, the experiences are discussed and summarized in the last section.

5.2. Grid model components and implementation

This subchapter presents the implementation of a representative low-voltage distribution grid model. The grid model is based on real data for summer and detached houses, for evaluation of a future smart-grid.

The grid properties are built via statistical approach by sorting the existing grid and their connections (e.g., the length of cables, the number of cabinets, the cross-section of cables, the number of customers per feeder, etc).

The aim of the models is to design, implement and test the proposed configuration and to investigate whether the low-voltage distribution grid is prepared for the expected future increase of PVs, heat pumps and electric vehicles.

The model is implemented in NEPLAN and DigSILENT Power Factory, based on a survey of the state of the art of network planning tools for distribution grids, to study different scenarios. A steady-state and a dynamic analysis of the grid model will also be presented based on time-series simulations with a comparison between different voltage profiles.

In addition, to test the previous mentioned functions, i.e., time series load flow, and control strategy implementation, sometime-series inputs and models are prepared.

The grid model contains many components, such as: PV systems, EV systems, HPs and conventional loads. The model has been designed to find out whether the proposed low-voltage distribution grid is prepared for the expected future increase of PV penetration, heat pumps and electric cars connected along the feeders.

5.2.1. Description of the grid models and scenarios

We have developed 23 scenarios based on conventional residential loads (houses), heat pumps (with 1 and 3 phases), electric cars (with 1 phase and 3 phases) and PV systems (with 1, 2 and 3 phases). In the case of one phase appliances it is assumed that all the devices are connected to the same phase. Similarly 2 phase PV systems are assumed to be connected to the same 2 phases.

The scenarios were developed using 2 different voltage limits, +6%/-10% and +10%/-10%. The first limit is based on DEFU recommendations no. 16/2001 [3]. These limits were used in Denmark during a grace period after EU legislation changed nominal voltage from 220 V to 230 V in order to allow for older 220 V household appliances to be phased out. The +10%/-10% limit is based on the latest version of DEFU recommendation 16, which closely mirrors European norm EN 50160 [4].

For PV systems 3 parameters were considered: rated voltage, tap position of the 10/0.4 kV transformer and the number of phases (1, 2 or 3). The position of the tap-changer normally depends on the primary voltage level on the 10 kV side. If the distribution transformer is located at the end of a long 10 kV feeder, the tap-changer is used to normalize the voltage level on the secondary side. In this study the tap changer position is used to allow a larger voltage drop/rise in some of the scenarios.

The components of scenarios are listed below:

Grid :

- a) feeder length
- b) numbers of customers
- c) types and lengths of cables
- d) the load of customers (comparing to the peak power)

New appliances:

- a) type (EV/HP/PV)
- b) connection to grid (three-phase connection/phase to phase connection/one phase connection)
- c) Size
- d) Numbers each node

Operation constraints:

- a) voltage variations (+6%/-10% or +10%/-10%)
- b) transformer tap positions

Given the above variables, the hosting capacity of the new appliances is analyzed. Table 1 in Appendix summarized all 23 scenarios indicating the state of variables.

By comparing the simulation results, we got the following statements:

1. Comparing Scenarios 1 and 2, there will be larger capacity in the network when enlarge the voltage limitation. The same result can be derived comparing the unbalanced systems in scenario 7 and 8.
2. Comparing Scenarios 1 and 3, if the transformer ratio is tuned higher, the voltage will still be into the limits when more PV are installed. However, the issue would be that when there is not so much PV production, the voltage drop in the feeder will exceed the lower limit.
3. Comparing Scenarios 1, 2, 3, and 4, when two procedures (raising the voltage and relaxing the voltage limitation) are both taken, the feeder can contain more PV (10 times of the size in 1st scenario). But the most critical constraint is the capacity of the cables and transformers. Scenario 4 is of interest to evaluate the relation between the hosting capacity and physical constraints of the grid.
4. Scenario 5, 6, 7 and 8 studied unbalanced systems. The load on a single phase makes the voltage unbalance very severe, depending on the unbalanced size. If the connection of PV panels goes for phase to phase connection, then the unbalanced voltage can be mitigated to some extent. However, special attention must be paid on the protection scheme of the feeder. When there is a short-circuit fault in the system, the complexity of the connection will make the condition even worse.

5. In Scenarios 9, 10, and 11 or in Scenario 14 and 15, the placement of loads are different. From the comparison results, we can tell that the more distributed allocation of loads can make the feeder have larger capacity to accommodate.

6. When the load connection is single phase, comparing Scenarios 12 and 13, the result is that when the allocation is close to the upper level connection point, less unbalanced voltage in the feeder would be. Comparing Scenarios 16 – 18, it can be found that when the loads are more evenly distributed, less unbalanced voltage in the feeder would be. After comparing Scenarios 13 and 19, it indicates that when the transformer ratio is tuned to raise the voltage along the feeder, the current loading is less, but the unbalanced voltage is higher.

7. If the chosen simulation feeder is shorter, the voltage difference in every node is not that obvious. The main limitation of the capacity of new components is the current loading of cables and the transformer.

5.2.2. Grid model implementation in NEPLAN and DIgSILENT PowerFactory

Given the grid model and scenarios, the static load flow is made in both NEPLAN and DIgSILENT PowerFactory. There is not much difference in results and setting up the calculations. The parameters of grid elements and loads are similar. The static load flow is the basis of steady state analysis. So it is well defined and integrated into the software's.

Based on investigations, calculations and assumptions presented in the previous section a grid model has been designed. The model contains an external grid, a distribution substation with a medium voltage transformer (10/0.4 kV) and with ten cabinets (switch boards) at which PV panels, residential loads, EVs and heat pumps (HPs) are connected.

To test the grid model 23 scenarios have been analyzed regarding the DEFU recommendations [3] and EN 50160 standard [4]. In the first four scenarios it was investigated how many solar cells can be connected to the grid along the feeder without to exceed the voltage limits defined in [3] and [4], when the PV systems have three-phases and 6 kW each with the residential load at 20 % of the maximum load. In the next five scenarios it was investigated what happens in the same conditions when one phase and 4 kW and two phases and 6 kW PV systems are connected along the feeder.

In the next seven scenarios we investigated how many EVs (3 phases EV of 11 kW and one phase EV of 3.7 kW each) can be connected to the grid, when the residential load is at the maximum load, without exceeding the lower voltage limit.

We have investigated in the last five scenarios the connection of heat pumps (3 phases HP of 2.8 kW each and one phase HP of 1.5 kW each), to the grid, evenly distributed along the feeder, with the residential loads at maximum load. In one of these last five scenarios we considered a mixed load case (the worst case scenario) when heat pumps (one phase and three phases) and electric cars are connected simultaneously on the same distribution grid.

The grid model was implemented in two different tools, NEPLAN and DIgSILENT PowerFactory, to study load flow, steady-state voltage stability and dynamic and transient behavior of the power system. These tools have been selected as they have the ability to simulate load flow and RMS fluctuations in the same software environment [5, 6].

In Fig. 5.1 is presented the implementation of the grid model for the low-voltage distribution system in NEPLAN (a) and DIgSILENT PowerFactory (b).

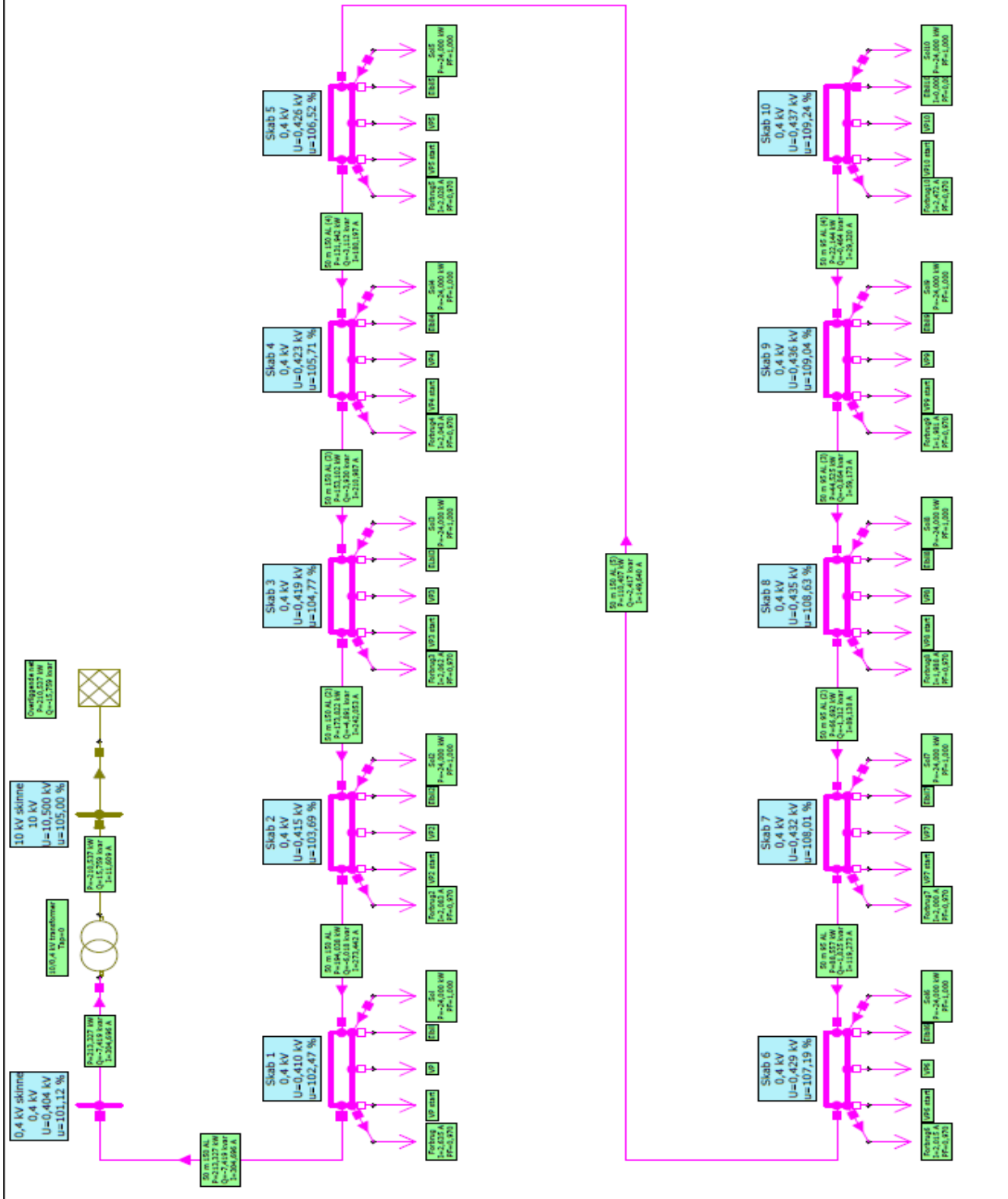
All components of the single line diagram, in Fig. 5.1, are built with standard blocks from the internal libraries of the software package tools.

The blue square above the cable cabinet (Fig. 5.1 a) shows the voltage on each phase, while the green squares show the power and current for each phase. Also, the arrows show that the components are active.

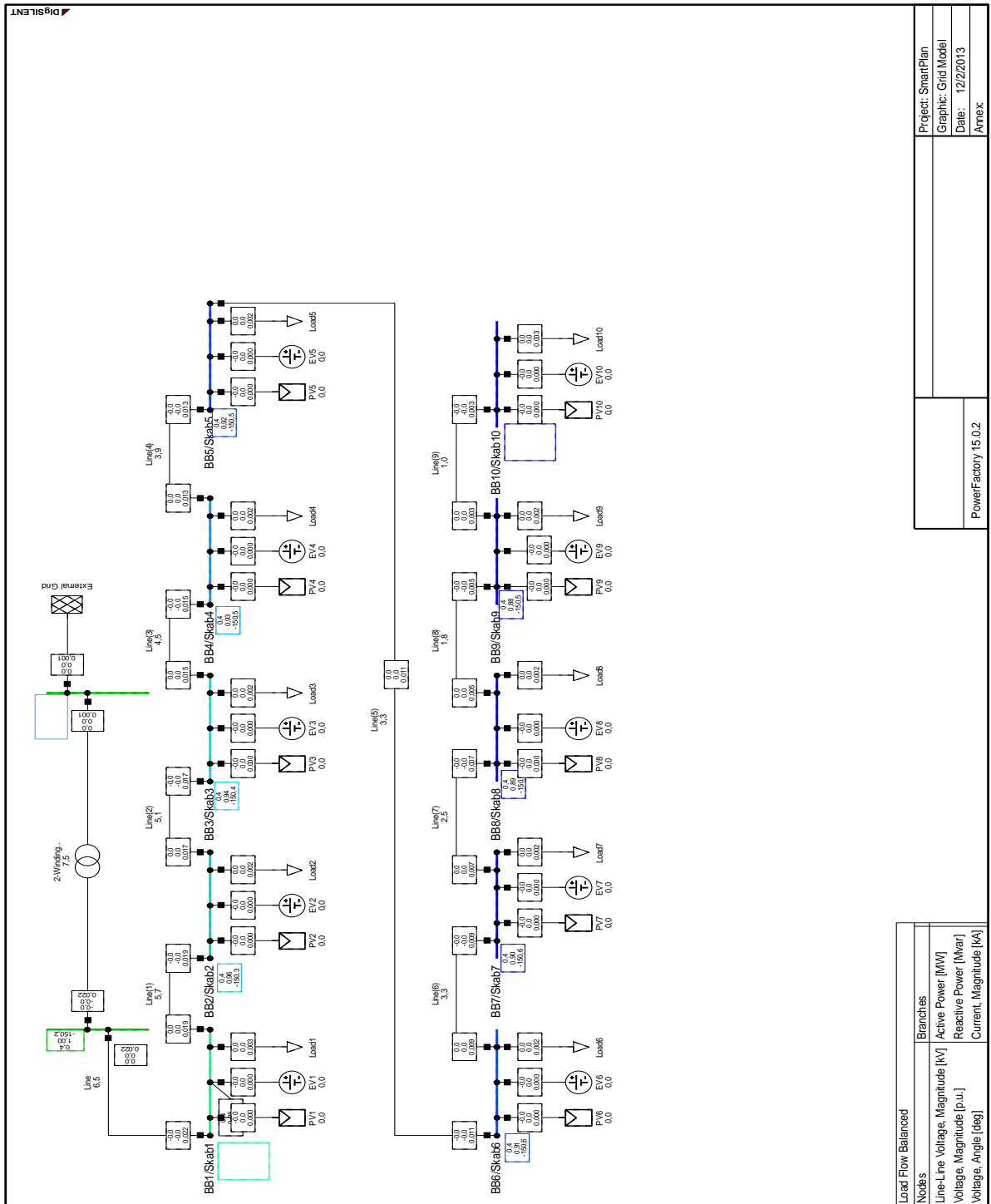
In DlgSILENT PowerFactory implementation (Fig. 5.1 b) the squares above the bus-bars contain the parameters of the cables and below the bus-bars show the voltages of each phase. Also, each component of the cabinet, such as PV systems, heat pumps and EVs has its own square block able to show internal parameters, such as: current, power, power factor.

Parcelhus 85% fraktil
 Solceller - 6 kW - 3 faset - 20% last - 4 stk. solceller i hvert skab
 253/438V
 Trin 1

Beregning 4



a)



b)

Fig. 5.1. Comparison between a) NEPLAN and b) DigSILENT PowerFactory implementation for the designed distribution Smart Grid model.

More details about components implementation, length of the feeders, types of lines and substation transformer parameters are presented in Fig. 5.2.

2-Winding Transformer Type - ...ipment Type Library\0.2MVA 10/0.4kV Dyn5.TypTr2

ANSI Short-Circuit | IEC 61363 | RMS-Simulation | EMT-Simulation | Harmonics | Optimization
 State Estimator | Reliability | Generation Adequacy | Tie Open Point Opt. | Description
 Basic Data | Load Flow | VDE/IEC Short-Circuit | Complete Short-Circuit

Name: 0.2MVA 10/0.4kV Dyn5

Technology: Three Phase Transformer

Rated Power: 0.2 MVA

Nominal Frequency: 50. Hz

Rated Voltage

HV-Side: 10. kV

LV-Side: 0.4 kV

Vector Group

HV-Side: D

LV-Side: YN

Phase Shift: 5 *30deg

Name: Dyn5

Positive Sequence Impedance

Short-Circuit Voltage uk: 4.35 %

Ratio X/R: 2.99

Zero Sequ. Impedance, Short-Circuit Voltage

Absolute uk0: 2. %

Resistive Part ukr0: 1. %

OK

Cancel

a)

Line Type - Equipment Type Library\0.4-0095ALPEX.TypLne

Reliability | Generation Adequacy | Tie Open Point Opt. | Description
 RMS-Simulation | EMT-Simulation | Harmonics | Optimization | State Estimator
 Basic Data | Load Flow | VDE/IEC Short-Circuit | Complete Short-Circuit | ANSI Short-Circuit | IEC 61363

Name: 0.4-0095ALPEX

Rated Voltage: 0.4 kV

Rated Current: 0.262 kA (in ground) | Rated Current (in air): 1. kA

Nominal Frequency: 50. Hz

Cable / OHL: Cable

System Type: AC | Phases: 3 | No. of Neutrals: 0

Parameters per Length 1,2-Sequence

Resistance R' (20°C): 0.32 Ohm/km

Reactance X': 0.07 Ohm/km

Parameters per Length Zero Sequence

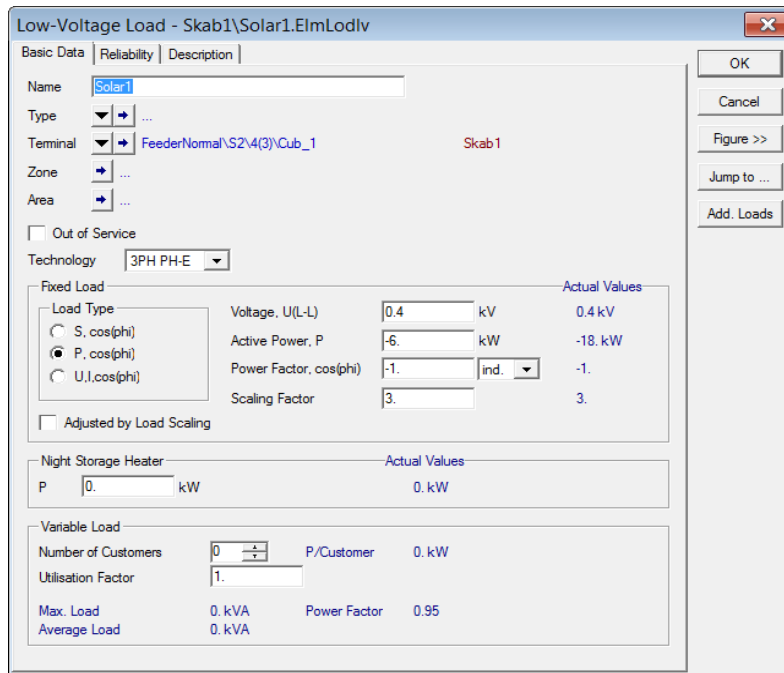
Resistance R0': 1.28 Ohm/km

Reactance X0': 0.33 Ohm/km

OK

Cancel

b)



c)

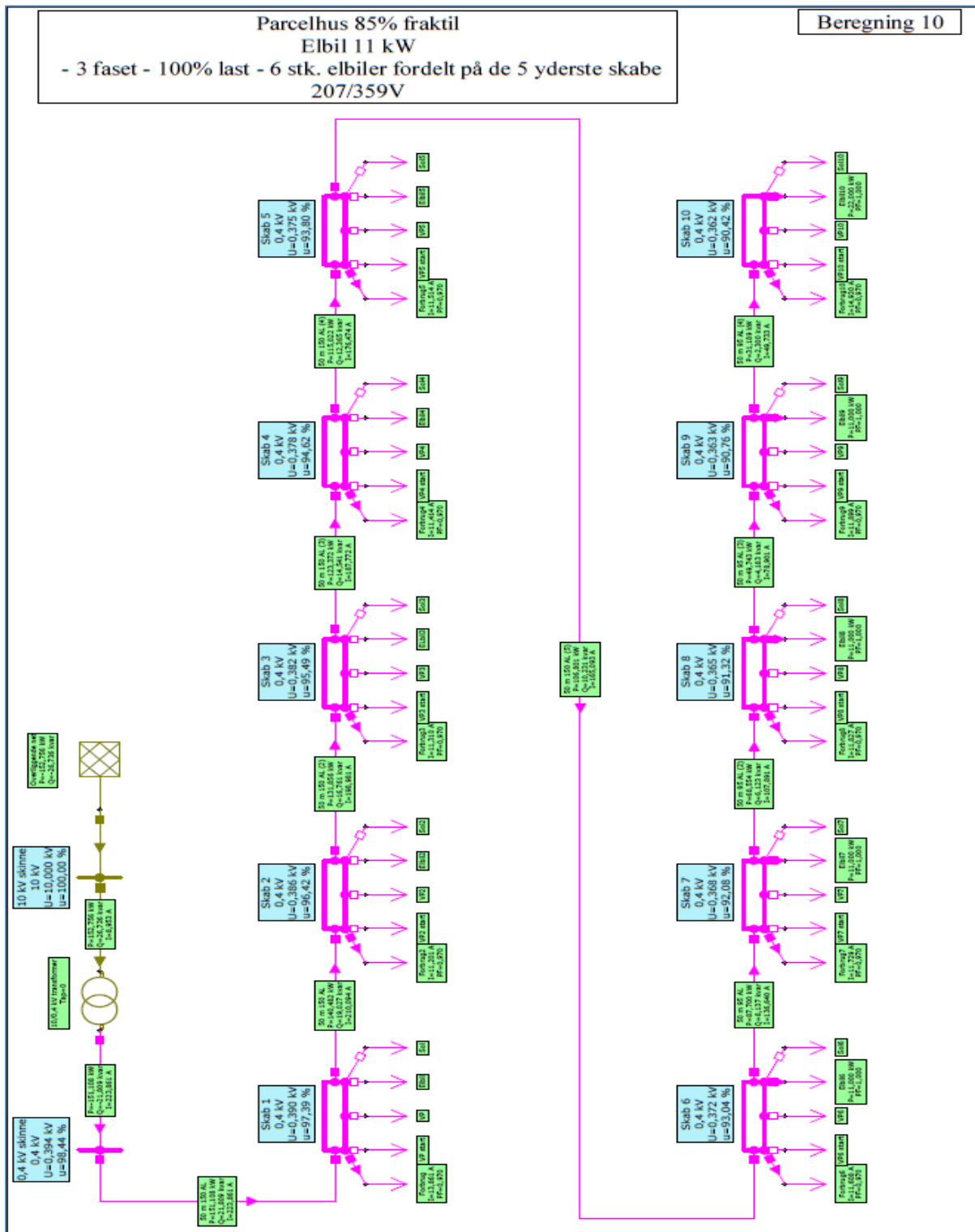
Fig. 5.2. Details about components implementation, length of the feeders, types of lines and substation transformer parameters

As can also be seen in Figs. 5.1 and 5.2, for the grid model analyses following parameters are taken into consideration: cable dimensions and lengths, the grid's age, category, substation no., no. of customers, no. of cabinets and the load per customer. The measured feeder length for the 85 % was 500 m for detached houses and 730 m for summer houses. We have considered only two types of cables (Fig. 5.2b), with a cross-section of 150 mm² AL and 95 mm² AL, because 240 AL and 50 AL cables represent a very small part of the total cable length investigated. The loads were implemented as in Fig. 5.2 c), defining the internal parameters, such as voltage, power and scaling factor.

5.3. Steady-state simulation results. Power flow calculation analysis

To compare the models implemented in both software packages, NEPLAN and DigSILENT PowerFactory, and to find out the differences between them, we have analyzed the results for all 23 scenarios using first a power flow calculation. The network contains 10 cabinets at which we have connected PV systems, EVs, HPs and general loads.

Fig. 5.3 shows a power flow calculation for the scenario no. 10, implemented in DigSILENT PowerFactory (a) and NEPLAN (b). The parameters of each cabinet (bus-bar), such as active and reactive power, power factor, current and voltage, can also be seen. In this case it was investigated how many electric vehicles (EVs) can be connected to the grid before voltage decreases below the minimum limit ($U_n - 10\%$). In this scenario, six electric cars (11 kW & 3 phase each) were distributed over the five most remote cable cabinets, two electric cars in the last remote cable cabinet and one electric car in each of the next four cable cabinets. A minimum voltage, at the end of the feeder, of 359 V was observed.

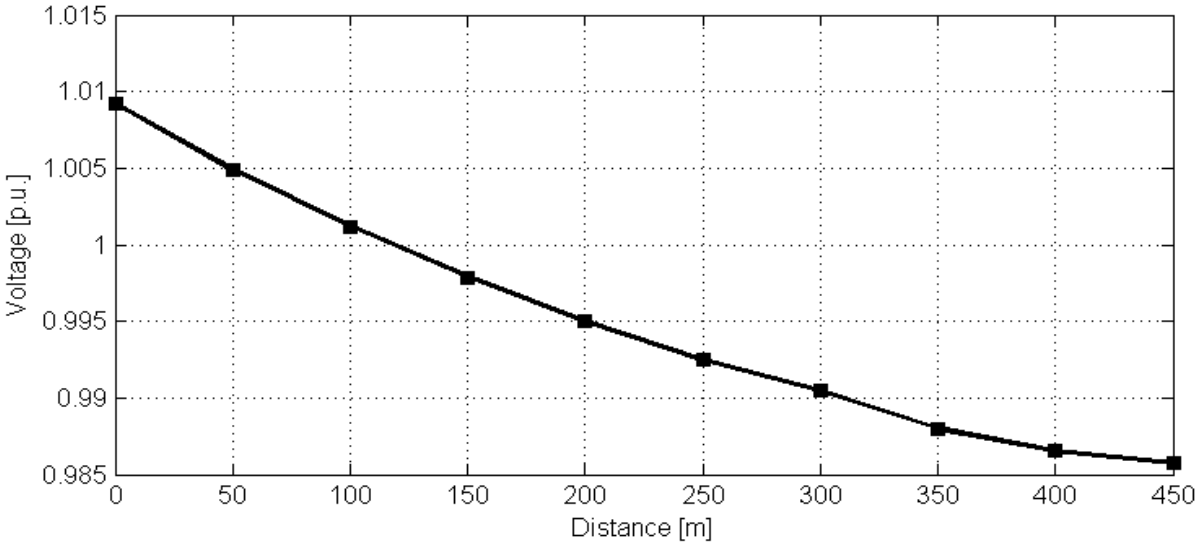


b)

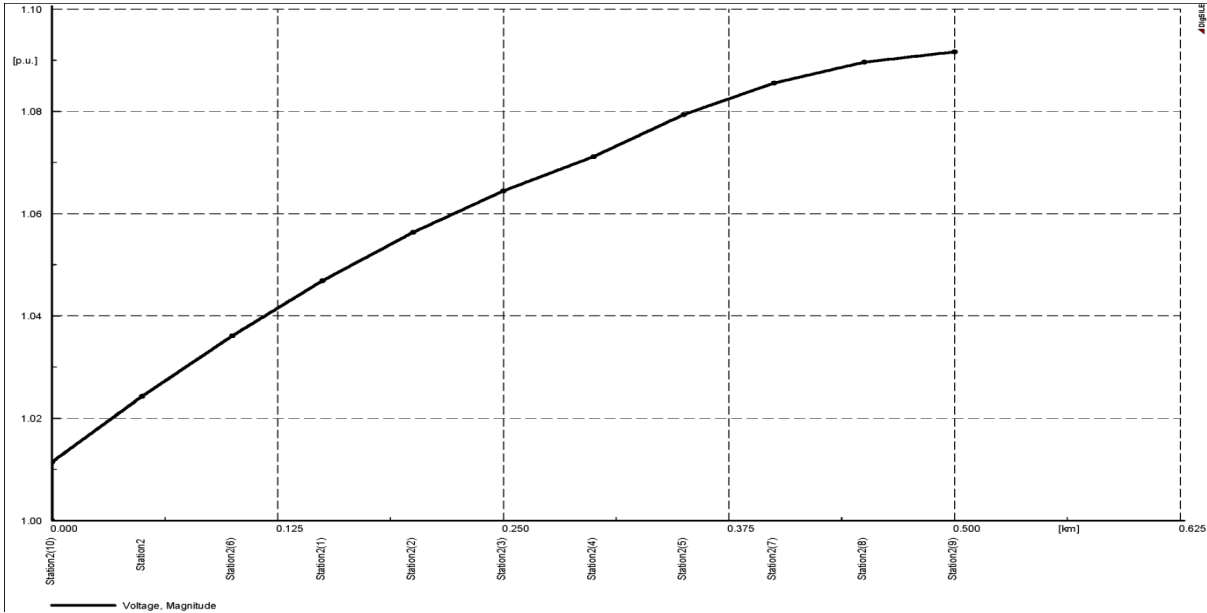
Fig. 5.3. Power flow calculation for scenario 10 using a) DlgSILENT PowerFactory and b) NEPLAN.

Voltage profile along the feeder can be seen in Fig. 5.4, for the same scenario analyzed before, without PV penetration and with 6 EVs connected over the last five cable cabinets. The voltage drops along the feeder (Fig. 5.4 a) because of the electric cars connection and reaches the minimum value of 359 V. In the contrast with voltage drops in scenarios no. 2 it was investigated how many solar

cells can be connected to the grid until voltage increase will not exceed the limit ($U_n + 10\%$). As can be seen in Fig. 5.4 b) the voltage increases up to 1.09 when 2 solar cells are connected in each cable cabinets.



a)



b)

Fig. 5.4. Voltage profile along the feeder a) for scenario no. 10, with 6 EVs connected and no PV, and b) for scenarios no. 2 with PV penetration (2 solar cells connected in each cable cabinet).

As a comparison between power flow calculations, using both software packages, we can conclude at this stage that there is an insignificant difference. The parameters and simulation models for all the components are slightly different. More than that DiGSILENT PowerFactory is able to import NEPLAN models.

5.4. Time-series simulation results

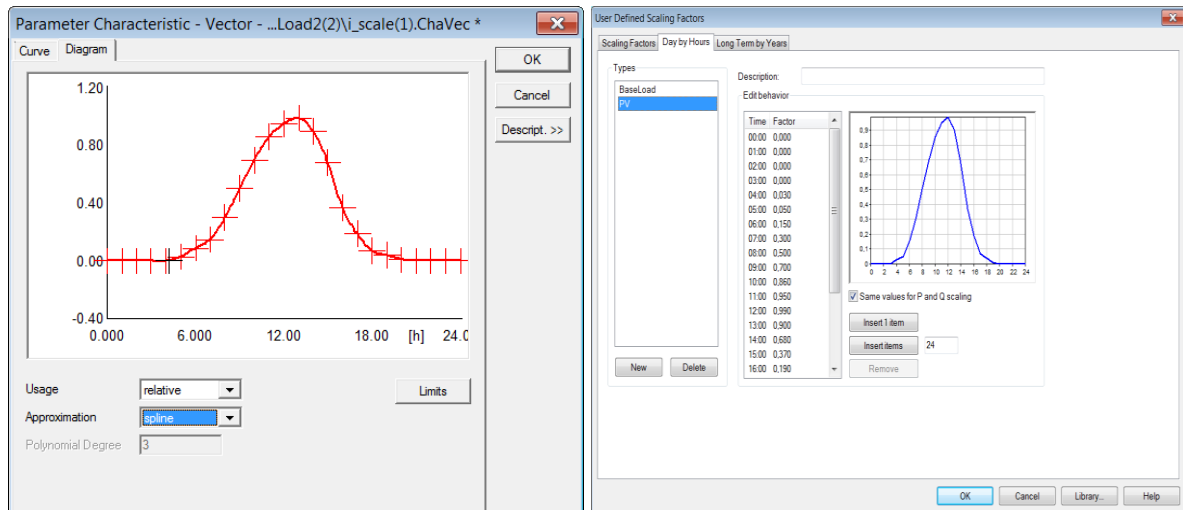
In this section a time series simulation is conducted using DigSILENT PowerFactory. To investigate the characteristics of the new components: PVs, EVs and HPs, we use the same grid model proposed in WP₁ and analyzed in the previously section of this report as well.

In the second part of the section will be analyzed a scenarios using two of the worth's case scenarios: a summer day with low load (20 % of max.) with the PV's connected to the grid and the Christmas eve with no PV production and the maximum consumption.

5.4.1. Steady-state simulations

This subsection presents a steady state analysis of the grid model using a time-series simulation. The PV production and the load consumption will be estimated using a Spline approximation.

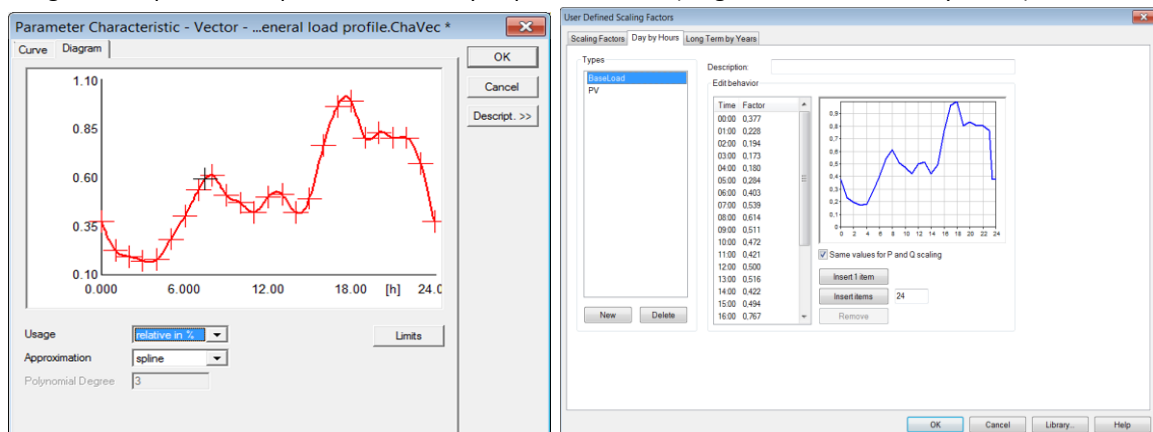
Fig. 5.5 and Fig. 5.6 show an estimated PV production (Fig. 5.5) and a load consumption (Fig. 5.6) profiles for one day implemented in PowerFactory (a) and NEPLAN (b) based on a polynomial Spline approximation.



a)

b)

Fig. 5.5. PV production profile for one day implemented in a) DigSILENT PowerFactory and b) NEPLAN.



a)

b)

Fig. 5.6. Load profile based on a daily consumption of a household implemented in a) DigSILENT PowerFactory and b) NEPLAN.

In NEPLAN it is easier to create and implement a simulation model for a time-series simulation. It is easier to create an individual profile of the load type using a scaling factor while in Power Factory it is necessary to develop a composite frame for each load of the simulation model.

Under a certain load, the composition of different types of load can also be modified in NEPLAN using the graphical interface used to define the user profile, as can be seen in Fig. 5.7. Also, the active and reactive power of the lines and loads can be modified.

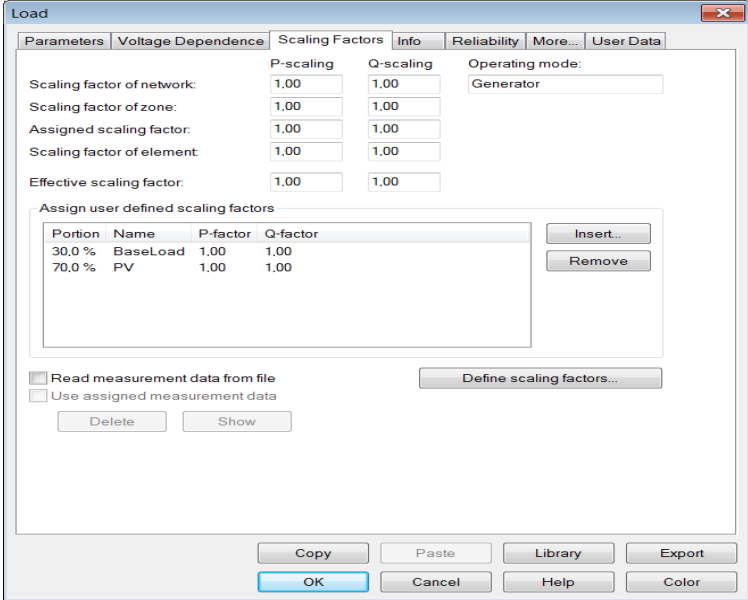
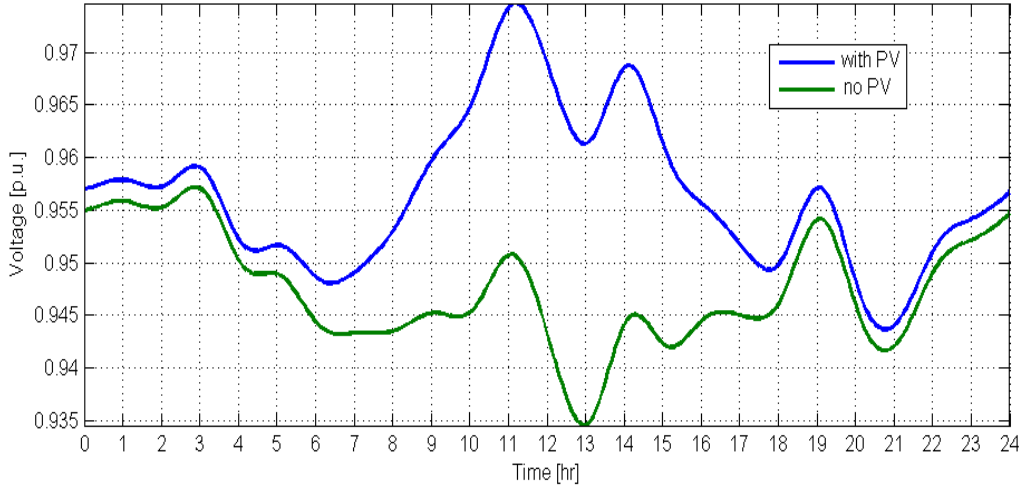


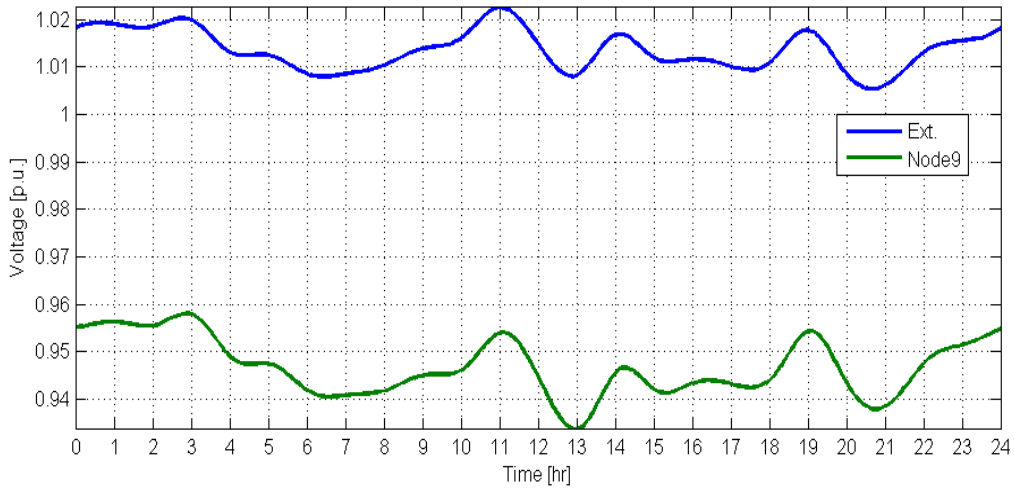
Fig. 5.7. GUI in NEPLAN to define load parameters.

These profiles presented before will be used to analyze the scenarios.

In Fig. 5.8 is depicted a comparison between two voltage profiles obtained at different connection points of the designed low-voltage distributed grid, using the estimated PV and load profiles, shown in Figs. 5.5 and 5.6, for the same scenario (no. 10). Fig. 5.8 a) shows a comparison between voltage profile at the end of the feeder node with and without PV panels connected to the grid, while in Fig. 5.8 b) is shown a comparison between voltage profile of the external grid and voltage profile at the last node of the feeder.



a)



b)

Fig. 5.8. a) Comparison between voltage profile with and without PV production at the end of the feeder and b) voltage profiles of the external grid and the voltage node of the last cabinet to the end of the feeder

To further investigate the proposed grid model and the characteristics of the new components: PVs, EVs and HPs, we used as inputs real data for external grid and PV production, acquired from SYSLAB, as can be seen in Fig. 5.9.

EV battery charges and load profiles are calculated based on driving and load pattern, as shown in Figs. 5.5 and 5.6.

The maximum load was calculated using the annual consumption multiplying the peak power based on the Velander correlation:

$$P_{\max} = \alpha \cdot w + \beta \cdot \sqrt{w} \quad (5.1)$$

In which P_{\max} represents the maximum load (measured in kW), w is the annual consumption (measured as MWh), α and β are the Velander constants.

In the first approach, only mature and existing functions inside the power system simulation software are used. More focuses are put on the interface between this and other simulation software's. As shown in Fig. 5.9, we can see that the DPL script helps to sweep the time for the time series simulation (where the example is given within the software). Other power system variables (e.g., voltage, active power and reactive power) are determined by the external environment. Only the time series is inserted into the corresponding elements. In our case, the blue blocks are prepared in MATLAB with self-defined models and functions.

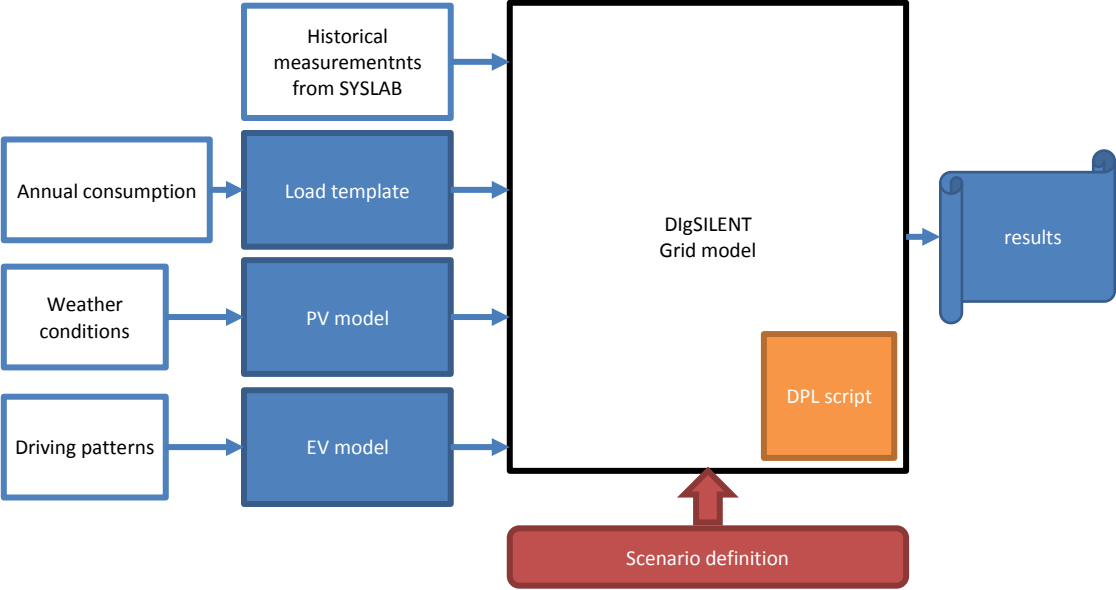


Fig. 5.9. Block diagram with details about how the simulation platform was built.

The daily time series in Fig. 5.10 (i.e. external grid voltage profile, PV production, EV charging consumption, and the detached house consumption) are the inputs of the simulation model. The data with voltage profile (the dash curve in Fig. 5.11) and PV production curve (06:00 – 20:00) is collected on 15-05-2012 from our laboratory with real components and renewable energy production (SYSLAB).

The capacities of PVs are adapted to 6 kW. EV charging profile, from (18–22), is calculated based on the driving pattern [7] with the rated charging power of 11 kW. The load profiles are calculated by the load pattern, from the aggregated historical data in Denmark, multiplying the peak power using the Velander equation (5.1).

By subtracting the production or adding the consumption new household load profile can be obtained. The time sweep load flow is executed by using DigSILENT programming language script DPL, as was shown in Fig. 5.9.

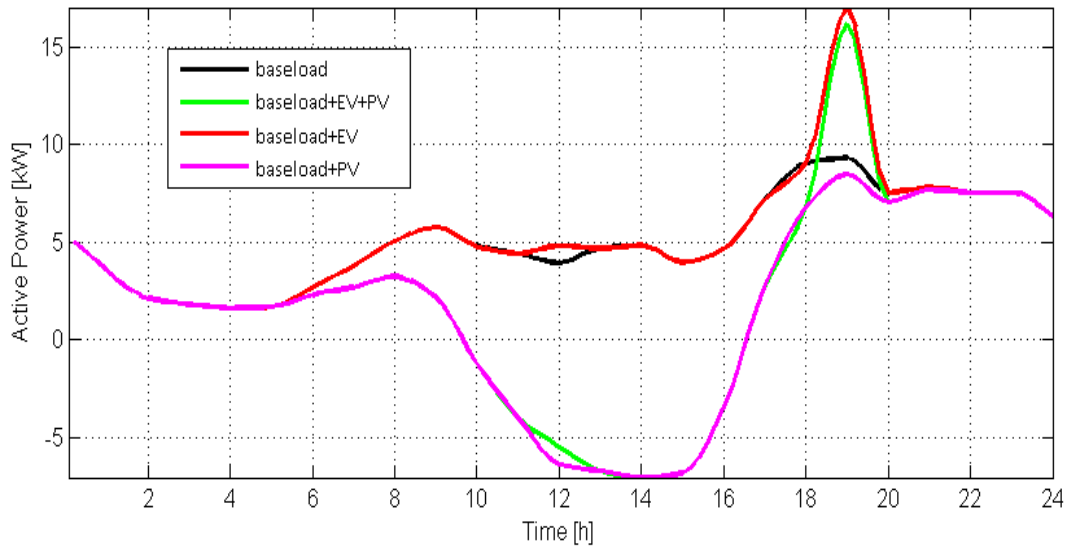


Fig. 5.10. Time series simulation of the load profiles for residential load (based on Velander correlation), EV load and PV load (distinguished from the conventional load with a peak power multiplication factor) based on the load pattern from the aggregated historical data in Denmark.

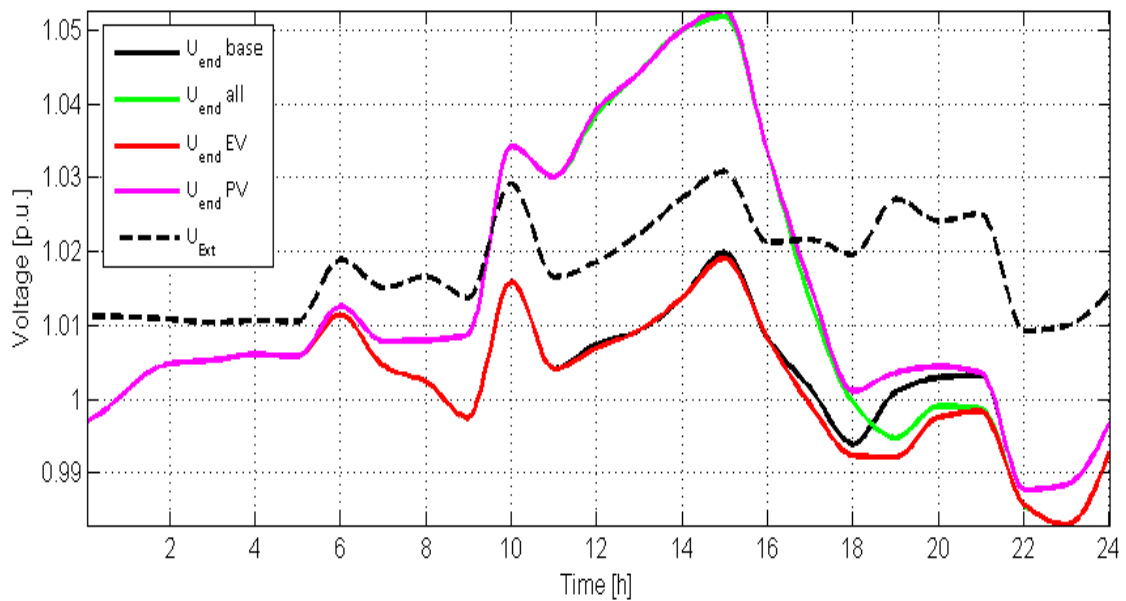


Fig. 5.11. Comparison between voltage profile of the external grid and the voltage profiles of the PV's, EV's, base loads and all loads connected at the last cabinet to the end of the feeders.

Fig. 5.10 shows that at 19:00, the modified load has a peak due to the EV charging (Scenario 10). However, considering the deviation of human behaviors (smoothing effect), the overall peak may be less than the sum of them. At 15:00, the reversed load reaches the peak where there is the largest mismatch between load and PV production (Scenario 2). A voltage rise of 1.06 p.u. can also be observed.

Fig. 5.11 shows the simulation results for one day with a comparison between voltage profiles in the last node (at the end of the feeder cabinet) versus voltage profile of the external grid. The voltage profile was plotted for one day as a function of time, giving the load profiles shown in Fig. 5.10.

In Fig. 5.11 can also be seen that we generated four different cases (scenarios): first case when the voltage profiles are similar (no PV production and no load consumption) from 0-6 a.m., the second scenarios from 6 a.m. to 6 p.m. when we have two different voltage profiles because of the PV production (with a maximum around 3 p.m.), the third case between 6-10 p.m is related to a maximum load with EV charging, and the last case from 10-12 p.m. with no PV production but a limited time for EV charging.

Using this approach (i.e., generate the profiles outside the power system software and use its traditional function) the complexity of the models can be avoided, but introducing a lot of manual work on modifying the inputs of the simulation model.

Time series simulation provides an overview of the potential problems (thermal loading and voltage rise in our case). Based on this the concurrency of a group of units can be investigated towards less conservative design.

Similarly, in NEPLAN, the profiles are prepared outside the power system simulation software. NEPLAN also provided the GUI to specify the scaling factors. Moreover, another option is provided: some files with certain format can be the information exchange interface with other software (see Fig. 5.13), instead of manually inserting the time series to the elements in the grid model in PowerFactory. However, NEPLAN does not support profiling the voltage characteristics whereas in PowerFactory there is no limit for the variable types. In order to represent the voltage variation in medium voltage level grid and present the effect from outside of the feeder, we used a weak connection point and a profiled load to adjust the voltage. Fig. 5.12 shows the rebuilt grid model in NEPLAN. Load U is the one used to profile the voltage at the MV/LV transformer.

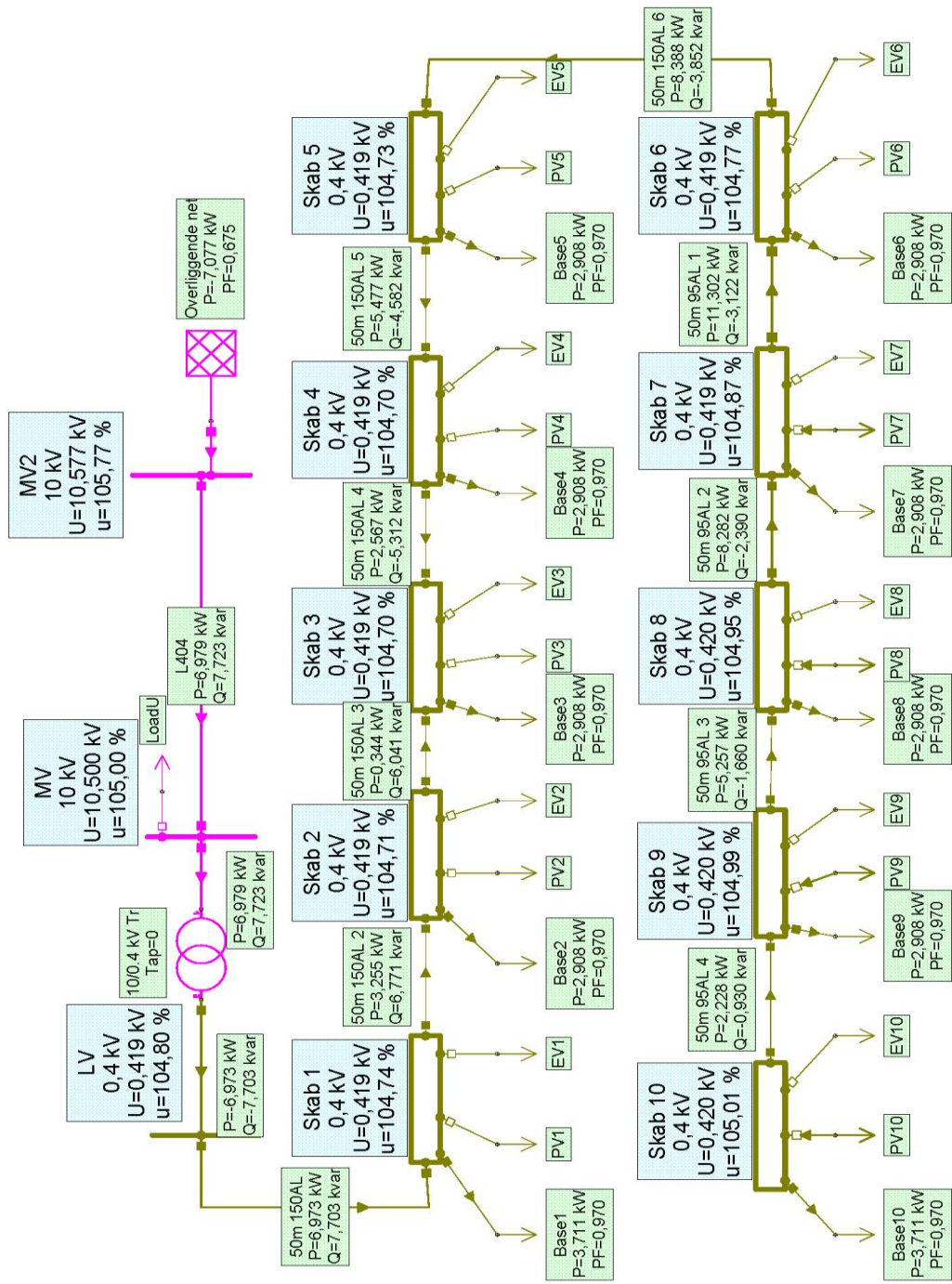


Fig. 5.12. Rebuilt grid model in NEPLAN combining scenarios no. 4 with 10.

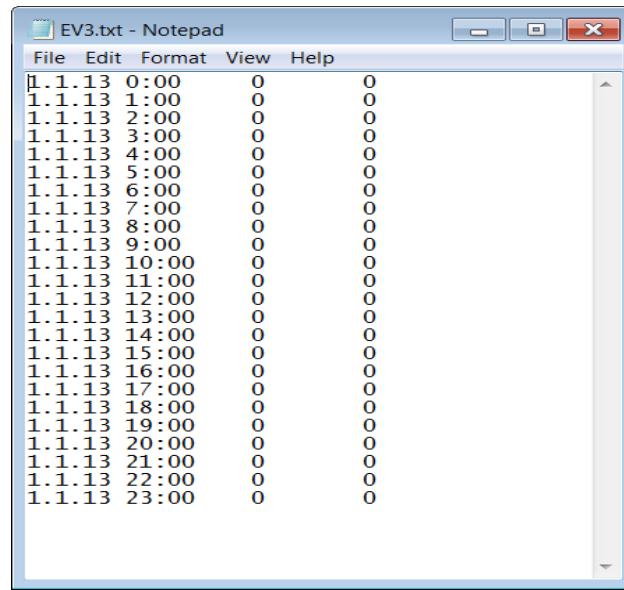


Fig. 5.13. Load profiling file.

The same profiles are prepared for three types of loads: base load (original residential house load), the PV production measurement from SYSLAB, and the EV charging profile given the driving patterns. All these three elements are connected to the same bus-bar (in our case, 'Skab', cabinet), as can be seen in Fig. 5.14.

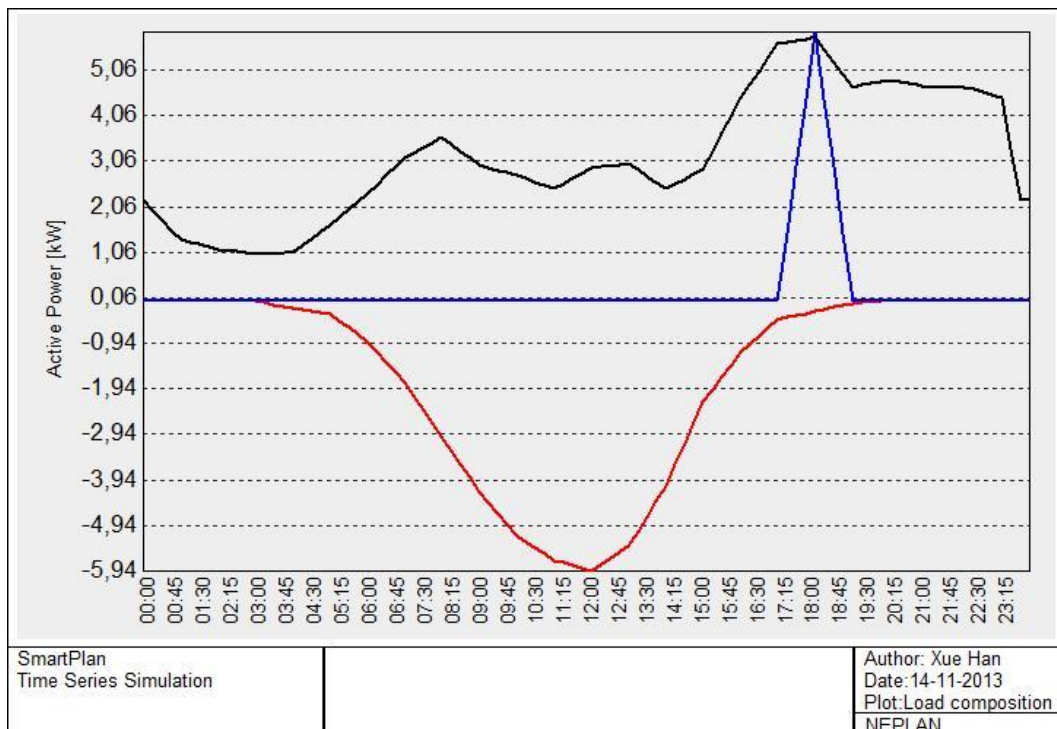


Fig. 5.14. PV production, residential load profile and EV charging profiles implemented in NEPLAN.

Fig. 5.15 shows the voltage profile at the transformer and at Skab 10 with (a) and without (b) PV connected to the grid. Similar results are obtained with Power Factory: there is an overvoltage along the feeder when PVs exist in the feeder and the production is higher than the consumption around noon. And for the rest of time, the voltage decrease along the feeder. It can also be observed from

Fig. 5.16 that due to the EV charging activities, the net load is larger and the voltage drop is rather severe.



a)



b)

Fig. 5.15. voltage profile at the transformer bus-bar and at Skab 10 bus-bar, a) with and b) without PVs.

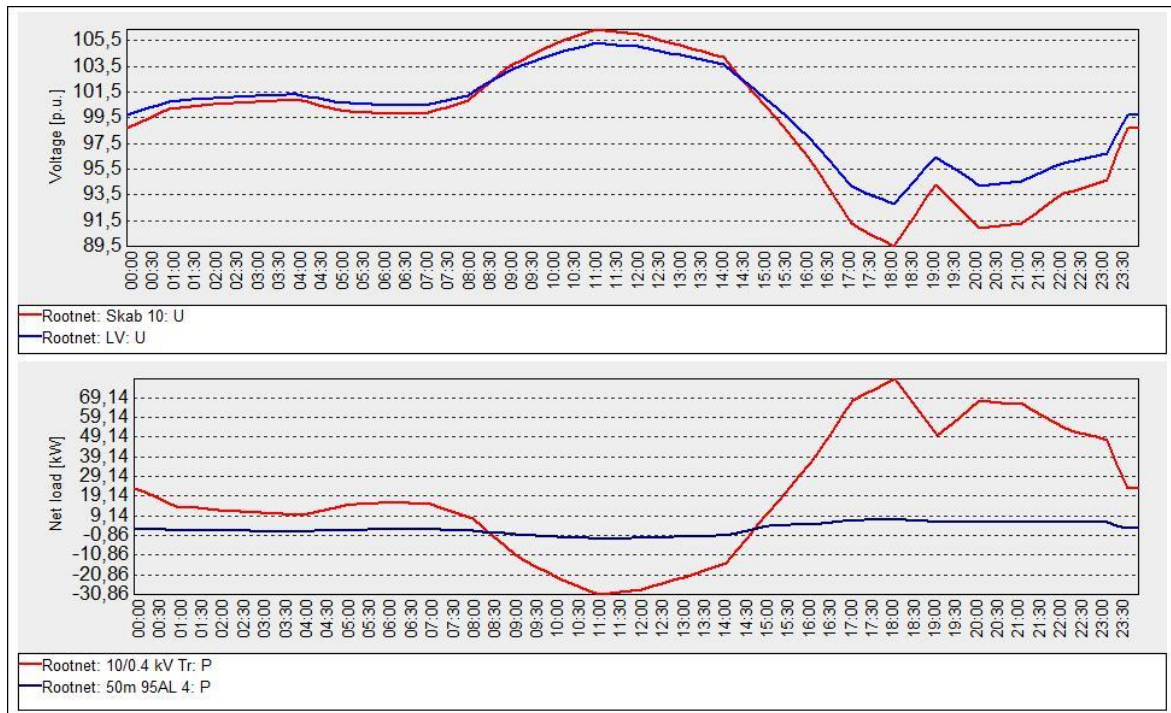
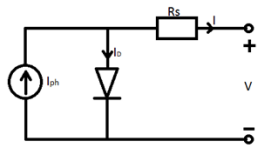


Fig. 5.16. Simulation results for voltage and load profiles in NEPLAN pointing out one of the worth's scenarios when the EVs were connected along the feeder.

5.4.2. Time-series simulations using dynamic models

5.4.2.1. PV system modeling

The dynamic model of the PV System (PV panels and PV inverter) has been built with standard block components from the Power Factory library and also using the dynamic simulation language (DSL) to implement the equations and to define the states and the parameters of the model. The model is based on a single diode equivalent electrical circuit for the PV model, described by an exponential equation [8-10], as can also be seen in Fig. 5.17.



$$i = I_{ph} - I_0 \left(e^{\frac{v+iR_s}{n_s V_T}} - 1 \right) - \frac{v+iR_s}{R_{sh}}$$

$$\frac{dP}{dV} = n_{sp} I_{sc} \left[1 - e^{\frac{v-n_{ps}V_{OC}+R_s i}{n_{ps}n_s V_T}} - \frac{v}{n_{ps}n_s V_T} e^{\frac{v-n_{ps}V_{OC}+R_s i}{n_{ps}n_s V_T}} \right] = 0$$

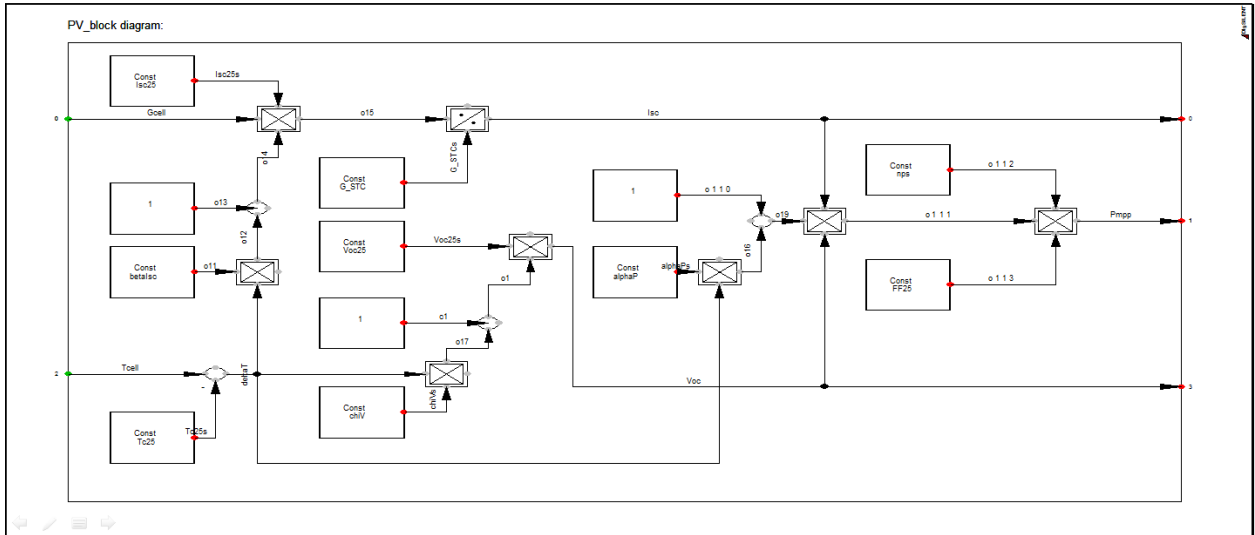


Fig. 5.17. Details about the single diode electrical circuit and the exponential equations of the PV model (on the top) and its implementation in DigSILENT PowerFactory

The model uses the cell irradiation G_{cell} and cell temperature T_{cell} as inputs, measured from a weather station and implemented as look-up tables.

The PV panels are mounted in three strings: two of them having 18 panels of 165 W each, and the 3rd one having 12 panels of 100 W. The strings of panels are connected to the low-voltage distribution network through a three-phase PV inverter. More details can be found in chapter 2 and also in [8] and [9].

The simulation model was validated using experiments carried out using RISØ experimental facility-SYSLAB ([8-10]). A block diagram with the PV model implementation and validation is shown in Fig. 5.18.

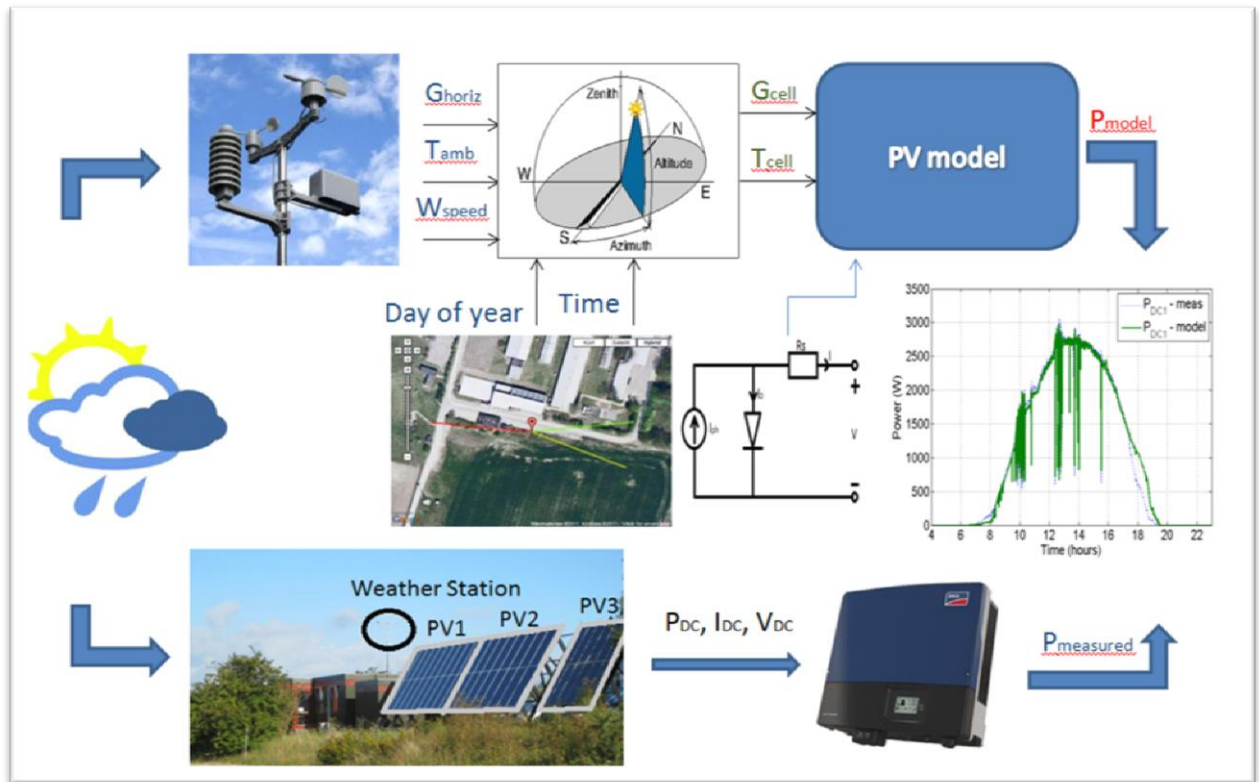
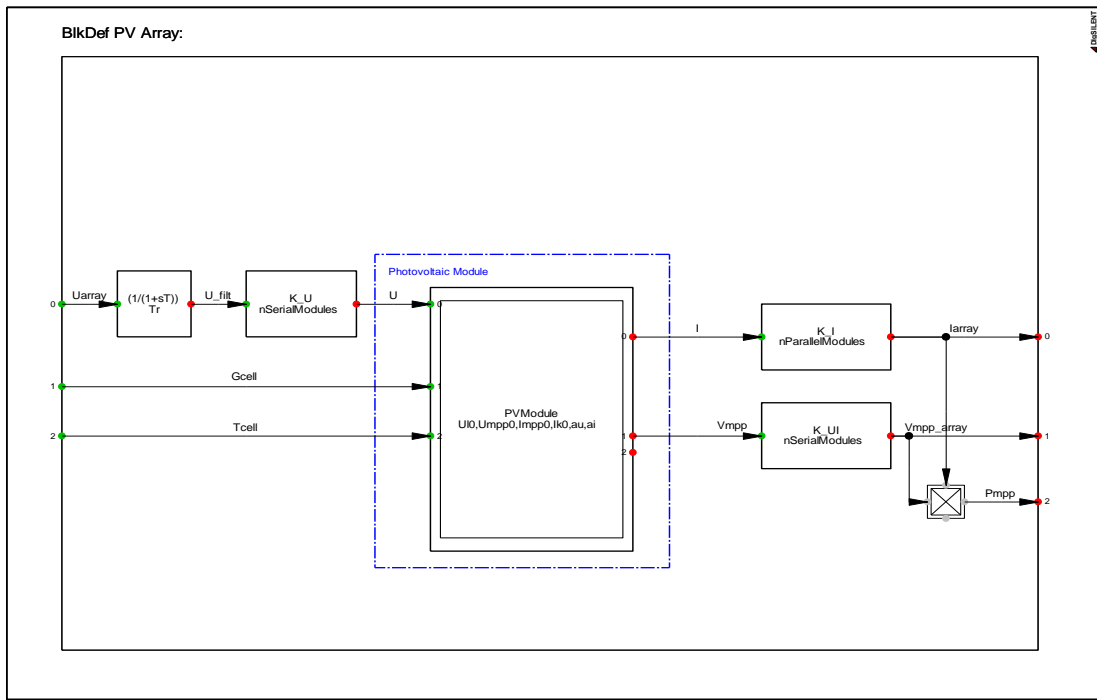


Fig. 5.18. A block diagram with details about the PV model implementation and validation.

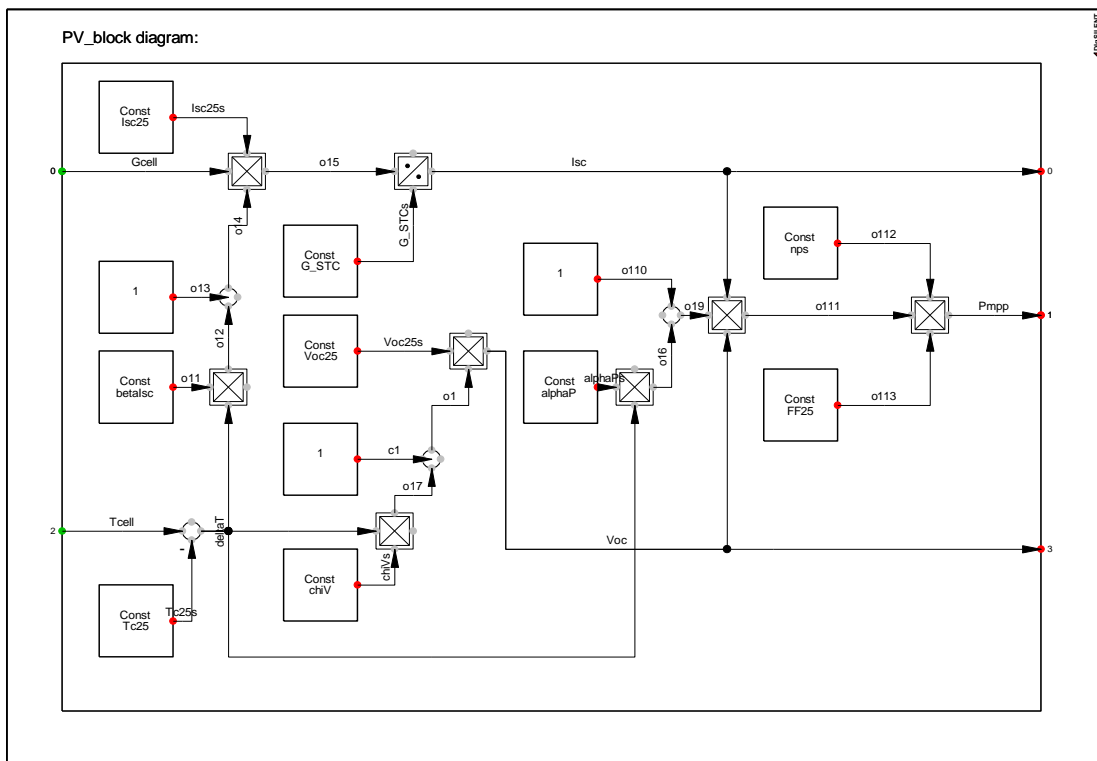
The PV array model is implemented in PowerFactory using block diagrams to define the PV module and the number of panels in series and the number of strings. The internal simulation language DSL was used to define the PV characteristics and equations, and to initialize the parameters and variables of the model.

The PV array model has as inputs the voltage array (U_{array}), irradiation (G_{cell}) and cell temperature (T_{cell}) and as outputs MPP of the current (I_{array}), voltage (V_{mpp_array}) and power (P_{mpp}) for the PV array, as can be seen in Fig. 5.19 a). To get the MPP values for i-v characteristics of the array two blocks references have been used.

Fig. 5.19 b) shows details about how the PV model frame has been implemented in PowerFactory.



a)



b)

Fig. 5.19. a) PV array block model frame and b) PV panels model implemented in PowerFactory.

In order to validate the simulation model developed in PowerFactory we compare the results with measurements, acquired from SYSLAB for one day.

In Figs. 5.20 is presented a comparison between measurements and simulations of inverter input power for two strings of panels with different PV modules (Schuko 165 and SOLEL 100).

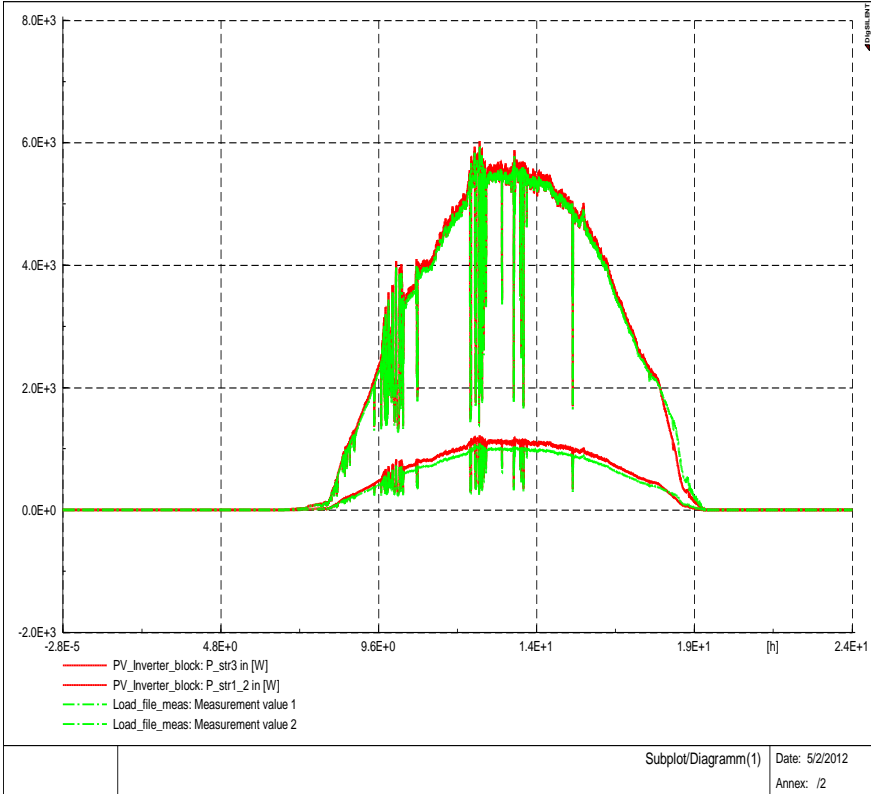


Fig. 5.20. Comparison between simulations and measurements of the PV panels for two strings with the data acquired from SYSLAB with a sampling time of 1 sec.

5.4.2.2. Active and Dynamic Loads Modeling

The traditional static load models are not suitable as they do not emulate the behavior of the loads. Accurate models of power system loads are important to study the dynamic performance of electric power systems.

A) Active Loads Modeling

The simulation model of the intelligent office building, called Flex-House, is based on the equivalent electro-thermal model of the building (Fig. 5.21) using a stochastic discrete-time linear state-space model (5.2) combining with physical knowledge regarding heat transfer inside the house together with statistical methods to estimate model parameters [8]-[10], [12].

The model for the building is formulated as a one room lumped-RC-model in accordance with the commonly used thermal-electrical analogy. Figure 5.21 shows the heat flow diagram for the building and the equivalent RC-circuit.

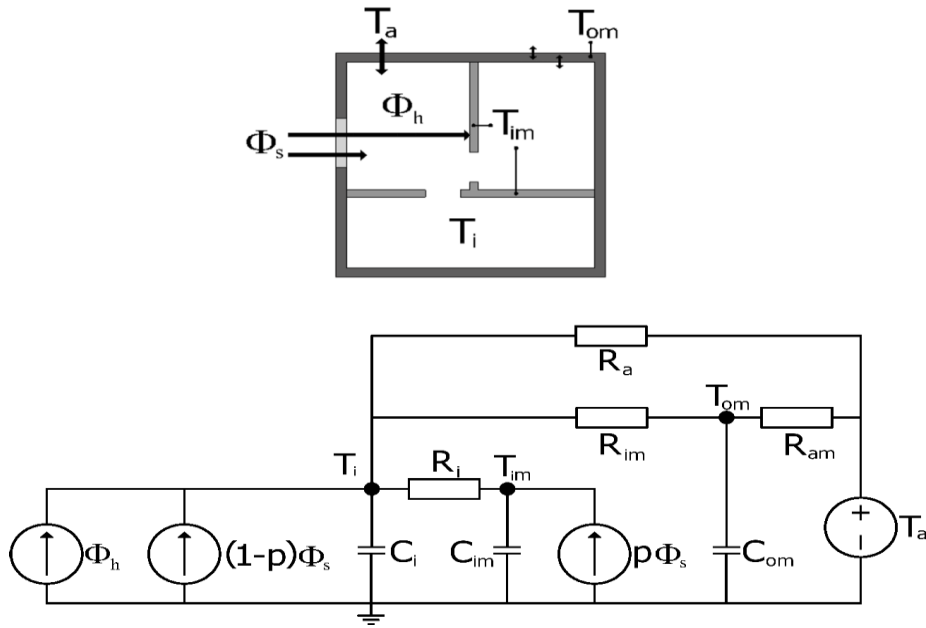


Fig. 21. Flex House single room RC-circuit diagram [12].

$$\left\{ \begin{array}{l} C_i \cdot \frac{dT_i}{dt} = \frac{1}{R_{ia}} \cdot (T_a - T_i) + \frac{1}{R_{im}} \cdot (T_m - T_i) + \frac{1}{R_{ih}} \cdot (T_h - T_i) + A_w \cdot G \\ C_m \cdot \frac{dT_m}{dt} = \frac{1}{R_{im}} \cdot (T_i - T_m) \\ C_h \cdot \frac{dT_h}{dt} = \frac{1}{R_{ih}} \cdot (T_i - T_h) + P_h \end{array} \right\} \dots(5.2)$$

Where C_i is the heat capacity of the house, R_{ia} represents the thermal resistance from the indoor to the ambient, A_w is the effective window area of the house with heating influence. The state space variables are: T_i – inside temperature, T_m – second inside temperature which defines an internal medium and T_h – temperature in the electrical heater.

B) Dynamic Loads Modeling

The dynamic load model was implemented in Power Factory (Fig. 5.22) using (5.3) and is based on voltage dependency of active and reactive power and it is described by ([5], [10]):

$$\begin{aligned}
 P &= P_0 \left[kp_1 \left(\frac{V}{V_0} \right)^{(p_1)} + kp_2 \left(\frac{V}{V_0} \right)^{(p_2)} + (1 - kp_1 - kp_2) \left(\frac{V}{V_0} \right)^{(p_3)} \right] \\
 Q &= Q_0 \left[kq_1 \left(\frac{V}{V_0} \right)^{(q_1)} + kq_2 \left(\frac{V}{V_0} \right)^{(q_2)} + (1 - kq_1 - kq_2) \left(\frac{V}{V_0} \right)^{(q_3)} \right]
 \end{aligned}
 \tag{5.3}$$

Where P_0 , Q_0 and V_0 are the initial values of active power, reactive power and voltage, $p(q)_1$ to $p(q)_3$ are coefficients that define the proportion of each component and k_p, k_q are coefficients that reflect the dependency of load ($k_{p1}=100\%$, $k_{p2}=0$). Typically, in dynamic simulation, a simplification is done and all loads are considered to be constant admittance type ($p_1=2, p_2=p_3=0$).

The implementation of dynamic load model, described by (5.3) is presented in Fig. 5.22 (on the top) together with a simulation of the bus-bar (BUS 2) voltage, at which the load was connected, and active and reactive power response of the load during a Short-Circuit event, when the voltage drops.

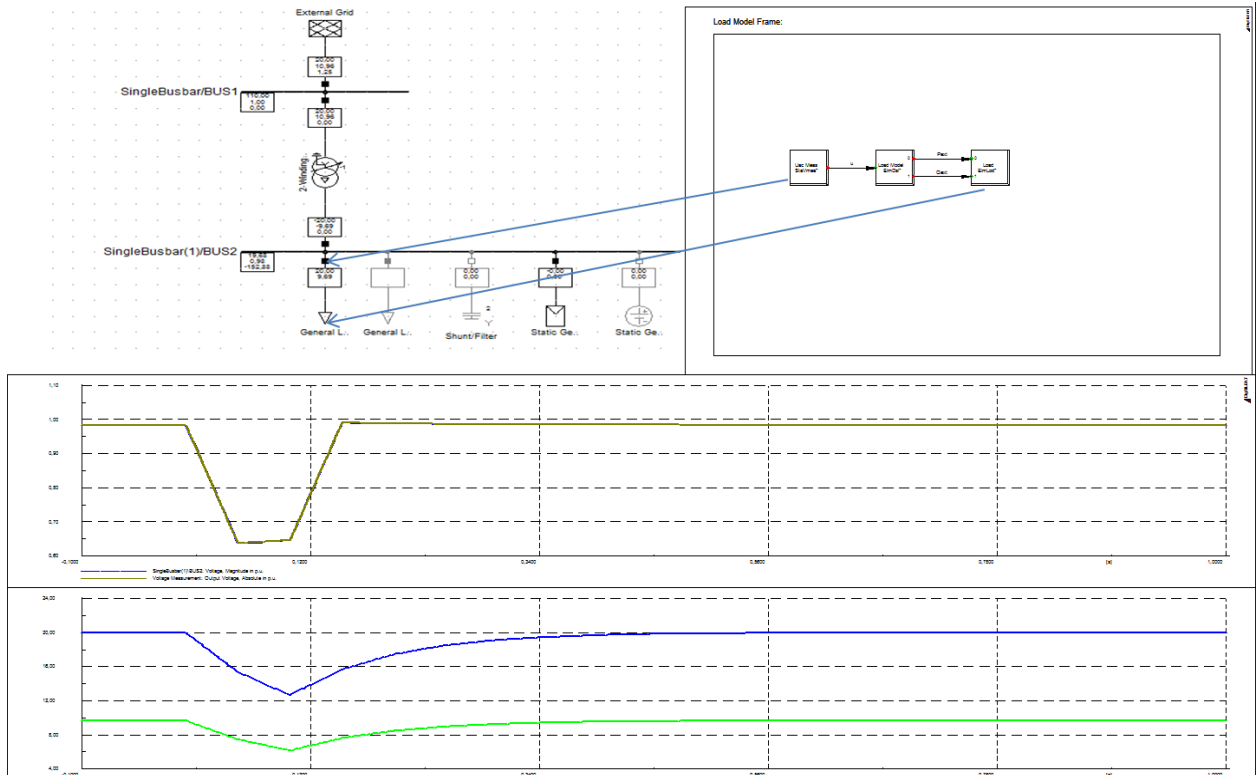


Fig. 5.22. Implementation of the dynamic load described by (2) in DigSILENT Power Factory (upper) and simulation results with voltage drop and active and reactive power of the dynamic load model.

5.4.2.3. EV battery modeling and implementation

An equivalent circuit modeling with one or two RC block model is the common approach for lithium-cell [14-17]. A single RC block model is adequate for many problems of industrial relevance and has also been used in this paper in combination with a runtime-based electrical battery model (Fig. 5.23).

The runtime electrical battery model (on the left in Fig. 5.23) represents the battery lifetime and contains a self-discharge resistor ($R_{\text{self-discharge}}$), a condenser (C_{capacity}) and a current-controlled source (I_{batt}). $R_{\text{self-discharge}}$ is used to characterize the self-discharge energy loss when batteries are stored for a long time and depends on SOC and temperature. C_{capacity} represents the whole charge stored in the battery (SOC) and can be express like in Fig. 5.23 [10].

Where C_n represents the nominal capacity of the battery and $f_1(\text{cycle})$ and $f_2(T)$ are cycle number and temperature dependent correction factors.

On the right side in Fig. 5.23 it is represented the Thevenin electrical circuit model which represents the voltage-current characteristic of the battery. The model contains a series resistor (R_s) and a RC parallel network (R_t, C_t) to predict the transient response of the battery. Each parameter of the Thevenin circuit is a function of SOC, current and temperature and was implemented in Power Factory using two-dimensional look-up tables based on the measurements shown in Fig. 5.24.

The series resistance voltage droop (V_s) and the equivalent voltage transient response (V_t) are combined with the open-circuit voltage (V_{OC}) to obtain the battery terminal voltage (V_{batt}), as it is described by the equations on the right side of the Fig. 5.23.

The model of the battery pack was implemented in Power Factory based on the equations presented in Fig. 3.5 and the measurements presented in the Fig. 3.6. The model provides the SOC, power of the battery and the battery voltage as a function of SOC, current and temperature. Each parameter of the Thevenin circuit is a function of SOC, current and temperature and was implemented using two-dimensional look-up tables based on the measurements at different SOC, current levels and temperatures using pulse current discharging/charging test.

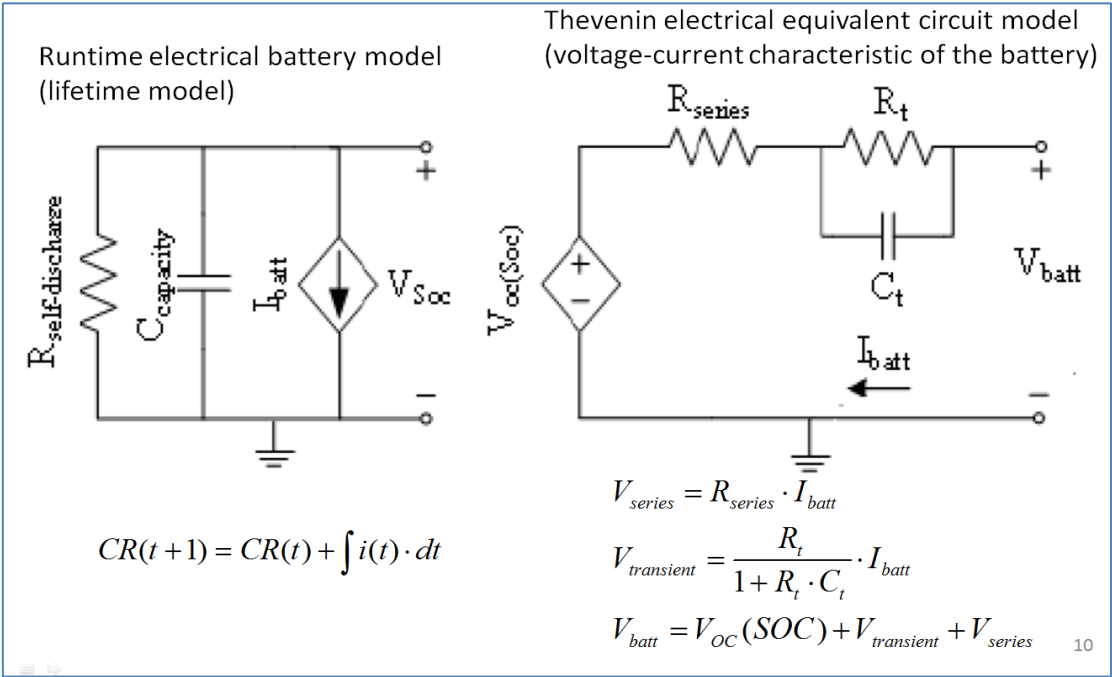


Fig. 5.23. The electrical equivalent circuit model of the EV battery.

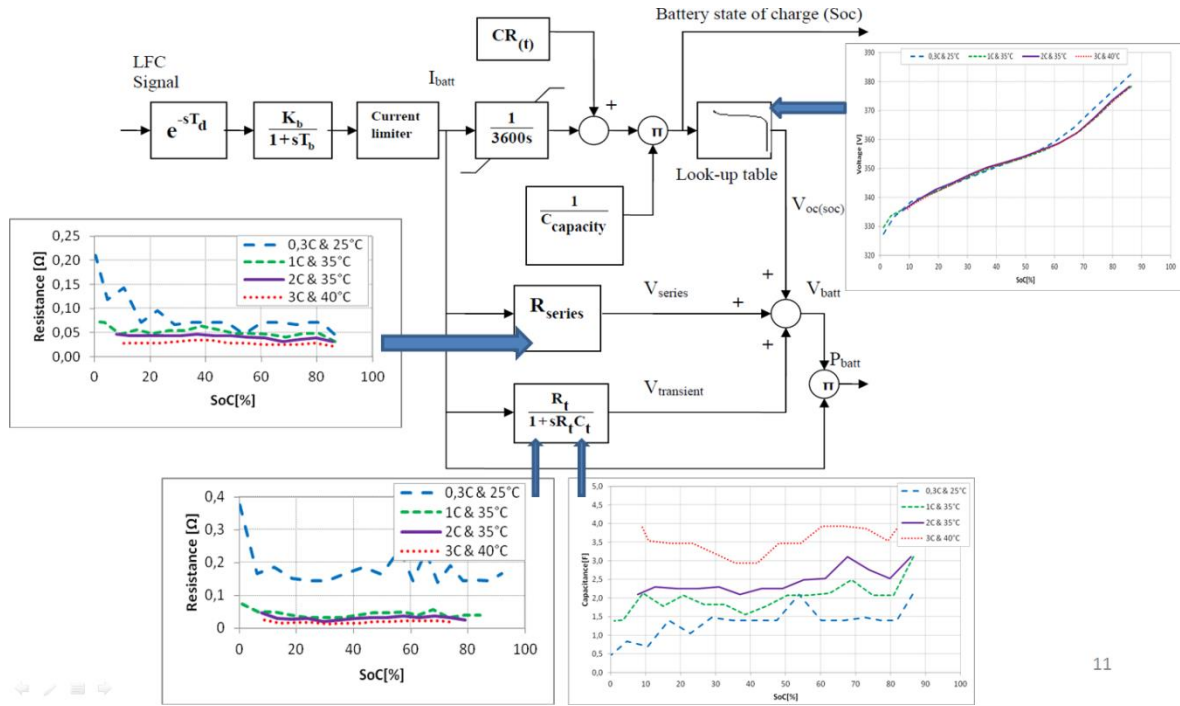


Fig. 5.24. Details with EV battery storage model implemented in DigSILENT PowerFactory.

Fig. 5.25 shows a time-series simulation results with EVs battery cell and package voltage and SOC during the discharging mode when the battery was discharged from full rate to zero and when a battery constant pulsed current of 25 A was applied.

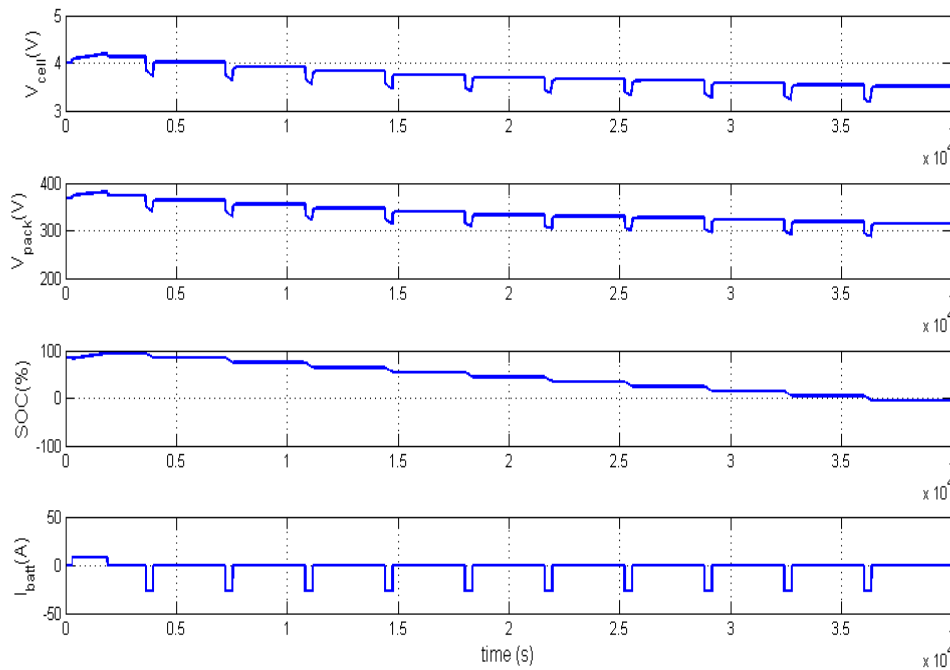


Fig. 5.25. Simulation results of the EV battery pack system with a pulsed current during discharging mode.

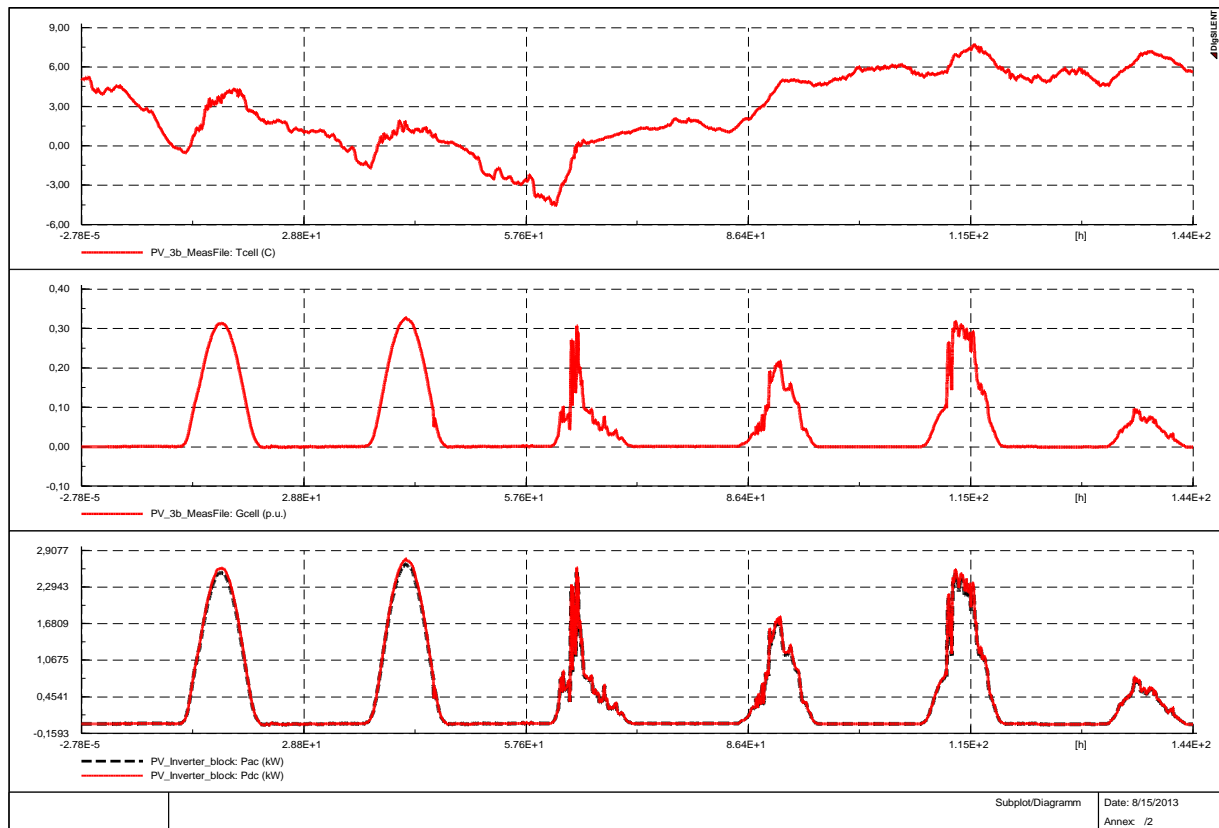
5.4.2.4. Simulation Results

In Fig. 5.26 are presented some time-series simulation results, with PV systems and loads connected together to the same bus-bar, for 6 days in November 2012. The input data for the simulation model (irradiation and temperature) was measured from the weather station placed on Risø campus with a sampling time of 1 second. The load profile was defined with and without voltage dependency of the active power.

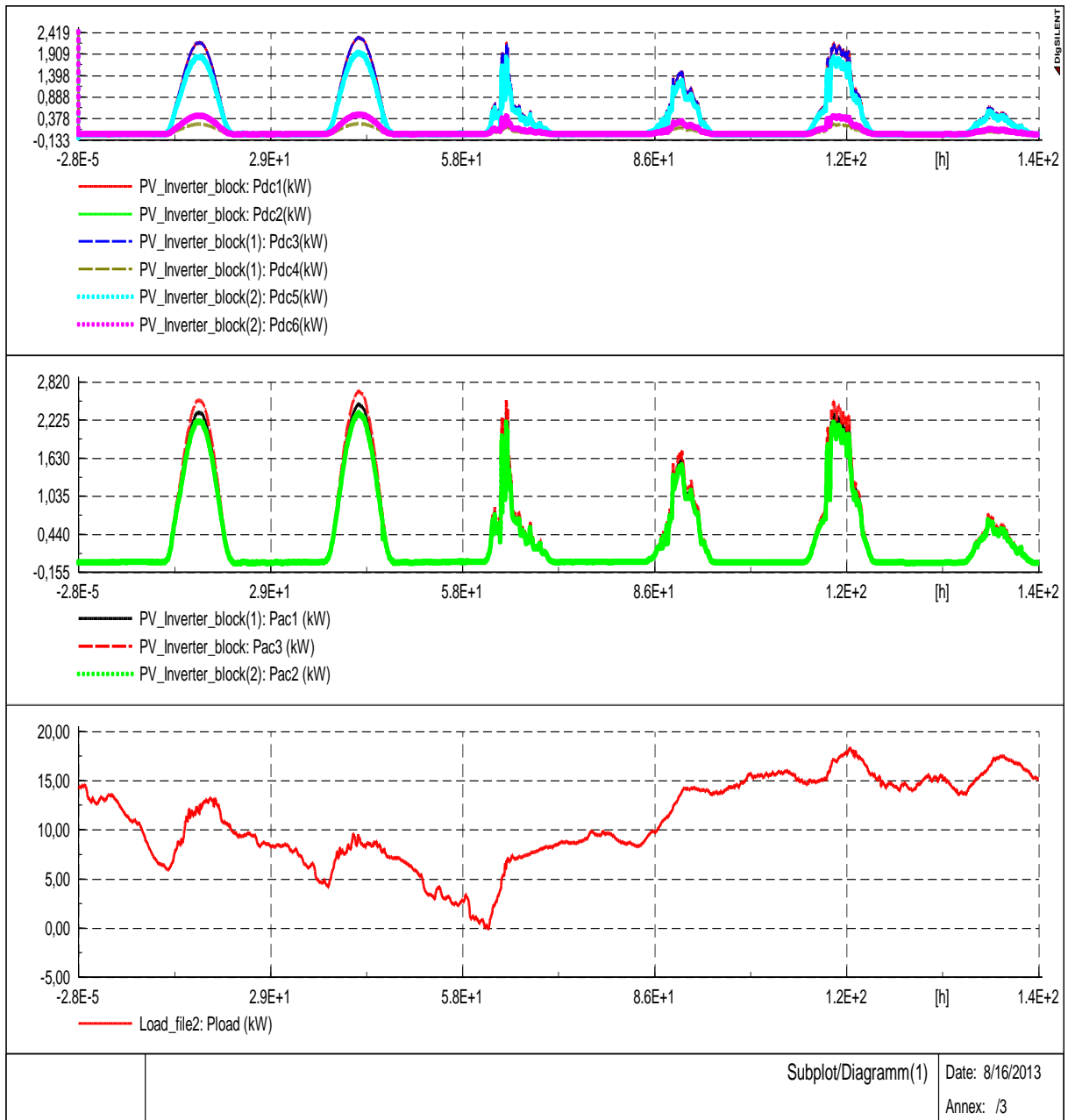
Fig. 5.26 a) shows a comparison between input data (T_{cell} between -4 and $+6$ °C and G_{cell} around 300 W/m² during the day) and the output parameters of the model [output power of the panels- $P_{dc1} + P_{dc2}$ ($P_{dc_total}=2.7$ kW) and output power of the inverter- $P_{ac}=2.6$ kW].

In Fig. 5.26 b) are shown the simulation results when 3 PV inverters are connected together with the loads at the last 3 cabinets of the grid model presented in Fig. 5.1. In this particular case, EVs and HPs are assumed to be an unknown proportion of the total load and the PV systems have the same parameters but the panels have a different orientation and tilt angles.

Fig. 5.26 c) shows a load profile defined by (5.2) with voltage dependency of active and reactive power.



a)



b)

Fig. 5.26. a) Time series simulation results of the PV system for 6 days with real data implemented as input and with DC and AC powers as outputs; b) Comparison between IN and OUT of the 3 PV inverters, connected to the last 3 cabinets of the grid model together with a load profile predefined in DSL.

5.5. Discussion and Conclusion

The purpose of this chapter was to identify limitations of existing simulation and planning tools for distribution grids, with a particular focus on the challenges imposed by the introduction of Smart Grid technologies.

Based on the survey of tools, we have been trying to find out the limitations during the implementation of smart grid solutions and corresponding functions. The simulations have been made in both software packages, DlgSILENT PowerFactory and NEPLAN, using the same grid model and parameters.

This chapter was also trying to identify critical load cases and voltage variations for the defined scenarios.

A steady-state and a dynamic analysis of the grid model have been presented based on time-series simulations with a comparison between different voltage profiles.

The low-voltage distribution grid model has been developed and implemented in NEPLAN and DlgSILENT PowerFactory to study load flow, steady-state voltage stability and dynamic behavior of the components.

As a comparison between power flow calculations, using both software packages, we can conclude that there is an insignificant difference. The parameters and simulation models for all the components are slightly different.

The comparison between both simulation tools has shown a good alignment and the possibility to use them for further developments, regarding the integration of smart-grid technologies. It means that this work could be used for development and improvements of the models for different components placed along the feeders in a future smart-grid distribution network.

Appendix:

The hosting capacity analysis of the new appliances (PVs, EVs, HPs) connected to the distribution grid developed and designed in WP1

Scenario	Phase	PV	HP	EV	FeederL	U range	T ratio	Cable	Trans	No de	Unbal	Comments	Distribution
1	3	*			85%	6/10	25,000	<10	<10	1,00		reference scenario for PV cases, 4st 6kW (-24 kW)	[0,0,0,0,0,0,1,1,1]
2	3	*			85%	10/10	25,000	>20	>20	1,06		larger voltage range, 20st 6kW (-120 kW)	[2,2,2,2,2,2,2,2,2,2]
3	3	*			85%	6/10	26,500	>20	>20	1,00		change transformer ratio, 23st 6kW (-138 kW)	[2,2,2,2,2,2,2,3,3,3]
4	3	*			85%	10/10	26,500	>80	100	1,06		both above changes, 40st 6kW (-240 kW)	[4,4,4,4,4,4,4,4,4,4]
5	1	*			85%	6/10	25,000	<10	<10	1,00	6V	1-phase, 1st 4kW (-4 kW)	[0,0,0,0,0,0,0,0,0,1]
6	1	*			85%	10/10	25,000	<10	<10	1,00	17V	1-phase, larger voltage range, 3st 4kW (-12 kW)	[0,0,0,0,0,0,0,0,1,1,1]
7	2	*			85%	6/10	25,000	<10	<10	1,00	2V	2-phase, 1st 6kW (-6 kW)	[0,0,0,0,0,0,0,0,0,1]
8	2	*			85%	6/10	25,000	>20	>20	1,06	13V	2-phase, larger voltage range, 9st 6kW (-54 kW)	[0,1,1,1,1,1,1,1,1,1]
9	3			*	85%	6/10	25,000	>80	100	0,90		reference scenario for EV cases, 10st 11kW (110 kW)	[1,1,1,1,1,1,1,1,1,1]
10	3			*	85%	6/10	25,000	>40	>40	0,95		change allocation, 6st 11kW (66 kW)	[0,0,0,0,0,1,1,1,1,2]
11	3			*	85%	6/10	25,000	>20	>20	0,95		change allocation, 5st 11kW (55 kW)	[0,0,0,0,0,0,0,0,0,5]

Part II: Future Plans for Career Development and Evolution

The second part of the Thesis, regarding to future plans for advancement and career development, is based on the proven skills to conduct and coordinate high-level research and teaching activities at academic level and to initiate successful international collaborations in the field of renewable conversion systems. As future plans I am trying to attract national and EU funds (Horizon 2020 grants) to extend and improve our research lab “Intelligent control of energy conversion and storage” from POLITEHNICA University of Timisoara, Electrical Engineering Department, and to extend our international cooperation and network. Another plan is to create and develop a Smart Grid platform, similar with that one from Danish Technical University (www.powerlab.dk), where I spent 3 years, and to use my experience to create a research center for teaching and education of Master and Ph.D. students, coordinated as a result of the Habilitation Thesis.

A) Main Directions for career development

Career development and evolution plans should be structured on several activities interconnected together, that fully complement each other in the same direction.

The plans include the involvement of dedicated persons (current and future advanced and early stage collaborators, as well as students) who will have the chance to benefit from the opportunities of the research system developed and via education and training anchored in the activity of the group coordinated as a result of the qualification attributed through this habilitation process.

Table I: Main directions and objectives for career development

Direction	Objectives	Expected outcome
1. Oriented research	1.1 Development of cost-efficient exploration tools for new components.	- set-up of a research facility for a smart grid platform; - new appliances and functional architectures;
	1.2 Investigation of novel control strategies.	- novel products and technologies.
	1.3 Design of new applications and technologies.	
2. Enlargement of the research potential	2.1 Identification of support for	- advanced investigation capacities;

	advanced lab equipment's	- involvement of adequate human resources for achieving the research goals.
	2.2 Funding for research collaborators.	
3. Improvement in teaching and academic career	3.1 Implementation of an improved educational offer.	- updated educational offer according to the current interest at international level;
	3.2 Advancement at professorship level.	- contribution to an improved institutional ranking and prestige.
4. Dissemination and transfer of knowledge	4.1 Scientific outreach.	- publications in high-ranked journals;
	4.2 Public outreach.	- public awareness on the importance of the activities developed; - collaborations with industry/companies.
5. International collaborations	5.1 Targeted research	- joint projects and partnerships;
	5.2 Networking.	- teaching and research collaborations.

Enlargement of the research potential

Based on the previous results and the continuing preoccupation for expanding the limits of the research and the capabilities to offer consultancy and training in the field of renewable energy sources and smart grids, the quest for support is going to be a continuous preoccupation. In parallel, funding will be sought to support the inclusion of new members in the research team, with focus on people looking for PhD and Master Degrees in the field of energy conversion systems using sustainable energy.

Scientific and technological challenge

The key challenges should be identified and investigated. They could contain the modeling and validation of the models, modeling the variability of the system and its impact on the control strategies, validation of the new control strategies for a smart grid with a large share of PV, WT etc, operational impact of the network and economic impact of the overall system.

The scientific and technological solutions should include the development and validation of the relevant models, development of new control systems, development of smarter

networks to achieve better controllability and integration of additional assets such as storage systems, and flexible demand into the overall power system operation (Smart Grid).

Improvement in teaching and academic career

As results of the habilitation, an expansion of the research-training activity is expected, that will favor the selection of students interested in pursuing a career in electrical engineering. Improved teaching materials will be prepared and the actualization of curricula for master and PhD courses will be a continuous preoccupation.

The educational activity in the framework of the university curricula and requirements will be complemented with the organization of summer schools, seminars and workshops, dedicated for training in smart grids and smart cities and investigation techniques, addressed to national and international students, and early stage researchers.

Dissemination and Knowledge Transfer

The valorization of the results is planned in scientific community and to the public interested in the subjects of the research activity.

In the scientific community, the dissemination will be made ensured by publishing the results in scientific journals with high impact factors. The exchange of ideas with the scientific community is planned to continue through participation in national and international conferences. In addition, the results will be published on the projects web page and the partners will also distribute the findings at workshops, conferences and journal papers. Each partner will compile its own report providing a detail description about the main tasks.

The transfer of knowledge related to the applicative results of the research will be a continuous preoccupation, with scientific and logistic support for start-up as well as established companies interested in developing the field. The partners in the projects should have good contact with DSOs and TSOs and can thus bring the results directly to the main stakeholders. This could be a main form of dissemination of project results.

International collaboration

The creation of long-lasting collaborative mechanisms in designing a smart grid platform (with focus on smart grids components and communication) with international partners is and will be a continuous preoccupation. It has already been materialized in several major collaborations and grants (*Smart Plan, Smooth PV, Improvements of the structures and efficiency of small horizontal axis wind generators with non-regulated blades*) that was developed based on the research activity in renewable energy conversion systems, providing support for innovation and its transfer from laboratory to pre-implementation phase of new components and control strategies. At this time, the following international collaborations are envisaged for the near future:

- Horizon 2020 planned application involving universities from Denmark (DTU and Aalborg University), from Canada(Ottawa University), Germany (Siegen University) and research international institutions: IWEAS (Germany) and Austrian Institute of Technology

B) Main Directions for research and planning objectives

The main direction for research development will cover the area of Smart Grid Technologies. In the context of Smart Grid, many new interfaces and new technologies emerge, as can be seen in Fig. 1:

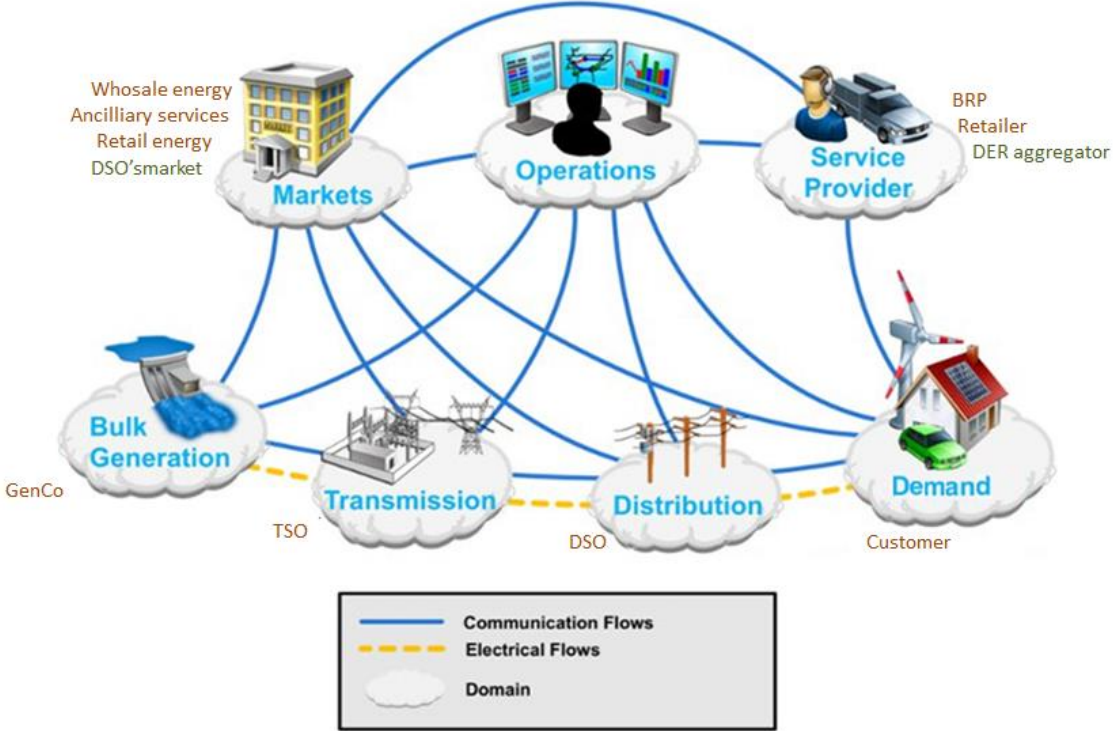


Fig. 1. A Smart Grid Architecture.

In a Smart Grid we have to redesign the power system, including new devices and protections, active loads, embedded generation, new control strategies, emerging solutions and new standards.

The transition from the existing to the smart distribution system requires building new distribution lines and feeder ties and installing new smart switching/protective devices, new distribution equipment, sensors, and meters for monitoring, controlling, and protecting the new lines. The improved methodologies and tools must help distribution engineers answer questions such as how many new smart devices, feeder ties, distribution lines, capacitor banks, voltage regulators, sensors, and other devices are needed and where they should be located.

More controllable devices may not be regulated by the DSOs. Because of that we have to find out new limitations considering new approaches in designing and planning objectives:

- Active load (customer assets)
 - Concurrency: change in concurrency due to control
 - Time dependence/memory: flexibility is limited due to user comfort requirements
 - Energy demand with deadline: flexibility is limited due to user comfort requirements
- Embedded generation (customer assets)
 - Negative load → active resource
 - RES with stochastic nature
 - Inverters offer the possibility of reactive power regulation
- Emerging market solutions
 - Real time market solutions (transactive control)
 - **Flexibility market for coordinating demand side flexibilities (TSO or DSO's)**
 - **Congestion management (Locational marginal pricing, or DSO's ancillary service market)**
 - Emerging entities (e.g. aggregator) could be active in the distribution level market and also by-pass the DSOs and provide services to transmission system
- Regulating options (DSO assets)
 - Devices: OLTC, AVR, switches
 - Network: dynamic topology
- A variety of control solutions for SG applications (when the targeted appliance are DERs, this can also be interpreted as different kinds of **DSM solution**) varying driven factors
 - Market-based: whole-sale spot market, ancillary service market, emerging markets (e.g. flexibility market)
 - Regulation-based control services: local vs. global
 - Multiple stakeholders: TSO, DSO, BRP, emerging entities
 - Diversified algorithms (transactive control, direct load control, model-based predictive control, coordinated voltage control, **distributed control**) for varying situations (normal vs. contingency) and architecture (distributed control vs. centralized control)
- Roll-out of measurements: AMI, Distribution Automation, Asset Management

---- available options of measuring devices and their aims (e.g. improved state estimation and load forecasting)

B1) Distribution planning objectives

Distribution planning objectives should contain general objectives regarding sustainable development and can be distributed on many levels to minimize the costs and power losses, improving the reliability of supply. A block diagram is presented in Fig. 2:

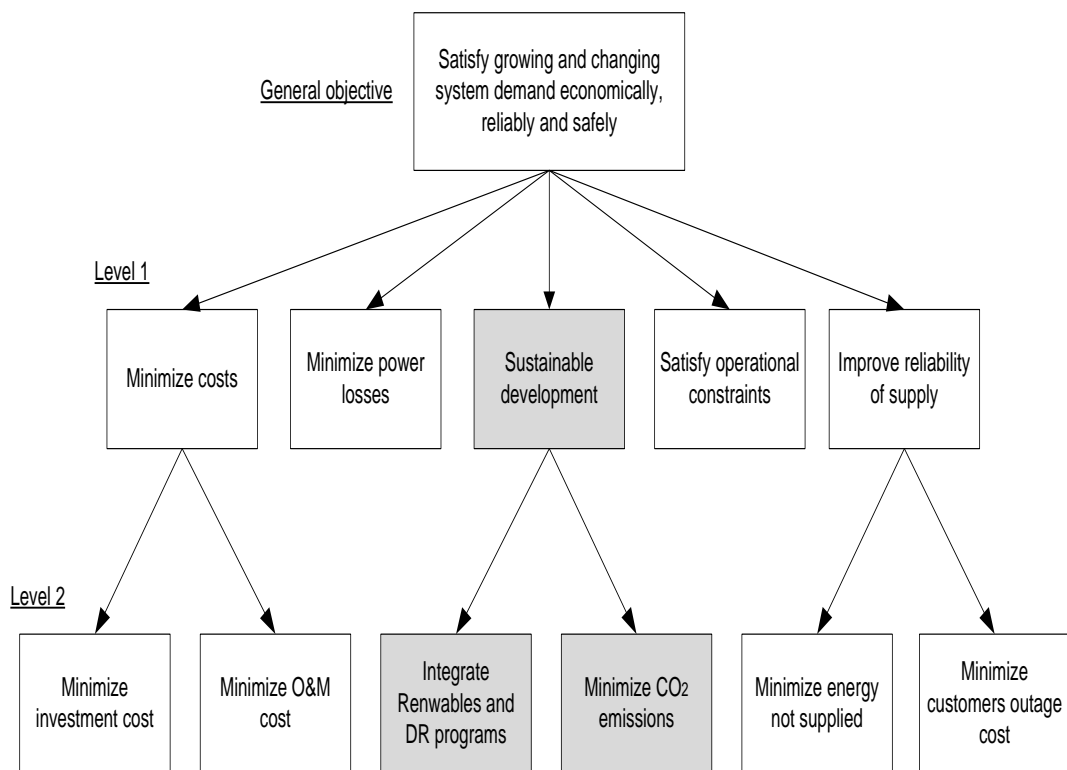


Fig. 2. Block diagram with general objectives and levels for distribution planning.

Common assumptions adopted in distribution planning can be summarizing as follows:

- Load forecast: passive load, DG taken as passive load, Concurrence factors are known, velandor correlations, temporal load profiles, peak load forecasting(annual, seasonal, and peak days), (new customer’s additions, and new uses of electricity), customer class identification
- Unidirectional load flow
- Distribution operation is out of the picture
- N-1 is the considered as the approach in contingency-based planning criteria
- Standards and planning guideline are the key material

The planning tools and functions are presented in the next table:

Table II: Planning tools and functions

Primary planning functions	Interface options
<ul style="list-style-type: none"> • Load flow (incl. OPF, and load profile time simulation) • Reliability assessment • Fault current analysis • Contingency analysis • Dynamic analysis • Transient analysis • Harmonic analysis • Protection coordination • Distributed generation modeling • Optimal capacitor placement and sizing • Distribution network optimization () 	<ul style="list-style-type: none"> • SCADA • Geographical information system (GIS) • Distribution management system (DMS) • Other tools (e.g., in-house developed tools, MATLAB)

B2) Recommendations for Smart Plan Tools: Analytical and Software Packages

---Near-term

- Metering data management and analysis: identify the present physical barriers (weakest point, capacity shortage, voltage unbalance.....)
- Reference network models (to improve DSO's understanding of its network and can use the reference models to test the integration impacts of SG and to formulate various scenarios)
- Screening tools for DG integration
- Improved forecasting: spatial and temporal load forecasting, better classification of loads and SG technologies, abstraction and estimation of the integration effects at different systems levels
- Representation of control as well as distribution operation in distribution planning:
 1. enable the better understanding of how SG technologies affects the current planning procedure and planning criteria
 2. ensure the accuracy of estimating the impacts of SG technologies on distribution network operation&planning
 3. allow the DSOs to evaluate the risk&return between using conventional planning alternatives and using SG-based planning options through detailed quantitative analysis
- Early-established strategies for worst-case scenario formulation and evaluation: For instance how to formulate worst case of PV integration in a given area while considering multiple factors (load condition, weather, other DGs, voltage rise, loading)

- Library of SG technologies (standardized technical models, flexibility characterization, economic information, associated uncertainties)
- Calculation model for deferred grid investments

--- Mid-term

- Well-established Framework for multi-scenario formulation and evaluation: SG-ready
- Cross-domain planning tools (modeling and simulation, cross-domain database)

--- Long-term

- Well-established planning procedure that is frequently-updated following the technology enlovement

As future research plans we will develop a research and education platform for a smart grid, including renewable energy conversion systems and control strategies, with energy storage devices and actively controlled loads. Afterwards we will implement the platform in a dedicated tool to be able to record limitations of the smart grid solutions, to identify critical load cases/voltage variations for defined scenarios and to design methodology for a future smart grid.

In conclusion, an extended set of activities are foreseen, at local, national and international level that are expected to significantly be enhanced in their results if the research team is going to be enlarged with Ph.D. students coordinated as a result of this Habilitation Thesis.

Part III: References

References for Chapter 2

- [2.1] Energynautics GmbH, Longen, Germany, 2010. Available: www.energynautics.com;
- [2.2] K. Richardson, D. Dahl-Jensen, J. Elmeskov, C. Hagem, J. Henningsen, J. A. Korstgård, N. B. Kristensen, P. E. Morthorst, J. E. Olesen, and M. Wier, "Green energy - the road to a Danish energy system without fossil fuels," Danish Commission on Climate Change Policy, 2010. Available: <http://greengrowthleaders.org/green-energy-the-road-to-a-danish-energy-system-without-fossil-fuels/>
- [2.3] S. Seme, G. Stumberg, and J. Vorsic, "Maximum efficiency trajectories of a two-axis sun tracking system determined considering tracking system consumption," IEEE Trans. On Power Electronics, vol. 26, no. 4, pp. 1280-1290, Apr. 2011.
- [2.4] W. De. Soto, S. A. Klein, and W. A. Beckman, "Improvement and validation of a model for photovoltaic array performance," ELSEVIER Solar Energy, vol. 80, pp. 78-88, 2006.
- [2.5] Y. Riffonneau, S. Bacha, S. Barruel and S. Ploix, "Optimal Power Management for grid connected PV Systems with batteries", IEEE Transaction on Sustainable Energy, vol. 2, no. 3, pp. 309-320, July 2011.
- [2.6] J. E. Skoplaki, A. G. Boudouvis and J. A. Polyvos, "A simple correlation for the operating temperature of photovoltaic modules of arbitrary mounting", ELSEVIER Solar Energy Materials, pp. 1393-1402, 2008.
- [2.7] A.D. Hansen, P. Sørensen, L.H. Hansen, H. Bindner, "Models for a Stand-Alone PV System", Risø National Laboratory, Roskilde, Risø-R-1219 (EN) / SEC-R-12, Dec. 2000.
- [2.8] H. Bidner, C. Ekman, O. Gehrke and F. Isleifsson, "Characterization of Vanadium Flow Battery", Riso-R-1753 Report, Roskilde, Denmark, October 2010.
- [2.9] L. Barote, R. Weissbach, R. Teodorescu, C. Marinescu, M. Cirstea, "Stand-Alone Wind System with Vanadium Redox Battery Energy Storage", IEEE, International Conference on Optimization of Electrical and Electronic Equipments, OPTIM'08, pp. 407-412, 22-24 May 2008, Brasov, Romania.
- [2.10] W. Wang, B. Ge, D. Bi and D. Sun, "Grid-Connected Wind Farm Power Control using VRB-based Energy Storage System", IEEE Transaction on Energy Conversion, pp.3772-3777, 2010.
- [2.11] H. Jiayi, J. Chuanwen, and X. Rong, "A review on distributed energy resources and MicroGrid", ELSEVIER Renewable & Sustainable Energy Reviews, vol. 12, pp. 2472-2483, 2008.
- [2.12] IEEE Standard for Interconnecting Distributed Resources with Electric Power Systems, IEEE Standard 1547-2008.
- [2.13] M. Jansen, R. Louie, M. E. Amoli and F. Sami, "Model and simulation of a 75 kW PV solar array", in Proc. 2010 IEEE PES Transmission and Distribution Conference and Exposition, pp. 1-5.
- [2.14] H. Liu, L. Jin, D. Le and A. A. Chowdhury, "Impact of high penetration of solar photovoltaic generation on power system small signal stability", in Proc. 2010 POWERCON, pp. 1-7.
- [2.15] <http://www.powerlab.dk/English/facilities/SysLab.aspx> ,
- [2.16] K. Murat, S. Mehmet, B. Yunus, D. Sedat, "Determining optimum tilt angles and orientations of photovoltaic panels in Saliurfa", IEEE Transaction on Renewable Energy, vol. 29, issue 8, pp. 1265-1275, 2004.
- [2.17] M. G. Villalva, J. R. Gazoli, E. R. Filho, "Comprehensive Approach to Modelling and Simulation of Photovoltaic Arrays", IEEE Transaction on Power Electronics, vol. 24, issue: 5, pp. 1198-1208, 2009.
- [2.18] <http://www.esrl.noaa.gov/gmd/grad/solcalc/>, Earth System Research Laboratory, National Oceanic & Atmospheric Administration, U.S. Department of Commerce.
- [2.19] D. Y. Goswami, *Principles of Solar Engineering*, (2nd ed.), Philadelphia: Taylor & Francis, 2000, p. 81-98.

- [2.20] S. Dezso, R. Teodorescu and P. Rodriguez, "PV panel model based on datasheet values", Proceedings of IEEE International Symposium on Industrial Electronics, Vigo, Spain, 2007, pp. 2392-2396.
- [2.21] Sera D.; Teodorescu R.; Rodriguez,P., "Photovoltaic module diagnostics by series resistance monitoring and temperature and rated power estimation", Proceedings of 34th Annual Conference of IEEE IECON- Industrial Electronics Conference, 2008.
- [2.22] D. Sera, "Real time modeling, diagnostics & optimized MPPT for residential PV systems", Ph. D. Thesis, Aalborg University, Denmark, 2009.
- [2.23] L. Mihet-Popa, C. Koch-Ciobotaru, F. Isleifsson and H. Bindner, „Development of tools for simulation systems in a distribution network and validated by measurements”, the 13th IEEE International Conference on Optimisation of Electrical and Electronic Equipment, OPTIM 2012, May 24-26, Brasov-Romania, pp. 1022-1031.**
- [2.24] L. Mihet-Popa, C. Koch-Ciobotaru, F. Isleifsson and H. Bindner, „Simulation Model developed for a Small-Scale PV-System in a Distribution Network”, Proceedings of the 8th IEEE International Symposium on Applied Computational Intelligence and Informatics-SACI 2012, Timisoara-Romania, May 24-26, pp. 257-261, ISBN: 1-4244-1234-X.**
- [2.25] L. Mihet-Popa, C. Koch-Ciobotaru, F. Isleifsson and H. Bindner, „Development of tools for DER Components in a distribution network”, the 20th IEEE International Conference on Electrical Machines, ICEM 2012, September 2-5, Marseille-France, pp. 1022-1031, ISSN 1842-0133.**
- [2.26] Y. Zong, L. Mihet-Popa, D. Kullman, A. Thavlov, O. Gehrke and H. Bindner, „Model Predictive Controller for Active Demand Side Management with PV Self-Consumption in an Intelligent Building”, IEEE PES Innovative Smart Grid Technologies Europe, Berlin-Germany, October 14-17.**
- [2.27] J.A. Gow and C.D. Manning, "Development of a photovoltaic array model for use in power-electronics simulation studies", *IEE Proceedings of Electronics Power Applications*, Vol. 146, No. 2, March 1999.
- [2.28] J.A. Gow and C.D. Manning, "Development of a model for Photovoltaic arrays suitable for use in simulation studies of solar energy conversion systems", *IEE Proceedings of Power Electronics and Variable Speed Drives*, 23-25 September 1996, No. 429, pp. 69-74.
- [2.29] DiGSILENT PowerFactory, User's Manual and Tutorial-Version 14.1, Gomaringen-Germany, November 2011.
- [2.30] Schuco S 165-SPU, Data sheet and technical data of the Photovoltaic Module.
- [2.31] PV Inverters: SUNNY TRIPOWER 10000TL Installation Manual, SMA Solar Technology AG.
- [2.32] C. Blanc and A. Rufer, "Optimization of the Operating Point of a Vanadium Redox Flow Battery", *Proceedings of IEEE Energy Conversion Congress and Exposition-ECCE'09*, San Jose, CA, 20-24 September, 2009.
- [2.33] C. Blanc and A. Rufer, "Multiphysics and Energetic Modeling of a Vanadium Redox Flow Battery", *Proceedings of IEEE International Conference on Sustainable Energy Technologies*, 24-27 November, 2008, pp. 696-701.
- [2.34] A. Gabash and P. Li, "Evaluation of Reactive Power Capability by Optimal Control of Wind-Vanadium Redox Battery Stations in Electricity Market", *International Conference on Renewable Energies and Power Quality-ICREPQ'11*, Las Palmas de Gran Canarias-Spain, 13-15 th April, 2011.
- [2.35] Global Smart Grid Federation, "Intelligent PV Integration into the Local Grid", January 23, 2012, www.globalsmartgridfederation.org/prod/news ;
- [2.36] A. Thavlov, "Dynamic Optimization of Power Consumption", Chapter 7- Master thesis submitted at DTU, Lyngby-Dk, 2008.
- [2.37] O. Gehrke, F.R. Isleifsson and C. Koch-Ciobotaru, "Priority-based local voltage control in distribution systems with high PV penetration", Solar integration workshop, Lisbon, November 2012.
- [2.38] O. Gehrke, A. Kosek, G. Tommaso-Costanzo, D. Kullmann and F.R. Isleifsson, "Generic interfaces for system services from heterogeneous DER units", the 5th Conference on integration of DER, Berlin, December 2012.
- [2.39] * * International Wind Energy Development, "World Market Update 1999". *BTM Consults Aps. Ringkobing, Denmark 2000 ISBN 87-987788-0-3.*

- [2.40] Anca D. Hansen, Poul Sorensen, L.Janosi and J. Bech, "Wind farm modelling for power quality". *IECON'01: The 27th Annual Conference of the IEEE Industrial Electronics Society*, vol. 3, pp.1959-1964.
- [2.41] * * "Guided Tour on Wind Energy", *Danish Wind Turbine Manufacturers Association, Denmark*.
- [2.42] E. Muljadi, C.P. Butterfield, "Pitch controlled variable-speed wind turbine generator", *Industry Applications Conference, 1999. IAS Annual Meeting. Conference Record*, Vol. 1, pp. 323 – 330.
- [2.43] S.A. Papathanassiou, M.P.Papadopoulos, "Dynamic Behaviour of Variable Speed Wind Turbines under Stochastic Wind", *IEEE Trans. on Energy Conversion*, vol. 14, no.4 1999, pp. 1617-1623.
- [2.44] A. Miller, E. Muljadi, D.S. Zinger, "A Variable Speed Wind Turbine Control", *IEEE Trans. on Energy Conversion*, vol.12, no. 2, June 1997, pp. 181-186.
- [2.45] * * DiGSILENT Power Factory user manuals, *DiGSILENT GmbH, Germany*.
- [2.46] G. Seguier, *Power Electronic Converters-AC/DC Conversion*, New York; McGraw-Hill, 1986.
- [2.47] L.H. Hansen, P. Sorensen, U.S. Paulsen, "Variable Speed Wind Turbine using Full Conversion", *Proc. of NORpie; 2000, Aalborg, Denmark*, pp. 115-119, 2000.
- [2.48] P.A.C. Rosas, P. Sorensen and H. Bindner, "Fast wind modelling of wind turbines". *Special topic conference. Wind power for the 21st Century*. Kassel, Germany, September 2000.
- [2.49] T. Thiringer, "Grid-Friendly Connecting of Constant-Speed Wind Turbines Using External Resistors", *IEEE Trans. on Energy Conversion*, vol. 17, no. 4, pp. 537-542. December, 2002.
- [2.50] F. Blaabjerg and Z. Chen, "Power Electronics as an enabling technology for renewable energy integration", *Journal of Power Electronics*, vol. 3. no. 2, April 2003, pp. 81-89.
- [2.51] Lucian Mihet-Popa, F. Blaabjerg and I. Boldea, "Wind Turbine Generator Modeling and Simulation where Rotational Speed is the Controlled Variable", IEEE-IAS Transactions on Energy Conversion, January / February 2004, Vol. 40, No. 1, pp. 3-10, ISSN: 0093-9994, Accession number:WOS: 000189128300001, (ISI Journal - ISI Web of Knowledge, Impact Factor 2.578, 47 Citations in ISI Web of Knowledge, 145 in Google Scholar).**
- [2.52] Lucian Mihet-Popa, O. Proştean and I. Szeidert, „The soft-starters modeling, simulations and control implementation for 2 MW constant-speed wind turbines”, The International Review of Electrical Engineering – IREE, Vol. 3, No. 1, January-February 2008, pp. 129-135, ISSN: 1827-6660, Accession number: WOS: 000264607500016 (ISI Journal, ISI Web of Knowledge, Impact factor: 1.4, 1 citation).**
- [2.53] Lucian Mihet-Popa and V. Groza, „Modeling and simulations of a 12 MW wind farm”, Journal of Advances in Electrical and Computer Engineering, Vol. 10, No. 2, 2010, pp. 141-144, ISSN 1582-7445, www.aece.ro, Accession number: WOS: 000280312600025 (ISI Journal, ISI Web of Knowledge-Impact Factor 0.7).**
- [2.54] Lucian Mihet-Popa, "Wind Turbines using Induction Generators connected to the grid", (monography) - 310 pg.), POLITEHNICA University of Timisoara, November 2007, ISBN 978-973-625-533-5.**
- [2.55] Lucian MIHET-POPA, „Modeling and simulation of a 12 MW wind farm",, Book Chapter, ISBN: 978-953-307-156-5, InTech 2011, indexed in IET Scopus, Google Scholar**

References for Chapter 3

- [3.1] Siegfried Heier, "Wind energy conversion systems", book, John Wiley & Sons Inc., New York, 1998.
- [3.2] L.H. Hansen, L. Helle, F. Blaabjerg, E. Ritchie, S. Munk-Nielsen, H. Bidner, P. Sorensen and B. Bak-Jensen, "Conceptual Survey of Generators and Power Electronics for Wind Turbines", Riso-R-1205 (EN), December 2001.
- [3.3] H. M. Hansen, A.D. Hansen, T.J. Larsen, S. Oye, P. Sorensen and P. Fuglsang, "Control design for a pitch-regulated variable speed wind turbine", Riso National Laboratory-Riso-R-1500 (EN), Roskilde-Denmark, January 2005.
- [3.4] Lucian Mihet-Popa, "Wind Turbines using Induction Generators connected to the grid", Ph. D. Thesis, POLITEHNICA University of Timisoara, October 2003.
- [3.5] Saifur Rahman, "Green Power. What is it and where can we find it?", IEEE power & energy magazine, January/February 2003, pp. 30-37.
- [3.6] A. D. Hansen, C. Jauch, P. Sorensen, F. Iov and F. Blaabjerg, "Dynamic wind turbine models in power system simulation tool DigSILENT", Riso-R, 1400 (EN), Riso National Laboratory, December 2003.
- [3.7] H. Polinder, M.R. Dubois and J.G. Sloopweg, "Generator systems for wind turbines", PCIM 2003, Nuremberg, Germany, 20-22 May, pp.
- [3.8] L. Mihet-Popa and J.M. Pacas, "Active stall constant speed wind turbine during transient grid fault events and sudden changes in wind speed", PCIM 2005, Nuremberg-Germany, 7-9 June, pp. 646-652.**
- [3.9] D. Schreiber, "Applied Designs of Variable Speed Wind Turbines and New Approaches", PCIM 2002, Nuremberg, Germany.
- [3.10] L. Mihet-Popa, F. Blaabjerg and I. Boldea, "Wind Turbine Generator Modeling and Simulation where Rotational Speed is the Controlled Variable", IEEE-IAS Transactions on Energy Conversion, January / February 2004, Vol. 40, No. 1, pp. 3-10.**
- [3.11] L. Mihet-Popa, F. Blaabjerg and I. Boldea, "Simulation of Wind Generator Systems for the Power Grid", Record of OPTIM 2002, Poiana Brasov – Romania, 16 – 18 May, Vol. 2, pp. 423-428.
- [12] *** www.windpower.org, Danish Wind Industry Associations, Guided Tour on Wind Energy.
- [3.13] S. Muller, M. Deicke and Rik W. De Doncker, "Doubly Fed Induction Generator Systems for Wind Turbines", IEEE Industry Applications Magazine, May-June 2002, pp. 26-33.
- [3.14] R. Pena, J.C. Clare, G.M. Asher, "Doubly Fed Induction Generator using Back-to-Back PWM Converters and its Application to Variable Speed Wind Energy Generation", 1996, IEE Proceedings on Electrical Power Applications, Vol. 143, No. 3, pp. 231-241.
- [3.15] Hirofumi Akagi and Hikaru Sato, "Control and Performance of a Doubly-Fed Induction Machine Intended for a Flywheel Energy Storage System", IEEE Transaction on Power Electronics, Vol. 17, No. 1, January 2002, pp. 109-116.
- [3.16] Rajib Datta and V.T. Ranganathan, "Direct Power Control of Grid-Connected Wound Rotor Induction Machine without Rotor Position Sensors", IEEE Transactions on Power Electronics, Vol. 16, No. 3, May 2001, pp. 390-399.
- [3.17] D.S. Zinger, E. Muljadi, "Annualized wind energy improvement using variable speeds", Industrial & Commercial Power Systems technical Conference, 1997. Conference Records, Papers presented at the 1997 Annual Meeting, IEEE 1997, 11-16 May 1997, pp. 80-83.
- [3.18] "Smart Grid i Danmark", joint report by energinet.dk and Dansk Energi, September 2010.
- [3.19] J. Kumagai, "The Smartest, Greenest Grid-What a little Danish island is showing the world about the future of energy", IEEE Spectrum, May 2013, pp. 38-43.
- [3.20] DEFU recommendations no. 16/2010.
- [3.21] European Standard-EN 50160.

- [3.22] DlgSILENT PowerFactory, Digsilent gmbh, November 2012.
- [3.23] NEPLAN, Tutorial manual, 2011.
- [3.24][Online].Available:http://www.scb.se/Pages/Product_____10616.aspx?Produktkod=TK1101&displaypublications=true;
- [3.25] C. Koch-Ciobotaru., L. Mihet-Popa, F. Isleifsson and H. Bindner, „Simulation model developed for a small-scale PV-System in a distribution network”, in Proc. of the 7th IEEE SACI Conf., 2012, Timisoara-Romania, May 24-26, pp. 257-261.**
- [3.26] L. Mihet-Popa, C. Koch-Ciobotaru, F. Isleifsson and H. Bindner, „Development of tools for DER Components in a distribution network”, in Proc. of ICEM Conf., September 2-5, 2012, Marseille-France, pp. 1022-1031.**
- [3.27] Y. Zong, L. Mihet-Popa, D. Kullman, A. Thavlov, O. Gehrke and H. Bindner, „Model Predictive Controller for Active Demand Side Management with PV Self-Consumption in an Intelligent Building”, IEEE PES Innovative Smart Grid Technologies Europe, Berlin-Germany, October 14-17.**
- [3.28] P. Kundur, Power system stability and control, McGraw-Hill, New York, 1994.
- [3.29] A. Thavlov, “Dynamic Optimization of Power Consumption”, Chapter 7- Master thesis submitted at DTU, Lyngby-Dk, 2008.
- [3.30] Global Smart Grid Federation, “Intelligent PV Integration into the Local Grid”, January 23, 2012, www.globalsmartgridfederation.org/prod/news;
- [3.31] M. Chen, G. A. Rincon-Mora, “Accurate electrical battery model capable of predicting runtime and I-V performance”, IEEE Transactions on Energy Conversion, Vol. 21, No. 2, June 2006, pp. 504-511.
- [3.32] S. Barsali, M. Ceraolo, “Dynamic models of lead-acid batteries: implementation issues”, IEEE Transactions on Energy Conversion, Vol. 17, No. 1, March 2002, pp. 16-23.
- [3.33] F. Marra, C. Traholt, E. Larsen and Q. Wu, “Average behavior of battery electric vehicles for distributed energy studies”, IEEE PES-ISGT 2010, Gothenburg, Sweden.
- [3.34] T. Huria, M. Ceraolo, J. Gazzarri and R. Jackey, “High fidelity electrical model with thermal dependence for characterization and simulation of high power lithium battery cell”, in Proc. of IEEE International Conference of Electrical Vehicles (IEVC), 4-8 March 2012, pp. 1-8.
- [3.35] L. Mihet-Popa and H. Bindner, „Simulation models developed for voltage control in a distribution network using energy storage systems for PV penetration”, in Proc. of the 39th Annual Conference of the IEEE Industrial Electronics Society-IECON’13, November 10-13, Vienna, Austria, pp. 7487-7492, ISSN: 1553-572X, ISBN: 978-1-4799-0224-8.**
- [3.36] Lucian Mihet-Popa, O. Proştean and I. Szeidert, „The soft-starters modeling, simulations and control implementation for 2 MW constant-speed wind turbines”, The International Review of Electrical Engineering – IREE, Vol. 3, No. 1, January-February 2008, pp. 129-135, ISSN: 1827-6660, Accession number: WOS: 000264607500016 (ISI Journal, ISI Web of Knowledge, Impact factor: 1.4, 1 citation).**
- [3.37] Lucian Mihet-Popa and Ion Boldea, „Dynamics of control strategies for wind turbine applications”, the 10th International Conference on Optimisation of Electrical and Electronic Equipment, OPTIM 2006, May 18-19, Poiana Brasov, Vol. 2, pp. 199-206, WOS: 000256418400033 (ISI Proceedings, ISI Web of Knowledge).**
- [3.38] L. Mihet-Popa, V. Groza, O. Proştean and I. Szeidert, „Modeling and design of a grid connection control mode for a small variable-speed wind turbine system”, IEEE I2MTC-International instrumentation & measurement technology conference, May 12-15, 2008, Vancouver Island-Canada, pp. 288-293, ISBN:1-4244-1541-1, ISSN: 1091-5281, IEEE Catalog Number: 08CH37941C, Accession number: WOS: 000261512100056; (ISI Proceedings, ISI Web of Knowledge).**
- [3.39] Lucian Mihet-Popa and Ion Boldea, “Variable speed wind turbines using induction generator connected to the grid”, Journal of Electrical Engineering –www.jee.ro, Vol. 2, July 2006, ISSN 1582-4594 (Inspec, SCOPUS, Google Scholar);**

- [3.40] Lucian Mihet-Popa and Ion Boldea, "Control strategies for large wind turbine applications", *Journal of Electrical Engineering-www.jee.ro*, Vol. 7, Edition 3rd, October issue 2007, ISSN 1582-4594 (Inspecc, SCOPUS);
- [3.41] L. Mihet-Popa, „Grid Connection Control Mode of a Small Variable-Speed Wind Turbine”, *Buletinul Științific al Universității POLITEHNICA din Timișoara (Scientific bulletin of POLITEHNICA University of Timișoara, Romania-Transactions on automatic control and computer science)*, România, Vol. 52 (66), No. 3, Decembrie 2007, ISSN 1224-600X; (Google Scholar, B+-CNCSIS).
- [3.42] L. Mihet-Popa, V. Groza, „Dynamic Modeling, Simulation and Control Strategies for 2 MW Wind Generating Systems”, *International Review of Modelling and Simulations-IREMOS*, Vol. 3, No. 6, December, 2010, pp. 1410-1418, ISSN: 1974-9821 (Cambridge Scientific Abstract, Elsevier Bibliographic Database SCOPUS, Index Copernicus (Journal Master List): Impact Factor 6.51);
- [3.43] L. Mihet-Popa, V. Groza, „Static and Dynamic Stability Analysis of Distributed Energy Resources Components with Storage Devices and Loads for Smart Grids”, *International Review of Modelling and Simulations-IREMOS*, Vol. 4, No. 6, December, 2011, pp. 1410-1418, ISSN: 1974-9821 (Cambridge Scientific Abstract, Elsevier Bibliographic Database SCOPUS, Index Copernicus (Journal Master List): Impact Factor 6.51);
- [3.44] Lucian Mihet-Popa and Ion Boldea, "Variable speed wind turbines using induction generator connected to the grid: digital simulation versus test results", *IEEE – the 9th International Conference on Optimization of Electrical and Electronic Equipment, OPTIM 2004*, May 20-21, Poiana Brașov, Vol. 2, pp. 286-294, WOS: 000255388800047 (ISI Proceedings, ISI Web of Knowledge);
- [3.45] Lucian Mihet-Popa and Ion Boldea, "A Laboratory System for Comprehensive Investigation of Wind Generators", Paper published in *Polish Journal – Przegląd Elektrotechniczny (SEP)*, R 80 Vol. 2004, No. 3, pp. 200-203, PL ISSN 0033-2097 (Scopus, Google Scholar).
- [3.46] Lucian Mihet-Popa, O. Prostean and I. Szeidert, „An experimental laboratory system for monitoring and detection of electrical drives systems with induction machines”, *International Scientific Journal Facta Universitatis – NIS, series Electronics and Energetics*, Aprilie 2008, Vol. 21, No. 1, pp. 45-54, YU ISSN 0353-3670 (Scopus, Google Scholar);
- [3.47] L. Mihet-Popa, V. Groza, „Indicators and signal processing techniques for detection of rotor faults in induction machines”, *International Review of Modelling and Simulations-IREMOS*, Vol. 3, No. 4, August, 2010, pp. 538-545, ISSN: 1974-9821 (Cambridge Scientific Abstract, Elsevier Bibliographic Database SCOPUS, Index Copernicus (Journal Master List): Impact Factor 6.51);
- [3.48] Lucian Mihet-Popa, Birgitte Bak-Jensen, Ewen Ritchie and Ion Boldea, "Condition Monitoring of Wind Generators", *Record of IEEE-IAS 38th Annual Meeting, Salt Lake City-USA, 2003*, 12-16 October, Vol. 3, pp. 1839-1846, ISBN: 0-7803-7883-0, Accession Number: WOS:7798516 (ISI Proceedings, INSPEC, IEEE Explore), 3 Citations in ISI Web of Knowledge, 70 in Google Scholar.
- [3.49] Lucian Mihet-Popa, "Wind Turbines using Induction Generators connected to the grid", (monography) - 310 pg.), POLITEHNICA University of Timisoara, November 2007, ISBN 978-973-625-533-5.
- [3.50] Lucian MIHET-POPA, „Modeling and simulation of a 12 MW wind farm", Book Chapter, ISBN: 978-953-307-156-5, InTech 2011, indexed in IET Scopus, Google Scholar

References for Chapter 4

- [4.1] K. Richardson, D. Dahl-Jensen, J. Elmeskov, C. Hagem, J. Henningsen, J. A. Korstgård, N. B. Kristensen, P. E. Morthorst, J. E. Olesen, and M. Wier, "Green energy - the road to a Danish energy system without fossil fuels," Danish Commission on Climate Change Policy, 2010.
- [4.2] L. Dow, M. Marshall, Le Xu, J. R. Agüero and H. L. Willis, "A novel approach for evaluating the impact of electric vehicles on the power distribution system", IEEE PES Smart Grids 2012.
- [4.3] X. Wu, M. Toshihiro and F. Hisashi, "Three-phase high frequency transformer isolated AC to DC converter for EV battery quick charging", in Proc. of IEEE-ECCE Conf., 2012.
- [4.4] P. Nørgård, O. M. Forero Camacho and N. Rao, "Electric vehicles in a distributed and integrated market using sustainable energy and open network", Riso-R-1753 Report, Roskilde, Denmark, April 2012.
- [4.5] [Online]. Available: <http://www.edison-net.dk/>, A. Foosnæs, "Electric vehicle technology", EDISON WP1.1 report, 2010.
- [4.6] S.S. Lee, H.T. Kim, S.J. Hu, W.W. Cai and J.A. Abell, "Joining technologies for automotive lithium-ion battery manufacturing-A review", International Manufacturing Science and Engineering Conference, vol. 1, pp. 541-549, 2010.
- [4.7] S. Xin, Y.G. Guo, L.J. Wan, "Nanocarbon networks for advanced rechargeable lithium batteries", Accounts for chemical research journal, Vol. 45, Issue 10, pp. 1759-1769, 2012.
- [4.8] S. Sundararagavan, E. Baker, "Evaluating energy storage technologies for wind power integration", Solar Energy Journal, vol. 86, issue 9, pp. 2707-2717, 2012.
- [4.9] D.G. Marinescu, I. Tabacu, F. Serban, N. Viorel, S. Tabacu, I. Vieru, "Plug-in hybrid vehicle with a lithium iron phosphate battery traction type", Lecture notes in Electrical Engineering Journal, vol. 191, issue 3, pp. 449-461, 2013.
- [4.10] N. Rao, "Interplay between EV battery and Power Grid", EV battery forum, Barcelona, Spain, May 2012.
- [4.11] [Online]. Available: <http://www.trafikstyrelsen.dk/DA/Groen-Transport/Elbiler/~media/7700C7669AB44627BCDC7CDE075ADBE3.ashx>
- [4.12] S. Sista and A. Sista, "Intelligent BMS solution using AI prognostic SPA", Lecture notes in electrical engineering journal, vol. 192, issue: 4, pp. 755-764, 2013.
- [4.13] C. Wu, J. Wan and G. Zhao, "Addressing human factors in electric vehicle system design: building an integrated computational human-electric vehicle framework", ELSEVIER Journal of Power Sources, vol. 214, pp. 319-329, 2012.
- [4.14] X. Yan, W. Li, J. Gu, X. Xiao and W. Li, "A simulated system of battery management system to test electric vehicles charger", in Proc. 2012 IEEE IEVC Conf., pp. 183-197.
- [4.15] H. He, R. Xiong, H. Guo and S. Li, "Comparison study on the battery models used for the energy management of batteries in electric vehicles", ELSEVIER Energy Conversion and Management Journal, Vol. 64, pp. 113-121, 2012.
- [4.16] David Andrea, Battery Management Systems for Large Lithium-Ion Battery Packs, ARTECH HOUSE book, London, 2010, ISBN-13 978-1-60807-104-3.
- [4.17] International Electrotechnical Commission IEC 61851-1 Standard, "Electric vehicle conductive charging system", 2010.
- [4.18] M. Kenichi, "Information and communication technology and electric vehicles-Paving the way towards a smart community", IEICE Transaction on Communication system for electric vehicle charging journal, Vol. E95B, Issue 6, pp. 1902-1910, 2012.
- [4.19] X. Fei, L. Xianzhang, Z. Yebiao, L. Hongchao and G. Ciurei, "A complex network-based method to evaluate smart charging and swapping network for electrical vehicles", Power system technology journal, vol. 36. Issue 9, pp. 20-24, 2012.
- [4.20] L. Yujin, K. Hak-Man, K. Sanggil and K. Tai-Hoon, "Vehicle-to-grid communication system for EV charging", Integrated computer-aided engineering journal, vol. 19, issue 1, pp. 57-65, 2012.

- [4.21] E. Sortomme and M.A. El-Sharkawi, "Optimal scheduling of vehicle-to-grid energy and ancillary services", IEEE Transactions on Smart Grid, Vol. 3, No. 1, March 2012.
- [4.22] BYD Battery parameters, BYD Company Limited FV 50 cells
- [4.23] [Online]. Available at: http://www.kokam.com/product/product_pdf, Technical specifications of Kokam battery.
- [4.24] R.A. Verzijlberg, Z. Lukszo and M.D. Ilic, "Comparing different EV charging strategies in liberalized power systems", in Proc. of the 9th International Conference on the European Energy Market (EEM'12), pp. 625-670, 2012.
- [4.25] J. Li, J.K. Barillas, C. Guenther and M.A. Danzer, "A comparative study of state of charge estimation algorithms for LiFePO₄ batteries used in electric vehicles", Journal of Power Sources, pp. 244-250, 2013.
- [4.26] G. Glanzer, T. Sivaraman, J.I. Buffalo, M. Kohl and H. Berger, "Cost-efficient integration of electric vehicles with the power grid by means of smart charging strategies and integrated on-board chargers", in Proc. of the International Conf. on Environment and Electrical Engineering (EEEIC'12), 8-11 May, Rome, 2012.
- [4.27] P. Bauer, N. Stembridge, J. Doppler and P. Kumar, "Battery Modeling and Fast Charging of EV", in Proc. of the 14th International Power Electronics and Motion Control Conference (EPE-PEMC 2010), pp. 39-45, 2010.
- [4.28] Gregory L. Plett, "Extended Kalman filtering for battery management systems of LiPB-based HEV battery packs. Part 2: Modeling and identification", Journal of Power Sources, pp. 262-276, 2004.
- [4.29] L. Mihet-Popa, O.M.F. Camacho and P.B. Nørgård, „Charging and discharging tests for obtaining an accurate dynamic electro-thermal model of high power lithium-ion pack system for hybrid and EV applications”, in Proc. of the IEEE PES Power Tech Conference, Grenoble, June 16-20, 2013.**
- [4.30] AKTA, "The road pricing experiment in Copenhagen", DTU Technical Report, Roskilde, Denmark, 2003.
- [4.31] H. Jiayi, J. Chuanwen and X. Rong, "A review on distributed energy resources and MicroGrid," ELSEVIER, Renewable & Sustainable Energy Reviews, vol. 12, pp. 2472–2483, 2008.
- [4.32] J. M. Guerrero, J.C. Vasquez, J. Matas, J.L. Sosa and L.G. de Vicuna, "Parallel Operation of Uninterruptible Power Supply Systems in MicroGrids", IEEE Transactions on Industrial Electronics, vol. 55, no. 8, August 2008, pp. 2845–2856.
- [4.33] W. Pan, W. Gao and E. Muljadi, "The Dynamic Performance and Effect of Hybrid Renewable Power System with Diesel/Wind/PV/Battery", IEEE Transaction on Industry Applications, vol. III, 2010, pp. 1–6.
- [4.34] B. Sedaghat, A. Jalilvand and R. Noroozian, "Design of a Predictive Control Strategy for Integration of Stand-Alone Wind/Diesel System", Proceedings of IEEE International Conference on Power and Energy, November 29-December 1, Kuala Lumpur, Malaysia, 2010.
- [4.35] IEEE Standard for Interconnecting Distributed Resources with Electric Power Systems, IEEE Std. 1547, 2008.
- [36] IEEE Guide for Synchronous Generator Modeling Practices and Applications in Power System Stability Analysis, IEEE Std 1110-2002.
- [4.37] B. Kroposki, T. Basso and R. DeBlasio, "Interconnecting Testing of Distributed Resources", IEEE 1547-2003, Standard for Distributed Resources Interconnected with Electric Power System, July 2003.
- [4.38] H. Bidner, C. Ekman, O. Gehrke and F. Isleifsson, "Characterization of Vanadium Flow Battery", Riso-R-1753 Report, Roskilde, Denmark, October 2010.
- [4.39] I. Boldea, "The Electric Generators Handbook" CRC Press, USA 2006, ISBN 084931481X.
- [4.40] H. Bindner, P.A.C. Rosas, R. Teodorescu and F. Blaabjerg, "Stand-alone version of the 11 kW Gaia wind turbine", Riso-R-1480, Roskilde-Denmark, September 2004.

- [4.41] N. Gyawali, Y. Ohsawa and O. Yamamoto, "Power Dispatching from Cage Induction Generator Based Wind Power System with Integrated Smart Energy Storage", IEEJ Transactions on Electrical and Electronic Engineering, vol. 6, pp. 134-143, 2011.
- [4.42] A. Karthikeyan, C. Nagamani, G. Saravana Ilango and A. Sreenivasulu, "Hybrid open-loop excitation system for wind turbine-driven stand-alone induction generator", IET Renewable Power Generation Journal, vol. 5, iss. 2, pp. 184-193, 2011.
- [4.43] L. Barote, R. Weissbach, R. Teodorescu, C. Marinescu, M. Cirstea, "Stand-Alone Wind System with Vanadium Redox Battery Energy Storage", IEEE, International Conference on Optimization of Electrical and Electronic Equipments, OPTIM'08, pp. 407-412, 22-24 May 2008, Brasov, Romania.
- [4.44] I. Bae and J. Kim, "Reliability evaluation of customers in a microgrid", IEEE Transaction on Power Systems, vol. 23, no. 3, pp. 1416-1422, August 2008.
- [4.45] A. Tsikalakis and N. Hatziargyriou, "Centralized control for optimizing microgrids operation", IEEE Transaction on Energy Conversions, vol. 23, no. 1, pp. 241-248, March 2008.
- [4.45] L. Mihet-Popa, O. M. F. Camacho, P. B. Nørgård and N. Rao „Electrical Vehicle Batteries Testing in a Distribution Network using Sustainable Energy”, IEEE Transactions on Smart Grid, Special Issue on „Energy Storage Applications for Smart Grid”, Vol. 5, Issue 2, March 2014, pp. 1033-1042, ISSN 1949-3053, Digital Object Identifier: 10.1109/TSG.2014.2299064, Accession Number: WOS:000331985300052 (ISI Journal, ISI Web of Knowledge).**
- [4.46] L. Mihet-Popa, O. M. F. Camacho, „Fast Charging and Smart Charging Tests for Electric Vehicles Batteries using Renewable Energy”, Oil & Gas Science and Technology – Rev. IFP Energies nouvelles (OGST Journal), March 2014, DOI: 10.2516/ogst/2014001, ISSN (Print Edition): 1294-4475, ISSN (Electronic Edition): 1953-8189 (ISI Journal, ISI Web of Knowledge, Impact factor: 1.258)
- [4.47] L. Mihet-Popa, V. Groza, „Static and Dynamic Stability Analysis of Distributed Energy Resources Components with Storage Devices and Loads for Smart Grids”, International Review of Modelling and Simulations-IREMOS, Vol. 4, No. 6, December, 2011, pp. 1410-1418, ISSN: 1974-9821 (Cambridge Scientific Abstract, Elsevier Bibliographic Database SCOPUS, Index Copernicus (Journal Master List): Impact Factor 6.51);
- [4.48] L. Mihet-Popa, F. Isleifsson and V. Groza, „Experimental Testing for Stability Analysis of Distributed Energy Resources Components with Storage Devices and Loads”, IEEE I2MTC-International instrumentation & measurement technology conference, May 12-15, 2012, Gratz-Austria, pp. 588-593, ISBN:978-1-4577-1771-0, Accession number: WOS: 000309449100113 (ISI Proceedings, ISI Web of Knowledge);

References for Chapter 5

- [5.1] "Smart Grid i Danmark", joint report by energinet.dk and Dansk Energi, September 2010.
- [5.2] J. Kumagai, "The Smartest, Greenest Grid-What a little Danish island is showing the world about the future of energy", IEEE Spectrum, May 2013, pp. 38-43.
- [5.3] DEFU recommendations no. 16/2010.
- [5.4] European Standard-EN 50160.
- [5.5] DIgSILENT PowerFactory, Digsilent gmbh, November 2012.
- [5.6] NEPLAN, Tutorial manual, 2011.
- [5.7][Online].Available:http://www.scb.se/Pages/Product____10616.aspx?Produktkod=TK1101&displaypublications=true;
- [5.8] C. Koch-Ciobotaru., L. Mihet-Popa, F. Isleifsson and H. Bindner, „Simulation model developed for a small-scale PV-System in a distribution network”, in Proc. of the 7th IEEE SACI Conf., 2012, Timisoara-Romania, May 24-26, pp. 257-261.**
- [5.9] L. Mihet-Popa, C. Koch-Ciobotaru, F. Isleifsson and H. Bindner, „Development of tools for DER Components in a distribution network”, in Proc. of ICEM Conf., September 2-5, 2012, Marseille-France, pp. 1022-1031.**
- [5.10] Y. Zong, L. Mihet-Popa, D. Kullman, A. Thavlov, O. Gehrke and H. Bindner, „Model Predictive Controller for Active Demand Side Management with PV Self-Consumption in an Intelligent Building”, IEEE PES Innovative Smart Grid Technologies Europe, Berlin-Germany, October 14-17.**
- [5.11] P. Kundur, Power system stability and control, McGraw-Hill, New York, 1994.
- [5.12] A. Thavlov, "Dynamic Optimization of Power Consumption", Chapter 7- Master thesis submitted at DTU, Lyngby-Dk, 2008.
- [5.13] Global Smart Grid Federation, "Intelligent PV Integration into the Local Grid", January 23, 2012, www.globalsmartgridfederation.org/prod/news;
- [5.14] M. Chen, G. A. Rincon-Mora, "Accurate electrical battery model capable of predicting runtime and I-V performance", IEEE Transactions on Energy Conversion, Vol. 21, No. 2, June 2006, pp. 504-511.
- [5.15] S. Barsali, M. Ceraolo, "Dynamic models of lead-acid batteries: implementation issues", IEEE Transactions on Energy Conversion, Vol. 17, No. 1, March 2002, pp. 16-23.
- [5.16] F. Marra, C. Traholt, E. Larsen and Q. Wu, "Average behavior of battery electric vehicles for distributed energy studies", IEEE PES-ISGT 2010, Gothenburg, Sweden.
- [5.17] T. Huria, M. Ceraolo, J. Gazzarri and R. Jackey, "High fidelity electrical model with thermal dependence for characterization and simulation of high power lithium battery cell", in Proc. of IEEE International Conference of Electrical Vehicles (IEVC), 4-8 March 2012, pp. 1-8.
- [5.18] L. Mihet-Popa, X. Han, H. Bindner, J. Pihl-Andersen and J. Mehmedalic „Development and Modeling of different scenarios for a Smart Distribution Grid”, in Proc. of the 8th International Symposium on Applied Computational Intelligence and Informatics-IEEE SACI 2013, Timisoara-Romania, May 23-25, pp. 257-261, ISBN: 978-1-4673-6400-3, WOS:000333188100079 (ISI Proceedings, ISI Web of Knowledge).**
- [5.19] L. Mihet-Popa, X. Han, H. Bindner, J. Pihl-Andersen and J. Mehmedalic „Grid Modeling, Analysis and Simulation of different scenarios for a Smart Low-Voltage Distribution Grid”, in Proc. of IEEE PES-ISGT Europe 2013, Lyngby, Denmark, October 6-9, ISSN: 2165-4816, ISBN: 978-1-4799-2984-9, Accession number: WOS: 000330939800241 (ISI Proceedings, ISI Web of Knowledge)**
- [5.20] L. Mihet-Popa and H. Bindner, „Simulation models developed for voltage control in a distribution network using energy storage systems for PV penetration”, in Proc. of the 39th Annual Conference of the IEEE Industrial Electronics Society-IECON'13, November 10-13, Vienna, Austria, pp. 7487-7492, ISSN: 1553-572X, ISBN: 978-1-4799-0224-8, Accession number: WOS: 000331149507049 (ISI Proceedings, ISI Web of Knowledge).**
- [5.21] L. Mihet-Popa, O.M.F. Camacho and P.B. Norgard, „Charging and discharging tests for obtaining an accurate dynamic electro-thermal model of high power lithium-ion pack system for**

hybrid and EV applications”, in Proc. of the IEEE PES Power Tech Conference, Grenoble, June 16-20, 2013, ISBN: 978-146735669-5 (Scopus, IEEE Explore, Google Scholar).

[5.22] L. Mihet-Popa, C. Koch-Ciobotaru, F. Isleifsson and H. Bindner, „Improvements and Validation of a PV System Simulation Model in a Micro-Grid”, Scientific buletin of POLITEHNICA University of Timișoara, Romania-Transactions on automatic control and computer science), Romania, Vol. 52 (66), No. 3, Decembrie 2012, ISSN 1224-600X; (B+-CNCSIS).